Physicochemical study of DNA biochips: DNA duplex stability, point mutation detection and beyond

Julia Fuchs

Thèse

présentée par

Julia FUCHS

pour obtenir le titre de

Docteur

de l'UNIVERSITÉ GRENOBLE I - JOSEPH FOURIER

Ecole doctorale de Physique

Spécialité : Physique pour les sciences du vivant

Physicochemical study of DNA biochips

DNA duplex stability, point mutation detection and beyond

Etude physico-chimique des puces à ADN

Stabilité du duplex d'ADN, détection des mutations ponctuelles et au-delà

soutenue le 5 novembre 2009 devant la Commission d'Examen :

JURY

M.	**Jacques DEROUARD**	**Président**
M.	**Malcolm BUCKLE**	**Rapporteur**
M.	**Joël CHOPINEAU**	**Rapporteur**
M.	**Didier-Luc BRUNET**	**Examinateur**
M.	**Jean-Charles BRES**	**Examinateur**
M.	**Roberto CALEMCZUK**	**Directeur de Thèse**
M.	**Arnaud BUHOT**	**Co-Directeur de Thèse**

Thèse préparée au sein du CEA Grenoble
Institut Nanosciences et Cryogénie (INAC)
Service des Structures et Propriétés d'Architectures Moléculaires (SPrAM)
Groupe: Chimie pour la Reconnaissance et l'Etude d'Assemblages Biologiques (CREAB)

To my family....

Acknowledgments

A three year Ph.D. thesis is rarely the result of one person's work, but most often a joint venture of different people. During this thesis I had the opportunity to work with a lot of different researchers and industrial partners whom I want to thank in the following for the numerous discussions and brainstormings that make this work so multifaceted and interesting.

First of all, I want to thank my supervisors Roberto Calemczuk and Arnaud Buhot. This work would not exist without their exceptional collaboration linking the laboratory's theory group and the experimental group CREAB. Although the orientation of this work is mainly experimental, I always profited from Arnaud's insight in the theory of DNA surface hybridization giving rise to numerical simulations like in the case of the salinity effects and the amplification method for the detection of a minority of mutated targets. Thank you, Arnaud, for all the helpful interpretation and your intuition when it comes to DNA surface interactions. But I was also fortunate to have Roberto always accessible just in the next room, to talk about experimental setups and results, to learn about background noise and all other kind of parameters and software options that might influence the SPRi signal. Thank you, Roberto, for your lively, creative and thoughtful spirit that gave rise to so many professional and personal discussions.

I want to thank the members of my jury and first of all, Malcolm Buckle and Joël Chopineau for critical, but also interested reading of my manuscript and their constructive remarks during my defense. I also want to thank the president of my Ph.D. thesis committee, Jacques Dérouard, and the examiners Jean-Charles Brès and Didier-Luc Brunet, each of them interested in other aspects of this work. The diversity of backgrounds of the members of this committee reflects the different aspects of the work and their interest in different subjects during my defense reminded me of the different challenges that are to be addressed in future work.

I want to thank Jean-Pierre Travers for welcoming me at the SPrAM, where I learned not only how to do good research, but also, how a research laboratory works and is financed. Thanks also to Catherine Pascal, the secretary of SPrAM who has always the good answer for administrative questions.

A special thank you is for Thierry Livache who followed my work with helpful ideas. Besides of giving me the funding to do the research and to participate in international conferences and the exchange program with Montréal, Thierry is always there also for small matters like how to pull down a tenacious roller blind to dim Grenoble's bright summer sun...

This Ph.D. thesis would not be what it is today without the numerous collaborations that provided this eclectic and creative research environment:

The biggest 'thank you' is clearly for Christelle Corne who spent a lot of time with me in front of the SPRi working on DNA repair enzymes on different DNA damage. Besides a very productive working climate, we also had a lot of fun together and I really appreciated her reliable work and her always good humor even in times of incredible stress. A big hug for you!

I also want to thank Didier Gasparutto and Alain Favier who initiated and guided this interesting collaboration to detect DNA damage by SPRi.

On the same subject, thanks a lot to Muriel Jourdan and Jean-François Constant for their complementary insight in FPG damage studies for multiple lesions and their enthusiasm to explore SPRi for their experiments. I hope you'll have a lot of good experiments!

Also good luck for the SPRi experiments of Christophe Morand Bounaix du Puch and Jean Breton and thank you for teaching me some facts about anti-cancer drugs. It was a real pleasure to work with you!

Thanks to Evelyne Lopez-Crapez without whom the project on PCR products would not exist. Thank you for the time you invested to provide me with PCR amplified targets and to discuss the results.

I want to thank Maryam Tabrizian for welcoming me at her lab at the McGill University in 2007. It was a rich experience, both, professional and personal and I am still glad about getting to know a lot of nice persons. Thank you Xuyen, Lidija, Julien, Marc, Marinella, Nadia, Sania, Simone, Jamal and all the others for giving me such a good time!

I am also very glad about the good collaboration with Karen Brengel-Pesce and Nadège Beaufet from bioMérieux, giving me the opportunity to learn a lot about NASBA. Thank you! Thanks also to Carole Lecossois who laid the foundations of this work during her Master thesis at our lab.

Thanks to Daniela Dell'Atti for the good time we shared during two months in 2007 in Grenoble. I wish you all the best. Thanks also to Marco Mascini for providing the funds for this exchange.

A very important paragraph here is dedicated to the members of the CREAB. One non negligible part of my decision to do my Ph.D. at this lab is surely based on the excellent atmosphere, where no day will pass without a lot of laughter and small jokes.

First of all thank you to Jean-Bernard Fiche who taught me the 'mystery' of DNA denaturation studies by SPRi and whose enthusiasm is simply infectious. Thank you is not enough to appreciate the great time during my 'apprenticeship' that we had in our shared office and the SPRi room on the third floor!

With the risk of being lengthy, just a few special words to some of the members and ex-members of the CREAB: Thanks to Radek Bombera for the good 'Eastern block' spirit we shared in our office and the coffee breaks always at the right time! Thanks to Emmanuel Suraniti for his attentive way to look at others and the right word at the right time. Thanks to Sebastien Laurent for his laughter and joy. I'm also happy to know Emeline Descamps who can be such a good friend! Thanks to Dayane Baptista-Tada, for passing three times at the lab and never forgetting to bring us the Brazilian summer! Thank you, Charles Agnès for sharing the 'Canadian Adventure' with me! Some days would have been disastrous without the magic hands of Sebastien Duménil. Also, every problem on instrumentation for SPRi could always be solved with the help of Loïc Leroy. Thank you! Thanks for all the tips and tricks I learned from Yoann Roupioz. I should not write but gesture the sign of 'merci' to Alexandre Thaumoux who always tried to teach me some more signs in French sign language. Thanks to Pascal Mailley for explanations about electrospotting and other recipes in every day life. Thanks to Martial Billon for taking some time to functionalize with me some QCM chips that are really sensitive to handle. Thanks to Malika Amdaoud for her good humor and the delicious cakes!

There are or were always a lot more people around the lab that make working there a good experience, so thank you to all of them and bisous à tous!

Thanks to all my friends, since work is only as good as the life around it and I am very happy to have a lot of good friends who joined me for every possible activity that can be done inside and outside Grenoble.

Last but not least, I want to profit from the few lines left to thank my family, especially my mother Doris Neu and her husband Robert Neu, for all the encouragement and help in every new adventure I headed for. Thank you for always being there for me, even when the distance was long!

And the very end is reserved for my love Sönke Pingel without whom life would be much less brighter and happier than it is. Thank you for being there and for joining me in every new adventure, those that passed and those that are still to come!

Résumé de la thèse

Ce travail de thèse a été préparé au sein du CEA Grenoble, au service des 'Structures et Propriétés d'Assemblages Moléculaires' (SPrAM) à 'l'Institut Nanosciences et Cryogénie' (INAC). Le projet de thèse s'inscrit dans la continuité du projet de thèse de Jean-Bernard Fiche qui a soutenu son travail en 2006. Pendant son travail au sein du groupe 'Chimie pour la Reconnaissance et l'Etude d'Assemblages Biologiques' (CREAB), J.-B. Fiche a conçu et monté une régulation de température pour un appareil d'imagerie par résonance de plasmons de surface (SPRi). Ce travail a donné lieu à la possibilité d'observer la dénaturation de l'ADN en temps réel par des rampes de température.

Dans ce travail-ci, nous allons valider et adapter cet outil par de nombreuses études du duplex d'ADN. Nous avons une approche à la fois fondamentale et applicative, qui pouvait être réalisée grâce à plusieurs collaborations internes et externes. Ainsi, nous allons profiter des connaissances approfondies obtenues par des études du système de l'hybridation et dénaturation thermique du duplex d'ADN sur support solide pour ensuite réaliser des applications pour la détection des mutations ponctuelles de l'ADN et la réparation de l'ADN portant des lésions. Tout le long de ce travail, nous profitons de la possibilité de pouvoir contrôler de façon précise la température pendant les expériences en SPRi.

Dans un premier temps, en chapitre 2, nous allons introduire l'objet clé de notre étude, la molécule de l'acide désoxyribonucléique (ADN). Il est important de comprendre le concept de l'hybridation et de la stabilité de la double hélice dans son environnement. Pour cela, le modèle du plus proche voisin sera utilisé pour obtenir des prédictions de la thermodynamique et de la stabilité du duplex d'ADN. Ensuite, le contexte biologique de ce projet sera posé, en introduisant la notion de gènes et du génotype pour définir les mutations ponctuelles et les enjeux pour la détection, objet d'une grande partie de cette étude. Les mutations ponctuelles sont les changements les plus subtils de l'ADN, où une seule base de la séquence est changée. Mais celle-ci peut altérer toute la fonctionnalité du gène associé. Etant donné que le mésappariement d'une base parmi un grand nombre de bases dans une séquence n'influence que peu la stabilité de la double hélice, il est donc très difficile de détecter cette mutation. C'est alors pourquoi des critères bien posés existent auquel doivent répondre les biopuces à ADN qui constituent dans ce travail la base de la détection de l'ADN. Le succès d'un outil de détection en format biopuce dépend notamment de sa capacité de discriminer les séquences d'ADN différentes mais très proches, comme les mutations ponctuelles, ce qui définit la spécificité du capteur. Mais aussi la sensibilité de la détection va jouer un rôle puisqu'elle définira les limites de détection et ainsi le nombre de molécules d'ADN minimum nécessaire pour une réponse positive. La spécificité et la sensibilité, ainsi que toutes les réponses du capteur doivent être reproductibles. Ces critères, associés à des critères de caractère commercial comme le coût, la facilité de manipulation, la possibilité d'intégration et le temps nécessaire pour obtenir l'information, seront des notions qui nécessairement accompagneront ce travail.

Le chapitre 3 expliquera les matériels et méthodes utilisés pour ce travail. Le focus de ce travail est la détection de l'ADN par la méthode de l'imagerie par résonance de plasmons de surface (SPRi). La SPRi est une méthode optique qui permet de suivre des changement de l'indice de réfraction à proximité d'une surface métallique, à une distance jusqu'à environ 100 nm. Notre

biopuce est composée d'un prisme, recouvert d'une mince couche d'or de 50 nm, qui sera ensuite fonctionnalisée par des séquences d'ADN synthétiques, appelées les sondes. La SPRi profite d'un couplage entre la lumière en réflexion totale et les électrons de la couche d'or pour sonder le milieu biologique aqueux sur la surface. Les changements de la lumière réfléchie sont suivis par une caméra CCD qui permet un traitement d'image pour obtenir des signaux en temps réel à des endroits spécifiques sur la puce. Nous pouvons alors fonctionnaliser notre puce par adressage pour obtenir jusqu'à environ 100 plots portant des séquences d'ADN bien définis. Le groupe CREAB a mis au point une méthode d'électro-spotting par co-polymérisation de poly-pyrrole avec des molécules modifiées par une fonction de pyrrole. Cette fonctionnalisation est bien compatible avec le format SPRi et montre des stabilités exceptionnelles. Néanmoins, pendant ce travail, une deuxième stratégie de fonctionnalisation de surface basée sur le principe d'auto-assemblage de molécules thiolées sur l'or a été dévelopée pour comparaison.

En plus de la SPRi et de la fonctionnalisation des puces, ce chapitre introduit aussi le principe de la synthèse d'ADN et des méthodes de détection complémentaires qui ont été utilisées pendant ce travail, à savoir la microbalance à quartz et la microscopie par fluorescence.

La première partie du travail est un mélange d'approches expérimentale et théorique, à travers de petites simulations dans le cadre d'un modèle de Langmuir approfondi. Ainsi, chapitre 4 commencera par une introduction théorique du principe de l'hybridation de l'ADN sur un support solide. La connaissance des paramètres thermodynamiques, notamment de l'enthalpie ΔH et de l'entropie ΔS à travers le modèle du plus proche voisin, nous permet de faire des prévisions sur la cinétique de la formation du duplex d'ADN sur la surface. Nous pouvons ainsi exploiter les modèles pour obtenir non seulement la cinétique d'association et de dissociation isotherme, mais aussi la dépendance en température. Comme nous allons le voir, cette possibilité d'observer la dissociation de l'ADN en fonction de la température est extrêmement utile quand il faut discriminer des cibles d'ADN qui ont une affinité comparable pour la sonde à la surface. L'hybridation d'une cible aura lieu sur plusieurs plots différents qui sondent l'endroit de la mutation par leur séquence en ayant des bases échangées. En appliquant une rampe de température, nous observons une dissociation à plus basse température sur des plots formant un duplex avec un mésappariement et ce n'est qu'à plus haute température que des plots avec le duplex parfaitement complémentaire montrent la dissociation de la cible. Puisque chaque sonde, en fonction de la cible injectée, peut porter le duplex parfait ou le mésappariement, nous pouvons déterminer par notre jeu de sondes l'identité de la cible dans l'échantillon. Le cas plus complexe de la présence d'un mélange de cibles avec une différence d'une seule base sera étudié. Ensuite, nous présenterons des extensions du modèle de Langmuir qui permettent de prendre en compte la salinité du tampon dans lequel l'ADN s'hybride.

Ces modèles théoriques seront ensuite vérifiés par des expériences en SPRi. Tous d'abord, une étude par rampe de température en équilibre, en présence de la cible d'ADN, sera présentée qui montre l'influence de la force ionique du tampon sur l'hybridation et la dénaturation thermique de l'ADN. Des prédictions empiriques et le modèle de Langmuir avec prise en compte de la salinité seront confrontés aux données expérimentales et les paramètres thermodynamiques résultants sont calculés. Il s'avérera que tandis que les formules empiriques établies pour la fusion en solution sont en accord avec la variation de la température de fusion sur puce induite par le sel, le modèle théorique prenant en compte la courbe complète en fonction de la température donne accès à des paramètres intrinsèques de notre système. Néanmoins, tandis que chaque approche fournit des informations valides, aucune des deux n'est capable de prédire exactement le comportement réel de l'ADN et nous en discuterons les raisons. Ces expériences ayant permis de mettre au point la force ionique nécessaire du tampon, nous allons dans un deuxième temps analyser l'influence d'agents dénaturants de l'ADN, notamment la formamide, sur les courbes de dissociation. Une prédiction de la variation de la température de dissociation par pourcentage de formamide sera obtenue et il sera montré que cette prédiction dépend peu de la présence de mésappariements et est indépendante de la méthode de greffage employée. Ces connaissances seront utiles pour des systèmes nécessitant une adaptation de la température de dissociation pour obtenir une meilleure discrimination.

Ensuite, nous allons présenter une méthode de détection de mutations ponctuelles avec des

cibles oligonucléotides synthétiques. Il sera démontré que notre système n'est pas seulement capable de détecter la présence d'une seule cible, mais aussi la présence de deux cibles mélangées qui s'hybrident sur un même plot. Cette fonctionnalité est intéressante pour des applications médicales ou il doit être même possible de détecter une séquence mutée d'ADN en faible concentration dans une forte présence de la cible sauvage. Ici, nous trouverons une limite de détection de 5% de mutant dans un solution à 250 nM. Nous allons discuter une méthode flexible d'amélioration de cette limite par une hybridation assistée par variation de la température qui résultera en une accumulation du mutant sur son plot complémentaire. La validité du concept est démontrée par des simulations et des expériences. Pour chercher de pousser la limite de détection d'avantage vers de plus basses concentrations, une méthode d'amplification basée sur la reconnaissance spécifique de la biotine par la streptavidine est ensuite évaluée. Cependant, il s'avère que cette amplification, alors qu'elle permet d'obtenir une amplification importante du signal, peut compliquer, voire fausser, une détection de mélange de cibles en solution. En vu des expériences avec des échantillons biologiques issus d'une amplification d'ADN génomique, nous avons également réalisé des expériences avec des cibles oligonucléotides de 80 bases ayant des queues vers la surface ou la solution. L'étude thermique démontera l'impact de la longueur et du positionnement, et révèle une pénalisation de l'hybridation par une queue en 3'. En même temps, la présence de structures secondaires dans la cible peut compliquer d'avantage l'hybridation à la surface en introduisant une compétition.

Nous allons profiter de cette compréhension des enjeux de l'hybridation d'ADN à la surface pour procéder au chapitre 5 avec la détection des mutations ponctuelles des cibles longues issues de l'amplification par 'Polymerase Chain Reaction' (PCR) ou par 'Nucleic Acid Sequence-Based Amplification' (NASBA). Le projet sur la détection des mutations ponctuelles dans les produits PCR est mené en collaboration avec E. Crapez du 'Centre de Recherche en Cancérologie' à Montpellier. Grâce à l'optimisation des paramètres d'hybridations, nous pouvons détecter le génotype d'un échantillon d'ADN dans le cas homozygote et hétérozygote. En même temps, nous découvrons un changement fondamental de la dénaturation sur puce entre les oligonucléotides courts et nos produits longs de la PCR. Tandis que les courbes de dénaturation des ODN sont larges, les courbes obtenues avec les produits PCR montrent une transition entre état hybridé et état dissocié beaucoup plus étroite, donnant lieu à de fortes pentes. De tels systèmes coopératifs de l'ADN sont possibles quand il y a une interconnectivité entre différents brins.

L'amplification d'ARN par la NASBA est brevetée par la société bioMérieux. En collaboration avec K. Brengel-Pesce et N. Beaufet de bioMérieux un projet sur la détection des ARN a été mené. En profitant de l'amplification isotherme d'ARN par la NASBA, nous pouvons dans un deuxième temps montrer que notre système de détection peut être compatible avec un système intégré où l'amplification et la détection ont lieu dans la cuve de la SPRi pendant la détection. Cette intégration permettrai de réduire les étapes nécessaires pour un diagnostique et constituent ainsi un gain de temps.

Le projet présenté au chapitre 6 est mené en collaboration avec D. Gasparutto, A. Favier et C. Corne du 'Laboratoire des Lésions des Acides Nucléiques' (LAN) à l'INAC au CEA Grenoble. Ce projet est une partie du projet de thèse de Christelle Corne et a été débuté avec notre laboratoire par J.-B. Fiche. Ayant précédemment focalisé notre recherche sur la stabilité du duplex d'ADN en présence de mutations ponctuelles, nous allons maintenant étudier l'effet de la présence d'une lésion dans la double hélice. Disposant de plusieurs enzymes de réparation faisant partie du mécanisme de réparation par excision de base, nous étudions les interactions entre enzymes et l'ADN endommagé. Différentes méthodes de révélation de l'activité enzymatique seront présentées, dont une qui est basée sur la dénaturation thermique de l'ADN coupé par les enzymes de réparation. Le contrôle de la température nous permet ici de libérer les brins incisés pour ensuite faire une révélation par réhybridation spécifique d'un petit oligonucléotide et la streptavidine. Le point fort de notre méthode est ici la possibilité d'observer l'interaction d'une enzyme sur différentes lésions. Par comparaison, nous pouvons ainsi identifier des compétiteurs avec le substrat naturel de l'enzyme pouvant jouer un rôle de piège qui inhibera la réparation efficace des dommages. Cette méthode parallélisée montre des applications très variées et peut notamment donner lieu à un screening

systématique de l'activité de réparation des cellules cancéreuses pour adapter des stratégies d'intervention. Ainsi, nous menons ici une étude de relevance biologique sur des lésions tandem, se trouvant au voisinage sur un même brin d'ADN. Nous trouvons notamment un comportement différent entre l'enzyme de réparation bactérienne FPG et son homologue humain hOGG1 par rapport à l'excision d'une base portant la lésion 7,8-dihydro-8-oxoguanine adjacente à une base de 7,8-dihydro-8-oxoadénine. Nous observons aussi un effet annexe sur le comportement de l'enzyme de réparation endonucléase IV, une enzyme de réparation de sites abasiques, qui s'avère capable de cliver une fonction commercial de fonctionnalisation avec la biotine quand celle-ci se trouve en 3' d'un brin d'ADN. Ce clivage peut-être important pour des études utilisant des interactions par la biotine dans des extraits cellulaires, par exemple.

Cette dernière étude des enzymes de réparation en format parallélisé sur une puce universelle offre des multiples applications dans la recherche enzymatique. C'est pourquoi j'ai assisté à la mise en place de deux nouveaux projets sur des lésions d'ADN. C. Bounaix du Puch et J. Breton du LAN étudient les lésions liées à la platine, comme cis-platine ou oxali-platine, des lésions induites par des médicaments anticancéreux. Les premiers résultats obtenus par SPRi confirment des analyses menées par méthodes classique en électrophorèse sur gel dénaturant. Le deuxième projet est mené par J.-F. Constant et M. Jourdan du 'Département de Chimie Moléculaire' de l'Université Joseph Fourier. Cette étude est en étroite liaison avec nos études sur la FPG et les lésions tandem, analysant les lésions multiples sur des brins d'ADN opposées. Des résultats encourageants ont déjà été obtenus sur puce.

Cette thèse présente ainsi un travail qui touche à des domaines assez variés autour de l'ADN. J'ai donc fait le choix d'introduire la bibliographie nécessaire à la compréhension et aux discussions au fur et à mesure. Le lecteur trouveras ainsi trois grandes parties (de 4 à 6), qui introduisent le problème en question et l'approche choisie de manière indépendante.

Abbreviations

8-oxoA	7,8-dihydro-8-oxoadenine, DNA lesion
8-oxoG	7,8-dihydro-8-oxoguanine, DNA lesion
A	Adenine, DNA base
aa	Amino acid, building blocks of proteins
AFM	Atomic Force Microscopy
AMV-RT	Avian Myeloblastosis Virus-Reverse Transcriptase, enzyme that polymerizes DNA in the 3'→5' direction
AP	Apurinic/apyrimidic, or more generally an abasic site in DNA
APE1	Human apurinic/apyrimidic endonuclease 1, also known as Ref-1, APEX1 or HAP-1
BER	Base excision repair
bp	Base pair
BSA	Bovine serum albumin
C	Cytosine, DNA base
C3	DNA lesion, abasic site
CA	5',8-cyclo-2'-deoxyadenosine, DNA lesion
CCD	Charge coupled device
cDNA	complementary DNA, obtained by reverse transcription
Cyt C	Cytochrome C, small protein used here as blocking agent
DABSYL	4-dimethylaminoazobenzene-4"- sulfonyl chloride, common FRET acceptor molecule
DMSO	Dimethylsulfoxide
DNA	DeoxyriboNucleic Acid
dNTP	DeoxyriboNucleotide TriPhosphate
dsDNA	Double stranded deoxyribonucleic acid
DTT	Dithiothreitol ($C_4H_{10}O_2S_2$), reducing agent
E.coli	*Escherichia coli*, bacterium
EDTA	Ethylenediamine tetraacetic acid, capture of divalent ions
EMSA	Electrophoretic mobility shift assay
Endo IV	Endonuclease IV, DNA repair enzyme for AP sites in *E. coli*
EtBr	Ethidium bromide, common dsDNA stain in gel electrophoresis
FA	Formamide, DNA denaturing agent
FPG	Formamidopyrimidine DNA N-glycosylase, base excision repair enzyme from *E. coli*
FWHM	Full width at half maximum, characteristic measure to determine the sharpness of a peak
G	Guanine, DNA base
GFP	Green Fluorescent Protein
hOGG1	Human 8-oxoguanine DNA glycosylase
HPLC	High performance liquid chromatography
LASER	Light Amplification by Stimulated Emission of Radiation
LED	Light emitting diode

MCH	6-Mercapto-1-hexanol ($HS(CH_2)_6OH$), blocking thiol
MM	Mismatch, non-Watson-Crick combination of opposite bases in the double helix
MMR	Mismatch repair, DNA repair pathway correcting replication errors
mRNA	messenger ribonucleic acid
NER	Nucleotide excision repair, pathway excising an oligonucleotide of 30 nt to remove a DNA lesion
NN model	Nearest neighbor model
NMR	Nuclear magnetic resonance
NP	Nanoparticle
nt	Nucleotide
NTD	Non-equilibrium thermal denaturation. Temperature scans are performed in absence of target DNA
ODN	Oligodeoxynucleotide (oligonucleotide): synthetic DNA chain up to about $\sim$60 bp
PAGE	PolyAcrylamide Gel Electrophoresis, method of DNA migration in denaturing gels
PBS	Phosphate buffer saline, common buffer in molecular biology
PCR	Polymerase chain reaction, DNA amplification method
PEEK	Polyetheretherketone, biocompatible material for tubings
PEG	Polyethylene glycol($C_{2n+1}H_{4n+6}O_{n+2}$), surface blocking
PID	Proportional-integral-derivative
PM	Perfect match, perfectly complementary double helix
Ppy	Poly-pyrrole
RNA	Ribonucleic acid
RT	Reverse transcriptase, generation of DNA strands from DNA or RNA templates in the 3'$\rightarrow$5' direction
SA	Streptavidin, protein with four recognition sites for biotin
SAPE	Streptavidin-phycoerythrine, biotin binding fluoreophore assembly
SNP	Single nucleotide polymorphism
SPR	Surface plasmon resonance
SPRi	Surface plasmon resonance imaging
SSB	Single strand break
ssDNA	Single stranded deoxyribonucleic acid
T	Thymine, DNA base
TCEP·HCl	Tris(2-Carboxyethyl) phosphine Hydrochloride ($C_9H_{16}O_6PCl$), reducing agent
THF	Tetrahydrofuran, DNA lesion
T_d	Dissociation temperature in NTD mode
TE mode	Transverse electric mode
T_m	Melting temperature
TM mode	Transverse magnetic mode
U	Uracil, RNA equivalent of thymine
U	Units, specifying the enzyme activity as provided by manufacturer
UV	Ultra-violet
$[X]$	Concentration of product X

Contents

Chapter 1

General introduction

Since the discovery of the structure of the DNA double helix in 1953 [1], our knowledge about DNA and its importance for life has made huge progress. The understanding of the function of genes and how a cell expresses some of them but not others gives rise to fundamental insight in a cell's metabolism. The information stored in our chromosomes is essential. DNA may be understood as the 'code of life', as it codes for all proteins and enzymes of a cell. Although the genetic information in human beings has been deciphered with the completion of the 'Human Genome Project', there are still a huge bundle of questions that are not yet answered [2]. So, genetic information and thus DNA is an ongoing subject in research. The last 25 years have seen the advent of biotechnology, and simultaneously a progressive shift from fundamental DNA thermodynamic studies to applications that provide biological understanding of cells and their function to develop medical tools.

The ability to manipulate DNA in a controlled way and the possibility to produce DNA by chemical synthesis has given rise to DNA chip technology [3, 4]. The concept of DNA chips is based on the recognition of complementary DNA sequences by hybridization. One of the strands is immobilized on a solid support. This chip can then be exposed to various biological samples to screen for the presence of complementary target DNA in these solutions. Indeed, DNA chip technology provides information about the presence or absence of a specific DNA sequence in the sample. DNA microarrays are probably the most famous representatives of DNA chips. Borrowing from microelectronic technology, it is today possible to study hundreds of thousands of DNA sequences on a small $\sim$1 cm^2 surface. However, the actual size of the DNA chip will strongly depend on its purpose and application. Gene expression arrays need many probe sequences to analyze RNA produced by the cell that reflects the expressed proteins [5, 6]. Also, Single Nucleotide Polymorphism (SNP) genotyping experiments compare huge amounts of sequences of genes to correlate DNA point mutations to disease susceptibilities or to screen for reasons of reduced or increased metabolism of drugs [7]. In SNP genotyping, one has always to choose if a large number of SNPs are screened for a few individuals or if a small number of SNPs is detected in a lot of patients. So, the amount of data generated in on-chip experiments is a non negligible factor. Other applications in environmental studies, food analysis or forensic sciences often look for only few but very specific targets. One purpose might here be the detection of presence or absence of specific bacteria in the analyte. These are only some examples of possible DNA chip applications, but they explain why DNA biochips are a powerful tool in biotechnology.

In the last years, researchers focused on different topics concerning DNA microarray technology. A lot of fundamental studies, experimental or theoretical, are carried out to characterize the properties of DNA surface hybridization under various conditions [8]. Here, surface chemistry, buffer conditions and factors like temperature, hybridization time and target concentration will be analyzed. But huge effort is also put in the creation of protocols and setups that improve critical factors like sensitivity and specificity of detection. A quite impressing amount of assay designs is available that use DNA amplification strategies, specific ligand recognition, sandwich

assays or nanoparticles to improve the technological performance of the device [9, 10]. For all DNA hybridization experiments, it is also necessary to guarantee the specificity of the detection. Stringent conditions have to be applied that allow distinguishing the perfectly matched duplex from hybridization with a mismatched target. When working with DNA microarrays, one important ingredient is also bioinformatics, as large amounts of data have to be statistically analyzed to provide reliable results. And, of course, besides these fundamental and technological aspects, the medical impact of DNA biochip data is of great interest. As microarrays rely on probe DNA sequences to recognize a certain target, each chip has to be carefully designed with special, carefully selected probes. Rigorous protocols have to be established so that the microarray analysis is reliable and reproducible. False positives are no option in personalized medicine, where DNA microarrays might possibly find their application.

After years of research on microarrays and with the advent of integrated systems called 'lab-on-a-chip', DNA biosensors have a great potential to find applications in DNA diagnosis [11, 12, 4]. However, some fundamental aspects of DNA surface hybridization are still uncertain or poorly understood. In this work we will analyze a wide set of parameters that have an impact on the DNA surface hybridization and the stability of the double helix. In a second time, we will profit from this knowledge to optimize a SNP genotyping assay and combine our on-chip approach to an in-situ detection system where target amplification and detection are carried out in a real-time detection system.

Brief description of this thesis:

This Ph.D. thesis profits from a temperature regulated Surface Plasmon Resonance imaging (SPRi) setup to study DNA interactions on a functionalized gold surface. The setup has been designed and optimized during the Ph.D. of Jean-Bernard Fiche at our laboratory [13]. This work aims to validate the previous work where the foundation for DNA point mutation detection is laid. Moreover, as SPRi is a real-time method that provides access to time resolve kinetics information, it provides a good basis to gain fundamental insight in the DNA surface hybridization process. So, the scientific results presented here will on one hand treat fundamental interactions and systems related to DNA solid phase experiments, and, on the other hand, we will optimize the system for applications like SNP genotyping and DNA repair studies with clinical relevance. Consequently, the experimental results will be separately presented in three main chapters with individual introductions and associated literature. Each of these chapters will present experimental results of different background, but all analysis will in some way or another study DNA stability and temperature related information.

The next chapter will start with a general overview over properties of the DNA molecule and how its stability can be predicted by the Nearest Neighbor Model. We will then introduce the concept of DNA mutations and how these alterations of the genetic material may arise. Then, we will present the challenge that the detection of SNPs constitutes and finally, we will introduce the basic concept and essential features of biosensor technology. In chapter 3, the materials and methods used in this study will be presented.

Chapter 4 introduces some theoretical concepts, notably the Langmuir adsorption isotherms and related extensions that will then be confronted to our experimental results. This chapter aims to provide fundamental insight in solid-phase DNA experiments. Two surface immobilization techniques will be presented and compared. Then, we will study the influence of the buffer composition on the stability of an immobilized DNA duplex. Here, the focus will lie on the influence of salt ions that screen the negative charges of the DNA backbone. Also, a typical DNA denaturing agent, formamide, will be characterized in our solid phase setup. Having determined optimal buffer compositions, we will shift our focus to point mutation detection. Here, the possibility to regulate the temperature will be exploited to denature surface hybridized DNA during a temperature scan, which provides an easy way to access the stability of perfectly matched from mismatched DNA duplex on the surface. Special attention is paid to the case when two targets with different affinity for the same probe are present in solution. In general, such cross-hybridizing systems are a challenge for detection, but since they have a real medical relevance, each genotyping system must be able to treat such cases of mixed wild type and mutant sequences. At the end of this

chapter, a study with longer oligonucleotide targets is carried out that prepares some points that will be essential for the detection of biological targets as presented in chapter 5. We discuss here the influence of dangling ends and target secondary structure on surface hybridization.

With the knowledge gained from our fundamental studies, we can set up in chapter 5 an optimized assay for Single Nucleotide Polymorphism (SNP) detection. The samples are now nucleic acids of 150-200 bp that are the product of amplification either by Polymerase Chain Reaction (PCR) or by Nucleic Acid Sequence-Based Amplification (NASBA). As these samples are produced by enzymatic reactions, unlike synthetic oligonucleotides used in the previous chapter, they are provided in special solutions and require either special purification protocols or adaptation of the biosensor to these new conditions. We will present detection of these targets for both, purified and unpurified targets. Further, the possibility to integrate NASBA in our SPRi flow cell to have an in-situ production of RNA targets will be demonstrated.

A third project of this Ph.D. thesis reaches beyond detection of DNA hybridization. In chapter 6 we will see that the DNA chip approach may also be used in the framework of DNA repair studies. Here, we demonstrate the possibility to study enzyme interaction with damaged DNA that is immobilized on our sensor surface. The parallelized layout provides easy comparison of enzyme affinity for different types of substrate. Further, we will demonstrate the possibility to reveal base excision repair (BER) activity on our DNA chip. Our method relies on thermal denaturation of enzymatically incised DNA followed by specific rehybridization of a reporter oligonucleotide that reveals the enzyme's activity. We use in this work bacterial (FPG) and human (hOGG1) glycosylases specific for the oxidative damage 7,8-dihydro-8-oxoguanine. Further, the associated apurinic/apyrimidic endonucleases Endo IV and APE1 are studied. To validate our DNA chip approach, enzymatic activity on clustered DNA damages is studied and confronted to classical gel electrophoresis analysis.

Conclusions and perspectives of this work will be presented in chapter 7 and 8.

In the appendix, the reader will find a table of all buffers employed in this study. Further, the protocol for fluorescence microscopy DNA hybridization revelation is explicitly given. The appendix finishes with a step-by-step description of the data treatment necessary to obtain the DNA denaturation curves as presented in this work. At the end of this thesis, the reader will find a small glossary with the most important definitions and some technical terms. Throughout the manuscript, the glossary entries will be emphasized upon first appearance. Also, to facilitate the lecture, an index of key words or protocols can be found after the glossary.

Chapter 2

Introduction to DNA and SNP genotyping

Ce chapitre introduira les notions nécessaires de la biologie de la molécule d'ADN (acide désoxyribonucléique) et de son rôle comme porteur de l'information génétique. La première section comportera une description physico-chimique de la molécule avec toutes les caractéristiques qui seront exploitées au cours de cette thèse. On se servira notamment du modèle du plus proche voisin introduit dans la deuxième section comme base de prédiction pour les interactions de chaînes d'ADN courtes, les oligonucléotides. Nous allons voir, que les oligonucleotides synthétiques, trouvent des applications notamment comme sonde locale dans des tests génétiques. Les sections suivantes introduiront des notions biologiques par une description simplifiée de la mutagénèse et du rôle important du génotypage pour des applications médicales.

2.1 Deoxyribonucleic Acid (DNA)

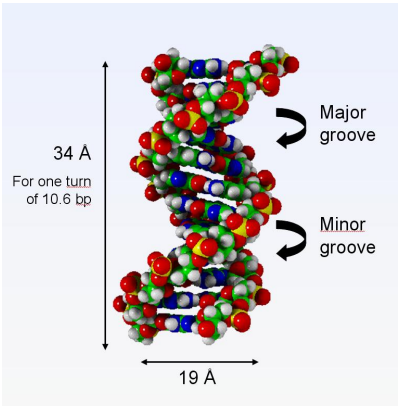

Figure 2.1: DNA double helix in the B-form. The arrows show the size of the molecule [14].

Deoxyribonucleic acid, the heteropolymer that codes for the genetic information in each creature, is composed of only four different bases. The bases can be divided in two groups: pyrimidines with one aromatic cycle and purines with a heterocycle formed of a pyrimidine and an imidazole ring. The bases adenine (A) and guanine (G) are purines, their complementary bases are pyrimidines: thymine (T) and cytosine (C), respectively, for DNA and uracil (U) and cytosine (C) for ribonucleic acid (RNA). The bases align by forming hydrogen bonds with their complementary parts: G and C form a more stable duplex with three hydrogen bonds compared to A and T with only two (see figure 2.2), forming so called Watson-Crick pairs [1]. The bases are linked by a phosphate-deoxyribose backbone and it is noteworthy that the DNA bases are isomorphous which means that the binding distance of each base to the sugar function is strictly the same. This fact allows DNA to combine in every imaginable sequence without major differences. The backbone, alternating phosphate groups with 2-deoxyribose, bears two different chemical end groups and is thus directional. The ends are labeled 3'(hydroxyl group) and 5'(phosphate group), according to the position of the carbon bearing those groups.

When two complementary DNA strands hybridize, they form the well-known double helix that can be seen in figure 2.1. The most common helical form is the B form, where the strands are anti-parallel (the forward strand is 5'→3', the reverse strand 3'→5', sometimes also called sense and anti-sense). The helix is then right-handed, and the bases are planar and oriented perpendicular to the axis in the center of the helix. Other forms, like for example, the B', A, and Z form appear for specific sequences or conditions [15]. The helix has not a perfectly cylindrical form, but presents two grooves which play an important role for DNA binding proteins (see figure 2.1). The bases are subject to stacking interactions inside the helix due to the dense packing of aromatic cycles. Stacking interactions are governed by Van-der-Waals, polarity, contact surface and dipole interactions. The strength of the stacking interactions differs in dependence of the neighboring base pairs and contributes to the stability of the helix. Some characteristic lengths in single stranded DNA (ssDNA) and double stranded DNA (dsDNA) can be seen in table 2.1. DNA as a polymer is subject to excluded volume interactions, preventing that two segments occupy the same space at the same time. This leads to a reduced number of possible conformations and increases the radius of gyration, which is inversely proportional to the diffusion coefficient. Also electrostatic interactions are very important for DNA interactions: since the phosphate in the DNA backbone is negatively charged, hybridization only takes place in a saline environment with ions ensuring the charge screening. Thus, the interaction between base pairs and consequently the DNA stability is influenced by the ionic strength of the surrounding solution. This becomes especially evident, when the *melting temperature* T_m, the temperature at which half of the DNA strands are in the double stranded state, is observed. There are several conditions causing DNA melting, i.e. the dissociation of the two strands, also called *helix-coil transition*: DNA double helix stability can be decreased by a variation of the pH to extreme acid or alkaline conditions (for example, reversible deprotonation of DNA bases at pH>9 [16]), by increasing the temperature, by decreasing salt concentration, by high dielectric constants compounds in aqueous solutions (for example alcohol, ketone) and by increasing the content of chemical agents like amides, urea or formamide in the solution [17].

DNA diffusion in solution has been treated by several approaches of poly-electrolyte linear polymer theory. The scaling law for the diffusion coefficient D in dependence of the length L of the DNA molecule is predicted as $D \sim 1/R_G \sim L^{-\nu}$ where R_G is the radius of gyration and

a) 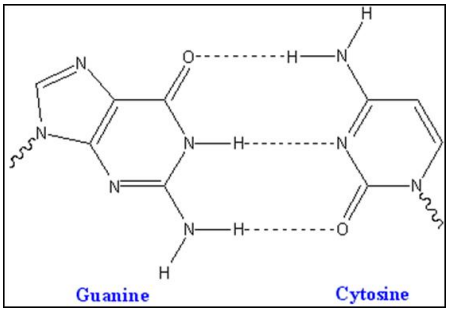

b) 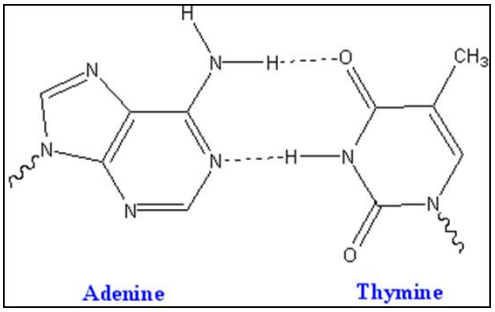

Figure 2.2: The four bases of DNA and their Watson-Crick hydrogen bonds between complementary bases. a) Cytosine and guanine forming 3 bonds b) Adenine and thymine forming 2 bonds (Figure from Wikipedia [18]).

parameter	**value**	**parameter**	**value**
diameter of dsDNA	1.9 nm	length added by on base pair to dsDNA	0.34 nm
persistence length of ssDNA	0.75 nm	persistence length of dsDNA[15]	50 nm
ssDNA base size	~ 0.6 nm		

Table 2.1: Characteristic length scales of single stranded and double stranded DNA

$\nu = 0.6$ is the Flory exponent. This law is applicable for polymers with relevant excluded volume effects. DNA diffusion coefficients have been measured using single molecule tracking of the Brownian motion of relaxed circular, linear and supercoiled DNA by Robertson et al. [19] using DNA with a length of ~6 to 290 kbp. A topology independent behavior can be determined with $\nu_c = 0.589 \pm 0.018$, $\nu_L = 0.571 \pm 0.014$ and $\nu_S = 0.571 \pm 0.057$ for circular, linear and supercoiled DNA, respectively.

2.2 The nearest neighbor model

The Nearest Neighbor (NN) model is one of the most commonly applied concepts to predict DNA thermodynamic parameters and, in this way, the stability of a duplex of a given sequence. As its name indicates, interactions are described between two neighboring base pairs and no long range interaction is included in the model. Pioneered in the 1960s by the groups of Zimm [20] and Tinoco [21], the nearest neighbor model has been developed mainly in the 1980s and 1990s by several groups [22, 23, 24]. It has been wrapped to a unified set of parameters by SantaLucia in 1998 [25]. The NN model applies accurately for short oligonucleotides up to about 20 bases, for which a two state melting transition can be assumed. For longer DNA strands, entropy induced bubble formation is expected [26] and the DNA has to be treated in other, more complex models. The NN model is thus suitable for the conception of assays in molecular biology that make use of well identified oligonucleotides. Applications can be found in the design of primers for DNA amplification by *Polymerase Chain Reaction (PCR)*, for the conception of *allele specific oligonucleotides* (ASO), probes on DNA biosensors and microarrays, *molecular beacons*, etc. to cite only some examples. A non negligible role in DNA duplex formation must be attributed to the stacking interactions between the bases which stabilize the helix. So, it is not astonishing that the stability of the duplex largely depends on the sequence i.e. on the neighboring bases. The NN model calculates the entropy and enthalpy of every DNA sequence using parameters for the 10 different duplex pairs that can be formed by the 4 bases. These duplexes are: AA/TT, GG/CC, AT/TA, TA/AT, CA/GT, GT/CA, CT/GA, GA/CT, CG/GC and GC/CG. The slash separates

the two complementary strands that are given in the sense 5'→3'/3'→5'. For a given duplex, the Gibb's free energy change ΔG during duplex formation at 37°C can be calculated taking into account corrections for terminal positions and self-symmetry of the strands:

$$\begin{aligned}\Delta G^0_{37^\circ\mathrm{C}}\,(total) = \sum_{i=1}^{10} n_i \Delta G^0\,(i) + \Delta G^0\,(\text{initiation with terminal GC}) \\ +\Delta G^0\,(\text{initiation with terminal AT}) + \Delta G^0\,(\text{symmetry})\end{aligned} \tag{2.1}$$

where $\Delta G^0\,(i)$ stands for the standard free energy of duplex i, n_i is the number of occurrences of duplex i, the second and third term are corrections for terminal A-T or G-C pairs [27] and the last term is the correction for self-complementary of the strands and is $+0.43\ \frac{kcal}{mol}$ if the duplex is self-complementary and 0 if not. Further contributions must be added in the presence of dangling ends ΔG^0 (dangling end), that are in most cases stabilizing as given in [28] or in the presence of mutations ΔG^0 (mutation type) that normally are destabilizing depending on their position in the duplex (reviewed in [29]). Also adjacent mismatches in the DNA helix have been evaluated and are in most cases destabilizing for the duplex [30, 31]. Analogous to ΔG, equations for ΔS^0 and ΔH^0 can be written as:

$$\begin{aligned}\Delta H^0\,(total) = \sum_{i=1}^{10} n_i \Delta H^0\,(i) + \Delta H^0\,(\text{initiation with terminal GC}) \\ +\Delta H^0\,(\text{initiation with terminal AT})\end{aligned} \tag{2.2}$$

$$\begin{aligned}\Delta S^0\,(total) = \sum_{i=1}^{10} n_i \Delta S^0\,(i) + \Delta S^0\,(\text{initiation with terminal GC}) \\ +\Delta S^0\,(\text{initiation with terminal AT}) + \Delta S^0\,(\text{symmetry})\end{aligned} \tag{2.3}$$

Note that the symmetry term for ΔH^0 is zero. All parameters for ΔS^0 and ΔH^0 can be found in Table 2 of [25]. Their knowledge permits to calculate the melting temperature of any ODN duplex for a given strand concentration c_t:

$$T_m = \frac{\Delta H^0}{\Delta S^0 + R \ln c_t} \tag{2.4}$$

By analyzing different thermodynamic data on DNA published by different groups, SantaLucia retrieved a set of unified thermodynamic parameters for DNA duplexes in solution at 1 M of salt [25]. These parameters have been completed by experiences analyzing mismatches between bases and dangling ends [32, 33, 34, 35, 36, 37]. It is noteworthy, that one mutation in a duplex has the highest destabilizing effect when placed in the middle of the sequence. Of course, the overall effect is stronger for shorter sequences. This is why, for *point mutation* detection, it is preferably to work with oligonucleotides of about 12-25 bases. The nearest neighbor parameters describe the thermodynamics of DNA in very particular buffer conditions (salt concentration of 1 M, neutral pH of the solvent). To take into account the actual ionic strength of the buffer, the thermodynamic parameters need to be corrected. Since G. S. Manning showed that salt effects are purely entropic, no correction is applied to the enthalpy change [38]. Several empirical equations have been proposed to take into account salt effects on the DNA helix stability, as given in [39]. One solution, proposed by SantaLucia, assumes that salt corrections are sequence independent, but depend on the length of the oligonucleotide:

$$\Delta G^0_{37^\circ\mathrm{C}}\left(\text{oligo}, \left[Na^+\right]\right) = \Delta G^0_{37^\circ\mathrm{C}}\,(\text{unified oligo, 1M NaCl}) - 0.144 \cdot N \ln\left[Na^+\right] \tag{2.5}$$

$$\Delta S^0\left(\text{oligo}, \left[Na^+\right]\right) = \Delta S^0\,(\text{unified oligo, 1M NaCl}) + 0.368 \cdot \frac{N}{2} \ln\left[Na^+\right] \tag{2.6}$$

where N stands for the total number of phosphates in the duplex and $[Na^+]$ is the total concentration number of monovalent cations from all sources. To include also contribution from divalent

magnesium ions, one should replace $\ln[Na^+]$ by $\sqrt{[Na^+] + 3.3\,[Mg^{2+}]}$ in ΔG [40]. ΔH is assumed independent of the salt concentration at least in the range 0.05 M$\leq [Na^+] \leq$1.1 M. Note that predictions of melting temperatures from the nearest neighbor model have an error of about 2°C. There are a lot of DNA stability prediction tools available online, but some of them are based on older models using empirical data for G·C content of the sequence and salt concentration. Predictions based on NN model parameters are integrated in HYTHER by J. SantaLucia and IDT scitool by R. Owczarzy [41, 42]. Hyther allows the determination of thermodynamic parameters and T_m of any sequence with mismatches and dangling ends in various salt conditions. The more recent IDT server is more application oriented and considers not only the DNA sequence, but also the influence of modifications by labeling, secondary structure predictions using Mfold etc..

2.3 DNA mutations

In living organisms, the genetic information in form of DNA is normally densely packed and stored in the cell's nucleus. The DNA is used as template for transcription to produce specific proteins necessary for the cell's function. This process transcribes the DNA into RNA sequences that are further treated and finally transported out of the nucleus the cytoplasm where ribosomes are responsible for protein production. Cells undergo growth cycles that are separated in different phases of growth, proliferation and division. Before cell division can take place, the genomic material of the cell needs to be replicated. This replication is carried out by DNA polymerases that copy the sequence information from the template DNA and synthesize the complementary strand in the sense 5'→3' [43]. Although DNA polymerases have a very high fidelity, errors occur at frequencies 10^{-4}-10^{-6} per nucleotide and extension [44]. Given the size of the human genome of 3 billion base pairs with its currently estimated 20,000-25,000 genes [45] it is evident, that error correction in form of DNA repair mechanisms is crucial. Not only replication may introduce errors in the genome, but also the attack from the environment in form of radiation, oxidative species or free radicals constantly induce damage. This may lead to DNA lesions, whereby the chemistry of bases or the backbone is altered, but also to strand breaks in the DNA. One of the most difficult cases is a DNA double strand break, provoking the separation of the two ends. When errors are not corrected before replication of the cell, DNA lesions can lead to sequence errors due to insertion of a non-complementary base at the position of the lesion. Later, these misinsertions will lead to point mutations in the DNA sequence. To avoid excessive mutagenesis, cells dispose of various repair mechanism addressing these damages. DNA repair mechanisms usually employ several enzymes and, often, there is not only one pathway that can lead to the replacement of the damaged part. The Base Excision Repair (BER) mechanism makes use of a variety of enzymes recognizing specific lesions that are then enzymatically cleaved. We will see examples of enzymes of this repair mechanism in chapter 6. In more complicated cases, several DNA bases have to be exchanged or in the case of strand breaks, the corresponding sequence must be repaired making use of the corresponding allele on the second set of chromosomes.

When DNA mutations due to errors in replication or DNA repair occur, several cases are possible:

- The mutation lies in an intergene region that does not correspond to a protein recognition site for transcription. In this case, the mutation will not affect the cell function and can so be transmitted without problems to the next generations.

- The mutation lies in a non-coding part of the gene. In fact, in human beings, genes have so-called exon, parts of the gene that are actually coding for a protein and introns that will be eliminated on messenger RNA. Although the mutation in an intron will not directly alter the amino acids of the protein, it can alter transcription factors and lead to up or down regulation of the gene's expression, for example.

- The mutation lies in the exon. Various cases can then be imagined. Since triplets of DNA bases code for the 20 amino acids (aa) and several triplets may lead to the same amino acid,

we can have the case of an altered codon still leading to the same amino acid. In this case, we speak of a silent mutation. When the associated amino acid changes, the sequence of the encoded protein will change and alter or inhibit its functionality, depending on the locus. A third case is the apparition of a stop codon before the actual end. The protein will then be truncated.

When mutations affect heavily the cells functioning, the cell will enter in apoptosis and will not transfer its altered genetic material to future generations. However, when the damage leads to mutations that permit the cell to survive and function, the abnormality will be transferred to the daughter cell and may give rise to tumor tissue formation or disease. However, not all mutations give rise to disease which would be disastrous because of their high frequency. Point mutations occur, for example, every 100 to 300 bases in the genome. More detailed information on mutations can be found in [46, 47]

When we look at the variety of living beings in nature, we will observe that each is an individual. Of course, we can easily classify each individual in categories of species or race, for example, but still each will have its unique visible appearance which is referred to as its phenotype. The phenotype, in turn, is an expression of the combination of a person's genotype and its environment. Normally, human beings possess two identical sets of chromosomes in a cell, i.e. they are diploid, and so each individual gene is encoded twice in the genetic material. However, two genes encoding for the same protein are not necessarily 100% identical from one person to another in which case we distinguish alleles. Moreover, since each person has two copies of each gene it is possible to have two different alleles. In the case of identical alleles inherited from both parents, the individual is homozygous and in the case of different alleles for one gene, the person is called heterozygous. We know since the establishment of Mendelian genetics that alleles can be dominant or recessive, determining if a gene is expressed or not. The genotype of an individual defines the combination of alleles which can either be homozygous dominant, heterozygous or homozygous recessive. Only in the last case, the encoded trait of the recessive gene is expressed and is a part of the phenotype. However, our genotype is not only expressed in our individual traits, but also comprises pathological changes in the genome either inherited or acquired, as is the case of inheritable diseases or cancer.

2.4 SNP genotyping

We can now understand, what genotyping or gene testing, i.e. the detection of an individual's genotype, can be used for. On one hand, the characterization of sets of alleles can be used for identification methods, like paternity tests or in forensic sciences. On the other hand genotyping is useful for diagnostic purposes to screen for carriers of inheritable diseases, obtain presymptomatic susceptibilities for the development of certain disorders or information concerning adult-onset diseases with possible risk evaluation, for example. It can also be used for determination of the malignant or benign nature of tumor tissue. It should not be forgotten, that also research on the evolution theory of species is based on genetics and variation identification [48]. Although DNA mutations can be of various types, for instance point mutations, deletions, inserts, translocations etc., the most current change is the exchange of one single base of the DNA. These point mutations are called Single Nucleotide Polymorphism (SNP) when having a significant frequency in population (normally above 1% as is the case for SNPs collected in databases like the human HapMap Project). Since SNP occur frequently, SNP genotyping encounters an increasing interest in research and industry. It gives access to individual diagnostic tools, and may lead in the future to so-called personalized medicine. We are however still a long way from the implementation of gene testing stations at a doctor's and technological as well as ethical question will have to be addressed to find a reliable way to transform the results into adapted medical surveillance and treatment without risking discrimination or social stigmatization. Also other fields like phamacogenomics, i.e. the influence of the genetic material on an individual's response to drugs, or gene therapy will profit from further insight in genetic variation and the interplay between different mutation sites.

2.5 DNA on-chip detection

To access the composition of DNA samples, many approaches make use of DNA biosensors or microarrays. Biosensors consist of a surface in contact with the sample solution. On the surface, identified biomolecules are immobilized at specific sites, for DNA detection, oligonucleotide probes are used. Surface grafted probes have one interaction partner, the target and hybridization will occur when the target is present in the analyte. This biomolecular recognition gives rise to a signal that can be for example, emission of fluorescence, electrons, light absorption, the colored product of an enzymatic reaction,... which is converted by the transducer to an electrical signal. The signal is then amplified and processed before being displayed and analyzed to obtain the biological information that is searched for. The principle of biosensors is schematically depicted in figure 2.3. Biosensors come in the form of real-time detection that gives access to the kinetics of the biomolecular recognition or as an end-point detection device, where the signal is read once the biomolecular recognition is completed. While biosensors typically detect one probe/target interaction at a time, DNA biochips and especially microarrays are miniaturized and permit recording of up to several hundred thousand hybridization events in one experiment.

Multiple techniques and biosensing strategies for SNP genotyping are available today. Each technology will present its own specifications and characteristics that describe its performance. We will especially pay attention to the following criteria:

- Sensitivity: Each detection method will be efficient in a certain range of target concentrations. The sensitivity gives hereby the slope of the signal to an increase of concentration. Often, sensitivity is also used to refer to detection limits, the lowest target concentration or quantity that leads to a positive signal.

- Selectivity/specificity: Selectivity is the capacity to recognize only the biological target to be detected, which is the DNA or RNA. Specificity then gives us the capacity to detect a specific target sequence and distinguish it from targets with similar, but smaller affinities for the probe, as it is the case for point mutations, for instance.

- Reproducibility: A key factor of biosensor and DNA microarray production is the capacity to obtain for identically produced sensors identical responses to target injection. This is often a limiting factor for quantification of the DNA in the sample.

- Multiplexing capacity: the capacity to detect a multitude of targets in a sample simultaneously. Multiplexing is often hindered by amplification steps or limited availability of markers, for example, fluorophores of different color.

- Cost, detection time, easy handling, automation...: For chip technology to become a widespread technique cost must be low, detection fast and the set-up must be user friendly by providing reliable, understandable results in an automated fashion.

It is evident that the first three points are essential and must respond to the samples that are to be treated. A high fidelity of the results is a prerequisite for application of a technology in medical diagnosis. Naturally, the last factors are of commercial interest, since often a lot of samples have to be analyzed for multiple SNP locations and thus integrated systems will be needed for automation, fast detection and data analysis.

Each step of sample treatment and detection must be optimized, from sample extraction, over eventual sample amplification, purification and labeling, to the detection module that will be composed of a biologically functionalized surface, a signal transducer and read-out system, eventually signal amplification and finally data analysis and interpretation. Various physical and chemical methods are available as SNP detection platforms, which will not be introduced here in detail. When appropriate, comparisons to other technologies than the one described in this work will be done throughout the manuscript. For a good summary of existing DNA detection methods, the reader may be referred to the Ph. D. thesis of J.-B. Fiche who laid the foundations

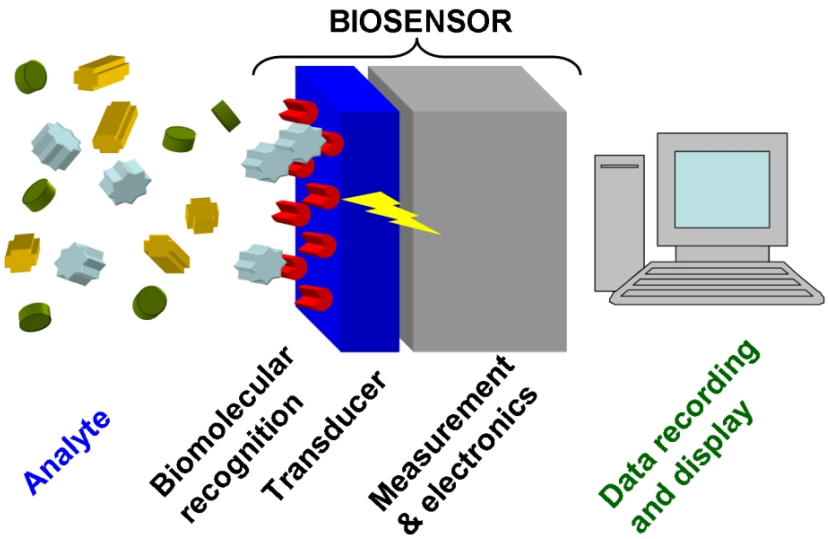

Figure 2.3: Principle of biosensors: The analyte is exposed to a surface functionalized with biomolecules (probes) that specifically recognize a part of the analyte (target). The transducer can be of any nature (light, electrons, chemical species, color, ...) and reports the recognition event. An electronic read-out system captures and amplifies the signal. Signals are then analyzed using bioinformatic tools.

of the work presented here by his former work at our laboratory [13]. Exhaustive reviews about microarrays and biosensor technology as well as SNP genotyping and its applications are also available [49, 50, 51, 12, 9, 52, 53, 5, 54, 55, 6, 56].

Chapter 3

Experimental techniques

Ce chapitre présentera les méthodes et appareillages qui constituent la base de ce travail. La première partie introduira les concepts de l'imagerie de la résonance de plasmons de surface, méthode clé des études menées. En particulier, on y trouvera les bases physiques de la méthode, les différentes mises en œuvres expérimentales disponible aujourd'hui et une description détaillée de l'instrumentation à disposition dans le laboratoire SPrAM. On trouvera les méthodes d'acquisition de données par la SPRi, les techniques d'analyse de données seront détaillées dans l'annexe 8. La troisième partie comprendra une introduction à la microbalance à crystal de quartz, technique utilisée pendant un séjour de 2 mois à l'université McGill à Montréal, Canada. On trouvera ensuite une brève introduction à la technique de marquage et acquisition des données par microscopie de fluorescence disponible au SPrAM. Après cette présentation des dispositifs physiques, les étapes chimiques de production de sondes d'ADN et les séquences d'ADN utilisées dans ce travail seront présentées. La dernière partie analysera différentes méthodes de greffage d'ADN sur un support solide et présentera les techniques d'immobilisation d'ADN par une fonction active de pyrrole ou de thiol.

This chapter will introduce the physical principles of experimental methods and setups used in this work. In particular, we will learn about the principles of Surface Plasmon Resonance imaging (SPRi) as well as the home-made temperature regulated setup, the principle of Quartz Crystal Microbalance (QCM), fluorescence microscopy, DNA synthesis and DNA immobilization methods on gold surfaces.

3.1 Surface Plasmon Resonance imaging (SPRi)

3.1.1 The dispersion relation

Surface Plasmon Resonance is an optical method which permits to follow refractive index variations close to a dielectric/metal interface of isotropic media. It is based on the coupling of incoming photons to plasmon polariton modes of the free electron gas in the metal.

Several conditions must be fulfilled to obtain photon coupling to the electrons. First, the light has to be in the transverse magnetic (TM) mode, in order to have a component of the electric field normal to the surface. Only under this condition, a surface charge density variation can be induced and the photon can excite surface waves.

The following considerations will be restricted to non-magnetic media ($\mu_r = 1$). When we consider the TM mode, in which the magnetic component $\vec{H}$ of the electromagnetic light wave is perpendicular to the incidence plane and thus parallel to the metal/dielectric interface, Maxwell's theory leads to the following condition (Reviewed by [57, 58]):

$$\frac{k_{z_1}}{k_{z_2}} = -\frac{\epsilon_1}{\epsilon_2} \tag{3.1}$$

This equation, relating the ratio between the z-components of the wave vectors in medium 1 (dielectric) and 2 (metal) to the ratio of the dielectric functions of each medium with a negative sign suggests, that the dielectric functions of the two materials have to be of opposite sign. This condition is, for example, fulfilled when one medium is a noble metal like silver or gold and the other is a dielectric medium. Then, one can retrieve the dispersion relation for surface plasmons in dependence of the dielectric functions of the two media:

$$\omega = \frac{c}{\sqrt{\epsilon_1}} k_x \cdot \sqrt{\frac{\epsilon_1 + \epsilon_2}{\epsilon_1 \epsilon_2}} \tag{3.2}$$

The dispersion relation (or energy-momentum relation) must correspond to that of the incoming light wave so that the energy and momentum conservation laws are respected. The x-component of the incoming wave vector of the photon is $k^x_{photon} = k_{photon} \sin\theta = \frac{\omega}{c}\sqrt{\epsilon_1}\sin\theta$. It has to match the plasmon wave vector k_x, or, in other words, the dispersion relation of the plasmon has to be cut by the light line of the incoming photon. The dielectric function of the metal is frequency dependent and, for high frequencies, can be expressed in the following way:

$$\epsilon_2(\omega) = 1 - \frac{4\pi n\, e^2}{m^*} \cdot \frac{1}{\omega^2} = 1 - \left(\frac{\omega_p}{\omega}\right)^2 \tag{3.3}$$

wherein m^* is the effective mass of the electrons, n is the number density and ω_p is the plasma frequency. Considering the condition $\epsilon_1 = -\epsilon_2$ following equation 3.1, we can conclude that there is a high frequency cut-off energy $\omega_{sp} = \frac{\omega_p}{\sqrt{1+\epsilon_1}}$ for the surface plasmon dispersion relation, showing that surface plasmons are a low energy phenomenon, contrarily to volume plasmons. In the limit of small wave vectors k, we find that the surface plasmon dispersion relation approaches asymptotically the light line of the photon in the dielectric medium. So, there is no intersection between the two dispersion relations in this two layer system, as can be seen in figure 3.2. To satisfy the coupling condition $k_{x,photon} = k_{x,surf.plasmon}$ we have to adjust the wave vector in order to 'couple' the light to the plasmon polariton modes. Two solutions to this problem have been put forward:

- Coupling via periodical structuring of the metal's surface, which permits to 'tune' the incident wave vector by diffraction. However, the incident light crosses the dielectric medium and may be perturbed by the inhomogeneities of the biological solution.
- Coupling by a third medium of high refractive index n_3 that permits to adapt the slope of the light line by changing the speed of light $v = \frac{c}{n_3}$. This is achieved by a glass prism where the incoming angle of incidence of the light lies in the domain of total reflection. The surface plasmons are excited by the evanescent wave, penetrating the adjacent medium and attaining the metal/dielectric interface. Here, the photons transfer their energy to the electrons in the metal, provoking oscillations at the interface.

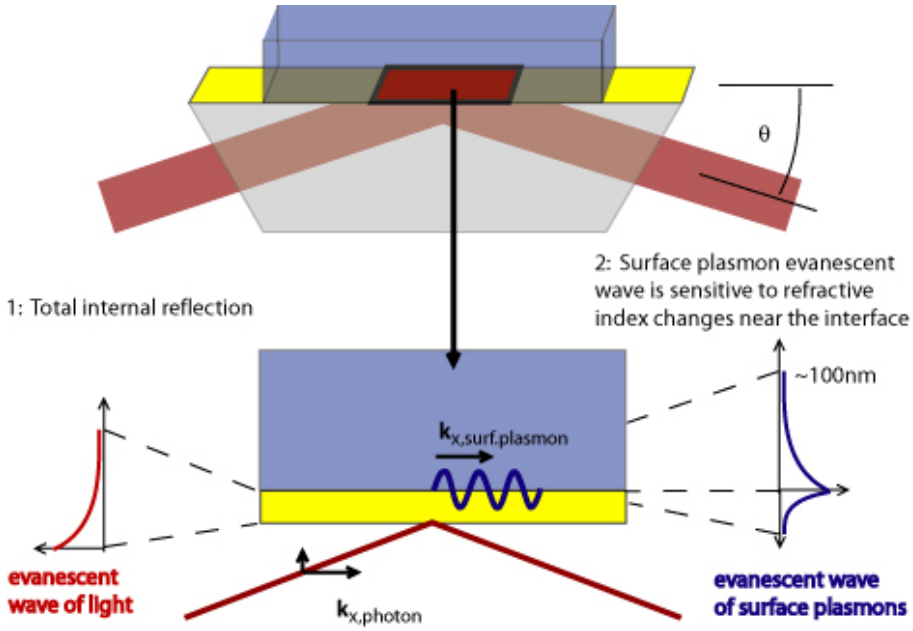

Figure 3.1: Surface plasmon excitation in the Kretschmann configuration: the incoming light is reflected at the glass/gold interface. Its evanescent wave couples to a surface polariton mode of the free electrons at the dielectric/metal interface, given that $k_{x,photon} = k_{x,surf.plasmon}$. Changes of the refractive index in the dielectric medium are sensed up to 100-200 nm from the interface depending on the quality of the gold coating and the wave length of the light. The lateral resolution is ~7-10 µm.

3.1.2 Resolution of SPR in the Kretschmann configuration

In the following, we will focus on SPR coupling via a glass prism. Two different configurations have been proposed by Otto [59] and Kretschmann [60]. In the Otto-configuration the dielectric is placed between the glass prism and the metal leaving a very tiny layer thickness of the dielectric medium to allow the evanescent wave to excite surface polaritons. Kretschmann chose a very thin gold layer directly damped on the glass prism, offering an infinite volume of the dielectric above. This is the configuration adopted for detectors in this work, enabling a functionalization of the gold surface that is then placed into contact with the biological solution. The evanescent waves of the surface polariton in the Kretschmann configuration is schematically depicted in figure 3.1.

Some precisions have to be made on surface plasmons and the resolution of SPR. Perpendicular to the surface, the electromagnetic wave is evanescent and decreases exponentially in both media. In the interface, surface plasmons have a finite propagation length due to the complex part of

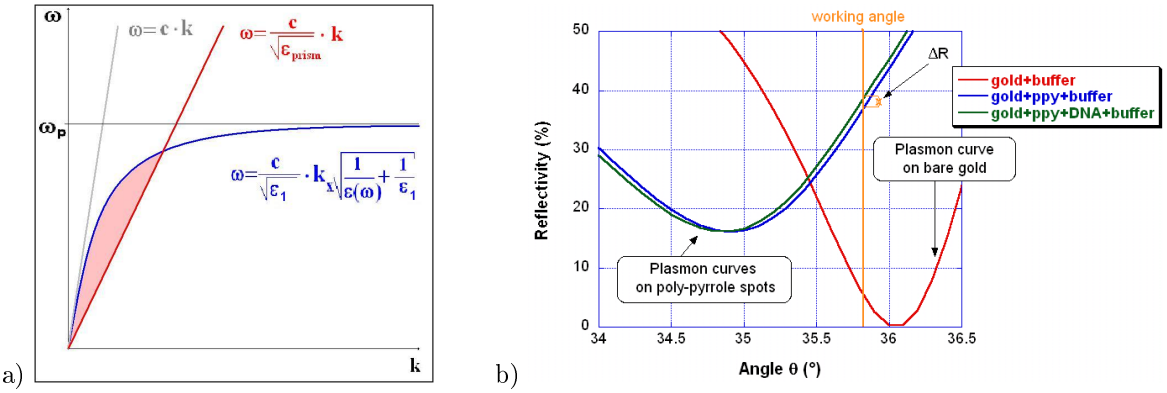

Figure 3.2: a) Representation of the dispersion relation of surface plasmon polaritons (blue), the light line in air (gray) and the light line after adaptation by a high-indexed glass prism (red). b) Theoretical plasmon curves in buffer. Curves are represented for a bare gold surface (red), an unhybridized poly-pyrrole spot (blue) and a DNA hybridized poly-pyrrole spot (green). While poly-pyrrole, having an imaginary part of the refractive index is adsorbing and deforms the plasmon curve, the hybridization of DNA leads to a simple shift of the plasmon curve. When measuring at a constant angle, this shift results in a refractive index change ΔR. The gold surface does not undergo any change when hybridization is specific.

$k_x = k_x^{'} + ik_x^{''}$. The following expressions can be found for the penetration of the evanescent waves in dependence of the dielectric functions of the dielectric (1) and the metal (2):

$$L_{z_2} = \frac{c}{2\omega}\left(\mathrm{Im}\left[\sqrt{\frac{\epsilon_2^2}{\epsilon_2+\epsilon_1}}\right]\right)^{-1} \tag{3.4}$$

$$L_{z_1} = \frac{c}{2\omega}\left(\mathrm{Im}\left[\sqrt{\frac{\epsilon_1^2}{\epsilon_2+\epsilon_1}}\right]\right)^{-1} \tag{3.5}$$

$$L_x = \frac{c}{2\omega}\left(\mathrm{Im}\left[\sqrt{\frac{\epsilon_1\cdot\epsilon_1}{\epsilon_2+\epsilon_1}}\right]\right)^{-1} \tag{3.6}$$

Taking for gold the refractive index $n = 0.14+i3.69$ and for water $n = 1.3316$ at λ =660 nm, we find $L_x \sim 7\,\mu$m, $L_{z_1} \sim 100$ nm and $L_{z_2} \sim 13$ nm [61]. The lateral resolution of SPR measurements is thus limited to $\sim 7\,\mu$m at 660 nm and decreases further for higher incident wave lengths [62]. In contrast, when moving to a higher incident wave length in the near infrared range, contrast and SPRi sensitivity is increased since the plasmon curve presents a smaller width. The sensing depth for SPR measurements is limited to ∼100-200 nm, depending on the medium, which should be kept in mind when big biological object like cells are imaged.

3.1.3 SPR methods

The excitation of oscillations of the free electron gas (surface plasmon resonance), describes in fact an energy transfer from the light to the plasmons. Therefore, when observing the reflectivity under the coupling angle, one observes absorption of the light in the total internal reflection angular range. The angle of the minimum reflectivity is strongly dependent on the refractive index of the dielectric. In our case, a change of $\Delta n = 10^{-4} - 10^{-5}$ already leads to a detectable shift of the plasmon curve. In most cases, the curve is shifted, but not deformed upon binding of a species to the gold surface. Deformation may occur when the material is absorbing, i.e. its refractive index has an imaginary component, as is the case for poly-pyrrole. Examples of plasmon curves

for unmodified gold, poly-pyrrole spots (5 nm) and DNA surface hybridization in buffer can be seen in figure 3.2.

The angular shift is explored for surface adsorption measurement systems and different techniques can be cited:

- Angular detection: using a LASER or the collimated light of a LED at one given wave-length, the angle of incidence is varied, permitting thus to trace the plasmon curve in proximity of the resonance. Signal read-out is achieved by a photo diode. Biological interactions are seen as an angular shift that can then be related to mass variation.
- Spectral detection: at a fixed incidence angle, the plasmon curve is traced in dependence of the wave length of the incident light by a spectrometer. Accordingly, biomolecular fixation on the surface leads to a shift of the curve.
- Surface plasmon resonance imaging: the incidence angle as well as the wave length of the incoming light is fixed. Variations of the reflectivity are then followed by a CCD camera. It is necessary to carefully chose the angle in order to be placed at the maximum slope of the plasmon curve where angular shifts result in a maximum variation of reflectivity [62, 63].
- Surface plasmon diffraction: this method uses grated surfaces to diffract the light and to enhance the surface plasmon signal. Once again the system is mounted in the Kretschmann configuration and the analyzed signal is the reflectivity at a fixed angle of incidence [64, 65, 66].
- SPR has been used to enhance other methods by coupling for example SPR to microscopy and a fluorescence detection [67, 68]. Also, SPR on grated surfaces has recently be coupled to electrochemical reaction detection (ESPR) [64]. Others used SPR signals on waveguides immersed in the analyte solution [69].

In this work, the method of surface plasmon resonance imaging has been applied to a multi-component biochip for the detection of immobilized DNA on gold coated prisms. The results are thus represented in terms of reflectivity changes in % that can be related to angular shifts knowing the plasmon curve of each observed spot.

3.1.4 Description of the experimental setup

All SPRi experiments are carried out on a flexible, home-made SPRi system with integrated temperature regulation. The system has been set up by Jean-Bernard Fiche and is characterized in detail in his Ph.D. thesis [13]. Figure 3.3 shows a scheme of the device. Exploiting surface plasmon excitation in the Kretschmann configuration, a gold coated prism is mounted in the optical detection system. The prism holder and flow cell is mounted on a rotation stage with goniometer and a flexible x-z-system to enable the user to change the prism's position as well as the angle of light source and camera with respect to the prism's horizontal plane. The incident light wave at 635 nm is delivered by a light emitting diode (LED). The diode is placed behind a pinhole. To get a well defined light source, transparent scotch is used to diffuse the light. A first optical lens parallelizes the light beam which is polarized before falling on the prism under total internal reflection conditions. The reflected light is focused by a second lens and imaged by a CCD camera (PixelFly VGA, PCO.Company, Kelheim, Germany, then replaced by Dolphin F-145B, Allied Vision Technologies (AVT), Stadtroda, Germany). For more detailed information on optimization of the optical system, the reader may be referred to the Ph.D. thesis of E. Maillart [61]. The prism is inserted in a holder and pressed against a temperature controlled flow cell of about 1 cm diameter and 5 µm volume, where the height is fixed by an aluminum ring placed around the o-ring. The flow cell depicted in figure 3.4 is made of stainless steel, in which in- and outlet of the flow system are screwed. On the metal, a heating resistance with maximum power of 12 W and a negative temperature coefficient (NTC) thermo-resistance are fixed. Both are inserted in isolating material to prevent heat loss. The whole SPRi installation is placed in a temperature

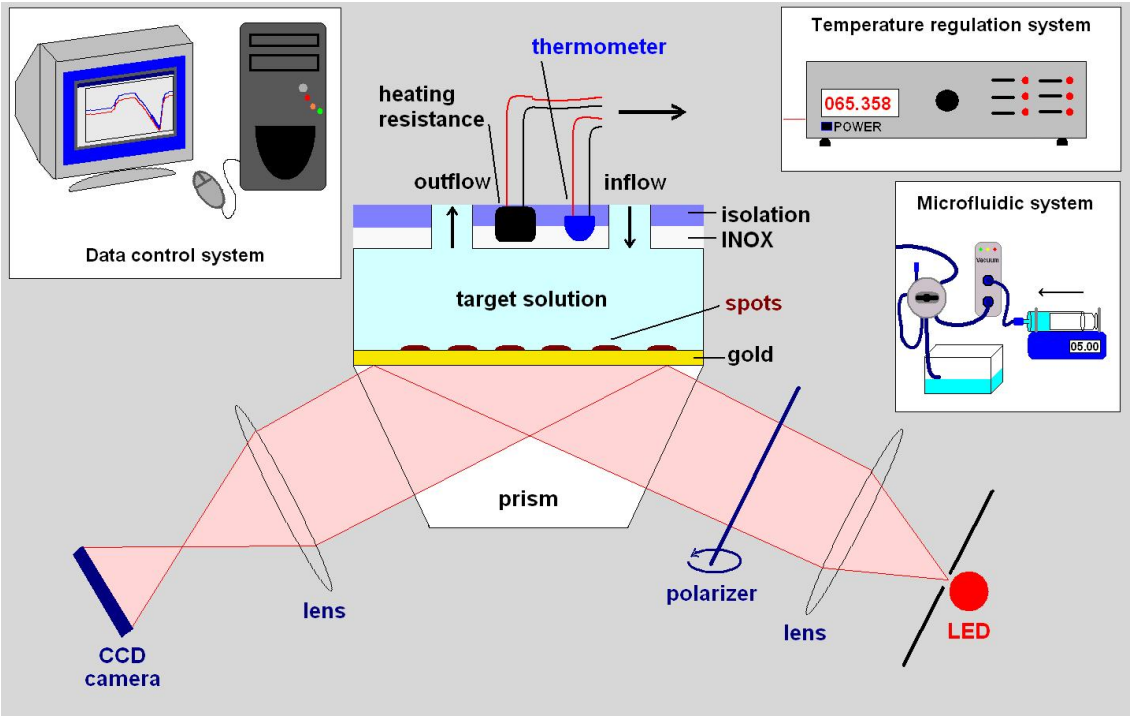

Figure 3.3: Setup for surface plasmon resonance imaging studies. The SPRi is connected to a fluidic device with a computer controlled syringe pump and a manual injection valve. A temperature regulation system is mounted on the flow cell. The temperature is applied by a heating resistance and read out by a spatially isolated NTC thermoresistance. The feedback loop is controlled by a regulator via a LabView interface. The reflectivity is monitored by the CCD camera using a LabView interface based on a program by GenOptics.

controlled incubator and the fluidic system is connected from the exterior to the flow cell on the prism. The flow is regulated by a syringe pump (Cavro XLP 6000, TECAN, Cavro scientific instruments, Sunnyvale, CA, USA) transporting the running buffer first through a degasser (Alltech Elite Degassing System, Deerfield, Illinois, USA), then through an injection valve before entering the incubator. The injection valve is a 6-way valve that permits to inject samples of volumes of about 500 µl to 1 ml into the system, depending on the injection loop connected. For injection of smaller volumes (∼20-100 µl), a three way valve is used, that is connected directly to peek tubing accepting introduction of a Hamilton syringe. The sample can then be injected directly from the syringe with only some microliters of dead volume.

Data acquisition and image processing is done by SPRi software from GenOptics (Spirit_V1.1.2 program for Pixelfly camera and adapted version of SPRi-ViewIt for AVT Dolphin camera). It permits the regulation of the acquisition time, the area of interest of the image and the definition of masks in order to obtain the reflectivity of the spots. The system automatically normalizes the reflectivity to the luminosity observed in TE mode and subtracts background noise from a reference image acquired while covering the light source. In this way, we obtain reflectivity curves for each spot inside the defined mask. The acquisition frequency is normally around 0.5 Hz with averaging over five images, so that one data point is taken every two seconds. A useful tool is the differential image that permits to follow changes by subtracting a reference image to the currently acquired one. In this way, local reflectivity changes can be followed and saved in image files permitting a rapid visibility of local reflectivity changes on the prism.

The integrated temperature regulation device permits rapid heating and direct measurement of the temperature on the prism. The temperature control is performed by a PID regulation system (ITC temperature controller, OXFORD instruments) with a stability of 0.05°C. A LabView (National Instruments, USA) home-made program assures the temperature regulation either at constant temperature or linear temperature scans at different rates up to 87°C given that the proportional and integral parameters of the feedback loop are carefully set. The thermometer is calibrated and has a very good precision. The solution entering the flow cell on the prism is heated during its passage through narrow channels in the steel heating cell, which itself is surrounded by the incubator's temperature. Therefore, the temperature on the prism can depend on the flow rate applied to the solution and, especially during controlled cooling, on the surrounding temperature. Measurements by SPRi at different temperatures up to 80°C show an increasing difference of the temperature sensed on the prism for a flow rate of 0 and 5 ml/h (Figure 3.4). For the highest temperature applied, the temperature on the prism may differ by about 1°C from the measured temperature, limiting the precision of the temperature measurements. Since this effect is flow rate dependent, and thus dependent on the conditions of each experiment, no systematic correction of the following temperature scan experiments has been applied. The measurement of the temperature for independent T-scans performed with defined feedback parameters have been controlled and show a very good reproducibility over the period of this Ph.D. thesis. The systematic error ΔT due to the flow rate and the temperature of the incubator is thus the same for each experiment with identical parameters. For scan rates of 2-5°C/min and hybridization temperatures of 25°C, the incubator is set to 20°C. Only for measurements needing fast cooling at 8 and 12°C/min, the incubator was set to 15°C or 10°C, respectively.

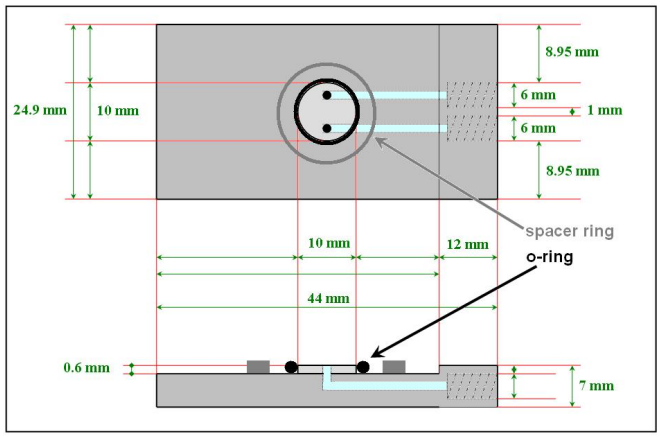

a)

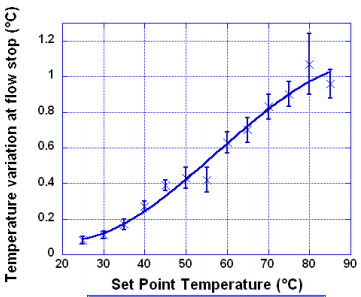

Y = M0 + M1*x + ... M8*x^8 + M9*x^9	
M0	0.3638
M1	-0.029579
M2	0.00086568
M3	-5.0117e-06
R	0.98902

b)

Figure 3.4: a) Representation of the flow cell geometry of the metallic part with fluidic connections. b) Systematic error of temperature measurement during flow rate changes from 5 ml/h to 0 ml/h at different set point temperatures measured by the SPRi reflectivity change.

3.2 Quartz Crystal Microbalance

Quartz crystal microbalance is a surface sensing technique that is based on the piezoelectric effect of quartz crystals. Deformation of the crystal produces an electric signal, and, the other way round, an applied electric signal induces a mechanical response in the crystal. These properties are exploited in resonance measuring systems where thin quartz disks are sandwiched between two electrodes. The quartz crystal is excited at its resonance frequency by an alternative current (AC) applied to the electrodes. Common devices use the thickness shear mode of oscillation with AT-cut quartz crystals (cut at 35°10′ of the crystal's z-axis) that are stable at room temperature. Most systems work in a frequency range of 5-20 MHz [70]. For biological applications, mostly gold coated quartz crystals are employed because of the inertia to liquid systems and the variety of surface functionalization methods available. The acoustic shear wave produced by the oscillation of the crystal is evanescent and the exponential decay limits the penetration depth to about 250 nm [71]. Therefore, QCM is a surface sensitive detection method, like surface plasmon resonance. In 1959, Sauerbrey established a linear dependence between the resonance frequency of the quartz crystal and the mass bound to its surface. The Sauerbrey relation is valid for rigid films [72]:

$$\Delta m = \frac{A\sqrt{\rho_q \mu_q}}{2nf_0^2} = -\frac{C\Delta f_0^2}{n} \tag{3.7}$$

where A is the surface area between the electrodes, ρ_q is the quartz crystal's density, μ_q is its shear modulus, f_0^2 is the fundamental frequency and n is the corresponding number of the overtone n=1, 3, 5,.... $C = 17.7\,\mathrm{ng\,Hz^{-1}\,cm^{-2}}$ for 5 MHz quartz crystals [73]. Biological films are often 'soft' films, containing a lot of water which gives a high viscoelasticity to the bound mass. In this case, the Sauerbrey relation breaks down and more complex models are needed. The soft films lead to damping of the acoustic wave which can be monitored as dissipation. The quartz crystal is excited at its resonance frequency, then the external drive is stopped and the free oscillation is recorded. From the decay of the oscillation amplitude, the dissipation can be obtained and is defined as:

$$D = \frac{E_{lost}}{2\pi E_{stored}} \tag{3.8}$$

with E_{lost}, the lost energy due to dissipation and E_{stored}, the total energy of the oscillator. The technology of QCM with dissipation monitoring (QCM-D) is patented and commercialized by Q-Sense [73]. Additional to the fundamental frequency, several overtones can be monitored. The data can then be fitted to the Voight-Model, giving access to the viscoelastic properties of the adsorbed layer [74]. Among the four parameters - film thickness, viscosity, elasticity and density - one parameter needs to be estimated before the other parameters can be extracted from fits. In the case of low dissipation, i.e., rigid films, the Voight-model yields the same result as the Sauerbrey relation for adsorbed mass [75]. Note that QCM-D measurements have a sensing depth between 250 nm (in water) and ∼1 µm. The signal is sensitive to buffer changes altering the viscoelastic response.

During a 2-month stay at the biomat'X lab of Prof. Maryam Tabrizian at the McGill University, Montreal, Canada, I had the opportunity to use the QCM-D technique on a Q-Sense D300 by Q-sense for surface analysis studies. The quartz crystals used are gold coated QSX3001-standard gold with an active area of 1.4 cm diameter. The system accepts one sensor covered by a volume of 80 µl. The minimum exchange volume is 0.8 ml, but samples of 2 ml volume are preferable for optimal exchange. The QCM-D system is temperature regulated at ±0.02°C and can be used at temperatures between 18 and 45°C. Data acquisition can be done at over 15 data points per second with a typical mass sensitivity in liquid of $3.5\,\mathrm{ng/cm^2}$ (0.2 Hz). The typical detectable dissipation change is 0.1×10^{-6} in liquid. The sensor is connected to a sample reservoir (5 ml pipette tip) and a peristaltic pump that allows injecting samples on the chip. A sampling frequency of 4 MHz is used in the experiments. The experimental setup is represented schematically in figure 3.5.

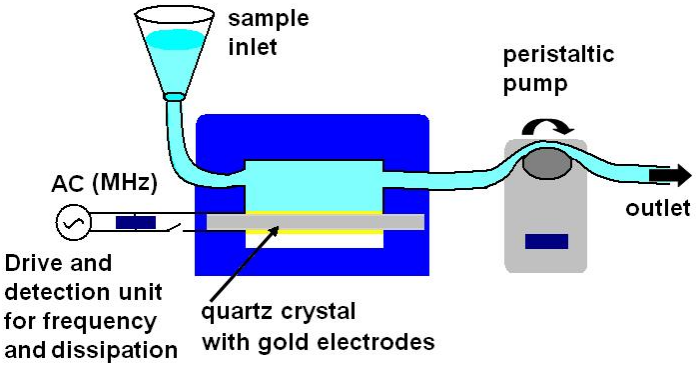

Figure 3.5: Schematic representation of the QCM-D device.

3.3 Fluorescence microscopy

Fluorescence microscopy is a very sensitive and commonly used method for the detection of biological interactions. While methods like SPR and QCM are so-called label-free methods, fluorescence microscopy relies on fluorophore labeling of the target itself or another biomolecule interacting with the targets, antibodies, for example. The principle of fluorescence microscopy is based on the excitation of molecules at their absorption wave length and the collection of the light emitted by the molecules at a second, different wave length ($\lambda_{excitation} < \lambda_{fluorescence}$). This is depicted in figure 3.6, showing a simplified Jablonski diagram and the corresponding absorption and emission spectrum. For DNA applications, there are a variety of fluorescent markers and methods available:

1. DNA intercalating agents: fluorophores that interact with the minor or major groove of the DNA duplex and therefore reveal specifically the formation of the double helix. Typical applications: gel electrophoresis

2. Molecular beacons: single stranded DNA forming a hairpin with a G/C rich stem of 5-8 base pairs and a loop with a specific, target complementary sequence of 15-30 bases. The ends of the DNA strand are tagged by a fluorophore and a quencher, so that, when the hairpin is closed, fluorescence is quenched due to the proximity of the quencher (7-10 nm). Fluorescence can be detected once the beacon hybridizes to its targets, thereby opening up the hairpin stem and emitting a fluorescence signal. Typical applications: Real-time NASBA, real-time PCR, hairpin probe labeled microarrays,... (recently reviewed by [76])

3. Chemical modification of the DNA target to allow the attachment of one fluorophore. The fluorophore can either be attached to the DNA before interaction is carried out or coupled after the binding event took place. Common strategies use biotin modified DNA that permits attachment of markers using the biotin-(strept)avidin interaction. Others attach the fluorophore covalently to the DNA target before carrying out biological interactions. Applications: DNA microarrays, gel pads, ...

The choice of the fluorescent dye is important and depends on the application and the experimental conditions. Parameters like the quantum yield, the size of the fluorophore, its tolerance towards photobleaching and quenching, for example will influence the essay conditions. The quantum yield defines the number of photons emitted compared to the number of photons absorbed and is often very poor for small organic compounds. Quantum dots have a very good quantum yield, but those huge metallic moieties alter the diffusion of the small DNA molecule and can therefore change interactions. Typical fluorescent proteins like the green fluorescent protein (GFP) and R-phycoerythrin are in the size range of 10-20 nm and thus are also big compared to ODN. Small dye molecules are available that are about 1 nm in size, but their emission is often lower. Another important factor is photobleaching, the light induced, irreversible destruction of

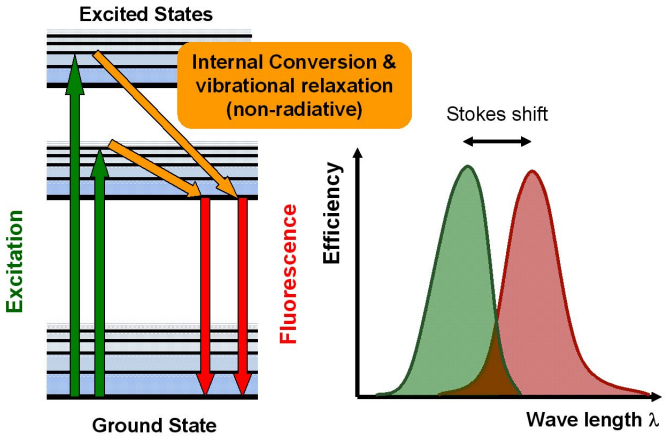

Figure 3.6: The principle of fluorescence: simplified Jablonski diagram and absorption/emission spectrum.

the fluorescent part of the fluorophore. Exposure times should be adapted to the fluorophore in use and for long observations, the fluorescent signal detected is likely to decrease over time. Other important factors for the choice of the fluorophores can be the temperature dependence of the light emission [77], compatibility with buffer conditions (pH, polarity, viscosity), pressure, quenchers [78], electrostatic potential, etc.

A standardized protocol for DNA hybridization and observation by fluorescence microscopy is used at our laboratory. It is based on the third strategy, using biotinylated DNA targets that are hybridized to immobilized DNA probes. After washing off unhybridized target molecules with a rinsing buffer, incubation with a streptavidin-phycoerythrin (SAPE) molecule allows attachment of the fluorophore to the hybridized targets. Another rinsing process eliminates the surplus of fluorophores before observation of the fluorescence signal using a Zeiss Epi-fluorescence microscope with a mercury arc lamp, the adequate excitation/fluorescence filter and a CCD camera. The detailed experimental protocol can be found in appendix 8.

R-Phycoerythrin has excitation peaks at 496 nm, 546 nm and 565 nm and emits in the orange-red at 578 nm, where biological background fluorescence is low. Fluorescence microscopy of phycoerythrin has the advantage of a high quantum yield (∼0.8) and a high absorption coefficient ($2.4 \times 10^6\,\mathrm{M}^{-1}\,\mathrm{cm}^{-1}$) leading to high brilliance [79]. Phycoerythrin is thermally stable up to ∼60°C. Fluorescence detection under these conditions presents a 1000 fold enhanced sensitivity compared to SPR imaging [80]. However, the protocol employed makes the technique an end-point detection method where no binding and dissociation event can be followed and the temperature is not controlled. Today, a variety of fluorescence technologies are put forward that allow not only high resolution for in-situ measurements of fluorescence in cells, but also real-time acquisition and temperature regulated observation. As it is the case in many technologies, many optimization steps have to be taken to adapt labeling with adequate fluorophores, photobleaching effects, image acquisition rates and resolution. There are still only limited applications in multiplexing since only a small selection of compatible fluorophores is available that absorb at approximately the same wave length while emitting distinguishable different colors.

3.4 DNA synthesis and sequences

Today, DNA is easily accessible for research because of its well known phosphoramidite chemistry. Since DNA sequences are easily synthesized and modified, the wide application of DNA for microarrays and biosensors is not astonishing. For this work, probes and oligonucleotides have been produced that correspond to the sequence of the SNP A870G codon 242 exon 4 of the protein

Cyclin D1. Cyclin D1 is a *proto-oncogene* that intervenes in the cell cycle and mutations in this gene are known to be involved in tumorigenesis [81, 82, 83]. DNA from patients of genotypes A/A and G/G (homozygous) and A/G (heterozygous) is amplified in order to find the mutation at position 147 of the 167 bases in the PCR sequence. In the probes, this mutation is placed in the center in order to decrease the stability of the mismatched duplex to a greater extent [84]. The discrimination of the targets is done by the denaturation temperature of the duplex formed on spots carrying probes complementary to each possible target sequence (see section 4.2.1). To facilitate the discrimination of the genotype, other probes presenting the additional mutation C/T one and two bases next to the analyzed position are designed [85]. These additional mutations decrease the melting temperature even further as loop formation occurs [15, 85]. Complementary oligonucleotides have two additional bases at each end (dangling ends) in order to increase their mass and, therefore, the SPR hybridization signal. All complementary oligonucleotides were purchased at Eurogentech, Angers, France. The DNA sequences used in this work are given in table 3.1.

The synthesis of the poly-pyrrole modified probes is carried out in our laboratory. The device EXPEDITE - nucleic acid synthesis systems - by 'Applied Biosystems' synthesizes DNA in the 3'→5' direction. During each cycle, one phosphoramidite (DNA base with modified phosphor function on the backbone, see figure 3.7) is incorporated. The first base is fixed on a solid support in columns that have been purchased. The bases have special protections that prevent involuntary reactions of the amine functions of the bases. A spacer of 10 thymine bases follows the sequence before the cytosine base carrying a pyrrole molecule is fixed. The pyrrole modified phosphoramidite is synthesized at our lab [86]. This last synthesis cycle has an extended coupling time of 15 min since the pyrrole coupled cytosine is more difficult to incorporate. The efficiency per cycle normally lies at 98%, but may decrease since reactive components become less efficient within two weeks.

The last detrithylation step (deprotection from DMT, see figure 3.7) is already performed by the synthesizing device, the bases still need to be cleaved from the solid support and to be deprotected entirely. This is done simultaneously by incubation in 1 ml of a 30% ammonia solution. After evaporation of the liquid under vacuum (SAVANT SpeedVac Concentrator), biologically functional sequences are obtained, still mixed with shorter sequences and all other molecules remaining from the synthesis. The purification of the pyrrole modified oligonucleotides is carried out using High Performance Liquid Chromatography (H.P.L.C.). The principle of selection is based on the more or less polar character of the molecules present in the solution. The oligonucleotides pass a so-called C-18 column filled with micro-spheres functionalized by specific molecules. The analyte entering the column will attach with more or less affinity to the spheres. Then, the solvent that continuously passes the column is gradually varied from being more to less polar. This is done by a mixture of solvent A consisting of 90% triethylamine acetic acid (TEA AA) at 25 mM and pH 7 and 5% acetonitrile and solvent B consisting of 50% TEA AA at 25 mM and pH 7 and 50% acetonitrile. Depending on their interactions with the column and the solvent, the retained molecules are eluted at a certain percentage and driven out of the column. Thereby, the most polar molecules are the last to leave the column. They pass a detector determining the absorbance at one wave length chosen in the UV / visible light. In our case, we observe the DNA absorption at 260 nm, the maximum of the absorption peak. The oligonucleotides carrying the pyrrole are the most retarded ones. Time-dependent collection at the outlet permits to get purified probes.

The desiccated oligonucleotides are later dissolved in 1 ml distilled water for quantification by UV spectroscopy (UVIKON XS, BIO-TEK instruments, or ND 1000 Spectrophotometer, NanoDrop® technologies, Wilmington, USA). For the Uvikon CS, small quantities are diluted and analyzed by a wavelength scan from 220 to 300 nm to obtain results in the linear range of absorption (0.2-1.2 OD). The NanoDrop uses 1.5 μl of analyte and has an extremely wide linear range due to measurements at two different light path lengths. In most cases, the sample does not need dilution before quantification. Both UV spectrometers have been compared and present no significant difference. The maximum value of the peak at $\sim$ 260 nm is taken for calculation of the solution's concentration. Additionally, a small amount of the solution is double-checked on H.P.L.C.. The spectra show one single peak, proving purity of the probes. Solutions used

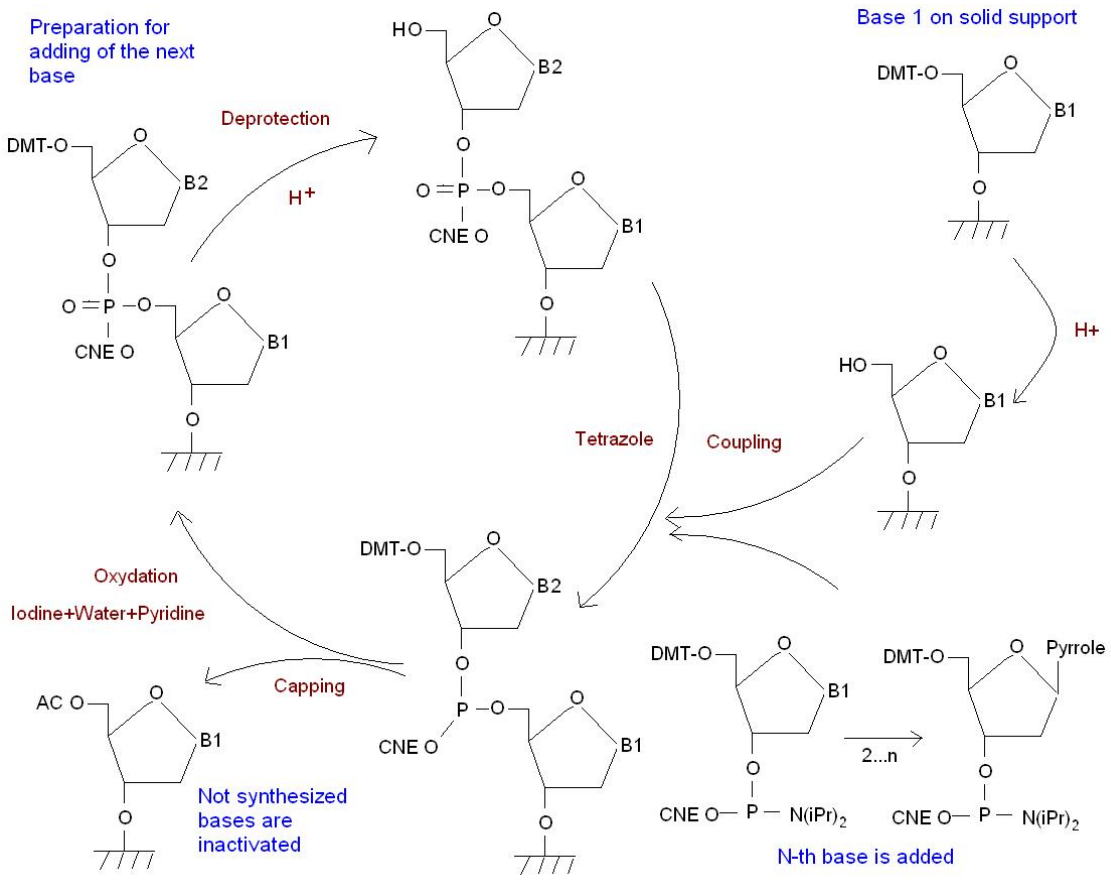

Figure 3.7: Oligonucleotide production: scheme of the DNA synthesis cycle performed for each base incorporated. The process proceeds in the direction 3'→5'. at the 5' end, a spacer chain of 10 thymines is added to the sequence. The last base on the 5' end is a cytosine modified by a pyrrole.

for measurements are thrown away in order to keep the original solution as clean and uniform as possible.

To calculate the concentration of the sample, the law of Beer-Lambert $A = \alpha\, l\, c$ is used, where A is the absorption, α is the absorption coefficient in l cm^{-1} mol^{-1}, $l = 1$ cm is the length of the quartz cuvette and c is the concentration of DNA in M. For short oligonucleotides, α can be estimated to be 10,000 per base. The prediction of the Proligo web site [87] is here adopted. To take into account the absorption of pyrrole, an adenine instead of the modified cytosine is used since it has one additional cycle and thus takes into account the absorption of the pyrrole monomer. Calculations showed that the total efficiency of the synthesis and the purification lay between 14% and 29%.

Thiol modified probes and all ODN targets are purchased from Eurogentech, France. The quality control at Eurogentech relies on mass spectrometry. At our laboratory, oligonucleotides from Eurogentech are controlled by H.P.L.C. and quantified by UV spectroscopy at 260 nm as described above. The H.P.L.C. spectrum shows no or negligible pollution as the relevant DNA peak presents always more than 92% of the total area and other eventual peaks are well separated in time and thus due to other components than DNA. The targets and probes are stocked frozen in distilled water until use.

Name	Sequence 5'→3'	Abbreviation
POLY-PYRROLE PROBES		
ASO-CCND1s-A-16	pyrrole-T_{10}-TGT GAC CC**A** GTA AGT G	A16
ASO-CCND1s-A-20	pyrrole-T_{10}-AGT GTG ACC C**A**G TAA GTG AG	A20
ASO-CCND1s-A-24	pyrrole-T_{10}-CAA GTG TGA CCC **A**GT AAG TGA GGG	A24
ASO-CCND1s-G-16	pyrrole-T_{10}-TGT GAC CC**G** GTA AGT G	G16
ASO-CCND1s-G-20	pyrrole-T_{10}-AGT GTG ACC C**A**G TAA GTG AG	G20
ASO-CCND1s-G-24	pyrrole-T_{10}-CAA GTG TGA CCC **G**GT AAG TGA GGG	G24
ASO-CCND1s-TA-16	pyrrole-T_{10}-TGT GAC CT**A** GTA AGT G	TA16
ASO-CCND1s-TcA-16	pyrrole-T_{10}-TGT GAC TC**A** GTA AGT G	TcA16
ASO-CCND1s-TG-16	pyrrole-T_{10}-TGT GAC CT**G** GTA AGT G	TG16
ASO-CCND1s-TcG-16	pyrrole-T_{10}-TGT GAC TC**G** GTA AGT G	TcG16
3'-PCR-T10	pyrrole-T_{10}-ATT GGA AAT GAA CTT CAC	3'-T10
3'-PCR-T20	pyrrole-T_{20}-ATT GGA AAT GAA CTT CAC	3'-T20
M3-15	pyrrole-T_{10}-TGG AGC TTG TGG CGT	M3
M4-15	pyrrole-T_{10}-TGG AGC TGA TGG CGT	M4
M5-15	pyrrole-T_{10}-TGG AGC TGC TGG CGT	M5
THIOL PROBES		
ASO-CCND1-A-thiol	$SH(C)_6$-T_{10}-TGT GAC CC**A** GTA AGT G	A16-thiol
ASO-CCND1-G-thiol	$SH(C)_6$-T_{10}-TGT GAC CC**G** GTA AGT G	G16-thiol
ASO-CCND1-TA-thiol	$SH(C)_6$-T_{10}-TGT GAC CT**A** GTA AGT G	TA16-thiol
ASO-CCND1-TG-thiol	$SH(C)_6$-T_{10}-TGT GAC CT**G** GTA AGT G	TG16-thiol
Zip7-thiol	$SH(C)_6$-T_{10}-TGC GAT CGC AGC GGT AAC CTG ACC	Zip7-thiol
Zip9-thiol	$SH(C)_6$-T_{10}-GAC CAT CGT GCG GGT AGG TAG ACC	Zip9-thiol
TARGETS		
ASO-CCND1c-Ac-20	CTC ACT TAC **T**GG GTC ACA CT	Ac20
ASO-CCND1c-Gc-20	CTC ACT TAC **C**GG GTC ACA CT	Gc20
ASO-CCND1c-Ac-26	Biotin-CAC CCT CAC TTA C**T**G GGT CAC ACT TG	Ac26
ASO-CCND1c-Gc-26	Biotin-CAC CCT CAC TTA C**C**G GGT CAC ACT TG	Gc26
M3c	ACG CCA CAA GCT CCA	M3c
M4c	ACG CCA TCA GCT CCA	M4c
M5c	(Biotin-)ACG CCA GCA GCT CCA	M5c or M5c-bio
ASO-CCND1t-Poly-T-solution	T_{56}-CCC TCA CTT AC**C** GGG TCA CAC TTG	PolyT-sol
ASO-CCND1t-Poly-T-surface	CCC TCA CTT AC**C** GGG TCA CAC TTG-T_{56}	PolyT-surf
ASO-CCND1t-PCR80	CCC TCA CTT ACC GGG TCA CAC TTG ATC ACT CTG GAG AGG AAG CGT GTG AGG CGG TAG TAG GAC AGG AAG TTG TTG GGG CT	PCR-80
ASO PCR amplified	3'-CAC TTC AAG TAA AGG TTA GGC GGG AGG TAC CAC CGT CGC CCC TCG CAC CAC CGG CGT CAC GTT CCG GAC TTG GAC TCC TCG GGG TTG TTG AAG GAC AGG ATG ATG GCG GAG TGT GCG AAG GAG AGG TCT CAC TAG TTC ACA CTG GG**C/T** CA TTC ACT CCC ACT ACA GGG -biotin-5'	PCR A/A, G/G or A/G
PCR PRIMERS AND HELPER ODN		
CCND1-forP-phosphorylated	phosphate-GTG AAG TTC ATT TCC AAT CCG C	primer-phos
CCND1-revP-biotinylated	biotin-GGG ACA TCA CCC TCA CTT AC	primer-bio
Helper oligonucleotide ASO-CCND1-20	biotin-CGC CTC ACA CGC TTC CTC TC	helper ODN

Table 3.1: Sequences of probe and target DNA used in this study. Probes are either modified by a pyrrole moiety to enable spotting by electro-polymerization or by a thiol function allowing self-assembling. Some targets bear a biotin at the 5' end for amplification using streptavidin. The PCR primers for forward and reverse strand are phosphorylated and biotinylated, respectively. The helper oligonucleotide designed for hybridization to the PCR strand is biotinylated.

3.5 DNA surface immobilization methods

As we have seen in the theoretical background of SPR in section 3.1, surface polaritons occur at the interface of a metal and a dielectric when light is shone through a material of high refractive index under the angle of total reflection. The DNA chips are hence prepared on glass prisms that are coated by a 50 nm gold layer. To assure better adhesion of the gold to the glass, a thin layer of 2 nm chromium is deposited between glass and gold. The prisms are purchased from Genoptics, Orsay, France and measure typically 1.25 x 2.4 cm on the top surface and exhibit an angle of 60°. Specifications on the thickness of the layers and their respective refractive indexes are given in table 3.2. Hereafter, two different immobilization strategies of DNA probes on a gold layer will be presented. The first one, electro-copolymerization of pyrrole modified DNA has been developed and employed at the CREAB for over 10 years. The second strategy, self-assembling of thiol modified DNA on gold layers is a common technique and has been optimized during this work for SPRi applications with multiple probes spotted onto one sensor.

3.5.1 Electro-copolymerization of poly-pyrrole

At our laboratory, DNA is immobilized by an electrochemical copolymerization process of pyrrole [86, 91]. Two different buffers are currently used as basic solutions of the reactive medium. Buffer 1, called FDZ, containing NaH_2PO_4, NaCl, glycerol, NaOH and water, is very stable when frozen and gives very reproducible results. Buffer 2, called GDALi, containing acetonitrile, dimethyl sulfoxide (DMSO), glycerol, lithium perchlorid and water has been empirically adapted and yields a better signal for DNA hybridization. However, the solution is not very stable with the acetonitrile being very volatile and no pH buffering done. It is thus preferable to prepare the solution directly before spotting. The spotting buffer is subject to on-going optimization, in this work the GDALi buffer has been used with slightly varying salt concentrations (0.1 M-0.15 M). The reactive medium is composed of buffer, pyrrole at 20 mM and pyrrole-modified DNA at typically 1 to 10 µM, for example, for oligonucleotides. So we have a ratio of DNA modified pyrrole monomers to pyrrole monomers of 1:2000 to 1:20 000.

To allow for confined spotting zones, the surface is rendered hydrophobic by immersing the prism for 10 min in an ethanol solution containing 2.5 mM of 1-Dodecanethiol ($CH_3(CH_2)_{11}SH$ - Sigma-Aldrich, France). Thiols are known to form spontaneously self-assembling monolayers on gold surfaces [92, 93, 94, 95, 96]. Dodecanethiol has a hydrophobic end group (CH_3), rendering the surface of the prism globally hydrophobic. After formation of the (unordered) layer, surplus thiols are eliminated by rinsing with ethanol. Note that the prisms are only thiolated when used with the pipette tip spotter Polypotter (see hereafter) and not with X-tend needles on the automatic spotter.

Our laboratory disposes of two different types of spotters. Polypotter (home-made, see figure 3.9) is a controlled device able to move in the three directions of space guiding a micropipette. It places the pipette tip on the prism, aligning the spots in a user defined matrix. Usually spots are spaced by 0.8 mm and the spotting area is chosen to fit into the fluid cell of the SPRi. Electro-

Specifications about the prism		
material	**layer thickness**	**refractive index**
glass	-	1.776
chromium	2 nm	$3.09+i3.34$
gold	52 nm	$0.14+i3.7$
poly-pyrrole [88]	1-12 nm	$1.7-i0.3$
DNA	variable, 5-10 nm	$\Delta n/\Delta c = 0.14 - 0.16\,\mathrm{cm}^3/\mathrm{g}$ [89, 90]

Table 3.2: Specifications on the SPRi prism and the refractive index of the different layers at a wave length of λ=660 nm. Information obtained from GenOptics.

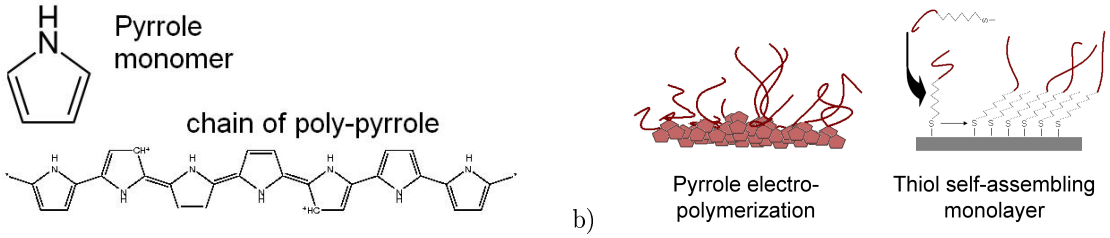

Figure 3.8: a) Chemical structure of a pyrrole monomer and poly-pyrrole. b) Morphology of pyrrole and thiol immobilized DNA.

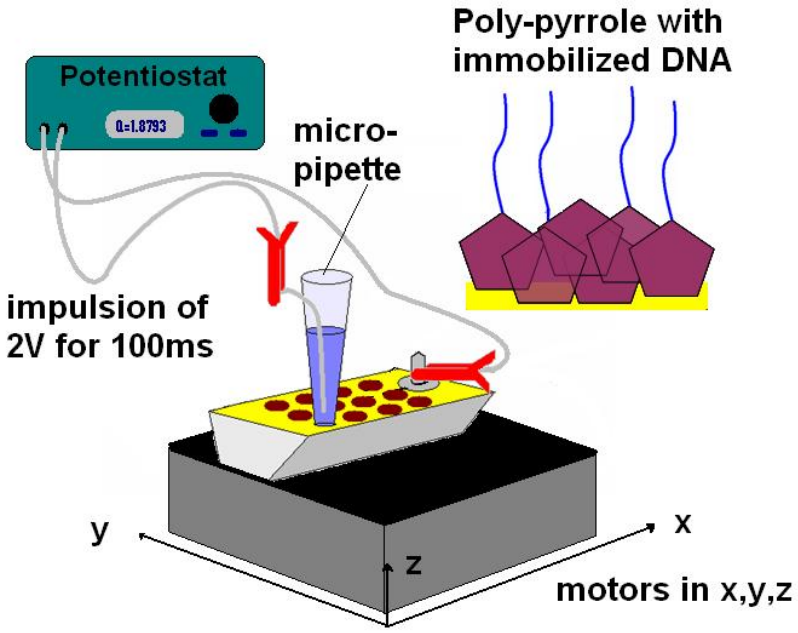

Figure 3.9: Schematic representation of the electro-spotting setup.

chemistry is done using a two electrode system, where the reference electrode is connected to the counter electrode. We therefore do not control the absolute potential in the cell, only the difference of the potential between working electrode and counter electrode. A platinum wire of 125 µm diameter introduced inside the pipette tip and the gold surface on the prism serve as counter electrode and working electrode, respectively. Using a potentiostat device (Potentiostat/Galvanostat Model 263, Princeton Applied Research®, Tennessee, USA) an electrical impulsion of 2 V is applied to the cell for 100 ms and leads to polymerization of the pyrrole molecules [97]. The charge is transported by the salt in the reactive medium loaded in the pipette tip and serves as indicator of the thickness of the deposited poly-pyrrole film. For DNA application, charges between $-1.2\,\mu C$ and $-1.8\,\mu C$ show empirically the best SPRi hybridization signal. The procedure needs an operator who manually charges the tip with the spotting solutions and controls the electrochemical process. The spots have a diameter of about 400 µm and a thickness of $\sim 5\,nm$. The probe density has been determined to be $10\,pmol/cm^2$ on thick pyrrole layers using 40 µM DNA [80]. We can not suppose that the grafting is directly proportional to the ratio of pyrrole monomers to DNA since the diffusion of the two species is significantly different. However, changing the DNA concentration leads to a variation of the grafting density. We estimate the grafting density to be around 1-5 $pmol/cm^2$.
Contrarily, the OmniGrid spotter by Genoptics, Orsay, France, is fully operated by a PC interface. The electro-spotting interface Labjack was integrated at the laboratory and is controlled by a Lab-

view interface. The robot uses a needle instead of the pipette and spotting solutions are taken up by capillarity. Spots can be precisely placed and have - in ideal cases - a diameter of 260 µm, the inner diameter of the Teflon covered needle. The electro-chemistry is usually set to 2 V for 100 ms, identically to Polypotter conditions. With the robot, spots of about 1 nm height are polymerized as determined by Atomic Force Microscopy (AFM) and Scanning Electron Microscopy (SEM) by E. Descamps at SPrAM.

Both deposition methods have advantages and disadvantages. In general it is preferable to deposit a very fine poly-pyrrole layer, since the plasmon curve is broadened when the layer increases. This increase leads to a reduced dynamic range of the biosensor [88]. On the other hand, the deposit of a thicker layer results in immobilization of more DNA strands that are able to hybridize and thus yield a higher mass and refractive index change in SPRi. The deposit of DNA in a polymer layer may introduce a probe length dispersion, since parts of the DNA strands may be hidden by the matrix and rendered inaccessible. Thus, the spotting with the Omnigrid robot may be a good approach once the DNA spotting conditions are optimized. However, when the pyrrole film is too thin, clear observation by SPRi before hybridization may be difficult since the contrast between the pyrrole layer and the bare gold surface is poor. It is absolutely necessary to distinguish the spots clearly in order to define SPRi masks for image analysis and signal averaging of each spot.

All chips are designed to present internal controls. A *positive control* DNA sequence differing from the target's sequence is spotted: it should not react to the actual target, since the two sequences are not complementary. When its complementary strand is injected, these spots give a specific signal. Additionally, every prism has some spots of poly-pyrrole without DNA. They are used as *negative control* since they should not respond to any DNA sequence injected. For all experiments, every sequence is deposited in multiplets to control reproducibility (3-6 spots per sequence).

The biochips can be used for several experiments over about 2-3 months when stocked thoroughly desiccated under argon atmosphere at +4°C. During storage over about 4 months, they may loose up to 50% of their signal. The poly-pyrrole can be regenerated from the gold surface by immersion in commercial bleach at a 10% dilution. The prism should be cleaned by a *piranha solution*, 70% sulfuric acid (H_2SO_4) and 30% hydrogen peroxide (H_2O_2) and immerged in dodecanethiol before second employment. *ATTENTION: Piranha solution is highly corrosive and should be handled with adapted, acid resistant security clothes and mask.*

3.5.2 Thiol self-assembling monolayers

A second DNA grafting method characterized and used in this work is the self-assembling of thiolated DNA on gold surfaces. Thiols have been known for some time and are today well characterized. A detailed review on this topic has been published by the group of Whitesides in 2005 [92]. Especially the self-assembling of alcanethiols on gold has been studied. Thiol self-assembling takes place spontaneously on clean gold surfaces when immersed in a solution containing the thiol of interest. While *physisorption* of thiols on gold takes place in a few minutes, the monolayer formation due to reorganisation of *thiolates* is a very slow process taking several hours, especially when the layer should be stable and free of defects. The final monolayer is not covalently bound, but thiols are chemisorbed. The concrete structure and thickness of the monolayer will depend on the length of the chains, the interaction time, the head group, etc.. The thiol-gold interaction is not covalent, but relies upon *chemisorption* of the thiol moiety SH to the clean gold surface. The stability of the monolayer will thus depend on the experimental conditions like pH [98], temperature [99, 100], electric potential [101], etc.. To immobilize thiolated DNA, I started with the protocol of Lidija Malic [102] during a 2-month stay at McGill University, Montreal, Canada which was adapted from Peterlinz et al. [103] to create uniform, DNA functionalized surfaces. This DNA immobilization method is well characterized in follow-up articles by Herne, Levicky and Steel [99, 104, 105], regarding grafting density, dependency on DNA probe length, stability of the self-assembled layer versus temperature, ... and is the most widely employed DNA surface grafting protocol using thiol-modified DNA strands.

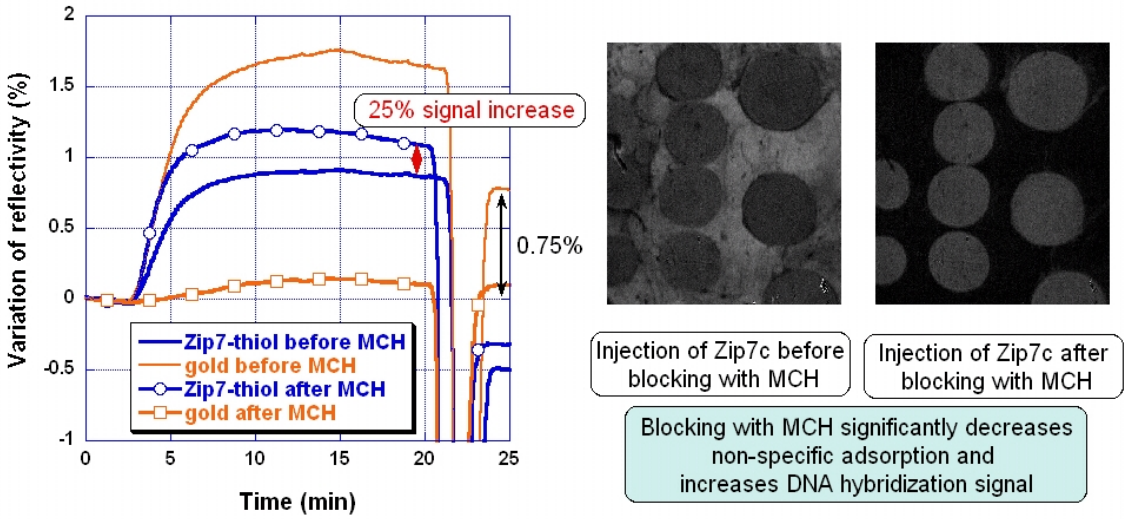

Figure 3.10: Comparison of two hybridizations by SPRi showing the efficiency of MCH blocking after spotting of Zip7-thiol probes. Hybridization before MCH treatment of the surface results in huge non-specific signal on the gold surface. After 90 min incubation with MCH, a second injection shows almost no signal on gold and increased hybridization signal on DNA spots. Images presented are differential images taken at the end of each injection. Regeneration si achieved by injection of NaOH 0.1 M for 1 min.

Gold coated prisms are cleaned in piranha solution for 5-10 min. The prism is then covered with 1 µM solution of thiolated DNA for 3-5 h in K_2HPO_4 at 1 M concentration, in a humid environment to avoid drying. After incubation, the prism is rinsed with deionized water and dried under argon or nitrogen stream. The prism is then immersed for 90 min in a 1 mM solution of 6-mercapto-1-hexanol (MCH) which serves as blocking thiol, replacing DNA that is not adsorbed by its thiol moiety and filling in imperfections of the layer [104]. After washing and drying, the chip is stored at 4°C and rapidly employed for SPRi studies. When only parts of the surface are functionalized by DNA, MCH also serves to block the remaining gold surface thereby rendering it insensitive to non specific DNA adsorption. In figure 3.10, we see functionalized areas of thiol (about 2-3 mm in diameter) that are hybridized to its complementary DNA. Before treating the surface with MCH, we observe a high DNA adsorption signal on the gold surface that is only partially recovered upon regeneration by NaOH. After treatment of the surface with MCH, the DNA hybridization signal is specific and we observe an increase of 25% of the hybridization signal on the spots.

In the course of this work, the described two step functionalization protocol has been adapted to be compatible with the spotting of thiolated DNA using the OmniGrid spotter with X-tend microarray pins (Lab Next Inc, Glenview, USA). Several parameters have been examined: Influence of DNA-thiol concentration, influence of the concentration of the K_2HPO_4 buffer, interaction time, humidity and rinsing methods. Especially rinsing gets important when thiols are spotted on a surface since upon rinsing the thiol-DNA solution gets in contact with thiol-free gold surface and may lead to contamination in form of 'comet tails', as shown in figure 3.11, or in the worst case, to cross-hybridization. This phenomenon can be overcome by letting the DNA-thiol solution dry before rinsing as shown in figure 3.11 on the right. Prisms can be regenerated from thiols by short immersion into piranha solution. Note that repeated application of piranha may damage the gold layer and lead to surface irregularities and irreproducible SPRi signals.

A detailed comparison of both spotting techniques by QCM-D, SPRi and contact angle measurements is presented in section 4.3.

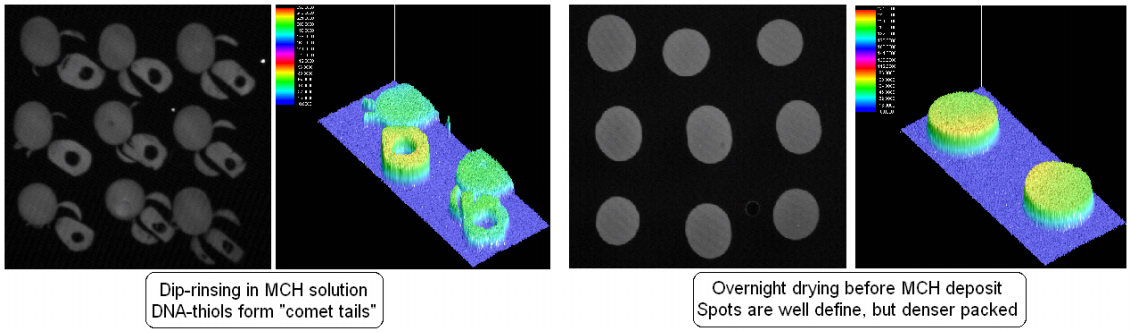

Figure 3.11: Images acquired after DNA hybridization and revelation using fluorescence microscopy. *On the left:* thiol spots that have been dipped in MCH solution for rinsing before MHC deposit show come-tails due to DNA deposit during rinsing. *On the right:* this effect can be suppressed when DNA-thiol spots are dried before MCH deposit. No DNA is found outside the original deposited spot, however, due to long incubation times, the grafting density is very high.

Chapter 4

DNA on a solid support: fundamental aspects of duplex stability

Dans ce chapitre, des concepts théoriques de l'hybridation de l'ADN sur puce seront introduits et nous les montrerons par la suite sur nos données expérimentales. Dans la première partie, le modèle de Langmuir sera utilisé pour une description détaillée de l'hybridation d'ADN sur puce. Des prédictions pour une analyse de cibles mutées par rampe de température seront faites pour le cas homozygote et hétérozygote. Ensuite, le modèle de Langmuir sera raffiné pour inclure les effets de la force ionique du tampon sur le duplex d'ADN à la surface. Après cette partie théorique, les premiers résultats présenteront une comparaison de deux méthodes de greffage d'ADN utilisées dans ce travail. Nous nous intéresseront notamment à la sensibilité obtenue sur des plots de polypyrrole ou de thiol et à la stabilité thermique de ces méthodes d'immobilisation. Cette partie introduira en même temps des concepts d'hybridation d'ADN sur puce à température constante. Toutes les parties suivantes traiteront l'analyse de dénaturation thermique de l'ADN hybridé à la surface. Après une clarification sur les différences entre les rampes de température à l'équilibre (en présence d'ADN) et hors équilibre (pendant rinçage de la puce), on s'intéressera d'abord à l'influence de la force ionique du tampon sur la stabilité du duplex immobilisé. Nous confronterons les résultats expérimentaux à la théorie introduite précédemment. La stabilité de l'ADN sera ensuite étudiée en présence d'agents dénaturants, notamment de la formamide.

Après cette étude de l'influence du tampon, on s'intéressera aux cibles. Un système modèle de mutations ponctuelles sera étudié. On essayera notamment de pousser les limites de détections le plus loin pour détecter une cible minoritaire et mutée en présence d'un large excès de la cible sauvage. Une méthode d'amplification du signal SPRi est ensuite étudiée pour évaluer si elle peut améliorer la sensibilité de notre détection. Les études sur les oligonucléotides seront complétées par une analyse de séquences plus longues ayant des queues d'un côté spécifique de la partie hybridante. Elles serviront également à établir les influences des structures secondaires d'ADN sur l'hybridation à la surface et prépareront ainsi l'étude d'échantillons biologiques présentée dans le chapitre 5.

4.1 Introduction

In this chapter, we will try to elucidate main issues in DNA duplex stability using thermal denaturation of DNA in a solid state experiment. Thermodynamic properties of DNA are usually analyzed in solution, as introduced in the previous chapter. DNA hybridization and melting are then studied in an 'ideal solution', where DNA is sufficiently diluted to prevent interactions between different 'neighboring' strands. A two-state association and dissociation model can then be assumed for duplex formation between oligonucleotides (ODN). When it comes to surface hybridization, however, new considerations have to be made, since grafting DNA to a surface implies serious changes to the hybridization environment. DNA may not only interact with the substrate by hydrophobic or electrostatic interactions, but immobilized DNA will also interact with each other, depending on the grafting density [8, 106]. The characterization and understanding of the biochip environment is thus a main issue in DNA microarray design. When no care is taken, results can be biased by non-specific signals, either from DNA in solution or other components. Selectivity, reproducibility and thus the reliability of the results are inevitable criteria in the design of diagnostic tools. Depending on the performance criteria, time consuming optimization steps are often necessary before the DNA chip can be considered for use in medical applications. Fundamental insight in solid phase hybridization will lead to more precise predictions on the system and therefore accelerate the validation of the microarray design. The here presented considerations and results will help to evaluate DNA interaction on biochips.

We will see in the theoretical section 4.2, how surface hybridization isotherms can be analyzed within the Langmuir surface adsorption model [107]. This simple model of hybridization between one target in solution that hybridizes to the immobilized probe is discussed and then extended to the case of a target mixture where two targets are able to hybridize to the same probe. Competition for the hybridization site will occur and we will see that the presence of two different targets with comparable affinities for the probe compromises the selectivity of the detection method [108]. However, there are medical applications where it is crucial to detect the presence of targets presenting one mutation, for example, when medical samples from a biopsy are to be analyzed. DNA samples from biopsies will reflect the DNA in the same proportion as the extracted tumor and healthy cells. The tumor cells often represent less than 10% of the sample, and the challenge lies in detecting not only their presence, but also in giving quantitative data on the sample's composition. Some representative scenarios are modeled. The competition may still get more complicated when the targets in solution are of relevant biological length, for example, >100 bp for samples amplified by PCR. Furthermore, targets in solution are usually double stranded or, after special treatment, in single stranded form and the targets may have important secondary structures that prevent efficient surface hybridization.

Next, we will study salt effects on solid phase hybridization. Since DNA has an anionic backbone, surface grafting creates a negatively charged layer. The surrounding bulk solution usually contains a certain amount of ions so that counter-ions from the bulk can be recruited to the surface to screen out negative charges. Different surface hybridization regimes can be encountered and are discussed here within the Langmuir model.

The first experimental results presented in section 4.3, will familiarize the reader with DNA surface hybridization kinetics via a comparison of two different DNA immobilization methods. In fact, chemical surface modification and grafting strategies for biological molecules are subject to continuous research. To date, no standard grafting method is established due to problems of adaptation to the detection systems or inert imperfections of the different chemistries, concerning especially their reproducibility, stability and ease of implementation. Here, we present poly-pyrrole electro-copolymerization [97] and thiol self-assembled monolayers [109, 110] as two possible surface modifications for gold substrates. The advantage and drawback of each method will be discussed.

In the following sections, we will focus on DNA stability on solid supports observed by thermal denaturation of DNA. Most detection systems that are able to distinguish point mutations in the

DNA sequence rely on stringent conditions for discrimination. Any condition that results in a significant destabilization of the duplex with one or more mismatches, as opposed to the perfectly complementary target, can be adapted to achieve specific hybridization and to confirm the target's identity. Current parameters that can be easily varied are ionic strength, temperature, addition of denaturing agents to the buffer, pH, electric field, ... We will analyze the following factors with respect to duplex stability thanks to time and temperature dependent signal acquisition using SPRi:

- **Ionic strength (section 4.5):** since DNA has an anionic backbone, hybridization is penalized in the absence of counter-ions that screen repulsive interactions between complementary strands. We acquire equilibrium melting curves and compare the results to existing literature and the theoretical model established in our laboratory's theory group.
- **Denaturing agents (section 4.6.1):** the influence of formamide on DNA non-equilibrium thermal denaturation is studied and compared to values from the literature obtained for DNA melting in 3D environments. We focus here on the influence of the grafting density and eventual interaction changes in the case of mismatched targets.
- **Point mutation detection on oligonucleotides (section 4.6.2):** the detection of mismatches is shown for non-equilibrium thermal denaturation experiments. Starting from the detection of the homozygous genotype, with one DNA sequence present in the sample, we go towards the detection of two targets in solution presenting one exchanged base pair and thus one mismatch when hybridized to the same probe. The possibility to distinguish the presence of mismatched targets on one spot is shown and pushed to the limit of detection for the case of a mismatched target in low abundance in high concentration of complementary target (case of biopsy samples). The results are once again compared to the theory.
- **Signal amplification using biotin-streptavidin interactions (section 4.6.3):** to increase sensitivity, many detection methods rely on amplification strategies. Here we evaluate one common method based on the strong affinity between the small molecular compound biotin and its recognition partner streptavidin. Thermal characterization provides here a more detailed insight in the interaction of streptavidin with biotinylated targets hybridized on the surface.
- **Dangling ends and secondary structure (section 4.6.4):** the influence of long dangling ends and their localization on synthetic targets of 80 nt length is determined. Furthermore, the influence of competition between surface hybridization and secondary structure in the bulk is observed.

We conclude this chapter with a summary in section 4.7 of the results obtained by the temperature scan method on SPRi measurements and a small discussion of the impact of our results.

4.2 The Langmuir model applied to DNA surface hybridization

4.2.1 The Langmuir model in the case of one or two targets

Hybridization and denaturation of DNA can, in the simplest case, be treated in a two state model, in which the strands are either hybridized or separated (target+probe $\underset{k_{off}}{\overset{k_{on}}{\rightleftharpoons}}$ double helix). When the probe DNA is attached to a surface, this can be modeled by the so-called Langmuir model. The DNA hybridization is assumed to follow first order kinetics. In our application with DNA on separate spots, it is useful to consider the surface coverage $\theta = \frac{\text{number of hybridized probes}}{\text{total number of accessible probes}}$ of each spot. We then have to solve the following differential equation:

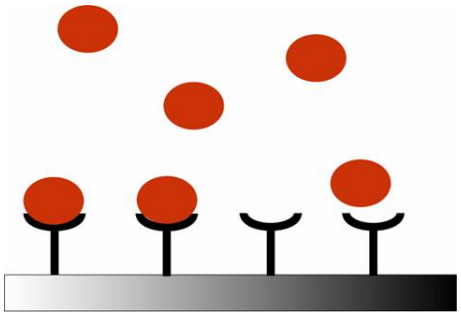

Figure 4.1: Sketch of the Langmuir Adsorption. Species can adsorb to free sites on the surface. The surface coverage θ is defined as the fraction of occupied sites.

$$\frac{d\theta}{dt} = k_{on} c_t (1 - \theta) - k_{off} \theta \tag{4.1}$$

where $k_{on}\left[\frac{1}{M \cdot s}\right]$ and $k_{off}\left[\frac{1}{s}\right]$ are the reaction constants and c_t is the concentration of targets in solution that will be considered constant during hybridization. Considering a spot initially not hybridized, i.e. $\theta = 0$, the following solution is obtained for isothermal duplex formation:

$$\begin{aligned} \theta_{on}(t) &= \frac{k_{on} c_t}{k_{on} c_t + k_{off}} \left(1 - e^{-(k_{on} c_t + k_{off})t}\right) \\ &= \frac{K\, c_t}{K\, c_t + 1} \left(1 - e^{-\frac{t}{\tau}}\right) = \theta_{eq} \left(1 - e^{-\frac{t}{\tau}}\right) \end{aligned} \tag{4.2}$$

where $\theta_{eq} = Kc_t/(1 + Kc_t)$ is the equilibrium surface coverage, $K = k_{on}/k_{off}$ is the equilibrium binding constant and $\tau = (k_{on} c_t + k_{off})^{-1}$ is the characteristic time scale of the reaction. Accordingly, we find the out-of-equilibrium denaturation isotherm ($c_t = 0$) when we consider the initial condition $\theta_{off}(t = 0) = \theta_{eq}$ at the beginning of the rinsing step:

$$\theta_{off}(t) = \theta_{eq} e^{-k_{off} t} \tag{4.3}$$

We are thus able to determine the equilibrium constant K by observing the hybridization and the denaturation process at a constant temperature.
It has to be mentioned that the Langmuir isotherm $\theta_{eq} = \frac{K\, c_t}{1 + K\, c_t}$ is only valid when the following conditions are fulfilled [111]:

- All probes on a spot should be of identical size and sequence
- Each probe hybridizes exclusively to one target. Note that this condition is not fulfilled when introducing two or more targets simultaneously that differ in one or two bases (mutations)
- Likewise, all targets hybridize only to one single probe. Dangling ends are thus not allowed to hybridize to neighboring sites
- There is no competitive hybridization in the bulk. The target can neither self-hybridize nor hybridize with another target in solution
- The grafting density should be diluted enough to inhibit all effects of interactions (excluded volume interactions or electrostatic interactions) between probes. Therefore, the distance between two sites should be larger than two times the Flory radius of a polymer chain $R = N^{\frac{3}{5}} a$ with $a = 6\,\text{Å}$ the characteristic size of a base and N the number of bases. To

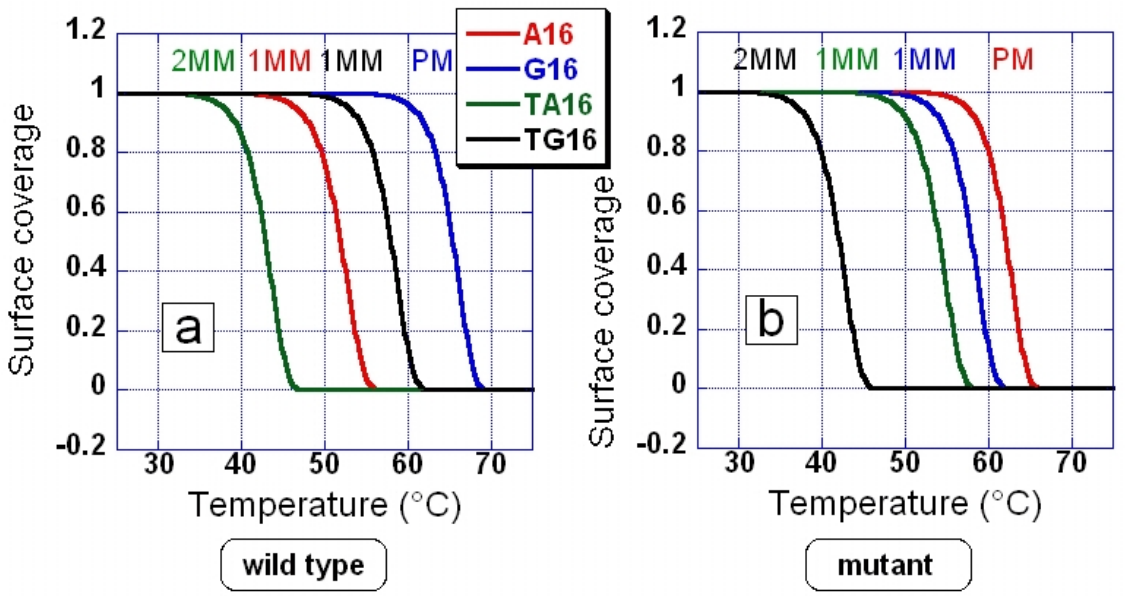

Figure 4.2: Simulation of non-equilibrium thermal denaturation curves for point mutation detection on the CCND1 SNP A870G. a) NTD curves after injection of 250 nM Gc20 target. b) Result on the same probes for 250 nM Ac20 target. Perfectly matched duplexes are well distinguished from mismatches.

avoid electrostatic interactions, the salinity of the buffer should have an ionic force that assures the *Debye length* to be smaller than the distance between two probe sites. The steric hindrance between hybridized probe sites modeled as rigid cylinders of 2 nm diameter should be negligible

The knowledge of the equilibrium constant permits further to access the thermodynamic parameters of the hybridized DNA using the equation

$$K(T) = \exp\left(-\frac{\Delta G}{RT}\right) \tag{4.4}$$

where R is the gas constant 8.31 J/(mol · K), T the temperature in Kelvin and $\Delta G = \Delta H - T\Delta S$ is obtained from the nearest neighbor model described in section 2.2. This relation also permits to calculate the melting temperature T_m determined by the thermodynamic enthalpy ΔH and the entropy ΔS of the DNA duplex formation. Knowing that T_m is defined as the temperature at which half of the available hybridization sites are in the double helical form i.e. $\frac{\theta}{1-\theta} = K(T_m)\, c_t = 1$, we find again equation 2.4 for the melting temperature. By observing melting temperatures for different target concentrations, we have access to ΔH and ΔS of the system:

$$\ln c_t = \frac{\Delta H}{R}\frac{1}{T_m} - \frac{\Delta S}{R} \tag{4.5}$$

When we plot $\ln c_t \left(\frac{1}{T_m}\right)$, we can calculate entropy and enthalpy from the slope and the axis intercept of the linear regression.

Furthermore, knowing the thermodynamic parameters of the DNA sequence either from experiments or from the NN model, we are able to simulate the melting curves of those sequences in thermodynamic equilibrium using the Langmuir model and calculating at each temperature the equilibrium surface coverage θ_{eq}. The thermodynamic parameters ΔH and ΔS are again considered constant and only ΔG varies with the temperature according to $\Delta G = \Delta H - T\Delta S$. It is

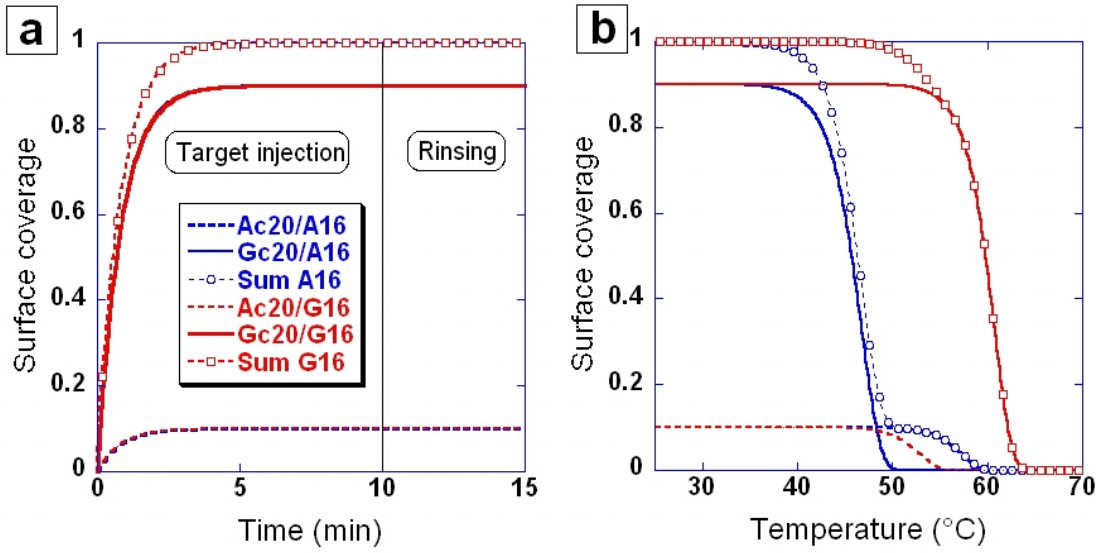

Figure 4.3: a) Association of target mix 90% Gc20 and 10% Ac20 of 250 nM total DNA concentration. At 25°C targets hybridize in the same way to PM and MM spots. The final surface coverage is composed of the percentages of matched and mismatched target on one spot and reflects the sample composition. b) During non-equilibrium thermal denaturation, the presence of a target mixture is revealed by a plateau which occurs in dependency of the T_d differences between PM and MM duplex on one spot. While it is clearly visible on A16, no clear stagnation appears on G16.

however more interesting for the experimental work hereafter to consider non-equilibrium thermal denaturation curves (NTD curves). The differential equation 4.1 for the surface coverage must then be solved numerically as the dissociation rate depends on the temperature which is varied over time. For a given temperature profile and by fixing the dissociation rate via the relation $k_{off}=k_{on}/K(T)$, equation 4.1 can be solved using a Mathematica routine. In figure 4.2, we can see NTD curves demonstrating the destabilizing effect of mutations on the DNA double helix. Probe sequences of 16 bp from the Cyclin D1 gene are presented after hybridization of Gc20 and Ac20 in figure 4.2a and b, respectively (see table 3.1 for sequence information). Each curve in one graph corresponds to a different probe being either perfectly complementary or having one or two mismatches toward the target. The melting temperature of the mismatched duplex is decreased by several degrees Celsius compared to the perfectly matched probe and mutations can so be discriminated. On one sensor surface with allele specific probes, we can determine, if the denaturation shows the signature of the wild type or the mutated target. The order of the curves on a chip with allele specific oligonucleotide (ASO) probes is changed when the probes hybridize to a mutated target instead of their perfectly complementary one as shown in the two subfigures. Our simple simulation will later be confronted to experimentally obtained NTD curves for these targets. These simulations do not consider any variation of the thermodynamic parameters ΔS and ΔH with the temperature. The correction due to the heat capacity change ΔC_p as determined by Zuker do not significantly alter our results [112]. For a detailed discussion of the influences of heat capacity changes on DNA melting, see for example [113]

As mentioned before, it may be interesting for clinical applications to observe mixed targets, i.e. the heterozygous case. When we consider a spot bearing one single probe and a target solution composed of target 1, the complementary strand, and target 2, the strand presenting a

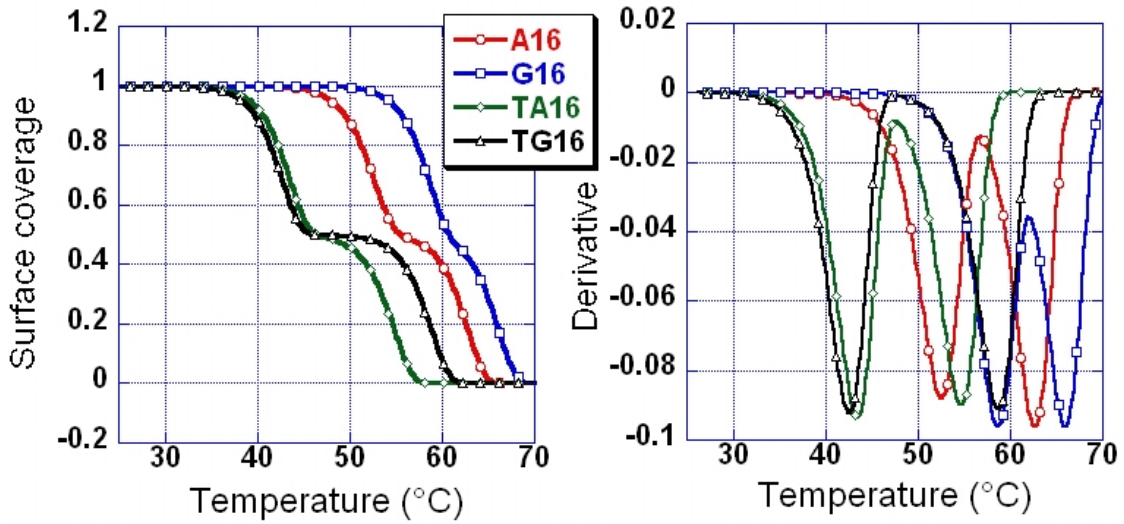

Figure 4.4: Simulation of non-equilibrium thermal denaturation curves for a heterozygous sample of genotype A/G of the CCND1 SNP A870G and their derivatives.

point mutation, we have to analyze the following equations [114]:

$$\frac{\partial\theta_1}{\partial t} = k_{on}c_1\left(1-\theta_1-\theta_2\right) - k_{off,1}(T(t))\theta_1 \tag{4.6}$$

$$\frac{\partial\theta_2}{\partial t} = k_{on}c_2\left(1-\theta_1-\theta_2\right) - k_{off,2}(T(t))\theta_2 \tag{4.7}$$

We consider, that the k_{on} of the complementary duplex and the mutated duplex are the same. This assumption has been shown to be consistent with experimental results [112, 108]. This can be explained by considering the DNA hybridization process as a zipper that closes up completely once a nucleus of about four base pairs has been formed. According to Wetmur and Davison [115], this rate limiting step depends on the complexity of the sequence. For two duplexes differing by one point mutation the sequence is very similar and thus also k_{on}. To predict the proportions of perfect and mutated duplexes on the spot, we have to solve the system of coupled differential equations numerically to find $\theta_1(\mathrm{T(t)})$ and $\theta_2(\mathrm{T(t)})$. We therefore apply a typical temperature profile with 10 min hybridization at constant temperature of 25°C. Then, unhybridized targets are washed off for 5 min before the temperature scan at 2°C/min is applied.

The hybridization process must be sufficiently short in order to avoid rearrangement of the targets on the spots caused by the higher affinity of perfect matches. At 25°C, however, target dissociation is almost absent so that the original hybridization proportions of matched and mismatched targets on one spot reflect the sample's composition. The association kinetics of a sample mixture containing 90% Gc20 and 10% Ac20 is shown in figure 4.3a. Since k_{on} is identical and both targets are stable at 25°C, the association of one target to a probe as perfect matched (PM) or mismatched (MM) duplex shows the same kinetics. Dissociation is absent under the conditions considered (400 mM NaCl, 25°C) and the surface coverage reflects the injected proportions. When solving the differential equations during the T-scan, we obtain the dissociation characteristics for θ on each spot from the sum $\theta = \theta_1 + \theta_2$. Figure 4.3b shows the NTD curves for a 2°C/min T-scan obtained after hybridization shown in subfigure a. Due to the difference of the dissociation temperature between complementary and mutated duplexes on the probe, we observe at low temperatures the denaturation of the mutated target. Then, the signal stagnates until the temperature is high enough to denature the complementary target. The stagnation occurs at the percentage of the surface coverage that equals the proportion of complementary targets on the spot. For genotyping, we can detect in this way heterozygous samples with equal proportions of

mutation and wild type target in the sample as shown in figure 4.4. In the derivative plot on the right, we find two minima per spot indicating the presence of two targets of different affinities for the probe in question. The NTD simulations are encouraging, since we seem to be able to detect not only if the sample contains the wild type or the mutated target, but also the presence of both at the same time.

4.2.2 Extensions: Taking into account experimental specifications

The Langmuir model is the simplest approach to evaluate DNA hybridization on a surface. However, as we have seen, the Langmuir adsorption isotherm is restricted to very limited conditions. In some cases, it may be useful to modify the Langmuir adsorption isotherm to take into account effects of the DNA's environment or the actual experimental protocol of DNA surface hybridization.

Probe length dispersion

We will first focus on the case, when the probe length is not unique but shows a certain distribution. In our experimental setup, a distribution of probe lengths possibly occurs because of the immobilization of the DNA in a pyrrole polymer film of about 5-10 nm thickness. Even in the presence of a spacer chain of 10 thymines, there can be probes that are partially entrapped in the polymer and thus not fully accessible for target hybridization. This may lead to a distribution P(n) of the probe length $n \leqslant N_{max}$ where N_{max} designates the originally synthesized probe length. The equilibrium surface coverage can then be expressed in the following way:

$$\theta_{eq}(T, c_t) = \sum_{n=N_{min}}^{N_{max}} P(n)\, \theta_{eq,n}(T, c_t) \tag{4.8}$$

Here, N_{min} describes the minimum length necessary for hybridization under chosen experimental conditions. When we assume, that the main fraction of 60% of the probes has the length N_{max} and that there is an uniform distribution of chain lengths $N_{max} - 7 \leqslant n < N_{max}$, we find that the resulting melting curve for a spot shows a broadened transition compared to curves obtained from the Langmuir model with one determined chain length N_{max}. This is due to the different dissociation constants of DNA duplexes of different lengths. The association constant k_{on}, meanwhile, is not affected by this probe length dispersion, as hybridization occurs spontaneously once a nucleus of $N_{min} \approx 4$ bases has been formed. This phenomenon has been analyzed by J.-B. Fiche in more detail in [112]. Other models are available like second order Langmuir models or the Sips model that describes the presence of heterogeneous binding energies and may be used to fit hybridization isotherms [89].

Salt effects

Another non-negligible factor, when working with denaturation curves of DNA, is the influence of the buffer's ionic strength on the melting temperature. The electrostatic interactions give rise to further corrections of the Langmuir model. Several groups have worked on this issue and have proposed empirical corrections. As most studies are led in 1 M sodium chloride (NaCl), this concentration is often used as the reference concentration for calculation of the melting temperature. Until today, there remain some uncertainties about the exact equation. Corrections of the thermodynamic parameter ΔS, convenient for a wide range of DNA probe lengths, DNA concentrations and salt concentrations have been put forward by Owczarzy et al. [39]. This article gives a good overview over existing corrections from various research groups and compares the different salt correction to data over a wide set of oligonucleotides. It concludes that the melting temperature can not simply be related to $\ln\left[Na^+\right]$ as proposed previously, but has also a quadratic term. Also, the authors find a salt dependency that is based on the percentage of G·C base pairs and not on

the sequence as the NN model. In the following, we will adopt the salt corrections by SantaLucia as stated in section 2.2 and the theoretical approach presented hereafter based on an extended Langmuir model to describe salt effects on a surface.

Henceforth, factors corresponding to *probes* will be indexed p, *targets* and duplexes between probes and targets are indexed t and pt, respectively. Hybridization of targets from the bulk to probe DNA grafted on a surface will be analyzed. Since probes usually have a spacer chain, we will treat the case where probes and targets are of different length N_p and N_t, respectively. We will consider a uniformly functionalized surface of grafting density $d_p = n/A$, with n the number of probes grafted on the surface A. We can also define a unit area per probes site Σ. Knowing the length of probe and target, we can now determine σ, the number of charges per unit area. Inevitably, σ depends on the surface coverage θ since each hybridizing target adds N_t charges:

$$\sigma = \underbrace{\frac{N_p}{\Sigma}}_{\sigma_0}\left(1 + \frac{N_t}{N_p}\theta\right) \tag{4.9}$$

where σ_0 denotes the density of charges on the unhybridized surface. The total charge density on the surface is thus $\sigma_{tot} = -\sigma\, e$.

A theoretical discussion of the influence of the electrostatic free energy per unit area γ_{el} is presented by Halperin et al. [107]. There, a general form of the adsorption isotherm is derived for probes and targets of equal size, which can be easily adapted to probes and targets of different sizes using σ as defined before. We then obtain a hybridization isotherm that takes into account surface charges:

$$\frac{\theta}{c_t\,(1-\theta)} = \underbrace{\exp\left(-\frac{\Delta G^0}{RT}\right)}_{K} \cdot \exp\left(-\frac{N_t}{kT}\frac{\partial \gamma_{el}}{\partial \sigma}\right) \tag{4.10}$$

with K the equilibrium constant and ΔG^0 the Gibb's free energy in the reference state. Note that the reference state in this model is *not* equivalent to the previously defined $\Delta G^0_{37°\mathrm{C}}$ of the NN model (1 M monovalent cations at 37°C). In fact, it corresponds to the energy of surface hybridization of uncharged chains. Equation 4.10 is generic since it is independent of the form of the electrostatic free energy γ_{el}.

To determine the electrostatic free energy, we have to characterize the relevant electrostatic length scales of our system. Since the polyelectrolyte DNA is immersed in buffer, its charges will attract cations that reduce the electrostatic potential. The screening length is given by the Debye length

$$\lambda_D = \sqrt{\frac{\epsilon_0 \epsilon_r kT}{N_A e^2 I}}, \tag{4.11}$$

where ϵ_0 is the vacuum permittivity, ϵ_r is the relative static permittivity of the medium, N_A is the Avogadro constant, e the elementary charge and I is the ionic strength of the electrolyte. It is also useful to introduce the Bjerrum length

$$l_B = \frac{e^2}{\epsilon kT} \tag{4.12}$$

in order to rewrite the Debye length as $\frac{1}{\sqrt{8\pi N_A l_B\, 10^3\, c_s}}$ in the Gauss system, where c_s is the salt concentration in M. The Bjerrum length describes the distance at which Coulomb interactions equal the thermal energy kT. A third relevant length scale is the Gouy-Chapman length $\Lambda = 1/(2\pi\, l_B \sigma)$ describing the diffuse layer of counter-ions attracted by the uniformly charged DNA surface.

One approach to obtain γ_{el} in the framework of the Langmuir model is based on the box model, where the charge of the DNA probes is modeled as a diffuse charged layer of height H over the surface. The model is valid for high grafting densities assuming the formation of a polyelectrolyte brush. The charged layer affects the ion distribution of the surrounding solution within $\Lambda > H$,

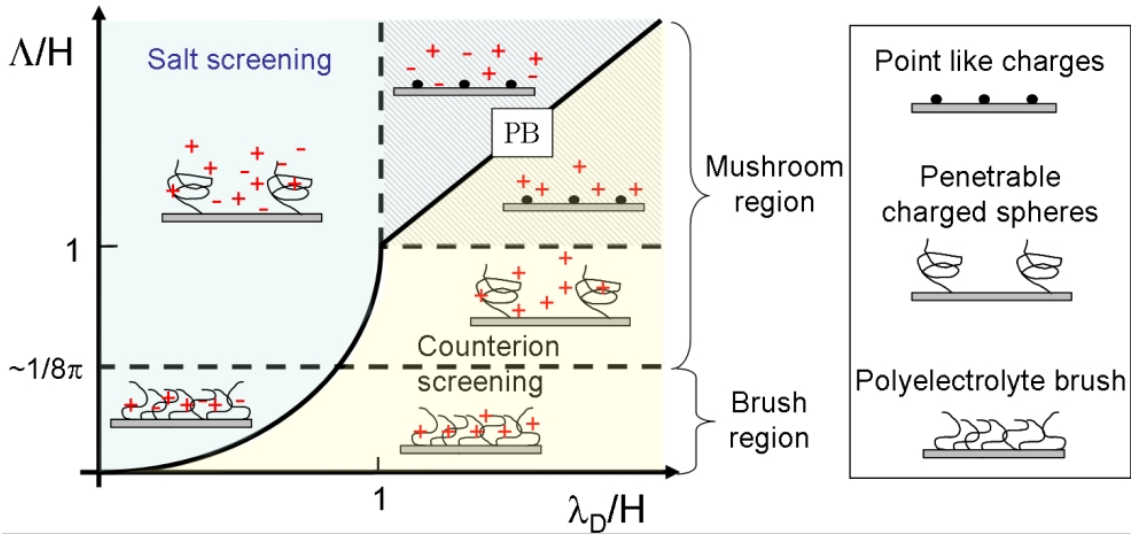

Figure 4.5: Phase diagram of DNA surface hybridization regimes. We distinguish the salt screening and the counterion screening, separated by a solid line. Each regime can then be separated in mushroom and brush region with diluted and high grafting densities of probe DNA, respectively. In the upper left corner, the Poisson-Boltzmann regime for point like charges can be found.

the neutralization length. For lower grafting densities, where probe-probe distances are higher than the average chain length, we find the mushroom regime. Here, probes can be modeled as penetrable charged spheres. For very diluted grafting densities, electrostatic interactions between probe sites become negligible and we can model the probes as point like charges or a uniformly charged surface.
Hereafter, we will analyze the following two regimes:

- The brush regime for salt screening where $\Lambda > \frac{\lambda_D}{H}$ and $\lambda_D < H$
- The brush regime for counterion screening where $\lambda_D < (\Lambda H)^{1/2}$ and $\Lambda < H$

Those and other regimes are depicted in a phase diagram in figure 4.5. The box model breaks down at lower grafting densities where charges are diluted. One approach to calculate salt effects for penetrable charges spheres has been presented by Pettitt et al. using the linearized Poisson-Boltzmann equation for a mean field approach [116]. However, we concentrate in the following on high grafting densities, i.e. the brush regime as described in [107]. Note that another regime may be found in the brush regime for very low salt contents at $\Lambda/H < (\lambda_D/H)^4$ in the case of a metal substrate screening the DNA charges by electrons in the metal. In this case, we obtain $\gamma_{el} = 2\pi k T l_B \sigma^2 H$, independent of the salt concentration. The screening is then very poor since the electrons can not penetrate the charged layer. However, since these low salt conditions are not relevant to our experiments it will not be discussed further.
In the salt screening regime, γ_{el} can be expressed in the following way:

$$\gamma_{el} = 4\pi k T \sigma^2 l_B \frac{\lambda_D^2}{H} \tag{4.13}$$

which then yields the hybridization isotherm by insertion of γ_{el} in equation 4.10:

$$\frac{\theta}{c_t\,(1-\theta)} = K \exp\left(-\underbrace{8\pi N_t \sigma_0 l_B \frac{\lambda_D^2}{H}}_{\Gamma_{ss}} \left(1 + \frac{N_t}{N_p}\theta\right)\right) \tag{4.14}$$

Accordingly, at low salt concentrations and thus in the counterion screening regime, we can determine the electrostatic free energy per unit area and the corrected isotherm from the box model:

$$\gamma_{el} = kT\sigma \ln\left(8\pi\sigma l_B \frac{\lambda_D^2}{H}\right) \tag{4.15}$$

$$\frac{\theta}{c_t\,(1-\theta)} = K \exp\left(\underbrace{-N_t \ln\left(8\pi\sigma_0 l_B \frac{\lambda_D^2}{H}\right) - N_t}_{\Gamma_{cs}} - N_t \ln\left(1+\frac{N_t}{N_p}\theta\right)\right) \tag{4.16}$$

The isotherms for salt and couterion screening at various salt concentrations are shown in figure 4.6a and b, respectively. We can see, that in the high salt regime, the melting curves have a narrow transition from $\theta = 1$ to $\theta = 0$. The melting temperature is shifted to higher temperatures with increasing salt concentration. For comparison, the Langmuir isotherm of the studied duplex of target Gc20 on probe G16 is plotted. In the limit of $c_s \to \infty$, we do not recover the Langmuir isotherm, revealing that the electrostatic penalty in the high salt regime is overestimated. In the low salt regime, one finds a flattened profile and a strong dependence on the salt concentration. At very low salt concentrations, spot saturation is no longer possible at room temperature and for 10 mM Na^+ no surface hybridization should be possible at all. For comparison, the simulation is shown up to 157 mM Na^+, although we should expect the salt concentration at the limit between counterion screening and salt screening to be ~0.06 M, depending on the grafting density and H. Note that the box model is an approximation and a more rigorous analysis should be based on the exact solution of the Poisson-Boltzmann equation.

Two parameters in the simulations are only approximately known in our application: the parameter H, giving the height of the charged layer, and σ_0, the charge of the spots which is not very well known for poly-pyrrole based DNA grafting. Poly-pyrrole is a conducting polymer which may have a positive charge after the usual spotting process. This yields a compensation of a part of the charge of DNA. This effect is absent in the case of thiol grafted DNA. In general, it has been observed that the nature of the substrate may not only influence hybridization kinetics of DNA, but also lead to conformational changes, which are not taken into account here ([116] and references therein).

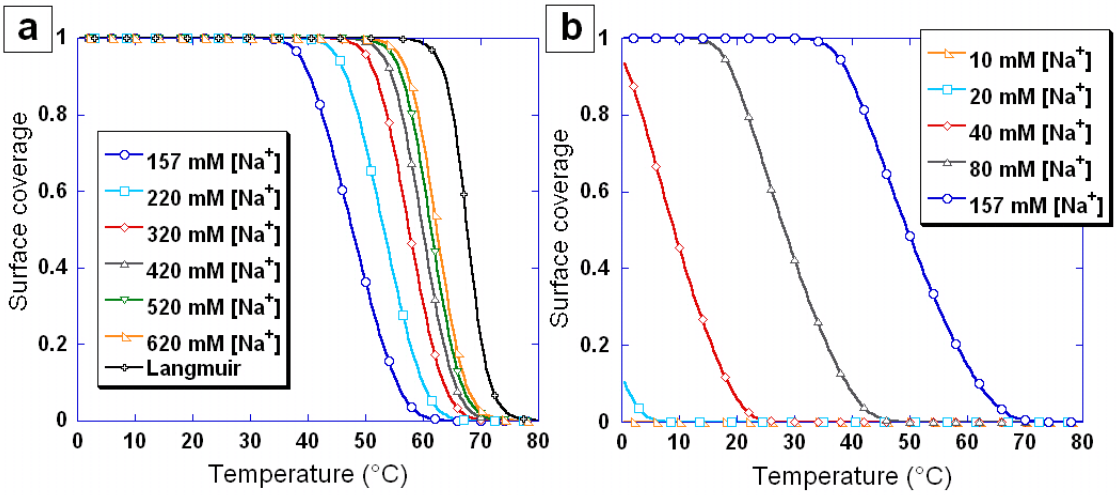

Figure 4.6: Simulation of the melting curves in the high (a) and the low (b) salt regime for high grafting densities for duplex Gc20/G16. Curves are shifted to higher temperatures with increasing salt concentration. The limit between salt screening and counterion screening, defined by $\Lambda = \lambda_D^2/H$, is experimentally at c_s ~0.06 M Na^+.

4.3 Influence of the immobilization chemistry on DNA surface hybridization

In DNA biochip fabrication, the surface chemistry employed for DNA immobilization has an important role. The functionalized surface plays the role of a transmitter between the sample and the physical detection system. Its quality will consequently influence the detection and finally the data analysis. Hence, the surface chemistry must be well controlled to yield reproducible signals of high sensitivity and with a good specificity toward the target. For surface functionalization with DNA, two main strategies can be cited:

1. In-situ DNA synthesis on a substrate

2. Grafting of ex-situ synthesized DNA

The first technique profits from technologies borrowed from microelectronics, especially photolithography, or from robot or ink-jet deposition technologies. DNA synthesis is carried out on the substrate in a site specific manner. The synthesis is based on phosphoramidite chemistry as introduced in section 3.4. The spots obtained by in-situ synthesis will show a certain probe length distribution since the efficiency of the base incorporation is ∼99% and some probes will thus be capped before reaching the full size. This strategy is suitable for middle to high density microarrays with thousands to hundreds of thousands of spots. We will not focus here on this technology and the interested reader may see the recent review of Gao et al., for example [117].

The second strategy, which is used in this work, uses presynthesized and purified DNA strands of uniform length. For fabrication of the biochip, the DNA must then be brought into contact with the corresponding surface grafting site (*addressing*) and be attached to the surface by stable interactions, preferably covalent. Addressing is often carried out with the help of robots and sequences are 'printed' at the desired localization. The quality of the spots can be characterized by parameters like the spot footprint (like area or diameter), the circularity (absence of comet-tails), the spot uniformity (inter and intra-spots), the signal to noise ratio and the coefficient of variation (CV=standard deviation/mean). Reproducibility is hereby a main issue in biochip production.

Various immobilization strategies are known and will depend on the type of substrate that is employed. Covalent grafting to glass slides can be achieved using silanization protocols, for example, surface chemistries using amino groups on the substrate or other anchoring groups like poly-L-lysine (PLL) [118, 119], for a review, see [120]. On gold surfaces, thiol self-assembling is often the foundation of subsequent attachment using mostly standard chemistries on 5' modified DNA. For SPRi applications, several surface modifications have been brought forward. Especially the group of Corn proposed a series of surface modification strategies for DNA grafting applied to surface plasmon resonance measurements [121, 122, 123, 124]. In their work, self-assembling of thiols is arrayed using structured gold surfaces or UV lithography. From the protocol of Peterlinz [103], Bietsch et al. adapted a technique to perform ink-jet deposit of thiols [125]. Also, microcontact printing of thiols on gold is a current method to obtain a localized surface functionalization [126]. Another approach of addressing gold surfaces with DNA has been developed at our laboratory [97]. The technique is based on the electro-copolymerization of pyrrole modified DNA with pyrrole monomers and allows spotting of about 100 spots in the classical format adapted to SPRi and up to 10 000 spots in a cantilever based format suitable for fluorescence microscopy [127]. The most current strategies for DNA functionalization adapted to SPRi, however, have been developed on Biacore platforms and are in most cases adapted to biosensors with a uniformly modified surface. A comparison of the functionalization of Biacore's dextran matrix which immobilizes streptavidin that subsequently captures the biotinylated DNA probe and the direct immobilization of DNA via thiols on gold has been published by Wang et al. [110]. Yang et al. compared the surface hybridization of DNA on 2D and 3D streptavidin surfaces, based on immobilization of streptavidin in a dextran matrix or directly on a thiol monolayer [128]. The multitude of surface chemistries available reflects the need of optimization in this area. Most

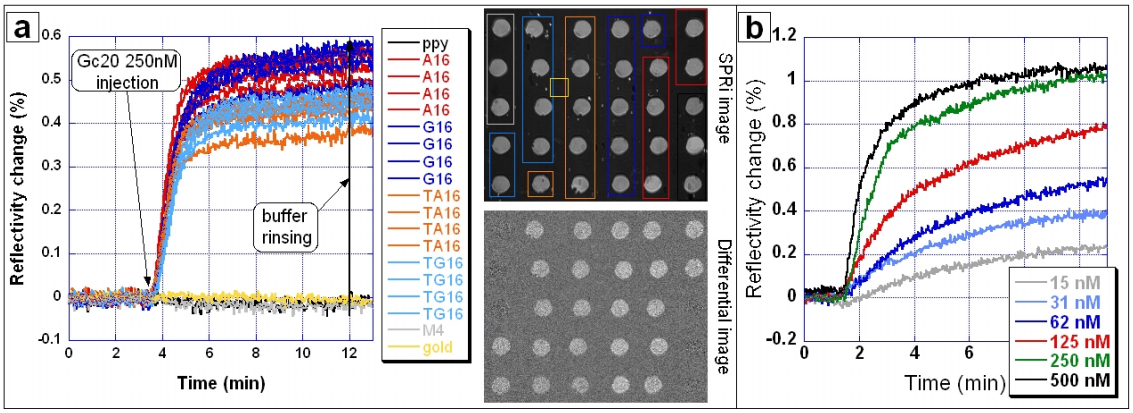

Figure 4.7: a) Hybridization of Gc20 on ppy probes of 16 bp length forming PM duplex (blue), 1 MM duplexes (red, light blue) and 2 MM duplexes. The corresponding SPRi image and differential image are shown. The injection is specific, since no signal is detected on control spots. b) Hybridization kinetics for Gc20 on G16 for various target concentrations on another ppy chip.

chemical methods are suitable for certain applications and have drawbacks on others. Main issues to be solved are the stability of the grafting, the reproducibility of the technique, the cost, production time, signal specificity and sensitivity, low background and a high signal-to-noise ratio, which is especially important for protein applications where non-fouling properties are needed.

Traditionally, our laboratory uses poly-pyrrole (ppy) functionalization for SPRi studies which is well adapted to a large variety of biological probes [97, 129, 130, 131]. As explained in the experimental section 3.5, poly-pyrrole immobilization is available in two flexible spotting strategies allowing precise addressing of probes on the chip. The probe grafting density can be varied by mixing different amounts of pyrrole conjugated DNA (usually in the range of 1-10 µM in 20 mM pyrrole monomers during spotting). The preparation is rapid and DNA chips are reusable over a period of about 3 months when the chip is regenerated after hybridization using sodium hydroxide (NaOH) at 0.1 M and stocked desiccated at 4°C.

In figure 4.7a, an exemplary injection of target Gc20 on probes of 16 bases length is presented. We can see that all spots hybridize globally at the same time, independent of their position on the prism. The injection signal is specific, which means here that the control spots, ppy, M4 and gold, show no adsorption signal during the injection. This can be seen from the kinetics curves and also in the differential image. We see that no significant difference in the hybridization signal is found for perfect matched and mismatched duplexes. The buffer condition being not very stringent with 350 mM NaCl, there is no significant difference in the affinity of the target to one probe or another. The kinetics also show the stable signal upon rinsing, no exponential decay can be seen and k_{off} is thus very small. In figure 4.7b, we see how the kinetics and the surface coverage are influenced by the target concentration. As predicted the Langmuir model, the characteristic time scale τ increases with decreasing concentration and surface hybridization gets slower. The equilibrium surface coverage decreases with decreasing target concentration. The detection limit on poly-pyrrole modified DNA chips is ∼10 nM. For thermal denaturation studies, poly-pyrrole grafting presents the advantage to be thermally stable up to high temperatures of minimum 90°C.

However, for DNA applications, poly-pyrrole seems to have some disadvantages, since the DNA is deposited inside a polymer matrix and may lead to artifacts like a probe length distribution on the spots. This has been observed by J.-B. Fiche during his Ph.D.. In parallel to poly-pyrrole, another common grafting method has thus been adapted to SPRi imaging studies: the self-assembling of thiol modified DNA, which is a well studied system for DNA biosensors [109]. This work has been initiated with the help of L. Malic at the Biolab'X of the McGill University in Montreal, Canada where Prof. M. Tabrizian generously welcomed me for two months. The thiol

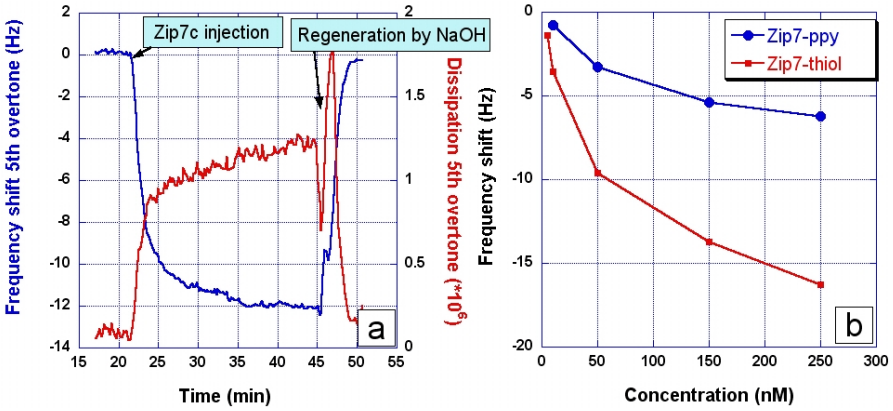

Figure 4.8: QCM signal upon DNA hybridization. a) Exemplary DNA hybridization kinetics observed for injection of Zip7c at 250 nM on thiol grafting chemistry. b) Comparison of calibration curves for injections of 2-250 nM on ppy or thiol grafted DNA.

functionalization protocol is now also used in our laboratory for certain applications.

Since our subsequent work will be based on temperature dependent analysis of DNA duplex stability, the crucial question is if DNA immobilized via a thiol group will be stable up to sufficiently high temperatures to allow thermal denaturation studies. Initial experiments were done on uniform DNA surfaces. Characterization of the thiol films and its hybridization properties is first carried out using a quartz crystal microbalance with dissipation monitoring. Zip7-thiol probes are brought into contact with the chip for 3 h in 1 M K_2HPO_4 (pH 9.25), leading to a frequency change of -35.5 Hz and a dissipation change of 0.95×10^6. Upon incubation with MCH in water for 90 min, an additional frequency change of -13.2 Hz and a dissipation change of 2.65×10^6 is measured. Although MCH adds little mass upon binding, it changes the viscoelasticity of the layer, bringing DNA chains upright, as shown by the dissipation change during MCH injection as compared to the DNA-thiol injection. This effect has also been observed by Boozer et al. using oligo(ethylene glycol)-terminated thiols (OEG) as diluent [132]. However, the overall dissipation change is low and proves the rigidness of the thiol monolayer. Similar functionalization protocols on a 9 MHz quartz have been used by Mannelli et al. [133]. Contact angle measurements show the hydrophilicity of both surfaces. With a contact angle of 26.2±2.7°, DNA-thiol functionalization shows better wetting capabilities as opposed to DNA-poly-pyrrole surfaces with 60.3±3.1°.

In figure 4.8a, hybridization kinetics observed for a Zip7c target injection on a thiol modified QCM chip is shown. Once again, the dissipation shift during injection is small, the hybridized layer has a rigid behavior. This is also the case on poly-pyrrole modified chips. In figure 4.8b, the hybridization signals of poly-pyrrole modified QCM-chips and thiol modified QCM-chips are shown for different target concentrations. We see that thiols yield a ∼2.5 times higher signal. The detection limit is 10 nM on ppy surfaces and 2 nM on thiol-DNA. It has to be noted, that the poly-pyrrole layer has here a thickness of several tenths of micrometers due to the altered electrospotting process on the large surface of the QCM sensor and in a big volume of 1 ml, as opposed to the thiol DNA monolayer of ∼1 nm optical thickness.

Thiol functionalized surfaces show generally an about two times higher hybridization signal as well in QCM-D measurements, as in SPRi experiments. This is due to two factors: the denser DNA packing leading to a higher grafting density and the higher sensitivity of surface plasmons on thiol functionalized prisms. Indeed, the absorbing nature of ppy reduces the SPR sensitivity by broadening the plasmon curves as can be seen in figure 4.9. Using the two-step protocol for DNA-thiol functionalization by Peterlinz et al. [103], the grafting density can be controlled by the incubation time of the DNA-thiol. Longer incubation leads to higher grafting densities which should ideally be in the order of $10^{11} - 10^{12}$ pmol cm^{-2} [134, 104]. For uniform surfaces, optimum incubation times lie between 3-5 h, as determined by L. Malic (personal communication). First

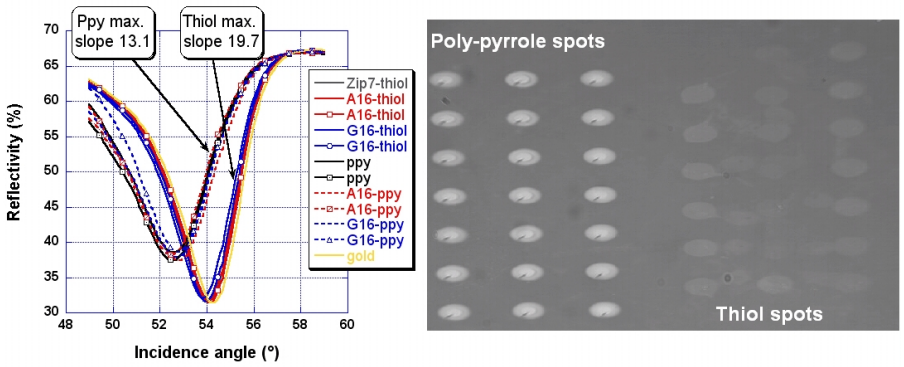

Figure 4.9: *On the left:* Experimental plasmon curves on one prism spotted with poly-pyrrole and thiol modified DNA. Poly-pyrrole changes the shape of the plasmon curves because of its imaginary refractive index part, contrarily to thiol monolayers. The SPRi sensitivity, related to the slope, is about 1.5 times higher on thiol spots. *On the right:* SPRi image of the prism. We see the high contrast of poly-pyrrole at the working angle as opposed to thiol spots that are barely visible.

temperature dependent experiments on DNA-thiols by SPRi showed a temperature stability of the hybridization signal of up to ∼75°C, when temperature scans of 2°C/min are applied and the end-temperature is maintained for 5 min. This thermal instability is in agreement with findings by R. Meunier-Prest and collaborators [135]. However, upon the first heating >50°C, every chip showed a signal loss of 5-10% of the initial hybridization signal, as indicated in figure 4.10a. Incubation at 50°C during formation of the thiol-SAMs does not prevent this initial signal loss. When T-scans are limited to 70°C, no important signal variation is detected over at least 18 heating cycles at 2°C/min, as shown in figure 4.10b. This proves the possibility to employ thiol functionalized gold surfaces for SPRi studies using thermal denaturation detection.

In a second step, the DNA-thiol immobilization method is adapted to the automated spotting system OmniGrid. The thiol solutions are deposited by X-tend microarray pins in a matrix and different sequences can thus be spotted. Since piranha cleaned gold is hydrophilic and the deposited droplets are thus very small, different thiol concentrations are tested to obtain an optimal grafting density with thiol functionalized DNA spots. As can be seen in figure 4.11, different regimes can be obtained in this way. While for a 1 µM concentration of DNA-thiol, a small hybridization signal is observed, indicating low probes density, 10 µM yield a high and stable signal. For 100 µM, we observe a lower hybridization signal on mismatched duplexes and a high k_{off} during rinsing. It should be noted that both, G16 thiol and A16 thiol at 100 µM grafting density show this high dissociation when Ac26 is used as target. The lower signal and higher dissociation upon rinsing is an indicator for too high grafting densities, leading to steric hindrance and multiple, repulsive interactions between probes and targets and different targets on the spot. This is also evident on the thermal denaturation scan. We observe a shift of the dissociation temperature to lower temperatures by about 15°C for high density spots due to higher stringency. This phenomenon has also been observed in the group of U. Krull for covalently grafted DNA on glass fibers [136]. When we observe closely, we can see in figure 4.11c, that there is a *bimodal distribution* of temperature dependent affinities on the spot and thus a small population dissociates at the same maximum temperature as observed on 1 µM and 10 µM spots. Further refinement between 10 and 100 µM of DNA-thiols showed a maximum around 40 µM for 3 h deposit at 85% humidity. However, these high concentrations caused parasite deposit of thiols on the surrounding gold during rinsing as we have seen in figure 3.11 previously. This has also been observed on other grafting methods that do not involve thiols for high product concentrations [118]. To avoid this problem, incubation times were shortened to 90 min at 85% humidity followed by overnight drying under the aspiration hood before rinsing off the DNA solution. The comet tails then disappear. For this protocol,

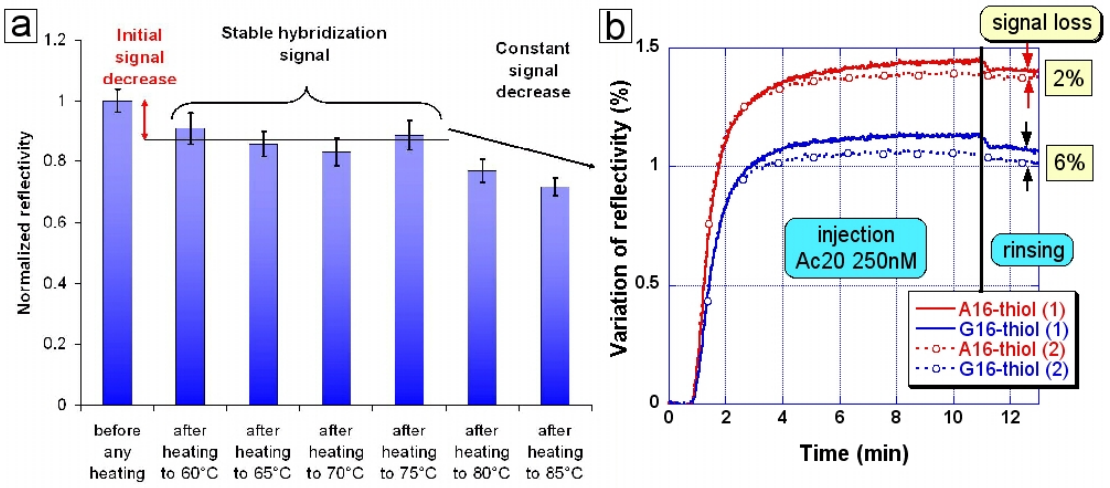

Figure 4.10: a) DNA hybridization signal on a DNA-thiol surface after heating to different temperatures. Signal stays globally stable up to ∼75°C and then decreases constantly.b) Comparison of hybridization signals achieved upon injection of Ac20 at 250 nM. Full lines represent first hybridization after initial heating, dashed lines correspond to injection performed after 18 heating cycles to 70°C and 4 days storage.

the optimal thiol-DNA packing is reached at DNA functionalization concentrations of 10 µM. It should be mentioned that the long drying period permits functionalization of medium to high density chips, for low grafting densities, the drying should be done more rapidly, under vacuum, for example.

It has to be mentioned that thiols in solution tend to form dimers which have reduced reaction kinetics as opposed to thiols [96]. This leads to reduced grafting efficiency over time for the same protocol even when small aliquots of thiol-DNA are stocked frozen until use. To restore the thiol groups, the disulfides may be reduced using Tris(2-Carboxyethyl) phosphine Hydrochloride (TCEP·HCl), an odorless and water-soluble reducing agent which has the advantage to present no thiol group itself, like for example the common reducing agent Dithiothreitol (DTT). This has been tested in our laboratory by R. Bombera.

In summary, QCM-D and SPRi experiments show that about two times higher hybridization signals can be obtained on thiol surfaces as compared to poly-pyrrole spotting. The spot reproducibility of thiol grafted DNA is generally much better than DNA immobilized by poly-pyrrole electro-copolymerization. Both techniques have a fair reproducibility when comparing independently prepared biochips with a coefficient of variation of about 15%. While chip preparation takes about 2-3 h for poly-pyrrole modified surfaces, thiol self-assembling with the presented two-step protocol takes about 24 h preparation time. Poly-pyrrole chips will loose about 50% signal in 3-4 months, depending on their manipulation and the regularity of employment, while thiol chips degrade about twice as fast, losing about 1% of the initial hybridization signal per day over the first two months (data measured every 2 weeks over this period). But the main reason to choose one technique or the other will depend on the intended grafting density and the necessary temperature stability. Dense surface packing may be unsuitable for long DNA targets where steric hindrance plays a crucial role. Thiol-SAMs should never be heated to high temperatures over 70°C for long periods, a fact that will also limit the length of the DNA probe for thermal denaturation protocols. The melting temperature should lie well below 70°C or be adapted accordingly by the use of DNA denaturing agents (see section 4.6.1 for more details). For poly-pyrrole immobilized DNA, no degradation has been observed for temperatures up to ∼90°C.

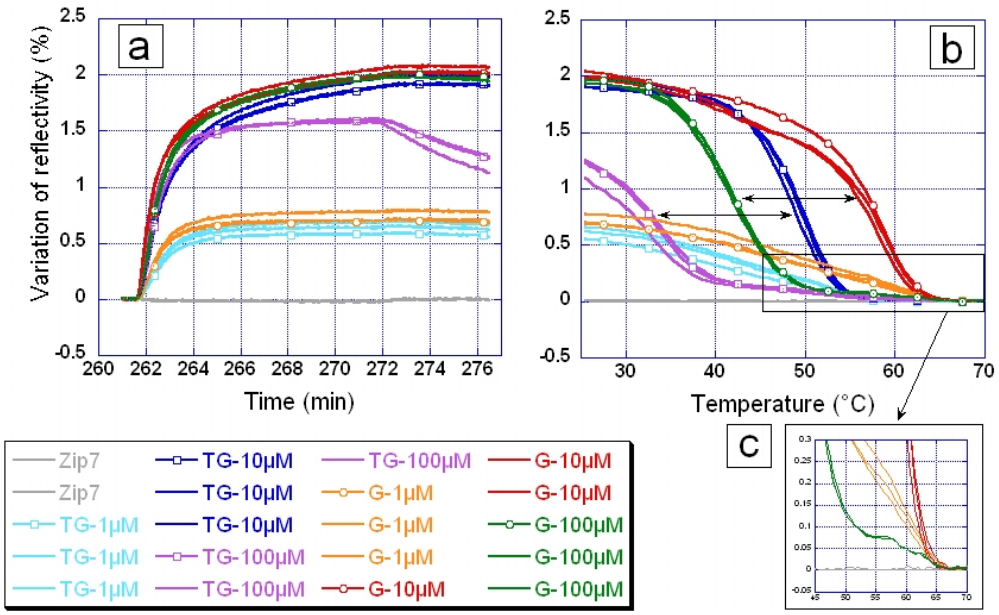

Figure 4.11: 3 different DNA-thiol grafting densities are investigated: deposit of 1 µM, 10 µM and 100 µM DNA thiols of sequence ASO-G and ASO-TG for 3 h before rinsing and deposit of 1 mM MCH. Signals correspond to injection of Gc26 at 250 nM in PBS 400 mM NaCl buffer. a) While 1 µM spots yield a low hybridization signal and thus a low grafting density, 10 and 100 µM spots show a very high signal. For 100 µM, the grafting density is so high that an important off-rate can be observed as soon as rinsing starts. b) While denaturation transitions are large for low density spots, 10 µM spots show a narrow transition at the expected denaturation temperature. Spots with high grafting density are shifted to lower temperatures as indicated by the arrows and show a two-phase behavior (c) with a small population having the same stability as DNA hybridized on spots with lower grafting density.

4.4 Differences between equilibrium and non-equilibrium denaturation studies

As we have seen in the previous section, the observation of DNA hybridization by SPRi gives access to hybridization kinetics. When probes are sufficiently long and hybridization takes place under soft conditions, i.e. at low temperatures and high salt concentration, it is difficult to distinguish differences from mismatches or other defects like DNA from DNA hybridization analysis. To get access to more detailed information on DNA surface stability, one has to apply stringent conditions that affect the duplex stability. One way to do so, is by changing the temperature and thus by denaturing the surface hybridized DNA. We will see in this section that temperature scans give access to interesting information on the DNA and permits to characterize its affinity in different environments. Two regimes have to be well distinguished in the following:

- Equilibrium melting
- Non-equilibrium thermal denaturation (NTD)

The first item refers to experiments in which the temperature scan is performed in the presence of DNA. The term 'equilibrium' describes the fact that we consider the DNA concentration in solution constant at all times. This is a valid approximation when the concentration is high and thus not significantly affected by the surface hybridized fraction. This condition is fulfilled for target concentrations bigger than ∼10 nM, giving way to a more than 100 fold excess of free DNA compared to available sites on the surface. We have to be careful with the term 'equilibrium' since

the fact that the temperature scan is performed in presence of free target DNA does not automatically imply that the surface hybridization and denaturation is in thermodynamic equilibrium. As we will see in section 4.4 and following, experimental factors like the rate of the temperature scan and mass transport to the surface will determine if thermodynamic equilibrium is established. One way to verify if thermodynamic equilibrium is established is to perform heating and cooling cycles and check that both overlap. We consider the temperature scan in thermodynamic equilibrium, when no hysteresis is detected and the initial hybridization signal is regained after the cycle. It is important to mention that only equilibrium melting curves in thermodynamic equilibrium permit to access the enthalpy and entropy change associated with the DNA duplex formation on the surface. Under these conditions, generalizations and predictions can be established that take into account the special environment of solid phase hybridization experiments.

From an experimental point of view, the non-equilibrium thermal denaturation method is more easily implemented on solid phase DNA detection. Here, the temperature scan is performed once hybridization is completed and excess DNA in solution is washed off. Since no DNA is present in solution, the composition on the DNA spot is only changed by DNA parting from the surface upon heating. No simultaneous annealing of targets from the solution to the now available probe intervenes. Although non-equilibrium kinetics are generally more difficult to access by thermodynamic models, the NTD condition can simplify data interpretation in some cases. In NTD experiments, we suppress any dynamic exchange of targets that might occur in the presence of a complex target mixture with different affinities for the probe. NTD conserves the initial hybridization proportions of the targets which, at low temperatures, is reigned by the concentration of the competing targets in solution. Hence, we are able to access the composition of the sample, which is a crucial step to quantitative analysis.

To obtain a better understanding of the differences between data obtained from equilibrium and from non equilibrium thermal denaturation studies, the influence of one experimental parameter, the temperature scan rate, will shortly be discussed.
Experiments under NTD conditions usually have the following protocol:

1. Hybridization of target DNA over a certain time period either under static conditions or in the presence of a steady flow.

2. Washing the chip with rinsing buffer to eliminate excess target DNA.

3. Under continuous flow of washing buffer, a temperature scan is started, from the hybridization temperature to a maximum temperature adapted to the stability of the DNA duplexes on the surface. At the maximum temperature, all targets are dissociated and the surface coverage equals zero.

4. For SPRi experiments, a second temperature scan with the same scan rate and temperature range is performed to acquire the background signal due to the temperature change and the corresponding change of the refractive index (see appendix 8 for details).

The hybridization signal determines the initial condition of the following analysis. For oligonucleotide experiments, DNA is injected at 250 nM, our standard concentration that is sufficient to saturate the surface grafted DNA in about 8-10 min under normal buffer conditions. Therefore we consider hereafter an initial surface coverage of $\theta_0 = 1$.
To analyze DNA melting curves in out-of equilibrium conditions, we have to solve the following equation:

$$\frac{d\theta}{dt} = -k_{\text{off}}\theta \rightarrow d\ln\theta = -k_{\text{off}}dt \tag{4.17}$$

To obtain the temperature dependence of the dissociation rate we consider the temperature dependence of the equilibrium constant for a given DNA probe-target pair:

$$K(T) = \frac{k_{on}}{k_{\text{off}}} = \exp\left(-\frac{\Delta G}{RT}\right) = \exp\left(-\frac{\Delta H - T\Delta S}{RT}\right) \tag{4.18}$$

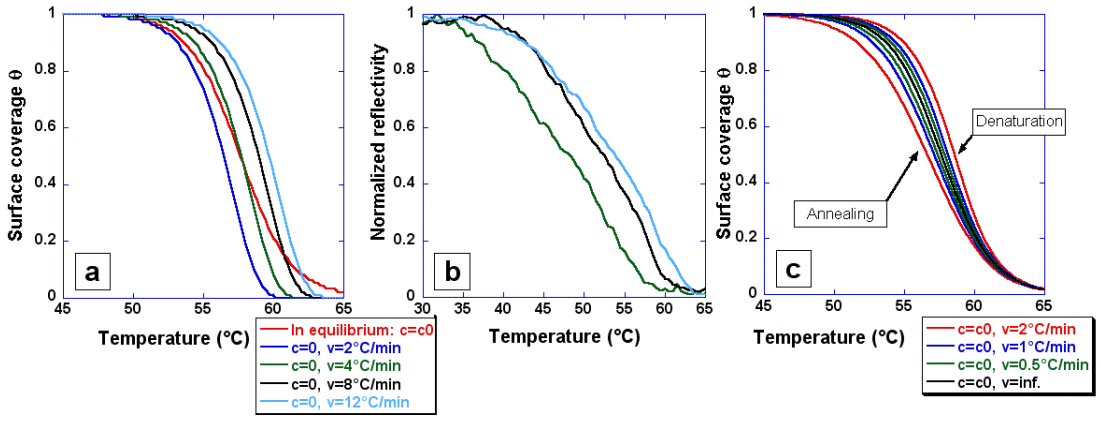

Figure 4.12: Comparison between equilibrium and non-equilibrium thermal denaturation curves. a) Numerical calculation of denaturation curves for different speeds of the T-scan and $c_t = 0$. For comparison, the equilibrium value at every temperature is plotted in red. b) Experimental results for different T-scan rates v_i for Ac20 on its complementary spot A. c) Prediction of the influence of the temperature scan rate on DNA equilibrium melting curves at constant DNA concentration. While for infinitesimally slow T-scans equilibrium is reached, the perfect matched duplex of Ac20 on A16 shows increasing hysteresis with increasing scan rate.

We then find $k_{\text{off}}(T) = k_{on} \exp(\frac{\Delta H - T\Delta S}{RT})$. By substituting $dt = \left(\frac{dt}{dT}\right) dT = \frac{1}{v}\text{dT}$, with v being the temperature scan rate in K/min, we obtain:

$$\ln \frac{\theta}{\theta_0} = \int -\frac{k_{on}}{v} \exp\left(\frac{\Delta H - T\Delta S}{\text{RT}}\right) dT \tag{4.19}$$

The temperature dependent surface coverage is numerically solved by Mathematica 5 [137].

For time dependent equilibrium melting analysis, we parameterize equation 4.1 for the surface coverage as a function of time, determined by the time dependent temperature profile.

$$\frac{d\theta(T(t))}{dt} = k_{on} c_t \left(1 - \theta(T(t))\right) - k_{off}(T(t))\theta(T(t)) \tag{4.20}$$

The association constant k_{on} and the target concentration c_t are considered constant at all times. In thermodynamic equilibrium, the result matches again the Langmuir isotherm with $\theta = \frac{Kc_t}{1+Kc_t}$.

In figure 4.12, we see a comparison of simulated and experimental NTD curves. We find that the temperature at which the target dissociates is shifted to higher values with increasing temperature scan rate. This demonstrates, that the dissociation temperatures for a given target-probe duplex will always depend on the experimental conditions. For comparison, the equilibrium melting curve for the same DNA duplex is plotted in figure 4.12a. We see that the equilibrium melting curve is broadened compared to NTD curves. However, while simulated NTD curves show a fast transition, the experimental curves, although reflecting the shift toward higher temperatures, are broadened. Note that for clarity of presentation, two different temperature scales have been chosen for figure a and b. The large transition on experimental NTD and melting curves is frequently found on biochip experiments and can here partly be attributed to probe length dispersion on poly-pyrrole grafted DNA chips [13, 138, 139, 116].

The effect of the temperature scan rate on equilibrium melting is considerably different. Figure 4.12c presents the surface coverage theoretically observed during one heating and cooling cycle of Ac20 on A16. Fast temperature scan rates provoke hysteresis of the curves. Annealing then takes place at lower temperatures than dissociation. The slower we perform the temperature scan, the closer we are to thermodynamic equilibrium at all points in time. Only for infinitely

slow temperature scan rates, thermodynamic equilibrium is reached and we find in this case the Langmuir isotherm. It should however be noted, that the Langmuir model reflects a simplified case, not taking into account any mass transport toward the surface other than diffusion of free, small molecules. An increase of the association rate, for example, due to higher target concentrations or improved mass transport towards the surface reduces hysteresis at a given temperature as controlled by simulations with varying k_{on}.

4.5 Equilibrium melting studies on solid supports

4.5.1 General considerations on equilibrium melting curves

Fundamental studies on DNA duplex stability and thermodynamics are traditionally carried out with free DNA in solution in thermodynamic equilibrium. DNA is then studied by UV-measurements based on the absorbance of the nucleotides at 260 nm, by nuclear magnetic resonance (NMR) or by calorimetric methods (see for examples publications from the group of J. SantaLucia [32, 35, 36, 34, 33, 37, 25] or R. Owczarzy [140, 141, 142] and [143]). More recently, fluorescence assays in thermocycler PCR amplification systems have been used to study the helix-coil transition of amplified DNA [144, 145, 146]. Systematic melting analysis of a huge number of oligonucleotides permitted to establish the nearest neighbor parameters for all possible combination of base pairs in the double helix including mismatches and dangling ends. The thermodynamic data is collected in databases and is at the basis of steadily improved predictions for melting temperatures, secondary structures etc. for any possible DNA sequence [147]. It should be mentioned that not only temperature induced DNA melting may be used for DNA stability studies, but some groups also put forward other methods, e.g. based on chemical gradients or force induced DNA melting by pulling on a DNA helix fixed between a surface and a cantilever or a bead in an optical trap [148, 149]. Since different groups studied DNA melting with different methods and analysis protocols, there are some discrepancies in the literature concerning the definition of the melting temperature [150]. We adopt here the definition of the melting temperature at the midpoint of the melting transition, with half of the DNA in the hybridized state, which finds its counterpart in solid-state experiments, where surface hybridized DNA is considered.

The determination of DNA melting curves still presents a powerful method for various applications, especially the detection of DNA mutations. So, today, multiplexed commercial systems are available using fluorescent analysis to determine real-time DNA melting curves, like the LightCycler 480 by Roche Diagnostics, for example, but also on-chip techniques are now emerging [151, 152, 153, 154].

Melting curve analysis is, however, not restricted to DNA in solution and today several integrated heating or denaturing systems are available that permit to obtain melting profiles on DNA microarrays. To date, most experiments studying melting curves on microarrays use fluorescence analysis on gel pad microarrays. Polyacrylamide gel pads are used to immobilize DNA in the 3D matrix and fluorescent labeling is then used as signal transducer. Several studies hereon are published by the group of P. Noble, like for example, Urakawa et al. analyzing the influence of formamide on melting curves obtained on a set of oligonucleotides bearing mismatches at position 1 to 5 from the 5' end during rinsing in a stringent buffer with low salt concentration [139]. A similar microchip technique is used in the group of A.D. Mirzabekov, and so Fotin et al. provided corrections of the thermodynamic parameters enthalpy H, entropy S and Gibb's free energy G for on-chip experiments [155]. These corrections are integrated in the prediction tool HYTHER [41]. Canadian researchers at the laboratory of U. Krull used DNA grafted covalently to an optical fiber in combination with fluorescent labeling to study solid-phase melting curves. The system is first characterized by Piunno using A·T duplexes of 20 bases and Watterson et al. then compare bulk and surface hybridization for different grafting densities and retrieve the van't Hoff's enthalpy from melting temperatures at different salinities [156, 136]. It is important to mention that those techniques working with fluorescent labeling at elevated temperatures need to take into account

the fluorescent yield of the fluorophore at each temperature [77]. Since many fluorophores are less efficient at elevated temperatures, the signal needs to be corrected. Moreover, it has been shown that fluorescent labeling, depending on the dyes and spacer chains employed may alter the free energy associated to DNA duplex formation [157], so that investigation of DNA thermodynamics for on-chip experiments should also use label-free techniques in order to study exclusively thermodynamic changes due to interactions between the DNA and its support. As a rare exceptions, Biswal et al. proposed a label-free melting curve detection system based on the deflection of microcantilevers [158], and Peterlinz et al. obtained melting curves by washing the biosensor surface with heated buffers using Surface Plasmon Resonance (SPR) detection [103]. With the increasing interest in nanoparticles and their application in biology, melting transitions have also been measured for DNA, immobilized on the surface of gold nanoparticles, for example [159]. While most systems have a time dependent temperature profile, some experiments on spatial gradients have been published. Zhu et al. used temperature gradient gel electrophoresis to determine point mutations in RNA [160]. Using microfluidic devices, several other temperature or chemical gradient mediated DNA melting analysis have been reported [161, 162, 163]. Erickson et al. provided a theoretical study of the formation of melting curves in a microfluidic device with stable spatial temperature gradient [164]. Interesting for integrated and miniaturized systems is also the flow rate dependent analysis of DNA melting transitions in microchannels as studied by Nagata et al. [165].

Melting analysis of surface bound DNA is an important tool for the understanding of DNA surface interactions. While DNA thermodynamics in bulk experiments are rather well understood, surface hybridization can be very different and thermodynamic parameters are altered due to molecular interactions. This issue has been critically noted by R. Levicky who solicited further experiments on solid phase hybridization to gain insight and control for microarray applications [8]. We have already seen in section 4.3, that immobilization method and especially the grafting density influence the DNA duplex stability. Well chosen immobilization chemistry must be able to avoid interactions between nucleotides and the substrate, and diluted grafting densities will avoid probe-probe interactions, excluded volume interactions and electrostatic attraction or repulsion that affect hybridization. However, some effects can not be avoided by changing the immobilization strategy. This is especially true for the accumulation of negative charges on the surface due to the polyanionic DNA molecule. We have already seen in the theoretical introduction of the Langmuir model, that surface bound DNA will always attract cations from the salt in the buffer to screen out the repulsive electrostatic interactions. The exact regime then depends on the probe density and the buffer's salinity.

4.5.2 Salt effects on poly-pyrrole grafted DNA chips

For this study, we used the temperature regulated SPRi system to acquire equilibrium melting temperatures on poly-pyrrole grafted DNA. Before discussing the actual results, we will make some general remarks explaining the experimental difficulty of this exercise. We want to obtain DNA denaturation and annealing curves in dependence of the buffer's salinity. We therefore need to place ourselves in conditions that allow thermodynamic equilibrium of surface hybridization at all times. To check this condition, we perform heating and cooling cycles at controlled temperature scan rate and check DNA curves for superposition. To regenerate the DNA chip completely in presence of target DNA in solution, we need to go to higher temperatures as compared to NTD curves (compare figure 4.12). So, using the ASO-CCND1 probes with 16 bases the chip is heated to 75°C repeatedly and stays at elevated temperatures for long periods. But long periods at high temperatures increase the risk of air bubble formation which disturbs the data acquisition. All buffers, including the one prepared for DNA injection, have thus been carefully degassed.

First experiments were carried out using static conditions, i.e. no flow is applied during the temperature scan. Under these conditions, we do not reach thermodynamic equilibrium. During cooling, the initial hybridization level is not regained and we observe a hysteresis. As it turned out, the annealing process is penalized mainly by insufficient mass transport. So, to improve

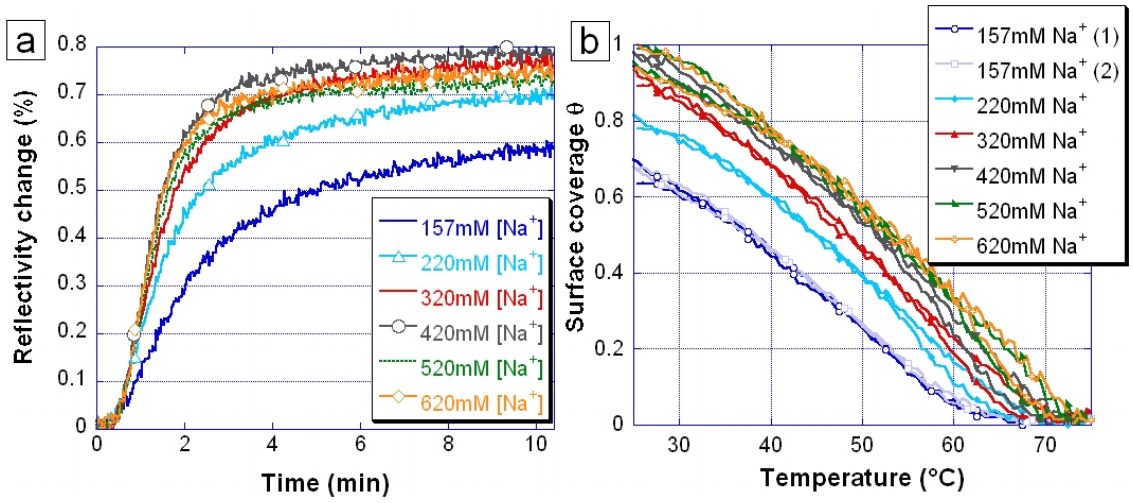

Figure 4.13: a) Hybridization of 250 nM DNA to complementary spot G16 in various concentrations of monovalent cations [Na^+]. b) Melting curves obtained in different salinities. For 157 mM [Na^+], signal reproducibility is shown.

the situation without decreasing further the scan rate of 2°C/min, agitation of the solution was applied during temperature scans. The automated syringe pump pushes the liquid back and forth without any net flow. In this way, we were able to establish thermodynamic equilibrium over most of the temperature range considered. This can be seen in figure 4.13b. Only one region, near the onset of annealing at high temperatures is perturbed and shows a slight opening. It must however be noted, that this region is possibly affected by temperature hysteresis due to the fast change of the set point at T=75°C and thus the change in power supply to assure temperature automation by the PI-temperature controller. Since heating and cooling do not take place by the same heat exchange pathways, we suggest that these high temperature perturbations can be the result of higher uncertainties in the temperature measurement (see considerations in figure 3.4b). We suppose the DNA to be in thermodynamic equilibrium for all salt concentrations studied. The curves show also a good reproducibility as can be seen from the two different temperature scans at 157 mM [Na^+] in figure 4.13. The curves have been set to their hybridization fraction at the onset of the temperature scan with normalization applied to the whole heating and cooling cycle simultaneously, so that any differences in heating and cooling would be conserved. The initial hybridization fraction of 220 nM has been corrected for melting curve analysis by ∼12%, since a systematic error occurred upon hybridization increasing the apparent hybridization signal.

To evaluate the salt effects on DNA stability, we have easily accessible parameters: the equilibrium hybridization surface coverage and the melting temperature. In figure 4.13, we see that hybridization efficiency decreases with decreasing salt concentration of the buffer. In absence of ions, for example in deionised water, no hybridization signal can be detected upon DNA injection. The salt concentration influences the affinity of the target for the probe and with increasing importance of electrostatic repulsion between the two partners, duplex formation is penalized. However, salt effects have a logarithmic behavior and thus provoke strong variations only in low salt regimes and become insignificant for hybridization and melting at elevated salt concentrations of $\geq$ 400 mM NaCl. For our grafting density and the hybridization temperature of 25°C, 400 mM salt is the ideal concentration to suppress electrostatic interactions without unnecessarily decreasing the specificity of probe-target interactions. In figure 4.13b, we observe that the stability of the probe/target duplex is shifted toward higher temperatures with increasing salinity. This shift is characterized by the melting temperature which gives access to the thermodynamics of the system. Figure 4.14a shows the melting temperatures in dependence of the salt concentration. The salt concentration affects the entropy change upon target hybridization, but does not affect the

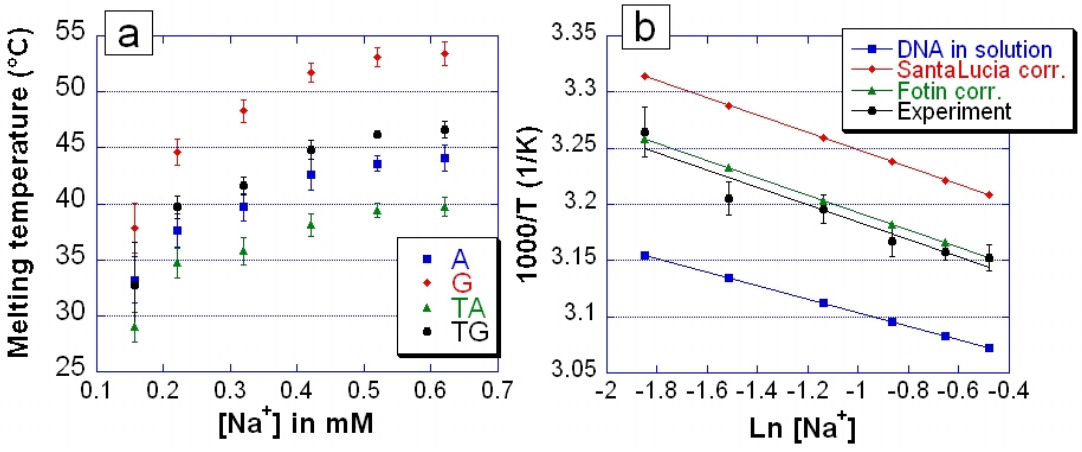

Figure 4.14: a) Melting temperatures obtained on all probes at different salt concentrations. b) Plot of $1/T_m$ versus Ln(Na^+). From the linear variation, enthalpy and entropy can be calculated. The results for probe A hybridized to Gc20 are compared to predictions for DNA in solution, Fotin's biochip corrections [155] and SantaLucia's biochip correction implemented in Hyther [41].

enthalpy change. We have already seen the empirical salt correction established by SantaLucia in equation 2.6. When we insert this equation in the expression for the melting temperature 2.4 and take the inverse, we obtain:

$$\frac{1}{T_m} = \frac{1}{\Delta H}\left(\Delta S^0\,(\text{unified oligo, 1M NaCl}) + R\ln(c_T) + \gamma\frac{N}{2}\ln\left([Na^+]\right)\right) \tag{4.21}$$

N represents the total number of phosphates in the hybridized duplex. In the case of our target Gc20 that is centered on the 16 bases long probes with one terminal mismatch at the 3' end and a 5' dangling end, we determine N=35. By plotting $1/T_m$ versus ln[Na^+], we thus obtain a linear dependency. Two conditions will alter the thermodynamic parameters so that they do no longer correspond to the standard ΔH andΔS of the NN model. One is the entropy salt correction as mentioned above; the other is a biochip correction of the thermodynamic parameters. When we consider the thermodynamic parameters of each sequence to be the same as for DNA in solution, we can obtain a 'biochip' salt correction γ as analog to the value of 0.368 for DNA in solution. When calculating γ for the different PM or MM duplexes, we obtain values between 0.73 and 0.44 with the highest value for the most stable, perfectly matched duplex. No universal, sequence independent parameter can be found and with the values determined, salt effects on biochips would have a similar, but slightly higher correction of entropy change than established for DNA in solution. In figure 4.14b, we compare our experimental data of target Gc20 on probe A16 to predictions from the literature using SantaLucia's salt correction. It gets clear that, while the slopes due to the variation of salinity are comparable, the absolute melting temperatures observed on our poly-pyrrole modified surface are considerably lower than those for DNA in solution. So, the second approach which includes a biochip correction of both, ΔH and ΔS, will be considered. For simplicity, we suppose the salt correction parameter γ =0.368 as in solution. We then can extract thermodynamic parameters for our sequences in the solid-phase experiment as shown in table 4.1. Figure 4.14b also represents inverse melting temperatures predicted for our sequences after application of the biochip correction based on the data of Fotin and their recalculated values by J. SantaLucia [155]. The represented duplex seems to match Fotin's correction, but doing the same comparison with the other sequences reveal this finding to be random. Since Fotin's experiments are carried out in polyacrylamide gel pads used for DNA immobilization, we can not expect the 3D matrix to be equivalent to our planar microarray. Differences can be seen from the thermodynamic parameters, which do not undergo in our case a simple additive correction

as applied by Fotin et al.. No fit was done on the 3 parameters ΔH, ΔS and γ simultaneously, since we only have two equations from slope and intersection and results would be rather prone to errors.

It gets clear from this first analysis, that the knowledge of the melting temperature is insufficient to retrieve valid predictions of the on-chip melting behavior. A better approach should take into account the melting curves containing relevant information on the surface hybridization process. Surface hybridization models must be used, and we will try to evaluate the data by applying the Langmuir salt corrections introduced in section 4.2.2.

Since the model distinguishes several regimes, we have to determine which one corresponds to our experimental conditions. Let us make some considerations on the relevant length scales in our setup.

- **Thickness of the surface grafted DNA layer:** to access the layer height, we determine the average length of the surface grafted DNA. In its single stranded form, the DNA chain is very flexible and we use the Flory radius to determine its average end-to-end length $l = aN^{3/5}$ with $a \cong 0.6 - 0.7\,\mathrm{nm}$, the average size per base. We obtain an average length of $\sim$5 nm. When DNA is in the single stranded helical form, we get a length of about 0.37 nm per base and thus find an average probe length of 10 nm. In the hybridized state, 16 bases will be in double helical form while the rest stays single stranded. As we have already seen, in the double helix we have 0.34 nm per base, thus in total we obtain a length of 8-10 nm depending on the random coil or single stranded helical form of the spacer chain. For the ss and ds helical state we have to consider further that the chain is not necessarily upright, but able to rotate in the semi-space due to flexible anchoring. The average height is thus the previously determined length divided by 2. We so obtain an average layer thickness of $\sim$5 nm for all configurations which is consistent with 4.8 nm determined by neutron reflectivity studies on ODN monolayers of 25 bases [104] and other methods [135]. Note that we consider the height as constant, although the layer of DNA chains might 'swell' in environments of low ionic strength [166]. Also the persistence length of dsDNA and thus its effective length is a function of cation concentration (see [167] and references therein).

- **Surface grafting density:** the poly-pyrrole spots are prepared at the grafting density d_p corresponding to electrospotting of 10 µM pyrrole modified DNA in 20 mM pyrrole monomers. Our probes consist of $N_p = 1 + 10 + 16$ bases with anchoring base, spacer and probe sequence, respectively. Considering a grafting density d_p of 5 pmol/cm^2, we find an interchain spacing of d$\cong$4 nm. This size is comparable to the average length of probes and we thus are located at the border between brush and mushroom regime as defined in section 4.2.2. From the grafting density, we can access the number surface charge of the unhybridized layer $\sigma_0 = N_p/d^2 = N_p \cdot N_A \cdot d_p = 8 \times 10^{17}\,\mathrm{m}^{-2}$, with N_A the Avogadro constant and N_p the total number of charges in the probe. When the surface is partially hybridized, we find the surface charge number $\sigma = \sigma_0(1 + \frac{N_t}{N_p}\theta)$ with $0 < \theta < 1$. Note that these considerations neglect any phenomenon of counterion condensation or osmosis on DNA which would reduce the effective charge seen by free ions in solution [38, 168, 169].

- **Electrostatic length scales: Debye screening length and Gouy-Chapman length.** The Debye screening length defines the distance over which the electrostatic potential decays. It is defined as $r_D = 1/\left(\sqrt{8\pi\, l_B\, c_s}\right)$ with c_s the salt concentration and $l_B = e^2/(4\pi\epsilon_r\, k\, T)$ the Bjerrum length. $\epsilon_r \sim 80$ is the dielectric constant of water, e the electron charge, k the Boltzmann constant and T the temperature. At room temperature, the Bjerrum length evaluates to 0.7 nm in water. The Debye screening length depends on the buffer's ionic strength and lies between 0.34 nm at 1 M NaCl and up to $\sim$10 nm in low salt concentrations. For a uniformly charged surface the diffuse layer of counter-ions formed to screen the charges is characterized by the Gouy-Chapman length $\Lambda = 1/(2\pi\, l_B \sigma)$, which depends on the surface charge number as defined earlier and thus on the chip preparation. In our case, $\mathbf{\Lambda}$ =0.2 nm.

To evaluate our equilibrium melting curves in the extended Langmuir model, we have to place our experiment in the correct regime. Considering the probe density and the estimated height

For target Gc20		$1/T_m$ vs. ln[Na^+] plot		DNA in solution		High salt regime	
Probes	# MM	ΔH	ΔS	ΔH	ΔS	ΔH	ΔS
G16	PM	-77.7 ± 10.4	-203.0 ± 30.5	-128.4	-346.5	-21.0	-32.7
TG16	1 MM	-97.3 ± 13.8	-270.5 ± 41.9	-116.7	-319.2	-25.4	-47.9
A16	1 MM	-92.1 ± 16.7	-256.5 ± 50.8	-107.3	-296.4	-30.3	-64.1
TA16	2 MM	-87.6 ± 11.8	-246.1 ± 36.5	-108.6	-309.6	-37.4	-118.6

Table 4.1: Thermodynamic parameters extracted from salinity melting studies: enthalpy ΔH in kcal/mol and entropy ΔS in cal/(mol $\cdot$ K) from linear fits based on plots or predictions as indicated.

H of the charged layer, we find $\Lambda/H = 0.04 \cong 1/(8\pi)$. Our results fall on the border between mushroom and brush regime as estimated from the interchain distance before. We further have to control if we are in the salt screening regime and thus if $\Lambda/H > (r_D/H)^2$, which is the case even for the lowest salt concentration of 157 mM [Na^+]. We now consider our results in the salt screened brush region where the charges of the polyelectrolyte are screened mainly by salt ions penetrating into the polymer brush from solution. We use the previously obtained equation for the surface coverage in the high salt regime:

$$\frac{\theta}{c_t\,(1-\theta)} = K \exp\left(-\Gamma_{ss}\,(1+\alpha\theta)\right)$$

where $\alpha = N_t/N_p$ takes into account the unequal length of target and probe. We take the logarithm of the equation and rewrite it in the following way:

$$\ln\left(\frac{\theta}{(1-\theta)}\right) + N_t \frac{c_p}{c_s}\,(1+\alpha\theta) = \ln c_t - \frac{\Delta H}{RT} + \frac{\Delta S}{R} \tag{4.22}$$

where $c_p = \sigma_0/(N_A\ H)$ represents the probe base concentration of the unhybridized DNA layer, c_t is the target concentration and c_s is the salt concentration in M. In the limit of $c_p = 0$, the model reduces again to the Langmuir model. When we consider surface grafting densities from 1-10 pmol/cm^2 and DNA charged layer thicknesses of 5-8 nm, c_p lies in the range of 0.034 and 0.54 M. When we plot the left hand side of the equation versus the inverse of the temperature at each salt concentration, the curves yield a linear dependency. All curves should collapse for one distinct value of c_p that is characteristic for our experimental chip conditions. Then, we are able to obtain the corresponding thermodynamic parameters ΔH and ΔS by linear regression.

To obtain the best value for c_p, the left hand side of the equation is calculated for the normalized reflectivity data that reflects θ at each temperature. Only the regions with $\theta = 0$ had to be excluded since no logarithm can be reasonably taken. For all other points, the standard deviation is calculated at each individual temperature and for every salinity in dependence of c_p. Then, all standard deviations are averaged yielding a function of c_p that can be analyzed. The function is minimized numerically to determine $c_p^{optimum}$, the parameter that causes the curves to collapse. The error is determined by calculating the differences between $c_p^{optimum}$ and the two c_p values that yield two times the function value found at $c_p^{optimum}$. Thus a sharp minimum gives rise to small errors while a broad curvature would yield larger errors. With the knowledge of $c_p^{optimum}$, we can plot the curves to reveal the quality of the collapse and determine the validity of the salt regime chosen for our analysis. All calculations are carried out by a program developed in Mathematica.

The optimal parameter c_p determined by this method is $c_p^{optimum}$ =13$\pm$1 mM. As expected, we find no sequence dependence of this parameter which should only depend on the surface preparation, that is, the grafting density and the height of the charged layer. The optimum c_p causes all results of the four DNA probe sequences to collapse. In figure 4.15a, we see the experimental curves collapsed using this optimum parameter. The collapse confirms the validity of the model we applied. When we go back from the optimum c_p value to the number surface charge σ_0, we find that there is a factor 20 between calculation and fitted parameter. This is astonishing, since the back calculation of the surface grafting leads to a 20 times diluted grafting density, which

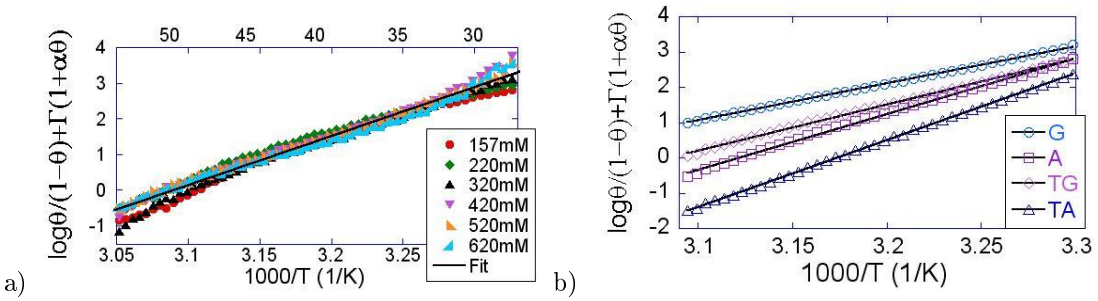

Figure 4.15: Superposition of the melting curves with one adjustable parameter c_p. a) Collapse of curves for Gc20 on TG with c_p=13 mM. b) Fit of collapsed melting curves for all analyzed probes hybridized to Gc20.

would place us closer to the mushroom regime. However, we should remember that the model we applied is not an exact determination, which would be derived from the Poisson-Boltzmann relation, but is an approximation. Also, there could be an effect of our electro-chemical grafting method, which can give rise to residual positive charges in the poly-pyrrole layer that reduce our effective σ_0. Repetition of the salinity experiment with heating to 70°C on thiol grafted probes at 10 µM and 50 µM yielded a c_p value of 39 mM and 0.53 mM, respectively. These parameters are obtained only from salinities ≥420 mM, since lower salinities displayed hysteresis and thermodynamic equilibrium is thus not reached. The three curves can however be considered as relevant since the melting temperature increases still significantly when passing from 520 mM to 620 mM Na^+. The c_p values are consistent with higher charge densities on thiol modified DNA surfaces and in the same order as found on poly-pyrrole modified DNA chips. A possible verification of the probe base concentration c_p could be done by hybridizing one probe to targets of different lengths. Since σ_0 is related only to the probes, the curves should collapse for the same c_p.

In figure 4.15b the average values of each salt concentration and each duplex is used for linear regression permitting extraction of the entropy and enthalpy change associated with duplex formation in our model. The thermodynamic parameters are given in table 4.1. Although these parameters reflect the different duplex stabilities for complementary and mismatched duplexes, we immediately note that the thermodynamic parameters neither are of the same order than unified NN parameters, neither do they have the same evolution with duplex stability, i.e. in the NN model, ΔH and ΔS decrease with decreasing stability, while we obtain an increase in the framework of the modified Langmuir analysis. As mentioned in section 4.2.2, our parameters do not have the same reference state as the NN model. To combine the parameters, we would need to know the thermodynamic parameters for uncharged chains. Hence, we can not directly compare the thermodynamic parameters to other models, although we would expect the tendencies to be conserved.

The whole analysis of the data reveals that although various models address the subject of salt effect on DNA surface hybridization, no satisfying predictions can be determined from their application. Biosensor surfaces are much more complicated than the assumptions in existing models. Further work will be necessary and it is quite impossible to imagine an integral theory that would apply to all kinds of substrates, grafting chemistries and experimental conditions.

4.5.3 Discussion of salt effects on the stability of DNA

The previously presented results might seem to give no concrete information, so that I will profit here to make a small resume of what we learned from these experiments. First, we have seen that mass transport to and from the surface plays a crucial role for establishing favorable conditions for hybridization. This is not only true in the case of equilibrium melting curves of short ODN, but can be generalized for microarray hybridization experiments which need a constant flow of targets to the surface to achieve optimum hybridization kinetics. To this purpose, a lot of work is

carried out in the field of microfluidics and chaotic mixing of solution by various groups [170, 171]. This is especially important in the case of bigger targets with comparatively slower diffusion as discussed later on in section 5.1.4. Second, we have learned in this section that DNA stability is influenced by the presence of the surface as compared to bulk experiments. We have especially seen that in the case of our setup, the melting temperature is lowered by several degrees compared to predictions from the NN model. So, thermodynamic predictions can not be applied directly to surface grafted DNA. Moreover, not only the grafting chemistry but especially the grafting density will influence this shift as suggested also by data presented earlier in section 4.3. Further, we argue that existing biochip correction by Fotin et al. on gel pads represent only a special case and should not be applied to different biochip environments without control of validity. Third, our data shows the influence of the buffer's salt content on hybridization and melting on DNA chips. We show that for concentrations below 400 mM NaCl, the hybridization kinetics is slowed down and it is preferable to work in higher salt concentration to diminish any hybridization penalization. However, one should be aware that too high salt concentrations are prone to decrease the target specificity. We show on the melting curves that the salt correction empirically found for DNA in solution can be, approximately, applied to the prediction of the salt induced shift of the melting temperature on chips. Current models, however, do not allow us to establish universal correction parameters. This would also need a much bigger diversity of probe/target duplexes than available for this study.

Traditionally, DNA stability and the salt dependency have been studied in bulk experiments and a collection of the various sequence dependent or sequence independent salt corrections can be found in [39] and references therein. Several theoretical investigations and experimental approaches have been undertaken to elucidate the behavior of charged DNA layers (poly-electrolyte brushes), the influence of the substrate and the DNA stability on a solid support [172, 173, 166, 135, 103, 136, 156]. Our findings on salt induced stability changes for surface grafted DNA can so be compared qualitatively to data from the literature. Globally, all experimental data on surface tethered DNA suggest that the salt variation observed is in good agreement with the findings in bulk experiments. There is, however, diverging information of whether surface tethered DNA is more stable or less stable than in solution. Vainrub and Pettitt developed a model for neutral or charged dielectric or metal substrates in different salt concentrations [173]. On metal surfaces, they find a distance dependent stabilization of the DNA duplex, presented as a shift of T_m toward higher temperatures. Using an electrochemical approach to obtain melting curves, Meunier-Prest also observes stabilization of the duplex when immobilized on a gold electrode as compared to melting in solution [135]. This could be produced by the charging of the metal surface. Contrarily, Peterlinz et al. report a decrease of about 5°C of the melting temperature for surface anchored DNA. Also Watterson and al. report this trend with a sensibly decreased melting temperature especially at high grafting density. Also DNA immobilized in gel pads show a decreased affinity as already shown for the data of Fotin. Recently, Gong and Levicky studied the effects of salt concentration and probe density on the hybridization content at a fixed temperature using an electrochemical detection [174]. They established an empirical map of different hybridization regimes encountered at different salt concentrations and different probe densities on biochips. Although this study spans only one order of magnitude in probe grafting density so that probes are always close enough to possibly interact, three different hybridization regimes have been found regarding the salt concentration. They introduce one way to compare buffer salinity and probe density using the fraction $\Pi = c_p/(1.61\, c_s)$, with c_p the probe base density and c_s the buffer cation concentration. Π is assumed to be in the order of one at the onset of hybridization and hybridization occurs at values below this threshold. Further, in the extended Langmuir model, Π is proportional to the quantity $r_D^2/H\Lambda$. The corresponding probe base density obtained here by scaling of our data to c_p in the high salt regime can be used to evaluate Π. It follows that the onset of hybridization should be found for salt concentrations of 8 mM which is clearly underestimated for our data. Onset of hybridization has not been experimentally determined but should lie at salt concentrations below 100 mM. The c_p determined here is thus about one order of magnitude below experimentally reasonable values. Further investigations of salt effects on biochips are clearly needed.

For completion, it should be mentioned that, although most experiments use monovalent

cations from NaCl or KCl for charge screening divalent cations are also relevant in DNA studies. Divalent cations shield the DNA backbone more efficiently than monovalent cations and already a small concentration of some mM $MgCl_2$ as commonly used for enzyme reactions sufficiently stabilizes DNA to allow surface hybridization [175, 176].

4.6 Non-equilibrium thermal DNA denaturation on solid supports

As we learned from the previous sections, DNA equilibrium melting curves, though necessary for thermodynamic analysis, present several experimental inconveniences. Long assay times and high temperatures may be inconvenient for surface chemistries and set-ups because of air bubble formation at high temperature, for example. Also, the thermal denaturation transition gets even larger than the already broadened NTD curves on solid supports. The small slope is a hindrance for point mutation detection, making the differences smaller and less easy to distinguish. A recent review on the virtues and traps of real-time DNA microarrays has been published by Chagovetz [55]. The authors present a clear comparison of available tools and their applicability to specific, multiplex target hybridization and SNP detection. We will now concentrate on non-equilibrium thermal denaturation to evaluate relevant parameters for DNA detection on solid supports. Here, we still work with synthetic oligonucleotides, but we will see later on that our findings will help to optimize DNA point mutation detection with long DNA or RNA targets.

Point mutation detection implies that the experimental device is able to make the difference between the perfectly matched target sequence and sequences with one, two or more exchanged bases that still have a high affinity for the surface grafted probe. In the case of SNP detection, the alleles and thus the mutation that may occur is normally well identified. Hence, it is not necessary to be able to detect the exact nucleotide that substitutes the original base, but it is sufficient to detect its presence in the target. Today, DNA sequencing methods, originally developed by Sanger and co-workers in the seventies [177] have become powerful and fast and have outrun DNA microarrays for sequence identification. We will focus here on the identification of the SNP G870A codon 242 exon 4 of the protein Cyclin D1, as the bases for detection of PCR amplified DNA provided by E. Crapez from the 'Centre de Recherche en Cancérologie' in Montpellier (see the following chapter 5.2). Experiments are carried out using allele specific oligonucleotide (ASO) probes with the SNP placed in their center as shown previously in table 3.1.

We have seen in section 4.3 that under 'normal' injection conditions, i.e. at low temperature and sufficient salinity, oligonucleotide probes with mismatches hybridize as efficiently to the probes as the perfectly matched duplex. To achieve good discrimination during hybridization, stringent condition of some type will be needed that suppress affinity of the mismatched targets while keeping a good affinity for the perfectly matched duplex. One first precondition has been fulfilled by choosing short probe sequences for which the mismatch yields a substantial reduction of stability. We can now choose two strategies to achieve mismatch discrimination with our real-time SPRi data acquisition:

1. Isothermal detection using stringent hybridization and washing protocols
2. Isothermal hybridization allowing good target hybridization followed by thermal denaturation of the duplexes

While the first approach needs relatively few instrumentation and good optimization of the buffer components, the second approach promises relatively few optimization steps for the buffer, but needs well controlled instrumentation for the heating device. Since SPRi is very sensitive to temperature variations, work from other groups adopts the first strategy for SNP detection. Stringent conditions are achieved during hybridization or rinsing or both using low salt concentrations, denaturing agents, pH variations, repulsive electrical fields or similar denaturing environments. In this case, to reproduce the result, all experimental conditions must be rigorously respected since the

result is based on the analysis of isothermal hybridization during injection and DNA dissociation during rinsing. The mutation is thereby distinguished either from the calculated affinity or by suppression of hybridization of the mutant to the wild type's probe. In this work, we adopted the second approach, based on non-equilibrium thermal dissociation of DNA as already introduced. Acquisition of thermal denaturation curves should not need optimization to obtain specific hybridization signals. On the contrary, all buffers will be chosen to allow hybridization of all targets that have a sufficiently high affinity for the probe, such as targets with one or two mutations. The term 'specificity' in our case includes mutations in the target, while injection of unrelated DNA sequences should yield no detectable signal. Sequence identification will be exclusively based on non-equilibrium thermal denaturation curves and the differences in the dissociation temperatures introduced by mutations. The probe design must thus be well adapted and each prism includes several duplicates of spots complementary to the wild type and the mutant sequence. Additionally, positive controls of non-complementary DNA and poly-pyrrole spots as negative controls serve to control specificity of the hybridization. Additional probes with supplementary mutation loci may be used for reasons explained later on.
A typical NTD scan experiment will have the following protocol:

- Equilibration of the SPRi system in running buffer at neutral pH of high salt content (typically $\geq$400 mM NaCl, see the buffer table 1 in appendix A). The typical flow rate is 5 ml/h (87 µl/min).
- Initial temperature scan at 5°C/min to the maximum temperature (T_{max}) to clean the surface at the beginning of the experiment. T_{max} corresponds to the temperature at which the surface will be fully regenerated. It will thus depend on probe length and buffer and is typically 70°C $\leq T_{max} \leq$ 87°C.
- Injection of 1 ml target solution at 25°C for about 10 min to allow hybridization.
- Washing for 5 min with running buffer.
- Start of the temperature scan at typically 2°C/min up to T_{max} under continuous flow.
- After cooling down to 25°C and signal stabilization, start of a reference T-scan needed for background subtraction of global refractive index changes. The reference can be valid for several target injections in the course of one SPRi acquisition, but needs to be done under the exactly same experimental conditions as the detection scan.

Data acquisition for one point mutation detection experiment on ODN targets thus takes about 1 h 30-2 h. To extract the NTD curves, data analysis is needed in form of subtraction of the reference temperature scan. A reference spot may also be subtracted to account for global refractive index changes and so to correct the base line.

As before, the main questions of this section will be: How do we efficiently control DNA hybridization to the solid support? How can we manipulate the DNA stability with the help of buffer components and the temperature? How can we optimize point mutation detection with regards to the sensitivity of our assay?

4.6.1 DNA denaturing agents

This first subsection will be closely linked to what we have learned about salt effects. Modulation of the buffer's salt concentration revealed a logarithmic dependence of the melting temperature on the salt concentration. We will now see that there is an easier way to modify the DNA dissociation temperature, the equivalent to the melting temperature but for NTD conditions. By addition of DNA denaturing agents to the buffer, the melting temperature of DNA is generally altered in a linear way. In molecular biology, numerous solvents are known to act as denaturing agents on DNA. Typical examples are formamide, glycerol, dimethyl sulfoxide (DMSO), urea and guanidinium thiocyanate, amongst others [178, 179, 180, 148]. Although some denaturing components may

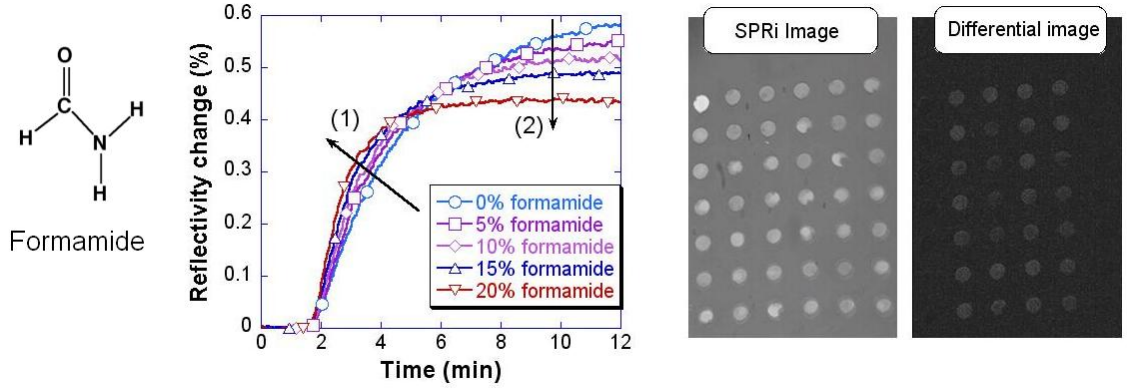

Figure 4.16: *On the left:* Chemical structure of formamide. *In the middle:* Hybridization kinetics compared for different injections of M5 on probe N (1MM). While the association accelerates in the presence of formamide (1), the total hybridized fraction on the spot diminishes (2). *On the right:* SPRi image and differential image for injection of Gc20 and M5c on a poly-pyrrole chip with ASO16 sequences and the M series (M5, M4 and N).

interact with DNA bases by hydrophobic interactions [181, 182], most denaturing agents interact with DNA by competing for hydrogen bonds (H-bonds) of the double helix. Formamide is the most common and probably strongest DNA denaturing agent. It is known for its ability to form hydrogen bonds and competes very effectively with the Watson Crick bonds [183]. The chemical structure of formamide is shown in figure 4.16 on the left. Amide functions in general have been reported to be likely to provoke DNA denaturation [155]. It has been shown that formamide lowers the melting temperature of free DNA in solution by 0.6°C [184] or 0.72°C [185] per percent formamide (volume to volume). We want to find out if formamide has the same denaturation power when DNA is grafted on a solid support and if the linear dependence is conserved. This project was initiated during the stay of Daniela Dell'Atti from the University of Florence, Italy, at our laboratory. To obtain generalizable results, we later used here both grafting methods available, i.e. thiol spotted SAMs and ppy electro-spotting.

For these experiments, the running buffer is PBS at 450 mM NaCl, 0.05% Tween20 and 1 mM EDTA and volume fractions of formamide from 0 to 20% in steps of 5%. Hybridization is carried out using targets at 250 nM suspended in running buffer for 10 min at 25°C with a flow rate of 83 µl/min. After 3 min washing, a temperature scan is done at 2°C/min up to 70°C. Since formamide destabilizes the DNA duplex, the hybridization efficiency decreases with increasing percentage of formamide in the buffer [139]. This effect is strongest on spots forming duplexes with two mismatches (MM) where less Watson-Crick base pairs are formed. At 20% formamide some probe/target duplexes with 2 MM have a signal to noise ratio below 10 and have been excluded from the thermal denaturation analysis. As we can see in figure 4.16, we observe an increased association rate k_{on} with increasing percentage of formamide on probes of the M-series. The association rate corresponds roughly to the slope at the onset of hybridization. Figure 4.16 superposes averaged data from probes N for different injections of M5c. While k_{on} increases, the total hybridization signal decreases. The denaturing agent seems to have two effects: while a fraction of probes is no longer able to hybridize to the target, probably because of a hybridizing part that does not correspond to the full length of 15 or 16 bases, the accessibility for hybridization is increased. Formamide may be able to suppress formation of secondary structures either in probes or in targets. If there are interchain interactions between targets in the bulk, they would be reduced. Similar observations are reported by Peterson et al. reporting better hybridization of mismatched targets after mild heating to 37°C which is attributed to facilitation of nucleation or conformational changes before hybridization [89]. Thus, competition between DNA structures in solution and surface hybridization is reduced and the kinetics of hybridization to the surface is

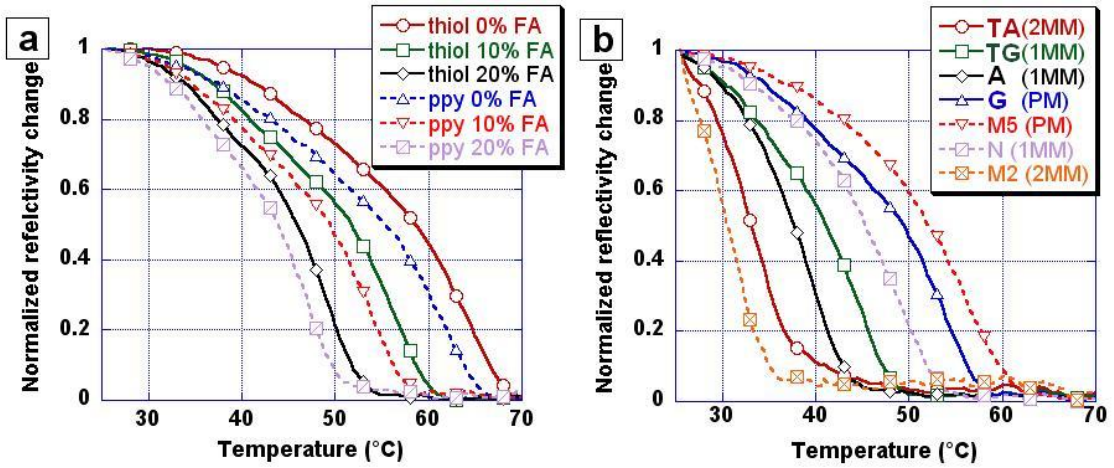

Figure 4.17: a) Comparison of non-equilibrium thermal denaturation curves observed on poly-pyrrole or thiol grafted DNA chips. While the absolute dissociation temperature varies, the destabilization with increasing volume fraction is equivalent on both grafting chemistries. b) Denaturation curves in 10% formamide observed on the ppy chip as presented in figure 4.16. We clearly distinguish each sequence from the other since mismatches decrease the denaturation temperature.

favored by addition of formamide. At the same time, formamide suppresses partial hybridization rendering the hybridized fraction more homogeneous.

To analyze the influence of formamide on the DNA helix stability, we use the dissociation temperature T_d defined as the temperature with 50% of the initial hybridization signal on the spots [139, 186]. SPRi dissociation curves are normalized to 1 and averaged over identical spots. The normalization is justified since we look at out-of-equilibrium data and no longer on equilibrium hybridization fractions. Figure 4.17a compares dissociation curves obtained for the PM duplex of Gc20 on G16 on poly-pyrrole and thiol chips. We observe higher dissociation temperatures on thiol chips compared to pyrrole grafting. This difference in T_d must be attributed to interactions between probes, targets and the substrate as a result of the immobilization method, but can not clearly be associated to one phenomenon. In spite of the differing hybridization environment, the T_d decrease due to formamide on DNA duplex stability is comparable for both grafting methods. A more precise study of the stability of mismatched DNA in the presence of formamide is also carried out. Figure 4.17b shows the dissociation curves of duplexes with 0 to 2 mismatches in 10% FA buffer. For the K-ras (dashed lines) and the CCND1 (full lines) probes, perfectly matched duplexes (PM) can be clearly distinguished from duplexes forming one (1 MM) or two (2 MM) mismatches with their targets M5c or Gc20, respectively. The addition of formamide to the buffer increases the slope of the DNA denaturation transition and thus assists the detection of mutated targets. Figure 4.18 shows measured dissociation temperatures and the standard errors on thiol and poly-pyrrole functionalized surfaces for target Gc20. Since thiol spots have a better spot reproducibility compared to poly-pyrrole spots, they lead to smaller experimental errors. T_d decreases linearly with increasing volume fraction of formamide as formerly observed for DNA in solution and in polyacrylamide gel pads by Urakawa [139]. The slope is calculated for each DNA duplex by linear regression yielding a determination coefficient of $R^2 \geq 0.98$. The calculated slopes representing the decrease of the dissociation temperature by addition of formamide are recapitulated in table 4.2.

Our results show that formamide has no significant sequence dependent destabilizing effect on the dissociation temperature and we obtain slopes from -0.49°C/% FA to -0.65°C/% FA. Urakawa et al. reported a higher T_d decrease for sequences where the mutation replaces a G/C base pair (-0.58°C/%FA) than for mutations replacing an A/T base pair (-0.52°C/%FA). It is, however, more accurate to evaluate the effect with respect to the intact hydrogen bonds in the

Poly-pyrrole grafting			**Thiol grafting**		
Sequence	H-bonds	ΔT_d per % FA	Sequence	H-bonds	ΔT_d per % FA
Target Gc20					
G16 (PM)	41	-0.59 ± 0.05	G16 (PM)	41	-0.62 ± 0.02
TG16 (1MM)	38	-0.61 ± 0.04	TG16 (1MM)	38	-0.65 ± 0.02
A16 (1MM)	38	-0.54 ± 0.02	A16 (1MM)	38	-0.62 ± 0.02
TA16 (2MM)	35	-0.49 ± 0.02	TA16 (2MM)	35	-0.57 ± 0.02
Target M5c			Target Ac20		
M5 (PM)	40	-0.63 ± 0.04	A16 (PM)	40	-0.64 ± 0.01
N (1MM)	37	-0.59 ± 0.04	G16 (1MM)	38	-0.55 ± 0.02
M2 (2MM)	34	-0.52 ± 0.02	TA16 (1MM)	37	-0.52 ± 0.01
			TG16 (2MM)	35	-0.57 ± 0.01
Mean: -0.57 ± 0.05°C per % FA			**Mean: -0.59 ± 0.05°C per % FA**		

Table 4.2: Slopes determined from linear regression to evaluate the decrease of the dissociation temperature with increasing formamide volume fraction in the buffer. Both grafting densities undergo the same change of -0.58°C/% FA.

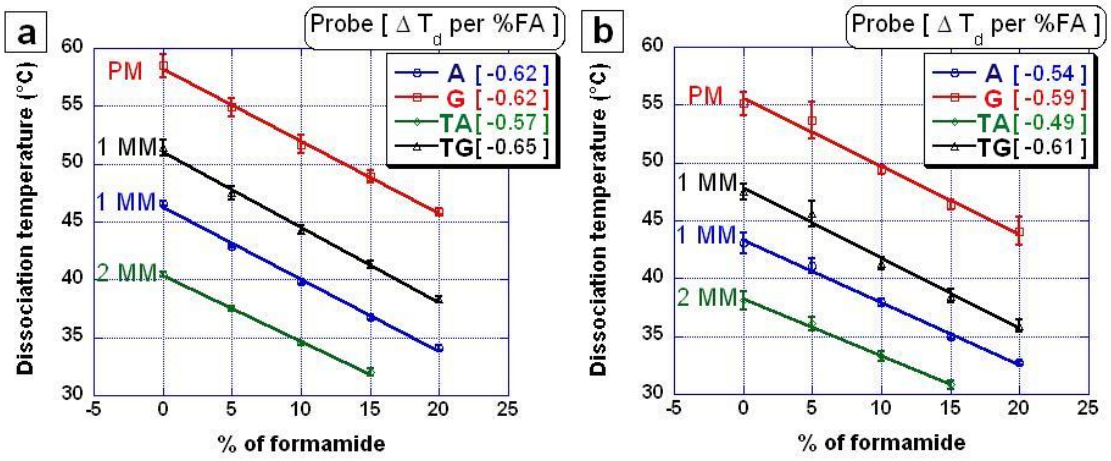

Figure 4.18: Representative fit to the dissociation temperatures observed in different volume fractions of formamide to obtain the slope as given in the legend. Data presented is obtained on ppy (a) and thiol (b) modified surfaces.

duplex since only those can be in competition with formamide. From the data of Urakawa et al. one can find a tendency of increasing destabilization by formamide with increasing numbers of H-bonds in the duplex, but the position of the terminal mismatches plays a crucial role and also large experimental errors are biasing the appearing order. Their slopes are in the range of -0.46°C/% FA to -0.63°C/% FA. In our study, no systematic dependency on the mutation type, the number of H-bonds in the duplex or the duplex sequence can be determined. Sequences with two mutations show a slightly lower response to the increase of formamide than the PM or 1 MM duplexes. This is probably related to their decreased number of H-bonds in the duplex. We find an average slope of -0.57±0.05 °C/% FA for poly-pyrrole surfaces and of -0.59±0.05 °C/% FA for thiol surfaces. There is thus no significant difference between the two surface chemistries. From Urakawa's data, one can calculate an average formamide shift of -0.56°C/% FA extending our result to another on-chip method. These values are lower than previously reported for DNA in solution since the results are obtained on immobilized oligonucleotides and for non-equilibrium thermal denaturation contrarily to equilibrium melting of long DNA chains (>800 bp) in solution. Thus, our results reflect the formamide destabilization of oligonucleotides in solid phase experiments.

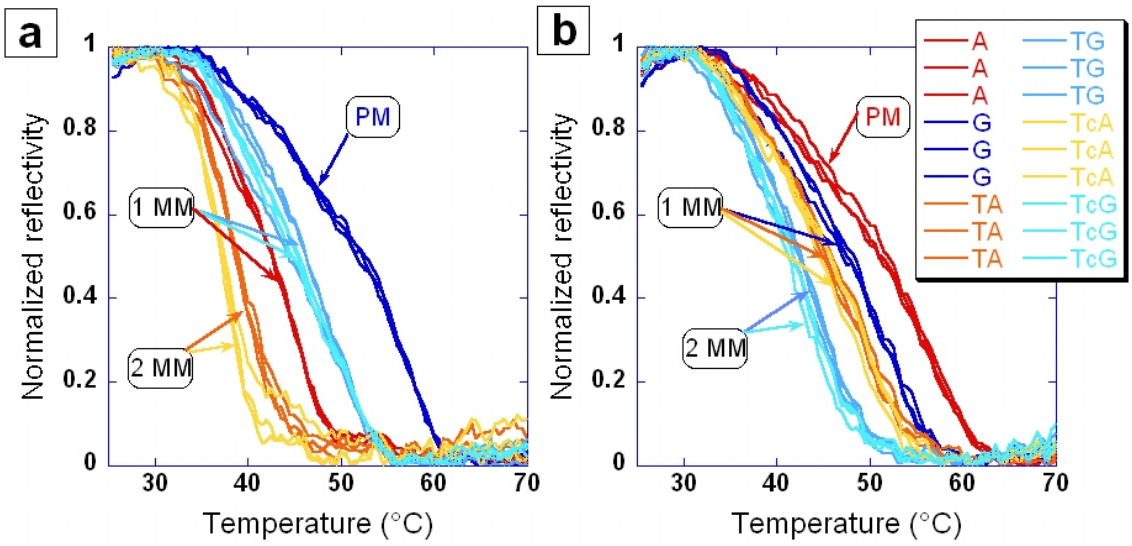

Figure 4.19: a) NTD scan as response to an injection of Gc20 at 250 nM. b) NTD response to Ac20 at 250 nM on the same prism. Mutations can be clearly distinguished by a shift toward lower dissociation temperatures.

We have learned here that formamide can help to suppress secondary structure in probes and targets and improve hybridization rates. To which extent formamide lowers the dissociation temperatures depends little on the DNA sequence, and can be fairly well approximated by an average decrease of -0.58±0.05 °C/% FA of the dissociation temperature on microarrays. Furthermore, the influence of formamide on oligonucleotides seems practically independent of the grafting method. For this reason the variation of the dissociation temperature found here can be applied to various biosensor and microarray platforms. The utility of formamide gets evident, since it may not only favor surface hybridization by decreasing other non-specific affinities or secondary structure thereby rendering the target available for hybridization, but it also increases the specificity of the surface reaction, lowering effects of probe length dispersion and providing an easy tool to shift the affinity to the optimal value. Since formamide induces a linear variation, it is easy to shift the denaturation temperature to adapted values, for example to allow the use of longer DNA probes on thiol modified targets without exceeding the heating limit of 70°C. It should be noted that the formamide effect may not be the same when samples are composed of RNA and DNA since RNA/DNA hybrids will be favored over DNA/DNA duplexes [187]. Finally, it is to be mentioned that not only denaturing agents may be employed for microarray experiments to increase the specificity of the assay, but also chaotropic agents like tetramethylammonium chloride and betain salts are available that equalize the difference of stabilities between A·T and G·C pairs [155, 188, 189]. In this way, the hybridization temperatures and stringency protocols are more easily adapted to a wide range of probes and targets. The only condition is that all probes are of equal length.

4.6.2 Point mutation detection

Physicochemical characterizations of the DNA biochip surface are an important step toward optimization for clinical applications. Although we already encountered mutations in the previous section, we will see here what challenges one has to confront in order to unambiguously identify the injected target or eventual target mixtures.

We can see in figure 4.19 NTD curves obtained after injections of 250 nM of either target Gc20 (4.19a) or target Ac20 (4.19b) on the same prism with probes of 16 bases length. Probes are complementary to wild type (G) and mutation (A) targets and may contain a supplementary mutation site at the first or second position 5' of the SNP site. For each specific target, the

complementary spots show the highest thermal stability. Going to lower dissociation temperatures, we then find duplexes with one internal mismatch. Duplexes with two mutations show the lowest affinity and dissociate at the lowest temperatures. We can see here that the method is even sensitive to the type of mismatch formed on the spot. The T·G mismatch formed on probes TG16 and TcG16 upon injection of target Gc20 is more stable than the A·C mismatch on probe A16. Contrarily, after injection of target Ac20, the T·G mismatch on probes TA16 and TcA16 are less stable than the G·T mismatch on probe G16, showing that the mutation's influence depends on the sequence context. This is in accordance with T_m predictions for the probe/target duplexes based on the nearest neighbor model as seen in section 4.2.1. It is, however, somewhat astonishing that we do not obtain a significant difference between the two targets having two mutations either at neighboring sites or with one base in between. We would expect the base flanked by two mismatched sites to be incapable of hybridization. The duplex would thus have a three base interior loop, yet we find its stability similar to duplexes with two neighboring mismatches. This is the case as well for TG16 and TcG16 hybridized to Ac20 as for TA16 and TcA16 hybridized to Gc20. Possibly, interior rearrangements take place where base stacking interactions or non-Watson-Crick hydrogen bonds may account for the stabilization. Targets with additional mutations such as TA16 and TG16 provide essentially the same information as the wild type and mutant complementary probes, but at lower temperatures which may be of advantage for experimental designs imposing moderate temperatures. The TcA16 and TcG16 probes do not provide additional information and are thus not useful in our SNP genotyping approach.

When comparing the experimental results to simulations obtained in the Langmuir model, we observe a broadening of the curves. The denaturation transition takes place over a wide range of temperature which decreases the mismatch resolution and the differences in T_d for PM or MM targets. When we compare part a and b of figure 4.19, we see that the dissociation temperature on one probe sequence changes with the hybridized target. For instance, while the PM duplex Gc20/G16 has a dissociation temperature of 52°C, it is reduced by 4.5°C to a T_d of 47.5°C when hybridized with the mutant Ac20. Differences between probes with additional mismatches like TA16 and TG16, were expected to increase their temperature difference to a greater extend. We here observe similar mismatch resolution, but on curves with higher slopes. So, from one single spot type, we are able to tell the target's genotype which would be G/G for injection of Gc20 and A/A for injection of Ac20. The double notation stands for the two possible alleles of one individual. So, when only one target type is present, we are in the homozygous case. Since for real biological samples, buffers and concentration may be less well defined as they are here for purified ODN, it is preferable to take into account the 'order' of duplex stability on the probes to identify the genotype and not only the dissociation temperature of one spot. Other criteria may use the signal at each temperature and thus take into account the s-shaped form of the curves. For example, a discrimination index defined in Li et al. reveals optimum discrimination at temperatures 5-10°C higher than the T_d of the PM duplex where the mutated target is almost completely washed off. Still, the observed order will define the genotype of the sample.

Being able to identify homogeneous samples, it will be interesting to look at target mixtures. One example of a 50%-50% target mixture of wild type and mutant is the heterozygous case with genotype A/G. In figure 4.20a, NTD curves obtained after target injection of 50% Gc20 and 50% Ac20 at a total amount of 250 nM ODN are presented. We now observe two phase dissociation on each spot. The first dissociation corresponds to the denaturation of the less stable duplex formed on one spot (1 MM for Gc20/A16 and Ac20/G16, 2 MM for the rest, accordingly). Then the signal stagnates at $\theta \sim 0.5$ before a second dissociation phase reveals the departure of the more stable target (PM for Ac20/A16 and Gc20/G16, 1 T·G MM accordingly on TA16, TG16, TcA16 and TcG16). The plateau indicates the proportions of the two targets since hybridization takes place fast with quasi identical association constants for both targets. Reorganization is essentially based on the difference of the dissociation constant k_{off} and would take infinitely long at the chosen hybridization temperature due to high affinities of both targets towards all probes. We are thus not only able to detect the presence of a mutated target in solution, but also to quantify its proportional abundance in the sample. These results show that our SPRi based temperature scan

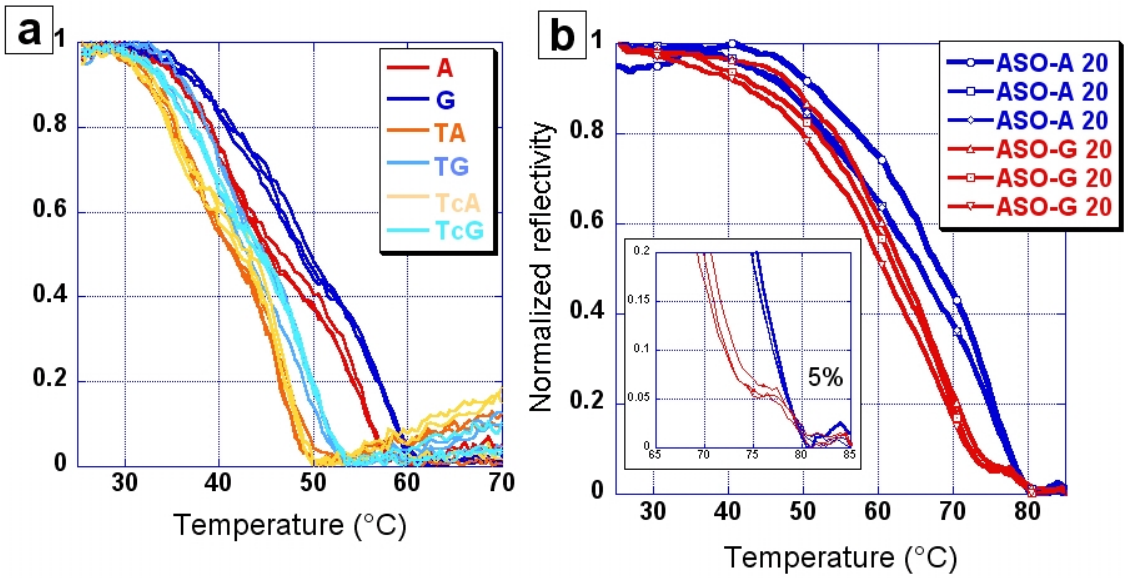

Figure 4.20: a) Detection of 50% of wild type and mutant corresponding to the heterozygous case. b) Detection of a target mixture of 250 nM total DNA, with 5% Gc-26bio and 95% Ac-26bio. It is possible to find the plateau due to the small fraction of complementary targets on spot G20.

method is a valid tool for SNP genotyping. For ODN samples, the genotypes can be categorized unambiguously. Furthermore, the method seems universal and simple to apply to other SNPs. The results presented here have already been presented by J.-B. Fiche on an SNP from the K-ras gene [112, 13]. That the method can be applied to several SNPs at one time can be seen in figure 4.17 in the previous subsection on formamide experiments. The main advantage of the approach is the absence of any sequence specific optimization. Although each probe sequences, of course, is optimized for mismatch discrimination while being sufficiently stable, there is no need for a uniform dissociation temperature for all PM targets. The hybridization temperature could even be lowered for shorter probes and the temperature scan must just be sufficiently high to denature every duplex formed on the chip. This is true in the case of ODN targets and will be later on evaluated for hybridization of long DNA targets (see chapter 5).

Since we are able to detect mutated targets in a target mixture, it will be interesting to know the detection limit of % mutated target in the overall sample. If we can detect and, better even, quantify very low percentages of mutated targets, the temperature scan method could prove useful for the analysis of biopsy samples. Biopsies are samples of tissues extracted from specific sites. The purpose is thereby often the classification of tumor tissue in benign or malignant. Since biopsies are often carried out at places in the body that are difficult to access, for example the stomach or the lung, the total extracted cell sample will contain a varying proportion of healthy cells and tumor cells. Sometimes, proportions of tumor cells are as low as one 1% of the sample. The extracted and amplified DNA will reflect the initial ratio and detection methods must thus be able to find low abundant amounts of mutated DNA in a large background.

Preliminary experiments by J.-B. Fiche showed a detection limit of 15-25% mutated target in the whole pool depending on the sequence to be detected. These limits could be further pushed to a detection limit of 5% mutated target in samples containing a total concentration of 250 nM. This is depicted in figure 4.20b, where we can see the plateau corresponding to 5% of Gc26 target on its complementary probe. The theoretically predicted initial decrease caused by 5% Gc26 on A20 can not be observed since the curves always show a steady signal drop in the expected temperature region. Accordingly, in figure 4.21b, another experimental result with this time 5% of target Ac26 is represented by the blue curve. The only conditions for the detection of the plateau are a

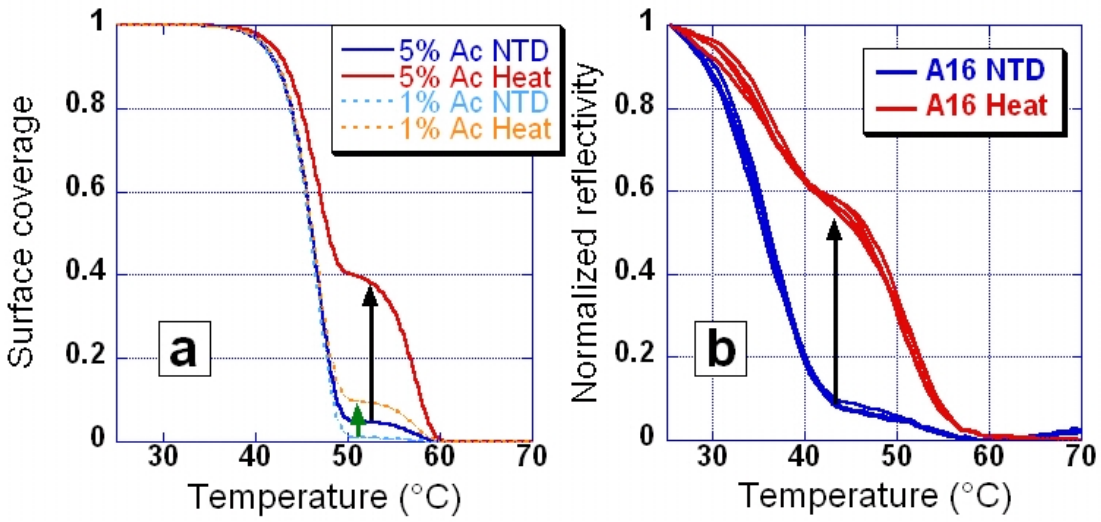

Figure 4.21: Detection of target mixtures on spot A16 with 250 nM total DNA. a) Simulations for direct NTD after hybridization (NTD) or performance of heating at 5°C/min to 70°C followed by return to 25°C at 1°C/min before NTD at 2°C/min (Heat). Full lines: 95% Gc26 and 5% Ac26. Dashed lines: 99% Gc26 and 1% Ac26. After only on heating cycle, both concentrations of Ac20 become detectable on the complementary spot. b) Experimental data corresponding to 95% Gc26 and 5% Ac26 detected on thiol probe A16 grafted at high density with (Heat) our without (NTD) heating of target solution before rinsing and NTD.

sufficiently big difference in the dissociation temperature of PM and MM target and sufficiently high hybridization signals.

While a detection limit of 5% mutated target is a low level, it is still insufficient for clinical applications. It is therefore necessary to think of more sophisticated detection protocols that will allow at the same time (at least rough) quantification of the sample composition and unambiguous detection of the presence or absence of very low percentages of mutated DNA. A two step approach to detection may hereby be suitable. Since the detection limit of 5% mutated DNA in the sample can be sufficient for quantification, a first NTD scan as the previous one would allow to tell either the proportions of the sample or classify the mutant as $\leq$5% or absent in target solution. The second step must be able to exclude or confirm the presence of mutated DNA in the sample. We propose here a strategy based on temperature cycles that will permit to accumulate the mutated DNA on its corresponding probe and thus shift the plateau in the detectable range.

To be able to predict the dynamic exchanges of targets on specific probes, a Mathematica routine is used that numerically solves the time dependent differential equation 4.7 for two targets with different affinity for one spot. A time dependent temperature profile can be chosen. To predict the affinity, thermodynamic parameters based on the NN model are used. We have seen that predictions from solution lead to higher temperatures than the actual dissociation on the biochip. This is why predictions can only be made on general dependencies and trends. Experimental protocols and temperatures can be adapted on the basis of two NTD scan with chosen buffer and either wild type or mutant target.

A first approach to minor mutant quantity detection could be the following protocol:

1. Hybridization of half of the sample to the chip followed by rinsing and NTD scan to T_{max} determining the percentage to be lower or greater than our detection limit.

2. Injection of second half of the sample at T_{max} and cooling slowly to 25°C under agitation of solution. For each individual probe sequence, first the hybridization of complementary

target will take place before coming into the range of hybridization of the mismatched target. In this way, the mutant in low abundance finds free hybridization sites on its PM probe that the competitor target can not occupy at $T_d(PM) \geq T \geq T_d(MM)$.

3. Washing and NTD scan on the second sample hybridization.

This protocol has the advantage of easy implementation to our system and assay time is optimized. In the beginning, we considered to have only one injection and perform a fast equilibrium detection scan to determine the composition of the target. It turned out experimentally that this approach is actually biased by the flattened denaturation profiles shifted to higher temperatures that do not allow a clear identification of the plateau at low percentages of mutant target. Further, simulations show that in the presence of targets, dynamic exchange will take place leading to continuous hybridization of mutant DNA to free sites on its complementary spot before reaching the T_m of this PM duplex. Quantification can thus not be achieved. Simulations of the proposed NTD assay protocol with cooling rates of 1°C/min are shown in figure 4.21a. Two cases are depicted: NTD curves obtained for first and second hybridization for a sample containing 5% Ac20 in 95% Gc20 and 250 nM total DNA (full lines, red and blue, respectively) and a target mixture of 1% Ac20 and 99% Gc20 (dashed lines, orange and light blue, respectively). We observe that in the case of 5% mutant, the second NTD scan shows the plateau at $\theta \approx 0.4$. For 1% mutant the percentage of complementary target on probe A can be increased to 10%. A cooling temperature of 1°C/min seems thus sufficient to shift even percentages of 1% in the detectable range. In figure 4.21b, an experimental result obtained on high density thiol DNA spots is shown for target solution with 5% Ac20. While the plateau is detected at 5% for the first NTD scan, after performance of the cooling scan of 1°C/min under agitation of the sample, we obtain a second NTD scan showing a percentage of about 55% Ac20 on probe A spots with a very good spot reproducibility. The experimental increase is hence even higher than expected from simulations. This fact is in clear relation with the high grafting density on the thiol chip. On hybridization curves for target Gc20, we obtain a visible dissociation on probe A16 during chip washing which is not the case for hybridization of Ac20 on the same spots. The high surface grafting thus increases the discrimination of PM and MM duplexes and leads to improved detection of minor target concentrations.

This result is encouraging and the second question was, if we could be able to accumulate even higher percentages of mutant on its complementary spot in a faster way. Several hypothetical temperature profiles with repeated heating and cooling cycles at various speed are analyzed for an overall 'target accumulation' time of 1 h which corresponds to the time needed of 1°C/min cooling from 85°C to 25°C. The analyzed mixture is composed of 1% Ac and 99% Gc on probe A16. Important factors are the cycle's maximum temperature T_c and the number of cycles related to the scan speed with heating and cooling being possibly different. We find that the efficiency is strongly dependent on T_c. It is clear that T_c must be sufficiently high to destabilize the MM duplex on the spot while being sufficiently low so that the PM duplex remains intact. It gets immediately clear that the optimum temperature will depend on the duplexes to be analyzed. As for the number of temperature scans, for symmetric temperature profiles it seems preferable to have more cycles at faster scan rates. Then, more time is overall passed in the temperature range where target exchange takes place. The best option is, however, an asymmetric temperature profile with fast heating rates and slower cooling rates since most rearrangement occurs during cooling. If it is experimentally feasible, it would be preferable to do scans around the dissociation temperature of the mismatched duplex, since at low temperatures (below ∼40°C), the displacement of Gc by the PM target Ac is inefficient.

Experiments with two heating and cooling cycles at 3°C/min are presented in figure 4.22a for the detection of 10% Gc26 and 90% Ac26 with 250 nM total DNA. Full lines represent the NTD curves obtained directly after hybridization at 25°C, dashed curves show NTD curves after two heating cycles in the presence of the sample. The figure reflects the different results one can expect for a chosen T_c with respect to duplex stabilities. While the two cycles to 47°C show visible, yet minor accumulation of Gc26 on probe G, a significantly higher increase is found on probe TG, sensing the same allele but at lower temperatures due to the additional mismatch. Figure 4.22b represents the derivatives of the NTD curves and reflects well the shift of proportions

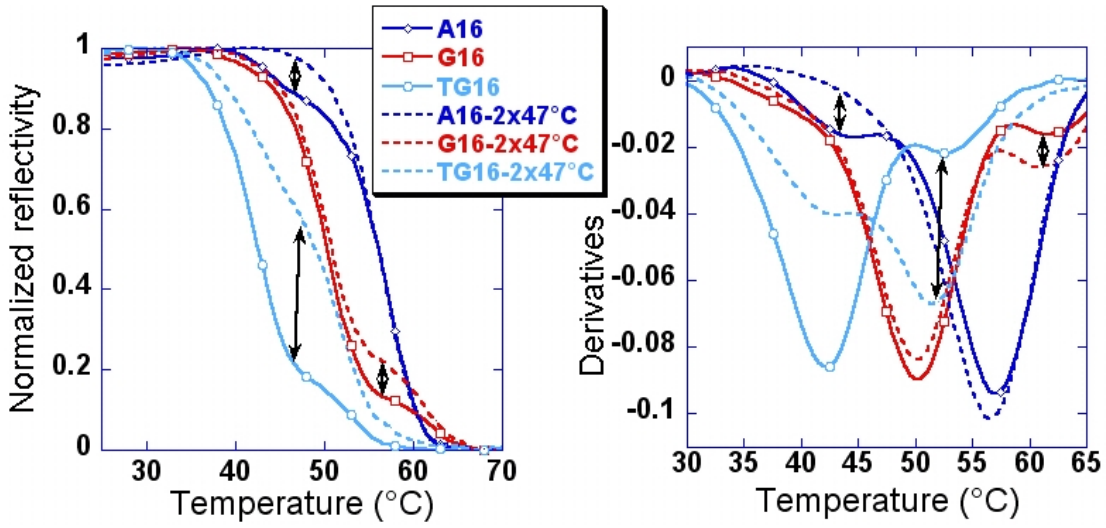

Figure 4.22: *On the left:* detection of a target mixture of 250 nM total DNA, with 10% Gc26-bio and 90% Ac26-bio. Full lines: NTD T-scan directly after hybridization and washing. Dashed lines: Under agitation of the solution, two consecutive heating cycles up to 47°C are performed before washing and NTD T-scan. The change of complementary target is indicated by arrows. *On the right:* The corresponding derivatives reveal the changed proportions.

of the minima corresponding to each target duplex. Arrows indicate the differences due to loss (A16) or addition (G16, TG16) of Gc26 on the spot. We see that our 'secondary reporter probes' with lower target affinities boost the detection of mutants at low concentrations and render the results more reliable.

To complete this presentation of the detection of target mixtures with one allele in low abundance, it has to be said that simple isothermal hybridization at an optimum temperature of $T_d(MM) \leq T_{opt} \leq T_d(PM)$ will provide the most time efficient accumulation of mutant target on its complementary probe. However, this approach is not flexible enough to be applicable to complex target mixtures sensing different SNP site, unless substantial effort is done for optimization of probe length and sequences. So, our temperature cycle approach with secondary reporter probes has the advantage to be more universal and less dependent on the nature of SNPs to be detected.

4.6.3 Signal amplification by DNA labeling

The previous considerations about detection of mutations and mixed targets reveal the need for sensitive detection methods allowing unambiguous target identification, and preferably also target quantification. One way to render SPRi more sensitive is by signal amplification using target labeling, the use of alternative strategies based on DNA binding ligands or enzymes or secondary detection using often a 'sandwich' type method, where the target is revealed after binding by a second recognition partner. Although SPRi generally is promoted as a label-free detection method, one should not hesitate to use labels in order to increase the sensitivity of the method when required. Although labeling increases the cost of the detection assay, one can see that today a lot of targets from DNA or RNA amplification protocols are routinely labeled.

SPRi measurements are generally 1000 fold less sensitive than fluorescence measurements, for example. However, some authors report very low detection limits on nucleic acids by SPR using target amplification by ligand binding, biological interactions as biotin-streptavidin recognition or coupling of gold nanoparticles [9, 190, 191, 121, 192, 193]. The purpose of this subsection is to evaluate amplification protocols based on biotin-streptavidin coupling with respect to their compatibility with subsequent heat denaturation detection. The main question is, if we can achieve high hybridization signals while keeping or improving our good discrimination of sequence specific

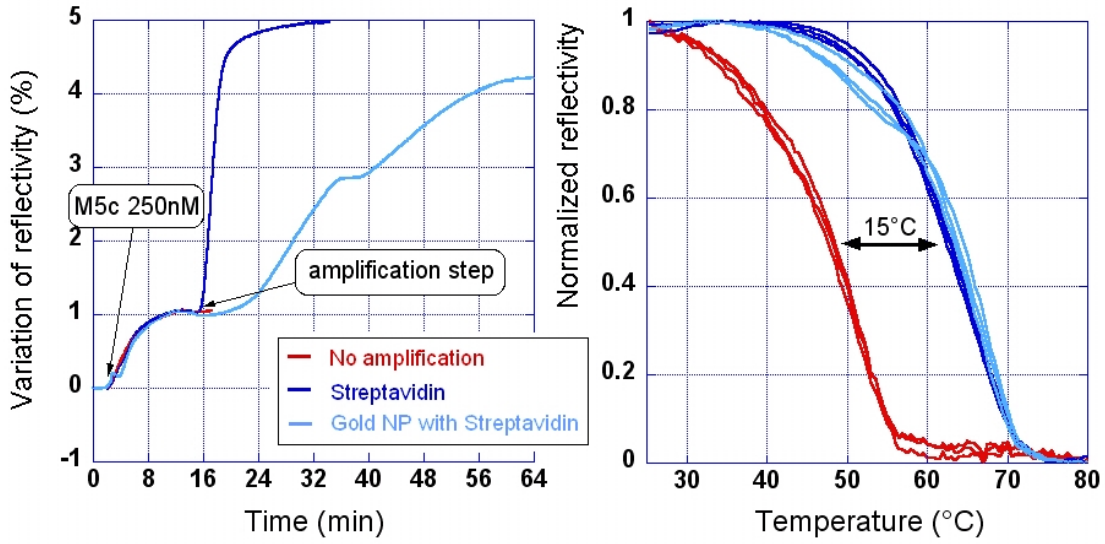

Figure 4.23: Amplification of biotinylated DNA. *On the left:* Hybridization of M5c on M4 probes (1 MM) at 250 nM on a poly-pyrrole chip. Red: streptavidin amplification (10 nM), blue: streptavidinated gold nanoparticles at 0.01 OD and light blue: no amplification. *On the right:* Denaturation curves of M5c and probe M4 (1 MM) on a poly-pyrrole chip observed after hybridization without amplification (red), with streptavidin-biotin amplification (blue) and amplification by streptavidin coupled Au nanoparticles (light blue). There is a shift of ∼15°C toward higher denaturation temperatures for amplified targets.

denaturation of mismatched targets using T-scans.

The biotin-(strept)avidin interaction is known as the most stable biological interaction and is therefore a welcome couple in molecular biology binding assays. The dissociation constant of $\sim 10^{-15}$M explains why the biotin-streptavidin complex is very stable and can not be destroyed under 'normal' conditions [194]. Streptavidin is reported to exhibit less non-specific binding than avidin and is therefore the partner of choice for on chip experiments. Its molecular mass is 52 800 Da and its *isoelectric point* is close to neutral conditions. Streptavidin is a tetrameric protein of $46 \cdot 93 \cdot 104$ Å. One strept(avidin) protein has four subunits with identical recognition sites for biotin.

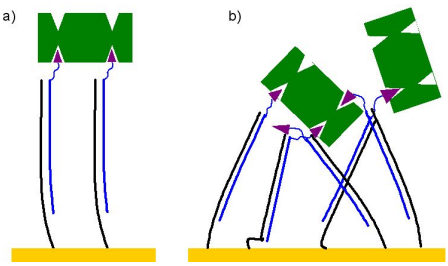

Figure 4.24: a) simplified model of streptavidin binding to a biotinylated DNA surface. b) more realistic model of binding events. One streptavidin protein can capture up to four biotin molecules in its binding sites.

Two amplification systems based on this specific interaction are available at our laboratory. The biotinylated target DNA is first hybridized to the probes and then 'revealed' by an injection of either 10 nM streptavidin or 0.01-0.05 OD of streptavidin functionalized gold nanoparticles. While the amplification of the SPRi signal by streptavidin is purely related to the additional mass, the gold nanoparticles (Au-NP) can couple to surface plasmon excitation and then exhibit signal amplification beyond simple mass addition. Figure 4.23a shows the superposition of injections of biotinylated M5c target on M4-ppy probe followed by no amplification (light blue), amplification by streptavidin (red) or a double injection of streptavidin functionalized Au-NPs. With a hybridization signal of 1% reflectivity, we obtain 5-fold amplification upon 10 min injection of streptavidin, displaying a very fast binding. For Au-NPs, we observe a much slower signal which after 20 min injection reaches a ∼ 4-fold amplification.

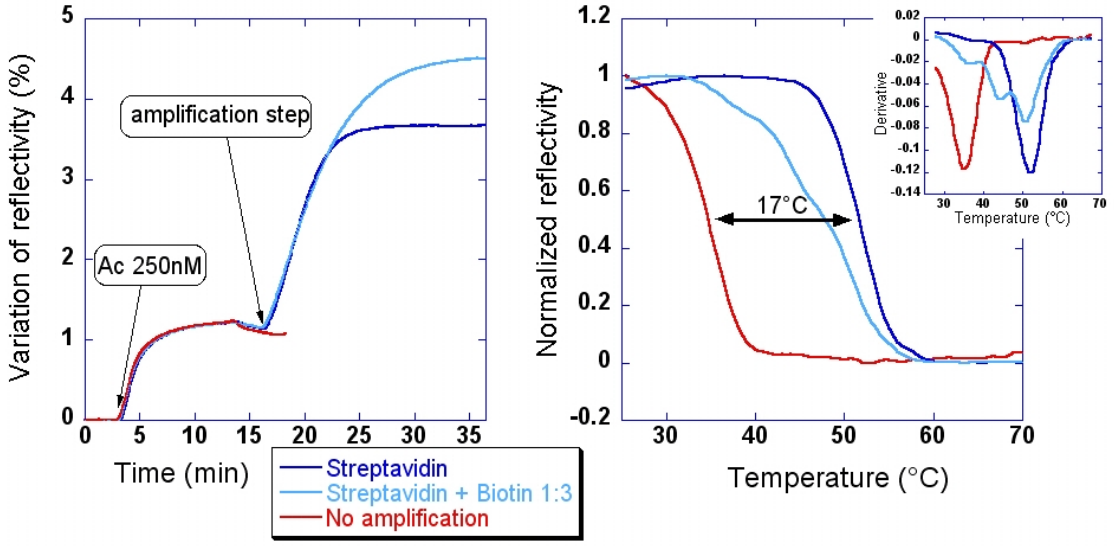

Figure 4.25: *On the left:* Hybridization of Ac at 250 nM on probe A-thiol followed by an amplification step. Red: streptavidin amplification (10 nM), blue: mixture of streptavidin (10 nM) and biotin with stoichiometry of 1:3 and light blue: no amplification. *On the right:* Temperature scan for ASO-Ac on probe A (PM) in 30% formamide on a thiol chip: without amplification (red), streptavidin amplification (blue), amplification with a streptavidin - biotin mixture of stoichiometry 1:3 (light blue). The inset shows the corresponding derivatives. While there is a simple shift as observed on M4 for streptavidin amplified targets, mixing of streptavidin with biotin reveals several complexes with various T_d. The temperature shift is cause by the coupling of several targets to one streptavidin protein.

The association of gold NPs to the surface is clearly limited due to insufficient mass transport towards the surface and can be seen from the delayed response curve at 16-24 min as compared to streptavidin. S. Laurent found at our laboratory that gold NPs also have a tendency to aggregate which he revealed by consecutive injections that never reached a clear signal saturation.

Since streptavidin has been reported to be thermostable up to 75°C in a free state and up to 112°C when coupled to four biotin molecules [195], we can perform temperature scans on our amplification system. From the NTD curves obtained by subsequent T-scans, we observe a surprising phenomenon: amplification using biotin-streptavidin interactions lead to significant stabilization of the surface bound state of the target DNA. We see in figure 4.23b that there is a 15°C shift to higher temperatures for both amplification strategies. We speculated that this important stabilization is the signature of multiple targets binding to one streptavidin molecule as depicted in figure 4.24 and thereby couples different hybridized targets. The complex will only part once all 1-4 streptavidin bound targets dissociate from their probe. However, temperature dependent phenomena are statistic and so targets that dissociate will stay close to the surface instead of being carried away directly. Targets may thus eventually find a new binding partner before other targets on the same streptavidin start to dissociate.

To put this model to the test, a comparison of streptavidin and streptavidin previously mixed at 1:3 ratio with free biotin is carried out this time on a thiol functionalized prism. From the hybridization signal in figure 4.25a we see that the premixed streptavidin leads to a higher amplification signal that can not be explained solely by the additional mass of biotin which corresponds approximately to the mass of one DNA base. So, the first observation is that more streptavidin is bound to the spots when some active sites of the protein are blocked before injection. When we observe the respective NTD curves in figure 4.25b, we observe that on thiol surfaces the shift

due to streptavidin coupling is conserved. Then, we notice that new properties appear on the curves corresponding to the streptavidin-biotin mix. There is not one clearly defined dissociation temperature as before, but a stepwise dissociation profile with two plateaus as revealed by the derivative shown in the inset. Tracing the parallel to the previous subsection on mixed targets, we can conclude that we have three species of different stability on the same spot. The most likely composition being here streptavidin proteins with one to three fixed DNA targets. By the way, one plateau could already be distinguished on the AU-NP NTD curve in figure 4.23b indicating that a varying number of biotin binding sites is already occupied by the functionalization on the nanoparticle. We can now also understand why more streptavidin is bound to the spot in the case of biotin premixed samples. While normally surface bound streptavidin captures a maximum of three or four target, yielding one single, stable dissociation temperature, more streptavidin will find now a free binding partner on the surface and thus increase the mass.

Let us come back to the original motivation of this work on signal amplification. The aim is to obtain higher signals especially to be able to find low abundant mutated targets in a complex sample. The fact that streptavidin connects neighboring targets on one spot is thus incompatible with detection of the specific target stability. When we find a plateau, we would not know if it corresponds to the fact that some streptavidin have less partners (cf. Au-NPs) or if it corresponds to intrinsic differences of the target's stability. Moreover, we should expect a broadened transition instead of a discernible plateau for target mixtures since among the streptavidin binding partners we will find a varying ratio of mutated and complementary targets. We can conclude that the T_d shift introduced by streptavidin coupling complicates target detection based on the prognosis of duplex stabilities. The streptavidin-biotin amplification scheme seems thus an invalid approach for thermal denaturation detection.

One solution of this problem could be provided by engineered streptavidin with only one binding site. A recent review on engineered streptavidin has been published by Laitinen and co-workers [196]. Although there exist dimeric streptavidin or even monomeric streptavidin fractions, they loose the prerequisite of the exceptionally stable binding to biotin and show binding affinities of K_d $\sim 10^{-7}$M [196, 197, 198]. Other amplification strategies must be found that are compatible with target stability detection using T-scans, when higher signal is needed.

4.6.4 Target length and secondary structure

Before discussing the point mutation detection on PCR amplified targets in the next chapter, we should discuss some preparative results concerning the differences encountered when passing from short oligonucleotides to longer targets. New effects are expected to arise, since longer targets are more likely to have stronger interactions on the chip due to stronger electrostatic interactions and steric hindrance. Long DNA or RNA sequences are also prone to self-hybridization in form of secondary structures, tertiary structures and hybridization between targets and background DNA in solution (so-called 'hitch-hiking' [199]) leading to reduced mobility and decreased availability for surface hybridization. Biological DNA and RNA targets as provided by current amplification protocols are usually longer than 100 nt and can have up to about 2000 nucleotides. Therefore, longer targets on oligonucleotide chips have dangling ends, in contrast to short ODN targets. Dangling ends that are either placed at the distal end of the probe or proximal to the surface are potential interaction partners for background DNA. As shown by Stedtfeld et al., already short homologies between the distal dangling end and background DNA can lead to substantial hybridization of background DNA to surface hybridized targets [199]. This effect is smaller for surface proximal tails, supposedly due to reduced availability and substrate influences. This is especially relevant when the target's complementary strand is present in the sample [200]. In the presence of dangling ends, hybridization depends strongly on the spacing between the probe sequence and the substrate [201, 202, 203, 157]. This is taken into account by incorporation of a chemical spacer between the hybridizing part of the probe and the substrate and is generally in the order of 45-90 atoms corresponding to $\sim$10 nucleotides [203]. Furthermore, the physicochemical properties of the spacers also have an influence on the hybridization yield and it is generally preferable to present

low negative charge density and to be hydrophilic to some extent. Probes without spacers are subject to increased stringency and show not only reduced melting temperatures as compared to more distant probe sites, but also exclusive two-state dissociation. Distant probes may yield multi-state dissociation curves due to partial hybridization and secondary structures in the target [202]. In this study, probes with a 10 thymine spacer are used, providing the required distance, but not necessarily optimal reduction of undesirable non-specific interactions.

Long DNA sequences containing all four nucleotides are very likely to form secondary structures. Those can be in form of hairpins, loops or pseudoknots. The influence of secondary structure in targets or probes in hybridization kinetics has been studied as well for bulk experiments as for surface hybridization [204, 205, 206, 207, 107, 208]. Although Bonnet et al. report an improved mismatched discrimination on melting curves for molecular beacons [205], in most applications secondary structures are an annoying effect since hybridization rates can be limited already in the presence of three paired bases in the single strand [206]. In general, target and probe design are aimed at avoiding secondary structures in the binding site. However, in applications like SNP genotyping, this may not always be possible since the locus of the target on the gene is determined by the SNP. Computational prediction of secondary structure is available in programs like MFOLD and Koehler and Peyret provide guidelines to optimize computational analysis based on secondary structure prediction for annealing of short ODN on long targets and the corresponding equilibrium kinetics [209, 40].

Effects of RNA structures on surface hybridization have been thoroughly examined by Mir and Southern [210]. Their study reveals that the exact type of secondary structure determines the hybridization yield. Surface hybridization takes mainly place when the hybridizing part contains some bases that are not Watson-Crick base paired in the target and a second part that spans one whole stem region. The unpaired bases can be free or stacked to neighboring helices and serve as nucleation site for surface hybridization. Stacking in hairpin adjacent sites plays potentially a favorable role for surface hybridization since the orientation of the bases facilitates the opening of the adjacent stem. The hybridization to the stem region is also favorable since little reorganization is needed to form the surface tethered heteroduplex. Partial hybridization of a stem region to the probe is generally suppressed, suggesting the reformation of the initial RNA secondary structure. Displacement by one or two bases of well-hybridizing regions may already result in a drastic signal decrease, since stabilizing stacking interactions may be lost [211] or a second stem region would be attained. The nucleation site can have as low as 3 nt and is not necessarily at one end of the surface tethered probe. The authors find similar hybridization patterns on reversely synthesized probe chips (3'→5'), showing that also surface proximal parts are accessible to nucleation. However, there might be a difference between normal (5'→3') or reversed probes depending on the orientation of the RNA target when hybridization initiates at the target's 3' end.

The following work is carried out on synthetic DNA of 80 nucleotides. The advantage of synthetic material for optimization is its availability in sufficient quantity and purity. All targets dispose of 24 bases perfectly complementary to probe sequence G24. Three targets are available: PolyT-sol has a poly-thymine dangling end of 56 nt on the distal 5' end of the hybridizing sequence, thus oriented towards the solution after hybridization. PolyT-surf has a poly-thymine end of 56 nt on the 3' end as surface proximal tail. PCR80 is similar to PolyT-surf but instead of 56 thymines, its dangling end is identical to the sequence of the PCR amplicon used later for detection of biological samples (chapter 5). This target is able to form a stable secondary structure with $\Delta G = -13.86$ kcal/mol. The hairpin shown in figure 4.26 is conserved for all 3 predicted secondary structures obtained using mfold. With these sequences, given in table 3.1 on page 28, we can thus study the effect of dangling ends with orientation towards the bulk or the surface and the influence of target secondary structures on surface hybridization and thermal dissociation.

First, hybridization kinetics for the 80mers are compared to a standard oligonucleotide hybridization. Therefore, injections of 250 nM target in PBS 400 nM NaCl at a flow rate of 5 ml/h are performed on a poly-pyrrole chip with immobilized A and G sequences of length 16-24 nt for grafting densities obtained with 2 and 10 µM DNA. Under identical injection protocols, the hybridization kinetics observed on the DNA chips depends on the target type. As shown in figure

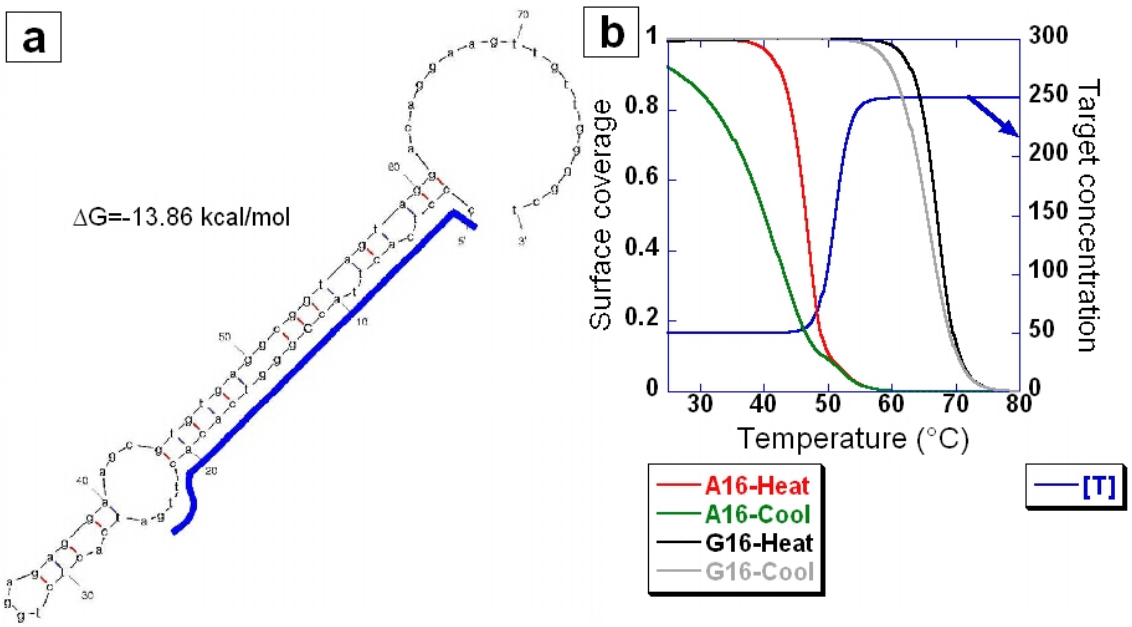

Figure 4.26: a) Secondary structure of PCR80 predicted by mfold. At 25°C and 450 mM NaCl, $\Delta G^{25\,^{\circ}C}$=13.86 kcal/mol. b) Simulation for melting curves in presence of variable target concentration that corresponds to secondary structure stability. Heating and cooling process are assumed at 2°C/min after 20 min hybridization of PCR80 on probe A16 and G16 (see explanation on page 80).

4.27a, the fastest association is obtained for the oligonucleotide, followed by PolyT-sol. The lower signal of Gc26 is due to the difference in mass. For PolyT-surf, we find a further reduced association rate. PCR80 associates even slower and tends to a lower equilibrium surface coverage than PolyT-sol. For the 10 µM grafting shown in the figure, spot signal is not saturated during the injection time for all 80mer targets. However, on 2 µM spots, saturation is fairly well reached. There, we find a 20% signal increase of PolyT-surf as compared to PolyT-sol although association takes place slower. This can be explained by the exponentially decreasing sensitivity of the SPRi signal perpendicular to the surface. An analysis of plasmon curves assuming a DNA layer extended over 8 or 16 nm on the poly-pyrrole spot assuming refractive indices of $n_{8\,nm} = 1.37$ or $n_{16\,nm} = 1.35$ yields a similar reflectivity increase for the thinner layer with higher refractive index, which corresponds to the target hybridized closer to the surface. PCR80 targets show only 60% of the PolyT-sol signal in these spots, leading to the conclusion that the equilibrium surface coverage for targets with secondary structure is lowered. During the dissociation phase, no apparent off rate is observed indicating that all duplexes are stable at 25°C.

To overcome the limited hybridization rate due to the secondary structure, hybridization of PCR80 at 250 nM is carried out at different temperatures from 25°C to 60°C in steps of 5°C. Figure 4.27b compares the kinetics obtained in average on probe G24 for the different injections. The association rate increases with increasing hybridization temperature. An optimum is reached for temperatures between 45°C and 50°C. However, the dissociation rate increases, too, and due to decreased affinity for the probe, the equilibrium surface coverage starts to decrease. The presence of secondary structure in the target hinders hybridization at low temperatures. Hybridization at higher temperatures increases the probability that the hybridizing part is in single stranded form and thus available for surface hybridization. It is clear that the competition between secondary structure and surface hybridization induces new constraints on the probe design. For example, probe G16 shows a strongly reduced hybridization signal when hybridization is carried out at 45°C and we do not obtain any signal at all on spot A16 with one mutation. Longer probe sequences

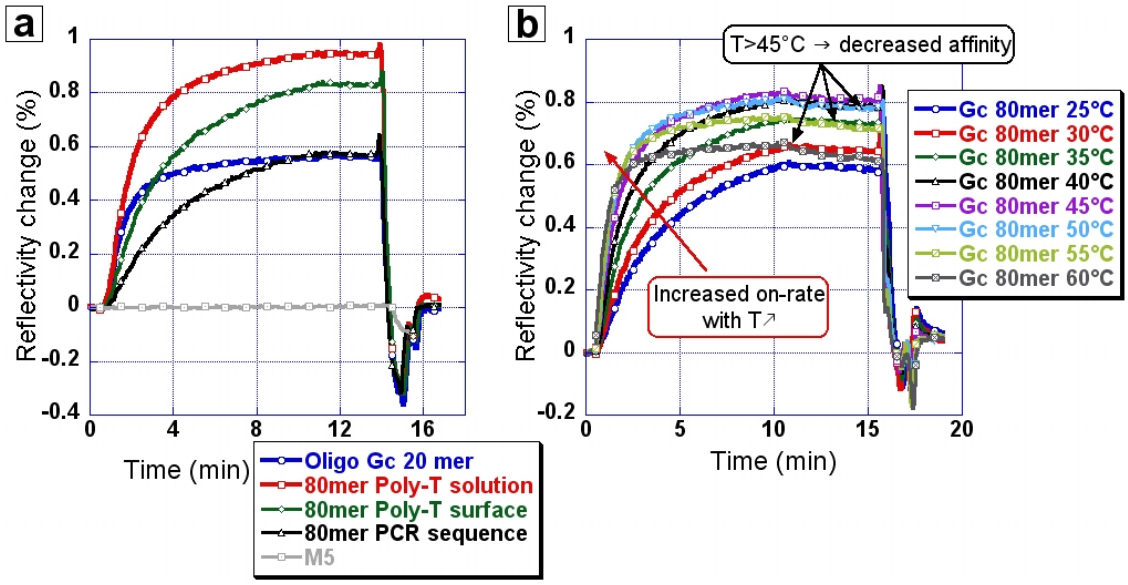

Figure 4.27: a) Hybridization kinetics of targets varying in length, position of the hybridizing part and secondary structure at 25°C on probe G24. While no off rate can be detected for all targets, on-rate varies by type. The slowest on rate is observed for target PCR 80mer forming secondary structure and having a surface proximate tail. b) PCR-80 target on probe G24 hybridized at different temperatures. On-rate increases with temperature and for T>45°C the equilibrium surface coverage decreases. An optimum is achieved around 45°C.

are needed that lead to $T_m(PT) > T_m(T^*)$, with T^* the melting temperature of the secondary structure. In our case, only the probes with 20 and 24 bases can be used.

To obtain further information on the interactions between long targets on ODN probes, NTD curves are acquired for all 80mer targets. Two details can be noted in figure 4.28a. While PolyT-sol results in a NTD curve identical to Gc26, PolyT-surf shows a reduced stability and dissociates at lower temperatures. Astonishingly, this decreased stability is not observed for PCR80, instead, a part of the targets seems to be hold back and dissociates only in a second step at temperatures where the other targets are already completely dissociated from the spot. Both effects are present as well on PM and MM spots. While the decreased stability for PolyT-surf might be explained by higher stringency in the proximity of the surface, the behavior of PCR80 has not been observed before for samples with one unique target. To obtain more information, equilibrium scans in presence of 250 nM target DNA with protocols as in section 4.5 are measured. In figure 4.28, we see that curves obtained with Gc26 and PolyT-sol are in thermodynamic equilibrium while the target with the surface proximal tail still dissociates at lower temperatures and shows a hysteresis effect. This finding is consistent with the NTD observations and reveals the penalized hybridization for targets with surface proximal tails. The equilibrium melting curve for target PCR80 is shown in figure 4.28c. Here, two probe types are shown, the mismatch forming probe A16 and the perfectly complementary probe G16. Targets are hybridized at 25°C and we then apply under agitation two successive temperature scans to 85°C at 2°C/min for heating and cooling. Reflectivity at the beginning of each scan is normalized to 1 to obtain easily comparable curves. From the first T-scan, we observe on both probes a plateau, indicating the presence of species of different stability on the spot. However, there is only one single target present in solution, so we can not explain this effect by different targets. We also observe that the percentage of duplexes with higher stability is not the same on PM and MM spots. While about 75% of targets on spot G16 dissociate at higher temperatures, this is the case for only ∼45% of targets on the mismatched spot. The plateau on G16 is also more pronounced. During the cooling process, no such distribution is observed, the curves regain smoothly the initial signal and in the case of G16, about 20% more mass is fixed

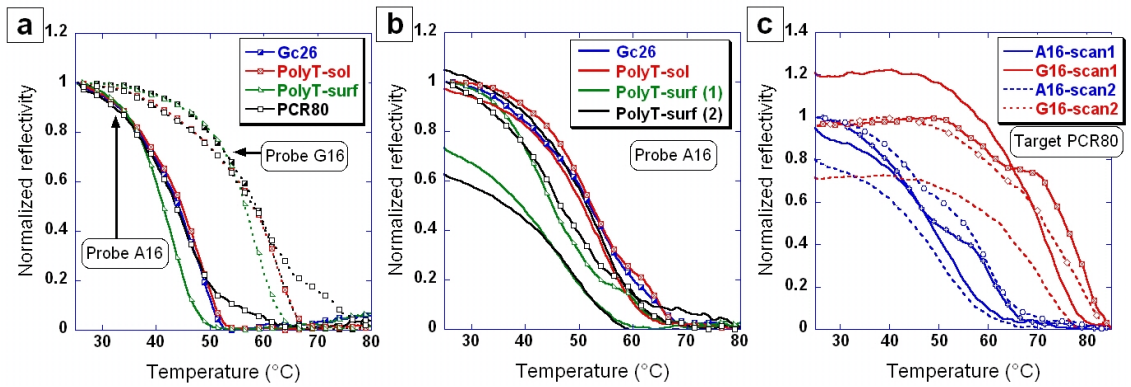

Figure 4.28: a) NTD scans obtained after injection of 250 nM target of either Gc26, PolyT-sol, PolyT-surf of PCR80. We observe a T_d decrease on target PolyT-surf and a level-off at the end of the PCR80 scan, here represented for probe A16 and G16, but present on probes of 20 nt and 24 nt, too. b) Heating (symbols) and cooling (full lines) in presence of target DNA under agitation. PolyT-surf is penalized and presents a hysteresis. c) Double heating and cooling cycle at 250 nM PCR80 observed on A16 and G16 (first scan → full lines, second scan → dashed lines). We find a plateau during heating, but not cooling. On G16, the plateau is completely absent for the second T-scan cycle, while it is still observable on A16 (1 MM). All curves presented are averages over identical spots.

on the spot. The second temperature scan is different from the first. While we still can observe the plateau on probe A16, it is smeared out on the PM spot. Both spots do not regain the initial hybridization signal. Although not shown here, spot A20 shows a distinguishable plateau during the first and second scan. No information is obtained on longer A or G probes since the spots are not totally dissociated at 85°C and normalization is thus difficult. Another experiment showed that the detection of the plateau on all spots is reproducible with $\sim 15\%$ variation on the absolute position of the plateau.

To find an explanation for the observed stability difference of PCR80 target on the spots, we first thought about effects of the secondary structure. Since probes are injected without any preheating, we must assume that targets form secondary structures. Two scenarios could then be found. First, at low temperature, only some targets are available for hybridization and we thus obtain an effective free target concentration [T] lower than the total target concentration c_T. In the absence of duplex formation, secondary structures in solution start to melt during T-scans and [T] increases until it reaches c_T. This concentration change leads to a shift of the equilibrium surface coverage and shifts the melting temperature to higher values. The reaction scheme can be expressed in the following way:

$$\mathrm{P} + \mathrm{T} \rightleftharpoons \mathrm{PT} \tag{4.23}$$

$$\mathrm{T} \rightleftharpoons \mathrm{T}^*, \; K_{T*} = \frac{[T^*]}{[T]} = \exp\left(-\Delta G_{T^*}/RT\right) \tag{4.24}$$

where P is the probe, T is the random coil target, PT is the hybridized duplex and T* is the stable secondary structures as predicted by mfold with the Gibb's free energy $\Delta G^{25\,^\circ C}_{T^*} = -13.86$ kcal/mol. K_{T^*} is the equilibrium constant of secondary structure formation and [X] indicates the concentration of X. Mass conservation equations for the target can be written as:

$$c_T = [T] + [T^*] + [PT] \tag{4.25}$$

with c_T the total concentration of the target. When targets are in large excess to available probe sites on the surface, we can consider [PT]≈0. Surface hybridization is treated in the Langmuir model and the secondary structure in equilibrium gives rise to a concentration $[T] = c_T/(1 + K_{T^*})$

that varies with temperature in the limits $0 \leq [T] \leq c_T$. With the thermodynamic parameters ΔH and ΔS for T*, we can determine the equilibrium constant and so obtain the target concentration in the random coil state. Numerical analysis of the Langmuir surface coverage are carried out for a variable target concentration [T]=50+200/(1+K_{T^*}), where only 20% of the targets are available for surface hybridization at low temperature and the rest forms equilibrium secondary structures with $T_m = 51$°C. The equilibrium of the secondary structure is supposed valid under the experimental conditions where Gc26 and PolyT-sol are in equilibrium with surface reactions. The somewhat arbitrary 50 nM open target fraction takes into account the existence of other secondary structures with low affinities that do not implicate the hybridizing part on the target. In absence, no hybridization would occur which is experimentally falsified. Analysis for T-scans at 2°C/min show the possibility to observe a plateau during melting and annealing on A16, as shown in figure 4.26b. Experimentally, we do not observe any stagnation in the annealing signal. However, since the secondary structures predicted for target PCR80 are all of about equal stability (predicted $T_m \sim 47 - 51$°C), this phenomenon only occurs in a distinct temperature range corresponding to hybridization to A16 (predicted $T_m = 50$°C). This is why already on probe G16, no particular influence is predicted since secondary structures are not stable at temperatures where PCR80 on G16 melts. So this model is not a satisfactory explanation of the signal stagnation on probes.

A second explanation of this two-state melting could be partial hybridization of the targets to the probes. To observe the plateau, two distinct conformations would be necessary, since multi-state dissociation would lead to a smeared out distribution. It would be possible to observe a distinct distribution when there is a competition between a part of the probe and a possible hairpin conformation of the secondary structure at one distinct point in the hybridizing part. Partial hybridization to the probe would lower the melting temperature of targets with shorter hybridization length. We can however conclude from comparison with oligonucleotide targets that we do not observe a destabilization, but, on the contrary, a stabilization of parts of the probes on the surface, except for PolyT-surf. So, partial hybridization, too, seems to be an invalid explanation for the plateau in PCR80. Once again it is astonishing that also on the melting curves, overall stability of PCR80 corresponds more to PolyT-sol and G26 than to PolyT-surf.

When we look closely at equilibrium melting curves obtained on the PolyT targets, we can also find a kind of plateau, but less pronounced as for PCR80 and at lower percentages. We must thus assume that the phenomenon should be at least partly assigned to the presence of dangling ends on the targets. The stabilization extends to a higher fraction of targets when dangling ends are composed of complex sequences and not only thymines. One could speculate that entanglements between dangling ends or even hybridization between parts of the dangling ends would lead to stabilization of the targets on the spot. It is even possible that hybridization between dangling ends of different targets takes place in the bulk before surface hybridization occurs. This scenario is similar to the observation discussed earlier for streptavidin. There we have seen that coupling of different probes increases the dissociation temperature.

Unfortunately, we can only speculate on the origin of the observed phenomenon since SPRi techniques are constrained to the observation of averaged phenomena and we can not gain further insight in the underlying microscopic phenomena. Other interactions than between dangling ends might intervene and could be dependent on the hybridization chemistry, the hybridization buffer, etc..

However, we can learn from these experiments that dangling ends and secondary structures of the target do not only penalize hybridization kinetics, but can also influence thermal denaturation characteristics. Since it has been shown in solution experiments that the dangling ends of different length do not alter the melting temperature [157], we must assign destabilization of surface proximal tails to the presence of the substrate and thereby to increased stringency. In the presence of secondary structures it is advantageous to use longer probes than for oligonucleotide observations since they are better competitors. Still, it is convenient to optimize the hybridization temperature to obtain fast surface hybridization. To overcome the plateau observed on NTD curves and melting curves, it could be helpful to adopt the strategy to inject targets at elevated temperatures and hybridize during cooling, as discussed for target mixtures before. In this way, surface hybridization occurs before formation of secondary structures. The results of the second

heating and cooling cycles performed on PCR80 suggests that such a strategy could smooth out the plateau.

4.7 Summary: real-time characterization of ODN chips

This chapter provided a global introduction to parameters that influence DNA duplex stability on a surface. We chose to work with synthetic oligonucleotides because of their stability, high purity and availability in large quantities. Target concentrations and buffer conditions can be freely chosen and there is no background signal due to the presence of complex components or proteins in the buffer. Although the last section on longer ODN targets indicates that we might be confronted to new problems with targets of biologically relevant length, the general tendencies and concepts that are presented apply also to longer targets.

We have presented here two different surface grafting chemistries, poly-pyrrole and thiol self-assembling, but a lot of other methods can be used and may be more suitable in other applications. Furthermore, not only DNA probes can be used, but also peptide nucleic acids (PNA) are now employed, since they have the advantage of an amide based, uncharged backbone which, of course, lowers the hybridization barrier in low salt environments [212, 213, 214, 215]. PNA is also capable of hybridization as well to normal, right-handed DNA as to its L-enantiomer, L-DNA that forms a left-handed helix upon hybridization to complementary L-DNA. Other methods use locked nucleic acids (LNA) which is in fact composed of modified RNA that is locked in a specific conformation dominant in A-form DNA and RNA and which enhances base stacking and phosphate backbone pre-organization, thus improving duplex stability. LNA has been reported to improve sensitivity and specificity for various detection strategies [216, 217, 218]. Here, we have chosen to study the stability of DNA-DNA duplexes which are commercially available and easy to implement. Consequently, it is important to characterize the duplex stability depending on the salt concentration. As we have seen, empirical salt corrections from bulk experiments apply rather well to the salt dependence found on biochips, while the prediction of the duplex melting temperature for surface tethered probes does not reflect values from solution. In general, as well melting temperatures as dissociation temperatures on biochips are lower than expected from prediction by the nearest neighbor model. We showed that our on-chip melting curves fit predictions from the Langmuir model taking into account salt effects. Although the model describes the salt dependence well as proved by the collapse of all curves for one single parameter, the fitting parameter is about 20 times lower than expected from estimations from the experimental conditions. Thus, all available models are currently only able to provide good predictions for the salt induced shift of the melting curves without giving us the possibility to model experimental melting curves beforehand. From salt experiments, we determined an optimal salt concentration of $\geq$400 mM NaCl for our experimental conditions. This salinity allows spot saturation of complementary and mismatched probes in 10 min for ODN concentrations of 250 nM. Contrarily to end-point detection methods, our setup requires hybridization of targets to all probes, regardless of mismatches formed on the spots. So, point mutations can not be detected during the hybridization process, but only from the subsequence temperature scan. The set of allele specific probes allows determining the genotype of the injected target from the order of stability obtained on thermal denaturation curves. We have analyzed the influence of denaturing agents on hybridization and non-equilibrium thermal denaturation. Every percent of formamide added to the buffer decreases the dissociation temperature by 0.58°C. Formamide can be used in any experiment to lower the temperature range that needs to be scanned. This can be especially useful for thiol grafted chips that do not support temperatures over 70°C. Formamide also affects hybridization of the targets and may favor surface hybridization over hybridization in solution, as for instance, secondary structures. It is possible to use different buffers for hybridization and chip washing during the temperature scan, but in practice, this type of protocol is not very suitable for SPRi experiments. Addition of solvents like formamide induces big changes of the buffer's refractive index and leads to high reflectivity changes in the signal. To obtain interpretable SPRi data, it is preferable to avoid these huge changes, unless sufficient time can be spent to wait for signal stabilization after buffer changes.

Otherwise, signals are likely to present drifts. Other stringent conditions like negative potentials applied to the sensor surface have not been treated here, but could also be used to modulate the DNA surface stability [214]. As soon as the buffer responds to the criteria of efficient target hybridization and adapted temperature range to perform T-scans, our ASO probes are able to detect the genotype of a target with assay times of about 90 min. While in end-point detection on microarrays it is difficult to define criteria for heterozygous samples, out NTD scans provide a simple classification system which can, for example, be based on derivatives of the target's dissociation curve and the order of dissociation from higher temperature to lowest temperature. Furthermore, when hybridization is carried out at low temperature and for short hybridization periods, the real-time detection method provides access to complex sample compositions in the case of target mixtures. We find a detection limit of 5% mutated target in a sample with 95% wild type DNA for 250 nM total DNA. Using a strategy of heating and cooling cycles, even lower percentages will be accessible. The method provides a semi-quantitative approach to sample characterization that can prove useful for medical analysis of samples from tissues extracted during biopsy. To lower the detection limits of our method, an amplification strategy using the specific recognition between biotin and streptavidin is studied. It turned out, that biotin-streptavidin amplification is unsuitable for our thermal dissociation approach since several targets can be coupled to one streptavidin molecule. Temperature profiles obtained after amplification are then not only shifted to higher temperatures by about 15°C, but may also present stepwise dissociation profile due to different numbers of targets coupled to streptavidin. These steps could bias our detection method for target mixtures and is thus not further applied for point mutation detection. Other amplification schemes based on DNA recognizing molecules or intercalators may be more convenient, but have not been treated in this work. Finally, this chapter finishes with a characterization of influences of dangling ends and secondary structures on target hybridization and dissociation. We show that it is preferable to have dangling ends that extend into the solution rather than towards the surface. Surface proximal tails are destabilizing to the duplex and lead not only to slower hybridization kinetics; they also lower dissociation and melting temperatures. However, at low grafting densities, SPRi shows a higher signal for these targets since most of the mass is accumulated in proximity to the surface, where the sensitivity of the SPR evanescent wave is higher. We further find a curious behavior of targets with strong secondary structures and surface proximal tails. The melting curves reveal the presence of two distinct stabilities on the spots that partly disappears when targets are hybridized during slow cooling of the solution instead of isothermal hybridization. The phenomenon can not fully be explained but is assigned here to interactions due to dangling ends that may cross-hybridize with neighboring targets or probes. Effects due to variable concentration or partial hybridization to the probes may appear but comparison of theory and experimental findings seems to rule out this explanation. Secondary structures in targets may be suppressed by the use of altered, structure free DNA as reported by Lahoud et al. [219, 220].

The phenomena studied in this chapter cover a wide range of interactions that take place on biochips. However, other types of interactions may occur when different substrates, surface chemistries, probes types, detection methods or strategies are employed. Separate characterization studies may be needed in these cases.

Chapter 5

Detection of biological samples on DNA chips

Ce chapitre utilisera les connaissances acquises par les études d'oligonucléotides sur puces présentées ci-avant pour adapter notre système de détection de mutations par rampe de température aux échantillons issu d'une amplification du matériel génétique d'un patient. Deux types d'échantillons seront traités :

- Les échantillons amplifiés par un protocole de la 'Polymerase Chain Reaction' (PCR). Cette méthode de la biologie moléculaire permet d'amplifier des régions précises sur un gène de manière exponentielle. L'amplification nécessite la présence d'une seule enzyme et fonctionne par des cycles de température. Les échantillons ainsi produits sont en forme d'ADN double brin.
- Des échantillons issue d'une amplification par 'Nucleic Acid Sequence-Based Amplification' (NASBA), un protocole d'amplification breveté par la société bioMérieux. La NASBA est une amplification linéaire et isotherme, faisant intervenir trois enzymes différentes. L'échantillon obtenu par cette méthode est en forme d'ARN simple brin. La méthode en produit environ $10^{12} - 10^{14}$ exemplaires.

Nous allons discuter d'abord la détection de mutations dans des échantillons issue de la PCR. Des méthodes de traitement et purification d'échantillon seront introduites. Les précautions expérimentales à prendre lors d'une hybridation d'échantillons biologiques sur puce seront discutées. Enfin, des résultats du génotypage par la méthode des rampes en température seront présentés.

La méthode d'amplification par NASBA sera étudiée ensuite pour montrer la possibilité de détection d'échantillons ARN sur puce. La méthode étant isotherme, s'apprête également à une utilisation in situ pour une amplification sur puce dans la cuve SPRi. La possibilité d'une amplification et détection intégrée sera démontrée et couplée à la méthode de détection par rampe de température. La méthode montre la capacité d'un système intégré pour la détection des mutations ponctuelles.

5.1 Introduction to DNA detection and genotyping of complex samples

A huge effort has been put in the optimization of DNA microarrays during the last decades. In the preceding chapter, we have seen the basics of DNA surface hybridization and the stability of the duplex: the impact of the surface chemistry, of various buffer components and amplification protocols for signal optimization. We also studied the impact of mutations and target mixtures on hybridization and thermal denaturation for solid phase experiments.

We will now shift our focus to on-chip detection of amplified DNA and RNA targets to be used in microarray experiments. For medical and environmental applications, DNA and RNA samples from bacteria, viruses or cells from specific tissues of plants, animals or human beings may be analyzed. For expression profiling, one will analyze the RNA in the samples to get to know the genes that the cells is currently expressing and thus the associated proteins necessary for the cell's function [221, 222, 223]. In other applications, as for example SNP genotyping, the target will lie in a certain region of the genome [224, 225]. For identification of cell lines or virus types, the conserved and variable parts of the genomic material are analyzed. Since targets from such sources are often available in low abundance, with concentrations in the attomolar range, for instance in bacterial detection, detection methods need very low sensitivity or adapted target or signal amplification. Most applications use a combination of target and signal amplification schemes to achieve the necessary sensitivity [9]. Signal amplification for SPRi experiments has been discussed earlier in section 4.6.3. We will thus focus here on the detection of amplified targets. The first and today probably most current DNA amplification method in molecular biology is the Polymerase Chain Reaction (PCR) [226]. This technique makes use of DNA extension by DNA polymerase in the presence of a small oligonucleotide hybridized to a longer DNA fragment. DNA samples can be amplified exponentially during repeated heating cycles. The final target represents a specific sequence of unique length and is in double stranded form. Other thermocycling methods and derivatives of PCR amplification like Ligase Chain Reaction, Long-distance Single Molecule PCR, random primer PCR (rPCR), Real-Time Quantitative PCR and Multiplex Ligation-Dependent Probe Amplification (MLPA) have been reported [227, 10]. Another possible amplification strategy is based on Rolling Circle Amplification (RCA). This is an isothermal method making use of circular DNA that serves as ligation template. The produced strand presents multiple repetitions of the amplified sequence. Other isothermal approaches like Klenow fragment-based amplification, strand displacement amplification and ϕ29 DNA polymerase-based amplification are available [10]. Also, Nucleic Acids Sequence-Based Amplification (NASBA) presents an isothermal amplification scheme that produces single stranded RNA form either DNA or RNA samples. The amplification is linear and yields up to $10^{12} - 10^{14}$ targets in solution. Some of the most current nucleic acid amplification and detection schemes are reviewed in [228, 229, 10].

In this work we will focus on two amplification protocols, PCR for DNA targets and NASBA for RNA targets. The first project on the detection of biological samples based on PCR amplified DNA is led in collaboration with E. Crapez from the Center of Cancer Research at Montpellier, France. The PCR samples are amplified at Montpellier from genomic DNA of cancer patients with homozygous or heterozygous DNA towards the SNP G870A on codon 242 exon 4 of the Cyclin D1 gene. The second project on RNA detection amplified by NASBA is carried out in collaboration with K. Brengel-Pesce and N. Beaufet from the Grenoble research and production site of bioMérieux. In fact, the NASBA amplification scheme is patented and commercialized by bioMérieux. This is why the reader may sometimes find limited information about specific DNA sequences and buffer components which are treated as confidential or have not been in our knowledge during the project.

Although each amplification protocol has individual requirements, all will have important parameters in common that create the need of adaptation of laboratory facilities and detection systems. Most amplification protocols are very sensitive and amplification initiates in some cases in the presence of only one single template DNA strand. The risk of contamination is important

and false positive results may arise. Special equipment regarding micro-pipettes and sterile environments are necessary. Usually, amplification and detection zones are well separated, so that an amplified DNA sample tube is never opened near the area where amplifications are prepared. In our case, PCR amplifications are carried out in external facilities by our collaborators and only NASBA amplification has been processed occasionally at the CREAB.

Since the samples are obtained from molecular biology protocols, they come in a distinct buffer containing special enzymes used for amplification and purification. Also, contrarily to oligonucleotides, only a limited volume at a certain target concentration will be available for detection. The microarray strategy must thus be adapted to complex sample conditions and low sample volumes in order to conserve a high signal to noise ratio with low background signal and specific target signal. Probe design and blocking strategies are now important factors and worth a detailed discussion.

5.1.1 Probe design for genotyping experiments

Probe design is a crucial step in microarray fabrication. On one specific gene several regions may be targeted by the probe, but the choice can heavily impact surface hybridization kinetics [230]. This is especially true when multiple targets are to be analyzed on one single array. Then, one must be sure to detect the correct target on each spot without the possibility of cross-hybridization and thus false-positives. For end-point based detection methods, probe length and composition have to be adapted so that all probes show high specificity for identical experimental conditions, i.e. temperature and buffer stringency. This implies that all perfect matched probe/target duplexes have about the same melting temperatures. Generally, the presence of secondary structures like hairpins in the probes is avoided. Some applications choose however to voluntarily introduce hairpins into the probe to increase specificity by competition arising between probe secondary structures and targets. For long targets with dangling ends, also the length of the linker or spacer chain will influence the hybridization efficiency as discussed earlier in section 4.6.4.

Not only the uniformity of probes in terms of duplex stability is important, but also the length of the hybridizing part of the probes [231]. For genotyping, it is important to discriminate between the perfectly matched duplex and a duplex with a single nucleotide polymorphism (SNP). The general rule that with increasing length of the duplex the specificity of the recognition is reduced has to be kept in mind. Nearest Neighbor predictions are here useful to simulate the impact of the mismatch on the melting temperature. The more Watson-Crick base pairs are formed in a probe/target duplex, the less likely a mismatch can be discriminated. Some applications like complementary DNA (cDNA) arrays, where probe DNA from reverse transcription of messenger RNA (mRNA) is immobilized, have intrinsically long probes. These arrays show a high sensitivity, but often a poor specificity. Likewise, commercial DNA microarrays, for example by Agilent or Affymetrix work with long DNA probes of 60 nt [221, 222].

Since our method is based on temperature scans for SNP genotyping, the probe length must be sufficiently short to yield a detectable temperature shift in the presence of a mismatched target hybridized to the probe. Three different probe lengths are designed for detection of SNP G870A of the Cyclin D1 gene with 16, 20 and 24 nt complementary to the target. In the case of RNA detection for target amplification by NASBA, probes have either 20 or 22 nt. Of course, the highest temperature differences between PM and MM duplexes are obtained on the shortest probes. However, we have already seen that a too short probe length may be incommensurate with in the presence of secondary structures in the target that prevent surface hybridization. In this case, probes need to be sufficiently long to effectively compete for the hybridization sites on the target and the melting temperature of the surface attached duplex should in any case exceed the melting temperature of the secondary structure.

In summary, critical probe design factors include the affinity for the target and thus the probe length, the affinity for non-target DNA in solution which should be as low as possible, the position of the SNP in the probe, the number of self-binding nucleotides in the probe giving rise to reduced sensitivity, and finally the linker length and its physicochemical properties. Empirical studies for different systems and probe lengths can be found in the literature [232, 233].

5.1.2 Importance of adapted blocking strategies

When working with biological samples, the target solutions always contain enzymes and proteins of some types and very specific reaction buffers. For on-chip hybridization, this is a rather disturbing fact; while DNA arrays are designed to show no adsorption of DNA on the surface, the same surface modification often does not withstand non-specific protein adsorption. Proteins are more complex than DNA. Their three dimensional structure is composed of a certain sequence of amino acids and may have various subunits and residues that present all kinds of physicochemical interactions, e.g. electrostatic, hydrophobic, hydrophilic, polar, etc. It is thus a big challenge to find a DNA functionalized surface that is inert to protein adsorption while showing a good sensitivity and specificity toward the target. Recent research is focused on the development of non-fouling surfaces that do not allow any protein interaction. Approaches based on poly(ethylene glycol) (PEG) modified surfaces, amongst others, show rather good results [234, 235, 236, 237]. PEG is also used in drug production to modify the physicochemical interactions of the active components within our body. However, many barriers still have to be overcome before a universal strategy might be found. In our poly-pyrrole or thiol based approach, another difficulty arises: while it is relatively easy to modify the bare gold regions with a PEG having a thiol anchoring group, this does not prevent protein adsorption on the DNA spots, where signal will finally be measured. Other strategies are thus needed that allow efficient blocking of the whole surface.

Common blocking strategies include bovine serum albumin (BSA) based blocking protocols. BSA is a big protein of 69.3 kDa. BSA is commonly used because of its availability, low cost, stability and its compatibility with most enzymes and proteins. BSA adheres to the sensor surface where it can find interaction possibilities. In this way, all possible interaction sites for proteins in the DNA sample are occupied before the sample is brought into contact with the array. As long as the components of the sample solution have no affinity for BSA, this approach works quite well. In this work, the blocking protocol developed by E. Mercey at our laboratory is adopted [238]. Three consecutive injections of 1% (= 1 g/100ml) BSA solutions in the running buffer (1 ml, 10 min) are carried out followed by an injection of 1.5 M NaCl in water for 1 min. The salt injection serves to screen eventual electrostatic interactions and weakly adsorbed BSA is thereby washed off. Other blocking components, like cytochrome C or succinic anhydride (SA), may be used [239, 118]. The choice will depend on the employed surface chemistry and the sample solutions to be injected. One indication if the blocking protein is well adapted is given by the *isoelectric point* (pI). At pH below their *isoelectric point*, proteins are positively charged and for pH>pI a net negative charges is found. The *isoelectric point* of the blocking protein should be similar to those of enzymes in the sample, so that all are at all times either positively or negatively charged and thus repellent in any pH of the hybridization buffer. The isoelectric point of BSA, for example is 4.7 in water at 25°C. Online calculation tools exist that help to find the isoelectric point of proteins and enzymes [240].

5.1.3 Enzyme deactivation

In most applications it is preferable to deactivate all enzymes used during certain amplification or purification steps before proceeding with the following sample treatment step or target detection. The deactivation protocol will depend on the enzyme and is usually provided by the manufacturer. Most enzymes can be heat deactivated. However, this is not the case for DNA polymerases employed in PCR amplification protocols which are thermostable. In this case, it is necessary to suppress the enzyme activity by suppressing the availability of its cofactor Mg^{2+}. This can be done by addition of ethylenediamine tetraacetic acid (EDTA), a molecule that captures divalent ions.

5.1.4 Low volume handling and mixing of sample solutions

Another concern of the detection of biological samples is their availability in small quantities. Often, molecular biology protocols are carried out in low volumes $<100\,\mu l$ and are difficult to scale up to larger volumes. It is thus not astonishing that DNA microarrays or recent developments of integrated components called 'Lab-on-a-chip' are miniaturized systems. Sample handling is a critical point, since low volumes have to be delivered to the hybridization area without loss or significant dilution [171]. Today, a lot of system use microfluidic approaches to deliver target solutions to the hybridization cell.

Our SPRi setup does not permit this approach since samples are injected outside the incubator and then delivered via PEEK tubing of about $100\,\mu l$ volume to the chip surface. Normally, a 6-way injection valve is used for samples of $>200\,\mu l$. For sample volumes below $100\,\mu l$, sample injections via a septum or a three-way valve have been tried. It turned out that the 3-way valve system is preferable since the septum is prone to leakage and leads to injection of air bubbles that hinder target detection in SPRi. The 3-way valve system works well with a Hamilton syringe that is inserted in a buffer filled PEEK tubing part that matches the size of the needle. During injections of samples with volumes down to $15\,\mu l$, the flow is stopped. The syringe is inserted in the PEEK tubing which is then connected towards the SPRi before injection of the sample in the system. The valve is close before retraction of the syringe and a user defined flow rate of usually $1\,ml/h$ is applied to deliver the samples to the heating cell. Of course, when available, more sophisticated injection systems may be used. 6-way injection valves with very low dead volumes of $1\,\mu l$ exist for example for H.P.L.C. applications, but they are rather cost intensive. Abrantes et al. reported a SPRi injection system for as low as $2\,\mu l$ samples using aspiration of sample sandwiched between air bubbles for Bioacore systems [241]. This is however not suitable in our case where air bubbles would hinder our T-scan detection. In microarray applications that do not have a closed fluidic system, also evaporation is an issue. Due to long hybridization times at sometimes elevated temperatures, evaporation must be avoided to avoid that the sample dries during the hybridization process.

Another important issue in the case of long DNA or RNA target is sample mixing. Since long targets have a larger radius of gyration, they will also diffuse more slowly than ODN targets. Especially in the case of low concentration, mass transport towards the chip surface may be limiting for hybridization. Up to date, several mixing systems have been brought forward that allow faster surface hybridization. A commercially available system for microarrays on glass slides is the MAUI hybridization system (BioMicro Systems, Salt Lake City, USA) [170]. The system relies on alternative forth and back movement of the sample volume of 10-65 µl by alternative pressurizing or depressurizing air chambers located at opposite edges. A more complex system based on chaotic advection is provided in the system TrayMix^{TM}2S by BioTray (Lyon, France), formerly called RosaMix. The system has been demonstrated to be compatible with efficient SNP detection, but uses rather large volumes [231]. Raynal et al. studied similar setups numerically [242]. In microfluidics, mixing may be achieved by structuring of the channels resulting in so-called chaotic mixers [171]. Mixing of target solution at low concentration significantly improves hybridization rates and thus decreases overall detection times. Some effort is undertaken to characterize the interplay of diffusion, convection and the parallel surface reaction for small detection systems. Squires et al. review the physical understanding of mass transport limits and reactions limits on biosensors and provide useful guidelines for the development of microfluidic devices [243]. While these authors assume a simple Langmuir model, a more complex DNA hybridization model is simulated by Erickson et al. with respect to mass transport in a channel with a steady spatial temperature gradient for mismatch detection [164].

At the moment, our fluidic system allows forth and back movements, providing only limited mixing capacities. Also, the hybridization chamber is not isolated from in- and outlet, so that diffusion occurs at the interface between samples and running buffer. This is why the injected volume should be large compared to the $5\,\mu l$ hybridization cell and well placed. Wherever possible, experiments are carried out at relatively high concentrations compared to surface hybridization

sites in order to get a reaction limited system rather than a diffusion limited system. Technological developments concerning sample mixing are, however, beyond the scope of this Ph.D. thesis.

5.2 Detection of samples from Polymerase Chain Reaction

5.2.1 Genotyping of PCR samples

DNA amplification has an important role in the analysis of genomic DNA from blood or tissue samples. Only few articles report direct detection of genomic DNA using real-time measurement methods [244]. Genotyping using DNA or RNA targets has been successfully demonstrated on biosensors and microarrays with all kinds of detection system, including fluorescence, as on microarrays, real-time PCR or molecular beacon based methods, electrochemistry, QCM, nanoparticle aggregates, SPR, cantilever based methods, minisequencing or other kinds of enzymatic base extension assays. Some current DNA detection techniques and applications are reviewed in the following articles [245, 11, 224, 246, 247, 53, 248, 4, 52, 227]. Here, we will try to summarize methods and protocols used in PCR surface hybridization and the strategies adopted to achieve mismatch discrimination with special focus on SPRi applications or methods using temperature gradients.

The first step for detection is a good hybridization signal. Typical PCR targets analyzed on solid supports are between 80 and 250 bp long. A first literature research shows that for PCR surface hybridization, research groups report very different hybridization times. While some use hybridization times between some minutes and 1 h [249, 250, 251, 252, 253, 254], others let targets hybridize overnight, often for more than 12 h [255, 256]. Possible denaturation strategies before PCR hybridization are based on heat denaturation, alkaline denaturation, formamide addition or the prehybridization of helper oligonucleotides, which can be, for example, the primers from the PCR reaction [257, 258, 259]. Heat denaturation often shows no efficient strand separation, unless it is used in low salt concentrations [260]. In general, it is advisable to perform either asymmetric PCR or a post-treatment to generate single stranded targets that are more readily available for surface hybridization [257]. Some SPR detection systems, instead of using immobilized ODN probes, fix the PCR targets on the surface and use ODN or short PNA probes as reporter sequence [261, 213, 253]. With this setup, PCR amplicons are rendered single stranded after surface capture by denaturation with 1 mM HCl or 50 mM NaOH. PNA probes in general can be helpful in PCR detection but buffer salt conditions must be specially adapted to optimize hybridization [262]. With SPRi systems, both, unpurified and purified PCR samples have been used. However, hybridization signals can only be followed in purified samples when no buffer change occurs. Secondary structures in the sample are of course an issue and targeted regions should be preferably free of any double helical regions.

For genotyping, most approaches rely on application of stringent washing protocols [106, 252, 263]. Thiel et al. used heating within SPRi to apply stringent conditions for genotyping in an end point detection approach [255]. Real-time analysis offers additional data since kinetics of hybridization can provide supplementary information to simple end point signal differences [213, 261, 55]. Hybridization time can so be shortened, since analysis can be stopped when sufficient discrimination between wild-type and mutant signal is obtained [260]. While wild type and mutant can most of the time be distinguished and classed using calibration curves or discrimination indexes, special signal characteristics often need to be defined for heterozygous samples. When different biosensor surfaces need to be used, this gets soon dependent on the reproducibility of the surface grafting. For SPRi applications, detection limits are usually in the range of 10-100 nM [263, 264], unless signal amplification or special strategies are applied [265]. An elegant genotyping method for SPRi is reported by Hayashi et al. [266]. The authors use a *L-DNA* tag which is introduced during PCR amplification to specifically detect the target's genotype on *L-DNA* biosensors. Since the tag constitutes a free end, surface capture can be achieved in 10 min and determines the genotype without further PCR treatment. A similar capture strategy has formerly been reported by Kai et al. [267]. Petersen et al. report the benefits of multi-thermal washer adapted to microarrays

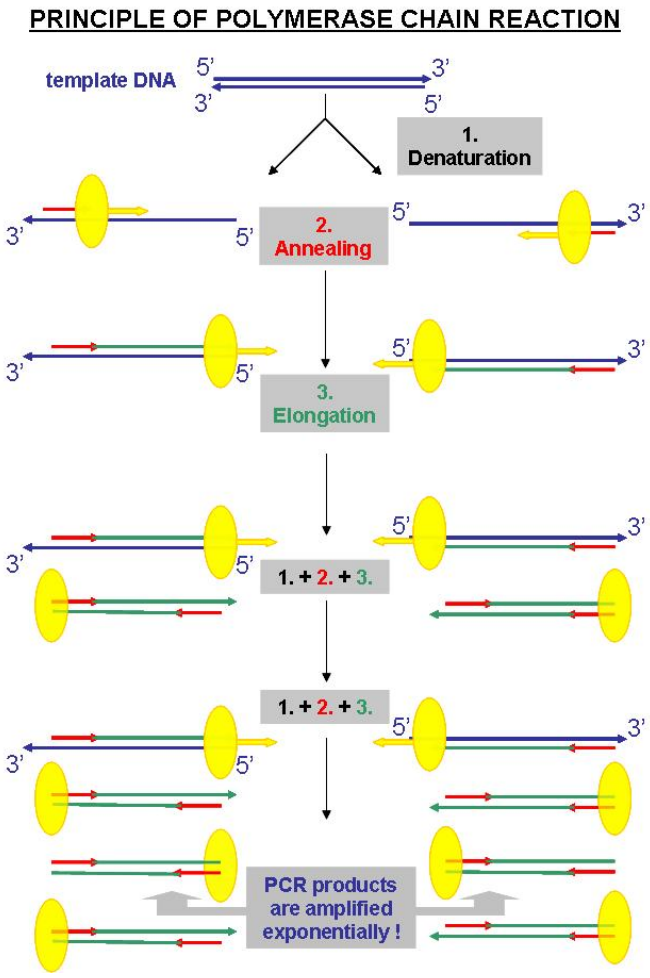

Figure 5.1: Polymerase Chain Reaction: After an initial denaturation step at 94°C (1.), primers are annealed at 60°C (2.) and then extended by Taq DNA polymerase at 72°C (3.). 20-35 cycles of 1.+2.+3. are carried out, leading to exponential amplification of the target sequence.

so that temperature or the rinsing buffer is controlled and SNPs can be identified [268]. Other thermal gradient based methods can be found in the literature [269, 146, 135, 138, 161].

5.2.2 DNA amplification by PCR

The advent of PCR technology has been a crucial break-through for environmental, microbial, forensic and disease studies, to give only a non-exhaustive list. It permitted the incredibly fast development of DNA based tests and promoted the development of DNA hybridization based technologies such as microarrays.

Polymerase chain reaction is a routine method in molecular biology. It permits amplification of any part of a genomic DNA sequence (template) obtained from cell samples or bacteria, for example, provided that adjacent regions are known so that primers can be found. Primers are the starting point of the amplified sequence. They are normally 20-25 nt long. Each primer matches perfectly the 3' end on either the sense or the anti-sense strand of the amplified region in the template. This is depicted in figure 5.1 in the annealing step. Since primers determine the specificity of the reaction, the primer length, sequence (generally with ∼50% G·C content) and concentration must be optimized to exclude any alignments to other parts of the sense or anti-sense strand of the template. Both primers should have the same melting temperature which

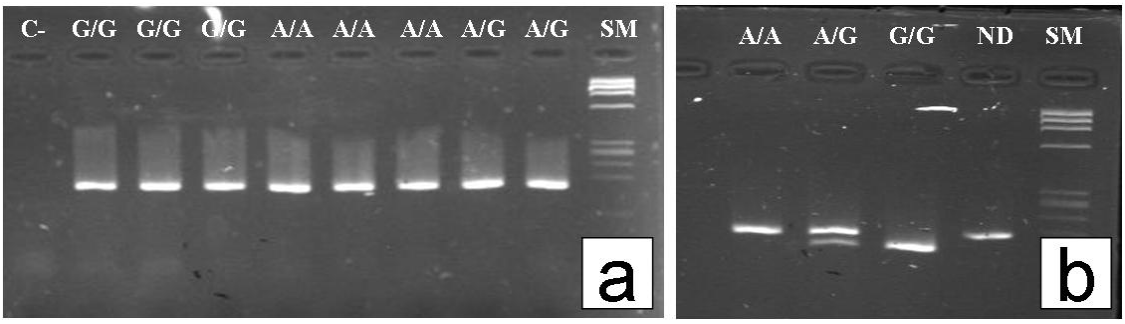

Figure 5.2: a) Quality control of PCR amplification of three different genotypes. All products present the correct length of 167 bp. C- is the negative control in absence of template DNA and SM stands for size markers. b) Genotyping using restriction enzyme *Nci*I cleaving specifically sequences with G at the SNP site. N specifies also fragments from genotype G/G that are not treated with *Nci*I. Results obtained in the group of E. Crapez.

will also determine the annealing temperature, normally about 5°C lower than T_m. Commonly, the method uses the thermostable Taq DNA polymerase that recognizes the double strand formed with the annealed primers and proceeds with its extension in the 5'→3' direction by copying the information from the template DNA. Before the first primer annealing can take place, a prolonged strand dissociation step is required to denature the template completely. Double strand separation, primer annealing and elongation are repeated about 20-35 times during the amplification process leading to an exponential amplification of the DNA sequence (2^n, with n, the number of cycles performed). The PCR process is schematically presented in figure 5.1.

All PCR amplifications are carried out at the 'Centre de Recherche en Cancérologie' at Montpellier. PCR and primer sequences are as specified in table 3.1. The 50 µl reaction mix contains 1X PCR buffer (Invitrogen), 1.5 mM $MgCl_2$, 0.2 mM dNTPs, 2.5 U Taq polymerase (Invitrogen), 0.4 µM of forward and reverse primer, 150 ng template DNA and MilliQ water. After an initial denaturation step of 1 min at 94°C, 35 cycles of denaturation at 94°C, primer annealing at 60°C and primer extension at 72°C are performed. The reaction is stopped after additional extension for 7 min at 72°C by cooling the solution to 4°C. The PCR reaction produces double stranded DNA of 167 bp length.

A quality control is carried out to check the presence of only one sequence of the correct length. This is controlled by electrophoresis on agarose gel. Only one DNA band can be found as shown in figure 5.2a. Further, to exclude contaminations, the presence of the correct genotype is checked using the restriction enzyme *Nci*I with its recognition site $CC|SGG/CCS|GG$, where S stands for either G or C. Since this sequence only appears for base G on position 870, the enzyme specifically cleaves the wild-type allele G as reported in [270]. The correct genotyping is demonstrated in figure 5.2b by the presence of a cleaved product migrating faster due to its reduced size. The heterozygous genotype A/G thereby presents both, cleaved and uncleaved strands with base G and A at the SNP site, respectively. The line N represents the genotype G/G that has not been treated with the restriction enzyme.

5.2.3 DNA purification and extraction

PCR amplicons are in double stranded form, a configuration that is extremely unfavorable for surface hybridization. The amplicons are therefore enzymatically purified to obtain single stranded DNA targets. First, Exonuclease I (New England Biolabs, Ipswich, MA, USA) is used to digest all primers that have not been used in the reaction. Exonuclease degrades any single stranded DNA specifically. Per 24 µl PCR product, 1 µl Exonuclease I is added for a final activity of 10 U/µl. The solution is incubated at 37°C for 30 min. The enzyme is then heat inactivated at 80°C for 20 min. After digestion of the primers, the 5' phosphorylated strand is digested using λ -exonuclease to

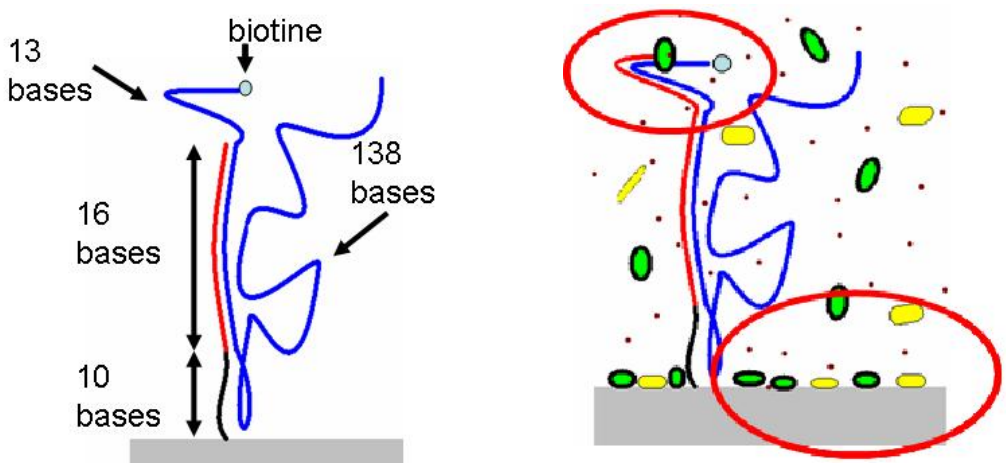

Figure 5.3: *On the right:* the PCR hybridization site and the length of the dangling ends is shown. The 5' end is labeled by a biotin. *On the left:* complex solutions lead to unspecific adsorptions on the surface and can give rise to enzymatic action on DNA like double strand synthesis starting from the probes during heating.

generate the single strand [271, 272]. Therefore, 1 µl λ-exonuclease (New England Biolabs, Ipswich, MA, USA), 3 µl of 10X reaction buffer provided by manufacturer and 1 µl DNAse/RNAse free water are added for each 25 µl PCR sample. The enzyme should at least have a final concentration of 5 U/µl and has in our case 20 U/µl. The solution is incubated at 45°C for 45 min and then heat deactivated at 80°C for 15 min. The enzymatic purification protocols can be up-scaled to 100 µl sample solution. Alternative protocols for single strand generation from PCR products have been reported in the literature [273, 274]. Also, asymmetric PCR amplification may be considered to obtain an excess of one single stranded target.

For SPRi detection optimization, it is convenient to further purify the solution in order to remove all enzymes and change the buffer. A common protocol based on phenol/chloroform extraction to remove proteins followed by an ethanol precipitation of DNA is used. The desiccated targets may then be taken up in deionized water and quantified by UV spectroscopy using the NanoDrop system. All DNA samples are stocked frozen at -20°C before use.

5.2.4 SPRi detection and genotyping

Optimization of the hybridization protocol

The first step to SNP genotyping and probably the main difficulty is the hybridization of the long PCR amplified DNA strand on the SPRi sensor surface. From ODN based experiments presented before, we know the crucial parameters that will influence the hybridization conditions. Target concentration is, of course a main issue since too diluted solutions will be limited by mass transport to the surface and also equilibrium surface coverage will be low. For oligonucleotides of 20 bases we found a detection limit at 10 nM. It is however preferable to work with high concentrations, in the limits of availability.

The target configuration is the next point: in figure 5.3 on the left, the hybridization configuration is shown for probes of 16 nt length. The hybridizing part of the PCR sequence is located near the 5' end of the target, thus leaving a surface proximal tail more than two times longer than in PolyT-surf and PCR80 studied in section 4.6.4. We must expect to find decreased surface hybridization due to steric hindrance and it might be useful to vary the grafting density to obtain higher spacing between the probes. Further, the target exhibits a strong secondary structure of $\Delta G_{25\,°C} = -32.52$ kcal/mol as shown in figure 5.4 for allele G. For the mutated target A, less stable secondary structures are predicted by the Mfold program [209]. We can see that the hybridizing

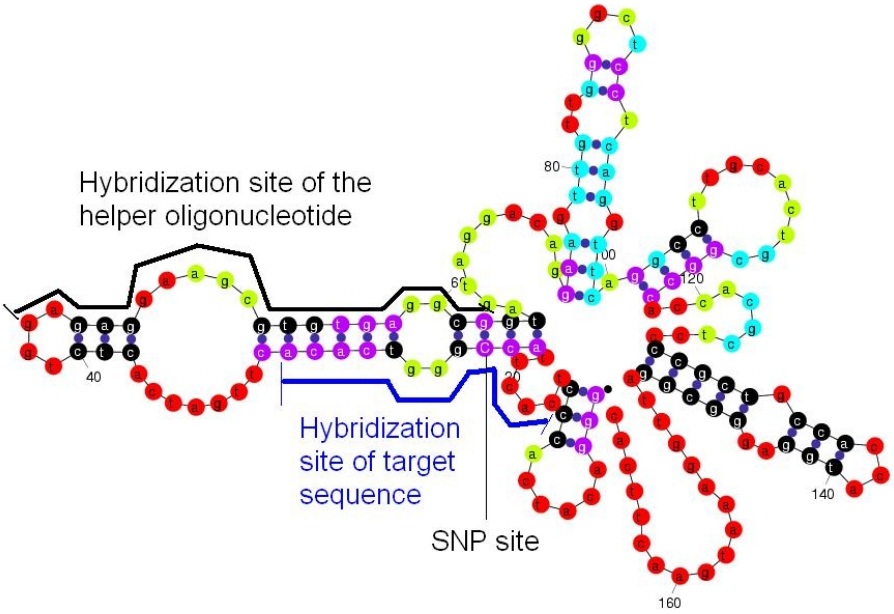

Figure 5.4: One possible secondary structure predicted for PCR amplicon genotype G/G using Mfold [209]. The color code describes the probability of bases to be in secondary structure, where red describes always unbound bases and black always bound ones. Violet represents a ∼75% probability and green ∼35% probability to be in bound state. The probe hybridization site, the SNP site and the helper alignment are indicated.

part, here shown for 16mer probes, is in the region of a stable hairpin. The melting temperature of the folding is predicted with T_m=58.4°C. Color code shows the probability of nucleotides to take part in secondary structure formation as indicated in the figure legend. In a first time, it will be useful to work with genotype G/G for optimization since it might be more difficult to hybridize. Secondary structures must be opened to reduce competition with surface hybridization. Longer probes are expected to be better competitors than short 16mer probes. Due to the presence of secondary structures, we know from work on PCR80 that the hybridization temperature will have a crucial influence on target association and dissociation as well as the final surface coverage obtained. When concentration and hybridization temperature are adapted to the hybridization configuration, surface hybridization might still be slow. So the last unknown parameter will be the hybridization time necessary to obtain detectable SPRi signals. Due to ∼8-fold increased mass of the target compared to Gc20, we expect a higher SPRi signal for lower surface coverage. In this work, no mass transport system is developed for low target volumes and these phenomena will thus not be further discussed, although they clearly are part of the set of parameters influencing on-chip detection.

First injections to SPRi sensor surfaces did not yield any detectable signal so that for first characterization and optimization studies of target surface hybridization fluorescence microscopy is used. Fluorescence microscopy is more sensitive so that small signals can be detected that could not be observed by SPRi. The protocol for fluorescence microscopy is given in appendix B on page 148. Figure 5.5 shows three independent experiments on the same sensor surface that is regenerated by NaOH after each assay. Absence of fluorescent signal after regeneration is controlled. Hybridization of genotype G/G and M5c simultaneously at 42°C during 30 min to 16mer CCND1 probes and M5 is shown as blue line. We find that best hybridization signal is obtained on M5, corresponding to spot saturation. Only one fifth of this signal is observed on complementary spots G16 and even lower signals for TG16 and A16 with one mutation. Almost no signal can be detected on 2 MM spot TA16. Three poly-pyrrole spots in the lower left corner

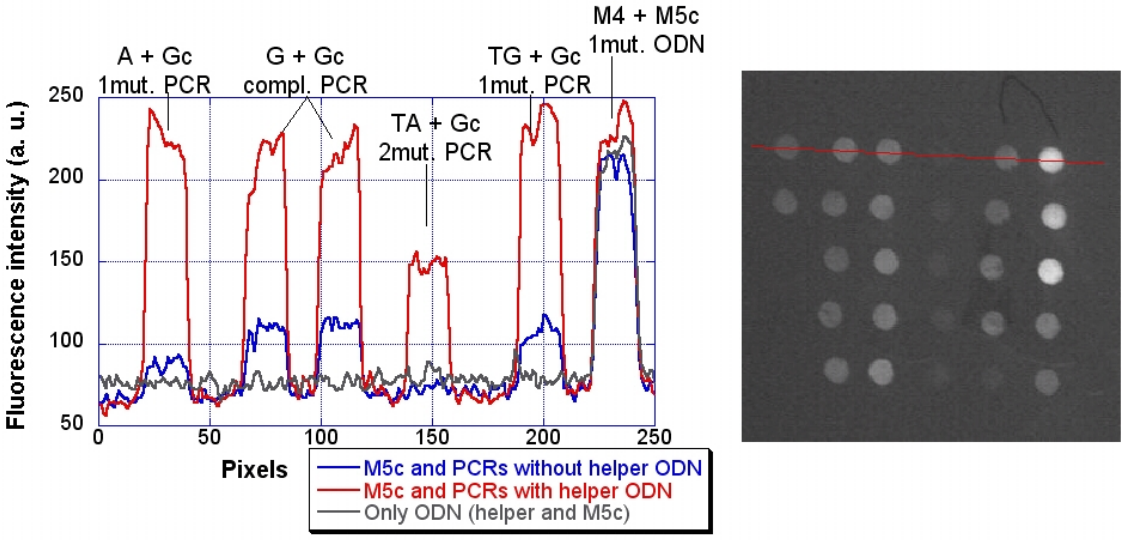

Figure 5.5: *On the left:* Line plot of fluorescence images over a series of spots. Three different experiments use targets 1. PCR G/G and ODN M5c (blue), 2. PCR G/G prehybridized to helper ODN and M5c (red), 3. and M5c and helper ODN alone (grey) at 42°C for 30 min. The control spot M5 (on the right) serves as reference signal for maximum detectable fluorescence. When PCR products are heated to 95°C and subsequently hybridized with their helper ODN at 60°C, the hybridization signal on poly-pyrrole spots reaches the same magnitude as M5c. The control experiment in absence of PCR targets shows no hybridization on CCND1 probes. *On the right:* Fluorescence image corresponding to hybridization 1. The plotted line is indicated.

of the matrix as shown in the figure on the right do not show any signal.

To decrease secondary structure formation at the hybridization site and thereby increase surface hybridization kinetics, a helper oligonucleotide of 20 nt length is designed that hybridizes to the side of the hairpin that is complementary to our hybridization site as indicated in figure 5.4. Its sequence is given in table 3.1. Helper oligonucleotides have been reported to increase solid state hybridization for double stranded DNA or single stranded PCR amplicons [259, 275] and to improve RNA accessibility in regions of strong secondary structure for fluorescence in situ hybridization experiments (FISH) [258, 276]. Here, the helper itself has some resemblance with the actual target and should thus not be used at low temperatures where excess helper ODN might compete with the target for surface hybridization sites. To effectively anneal the helper to the target, the target solution is heated in presence of 10% excess of helper ODN for 3 min to 95°C before annealing of the helper for 1 min at 60°C. The annealing temperature is slightly lower than the predicted melting temperature of the helper, analogue to primer annealing in PCR. In figure 5.5, the blue line demonstrates the increase of hybridization obtained for the same hybridization condition with PCR G/G and M5c as before. We see that this time, complementary spots and spots with 1 MM show hybridization signals equivalent to ODN spot saturation of M5c on M5. We now obtain also a signal on spots with two mutations that elevates to about one half of the maximum signal obtained in PM spots. The helper oligonucleotide thus increases significantly the hybridization rate and favors surface hybridization. A control experiment with only helper ODN and M5c under equal conditions shows not signal on CCND1 probes confirming the previous signal to be due to hybridization of PCR amplicons and not the biotinylated helper ODN.

Different injection protocols are also studied by SPRi using the synthetic PCR80 sequences to confirm results from fluorescence microscopy. Upon hybridization of PCR80 annealed to the helper ODN in PBS 450 mM NaCl, 1 mM EDTA, 0.05% Tween20 at 25°C, we find an increased association rate, es expected. This is shown in figure 5.6a. Although injection is not performed

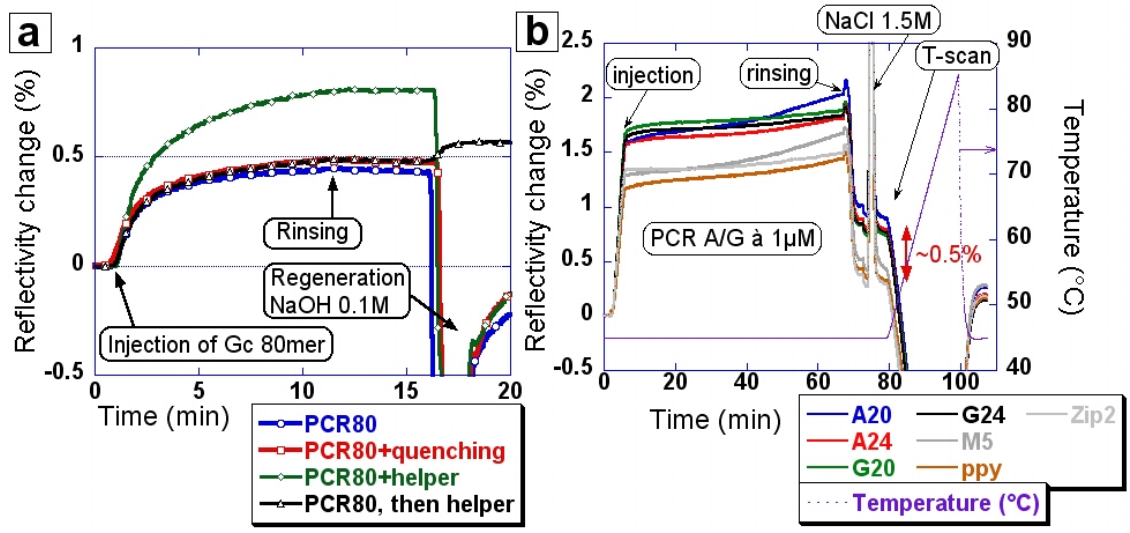

Figure 5.6: a) Hybridization kinetics of different Gc PCR 80mer injections at 250 nM with various pretreatments. Best association is obtained in the presence of helper ODN. b) SPRi signal averaged over spot types for an injection of purified PCR amplified sample mix A/G at 1 µM for 1 h. A hybridization signal of ∼0.5% is obtained at the beginning of the T-scan for 0.3% background signal. Corresponding NTD curves are shown in figure 5.9.

long enough to reach equilibrium, it gets clear that hybridization in the presence of the helper ODN tends to a higher equilibrium surface coverage. To determine if the increase in signal is simply due to the additional mass of the helper, a subsequence injection of the helper after hybridization of PCR80 is shown. The helper increases the signal, but not to the extend we observe for association of helper annealed targets. We also examine another common denaturation method which is based upon heat denaturation for 3 min at 95°C and then rapid cooling for 1 min on ice. The sample is then injected at room temperature into the SPRi system, but no signal difference to hybridization of untreated PCR80 targets can be found. Fast reannealing after heat denaturation has also been reported for PCR hybridization which could be overcome using alkaline denaturing conditions [257]. Only the helper oligonucleotide seems capable of effectively reducing secondary structures that involve the hybridization site in our target.

The study of the synthetic analog PCR80 as presented here and previously in section 4.6.4, alongside fluorescence microscopy experiments finally succeeded to provide optimal conditions for hybridization of the purified DNA target on poly-pyrrole grafted biochips. First results are obtained for 1 µM purified G/G target concentration in the presence of the helper ODN in a total volume of 40 µl in PBS 400 mM NaCl and 1 mM EDTA. Hybridization is allowed to take place for 3 h at 45°C with no-flow conditions. The hybridization is carried out on a poly-pyrrole chip having grafting densities that correspond to 2 µM and 10 µM DNA in 20 mM pyrrole. Signal intensities vary between 0.55 and 1.1% reflectivity. No hybridization signal is found on probe A16 due to the elevated hybridization temperature. In general, hybridization signals are higher on 10 µM spots than on 2 µM spots. An exception is G16, where both reach about the same signal. Furthermore, hybridization signals are generally better the longer the probe, consistent with their higher stability. Since the hybridization signal seemed to indicate only minor increase after 1 h hybridization, the hybridization time is shortened accordingly. Subsequence SPRi prisms are based only on chips with probes of 20 and 24 bases length, since 16 bases are not efficient at the hybridization temperature chosen.

In figure 5.6b, the SPRi signal obtained for a 1 h hybridization of a sample mix mimicking genotype A/G is shown. Due to refractive index changes during target injection, and signal drifts during the hybridization period, the hybridization signal can only be detected at the end of

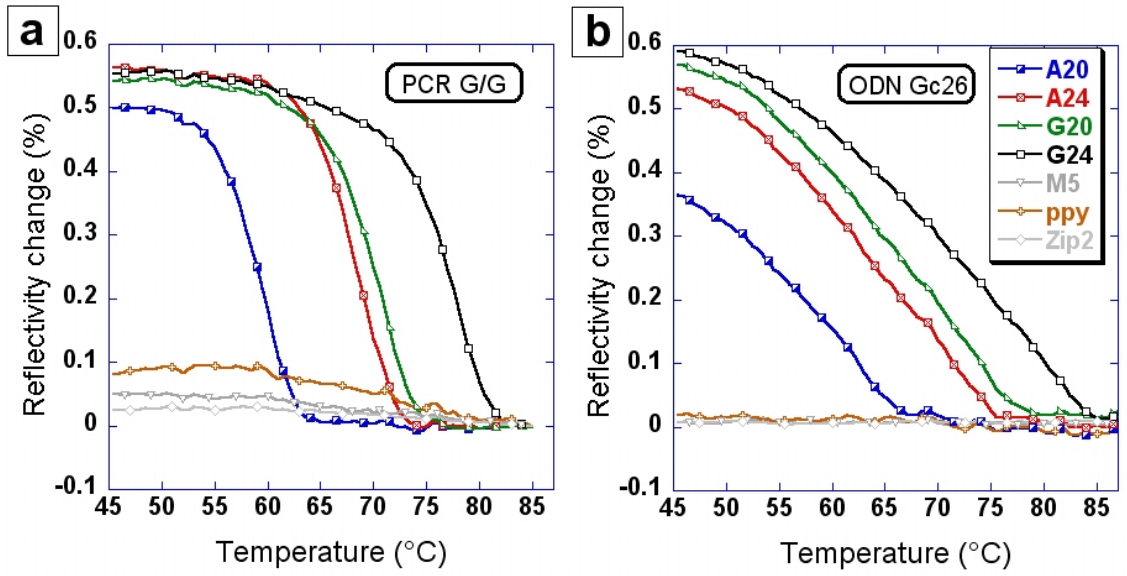

Figure 5.7: a) NTD curve of PCR G/G amplified DNA at 1 µM. b) NTD curves for ODN Gc26 at 250 nM obtained on the same chip. While the ODN curves are large, PCR products show a pronounced, sharp transition.

injection after rinsing. The refractive index change is due to sample preparation from 5X buffer, targets at ∼1 µM, helper in 10% excess to target and deionized water, as well as the subsequent annealing of the helper ODN. A specific hybridization signal is found on CCND1 spots with an average signal of 0.5% reflectivity. Note that the quantity of injected target corresponded here to one PCR of 50 µl. Also, some non-specific signal is found at the end of hybridization. It has been found useful to inject during 1 min a 1.5 M NaCl solution to wash away eventually species on the chip that is weakly bound. This procedure avoids desorption of any such component during the subsequence temperature scan where it would induce additional noise. Hybridization and rinsing is then followed by a temperature scan to identify the hybridized target genotype.

We successfully hybridize targets corresponding to all three genotypes: homozygous wild-type G/G, heterozygous A/G and homozygous mutant A/A. However, contrarily to our expectations, we do not obtain an 8-fold signal increase due to the increased mass of the PCR amplicon as compared to ODN targets. For 1 h hybridization on 10 µM poly-pyrrole chips, we obtain signals that are in the same order as found for Gc26. Longer hybridization times might increase the surface capture, however, it is unlikely that the same target density as obtained for ODN targets can be reached. Already the 80mer synthetic targets did not show the same surface coverage as short ODN targets.

Mutation detection using temperature scans

Due to the very complicated configuration and the unfortunately strong secondary structure, the biggest problem of genotyping using our SPRi system is the surface hybridization. Once this is achieved with a minimum reflectivity signal, T-scans can be used to detect the genotype of the target. When acquiring NTD curves for PCR amplified targets, we observe another interesting feature of DNA thermal denaturation. The dissociation curves obtained on PCR samples are not flat as curves found with ODN targets, but show a rather narrow transition over a temperature range of about 10°C. A comparison of averaged NTD curves obtained on the same sensor surface for (a) PCR G/G and (b) Gc26 is presented in figure 5.7. The signals are not normalized so that hybridization signals at the onset of the temperature scan can be compared. Due to long hybridization times, signal background is slightly increased for PCR targets. As already mentioned,

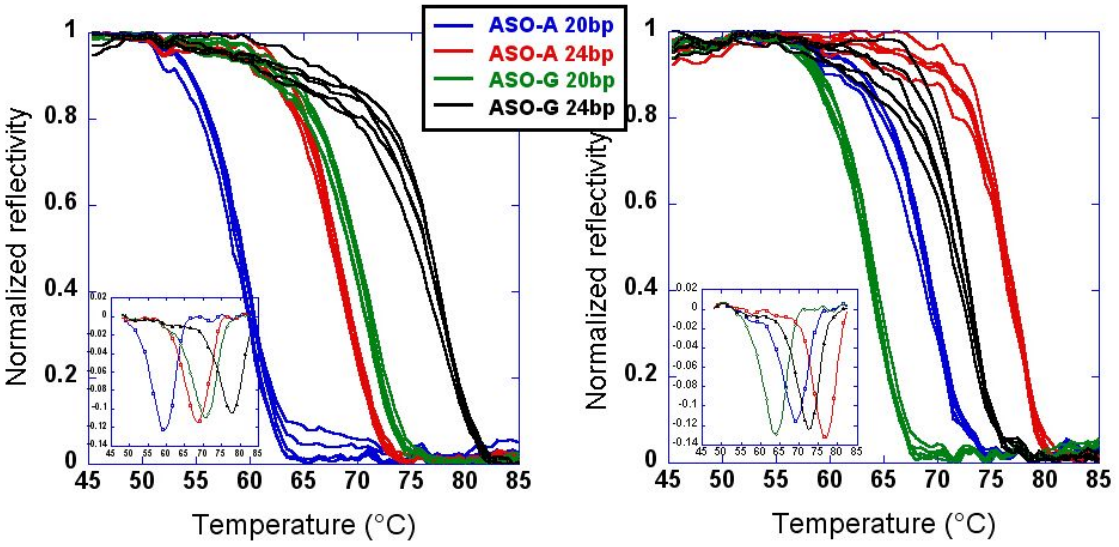

Figure 5.8: Thermal denaturation curves of PCR amplified, purified targets genotype G-G (left) and A-A (right). Mutations towards the probe can be clearly distinguished from the dissociation temperature or the peaks of the derivative (insets).

the fact that we find an equal hybridization signal indicates a lower surface coverage obtained with PCR targets. A comparison of the curve shape clearly shows that the physicochemical environment of the PCR sample is distinguishably different from ODN targets. The sharp transition displays strong interactions that are absent in ODN dissociation curves. This cooperativity is a welcome effect since the sharp transition increases the selectivity of our assay. Dissociation curves between matched and mismatched duplex are also more readily distinguished. The hybridizing length on the surface is identical for both, ODN and PCR targets, so the reason may not be found in duplex interactions but other types of physicochemical interactions.

In general, for probes of 24 bases, we find more noise at temperatures smaller than T_d before target dissociation. This might be attributed to the dissociation of helper oligonucleotides from the surface proximal dangling end. The helper ODN has 20 nt which represent about 10% of the total mass per hybridized target site. Since it has a theoretical melting temperature of 66°C, it should be sufficiently stable at 45°C but dissociate earlier during the temperature scan from the target than the target from probes of 24 nt length. So, on longer DNA probes, we expect a signal loss due to helper denaturation. While curves of 20 bases are very reproducible, the helper dissociation appears on long probes as noise and depends on the spot. The conclusion that the helper is present on some targets during dissociation and absent for others leads to the conclusion that the helper ODN has no influence on the observed cooperativity. DNA cooperativity has been known for some time now for long dsDNA in solution. Several theoretical models have been put forward and bubble formation and DNA melting has been successfully predicted for several DNA sequences [277, 278, 279, 280]. In biotechnology applications, sharp melting curves have been observed on DNA-modified gold nanoparticles hybridized to ODN microarrays [281, 282]. There, Taton et al. report a full width half maximum (FWHM) of the curve's derivative of 3°C revealing even sharper curves since we find here a FWHM of ∼6.5-8°C. For comparison, for AU-NP or streptavidin coupled dissociation, we detect here a FWHM of 10-16°C which is much higher. Taton et al. show also that dissociation of fluorescently labeled targets from the same array is much larger, similar to our findings on ODN. Also comb polymer-DNA hybrids can show cooperative melting. Possible explanations are based on the formation of aggregates or networks that interconnect DNA and thus stabilize the conformation until T_m is reached. Another model explained cooperativity of melting by ion clouds shared between neighboring strands and confined

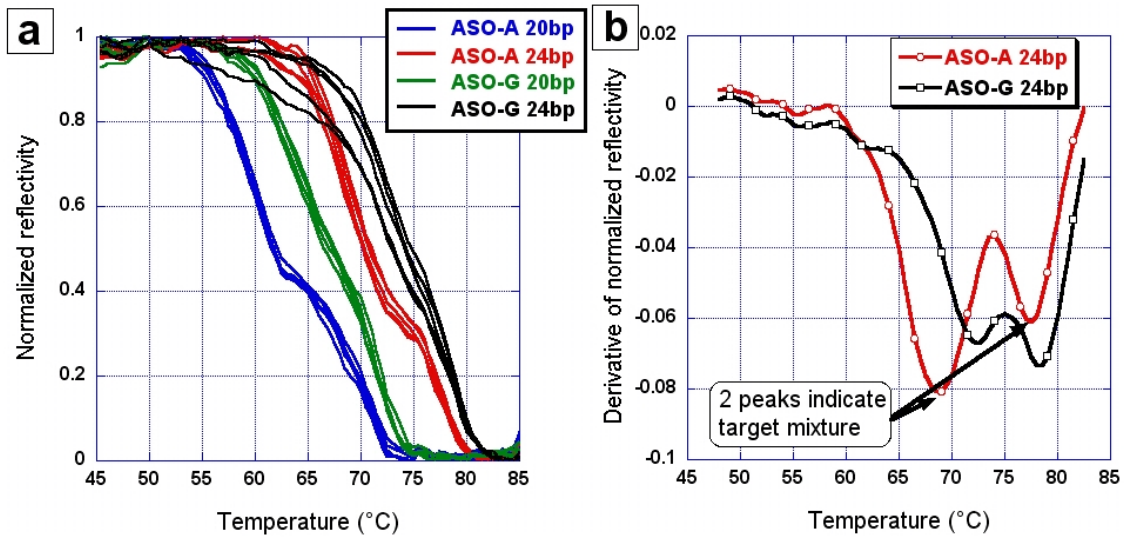

Figure 5.9: Thermal denaturation curves of a mixture of PCR amplified, purified targets PCR-Ac and PCR-Gc (left). A plateau indicates the presence of mutated targets. In the derivative we find two distinct peaks (right).

zones that stabilize the hybrids. DNA cooperative melting on comb polymer-DNA has recently been more deeply analyzed by Gibbs-Davis et al. and Park et al. [283, 284]. Their experimental concept and the obtained data is compatible with the neighboring duplex cooperative model based on ion clouds. However, cooperativity is exclusively found when hybridization takes place in between structures that link DNA. Then, the dissociation of an individual, free DNA strand is found coupled to the dissociation of surrounding DNA, leading to a switch-like dissociation. Here, hybridized targets are not physically linked to other targets. We can however not exclude that the proximity does not lead to entanglement and partial hybridization between dangling ends of neighboring targets. In this case, an interacting network might occur that, similar to the polymer combs exhibits cooperative melting. With the present data, we can however not conclude on the exact interpretation of our observations. We can only state that the phenomenon seems to be independent of the presence of the helper ODN and shows not a big dependence on the amount of surface hybridized targets, since we will find the same steepness for $\sim 50\%$ lower hybridization signals after injection of unpurified targets later on.

Figure 5.8 shows the NTD curves obtained for homozygous targets G/G and A/A. The normalized curve of G/G corresponds to figure 5.7a. Here, the result of each individual spot on the sensor is shown and demonstrates very good signal reproducibility amongst different spots. From the order of dissociation, the genotype is readily determined, as well from probes with 20 nt as from the longest probes used here with 24 nt. In each case, the perfectly matched spot shows higher dissociation temperatures, i. e. G20 and G24 dissociate at higher temperatures for injection of G/G than probes A20 and A24 and, in analogy, for A/A, probes A20 and A24 are more stable than probes G20 and G24 specific for the wild type allele. Differences between PM and MM are more pronounced on shorter probes, as expected. The inset in each figure shows the derivative of the curves. Since they essentially display the same information, they might be used for automated genotyping. Therefore, the minimum of each curve is extracted and the corresponding temperature compared to determine which spot is perfectly matched to the target and which forms one mismatch. Alternatively, temperature ranges can be defined to classify the genotypes, provided that dissociation temperatures are reproducible. The first method, based on the order rather than absolute temperatures is, however, more flexible with respect to alternative buffer conditions, T-scan speeds and other factors influencing the dissociation temperature.

The next challenge is the detection of the heterozygous genotype A/G. Figure 5.9a shows dis-

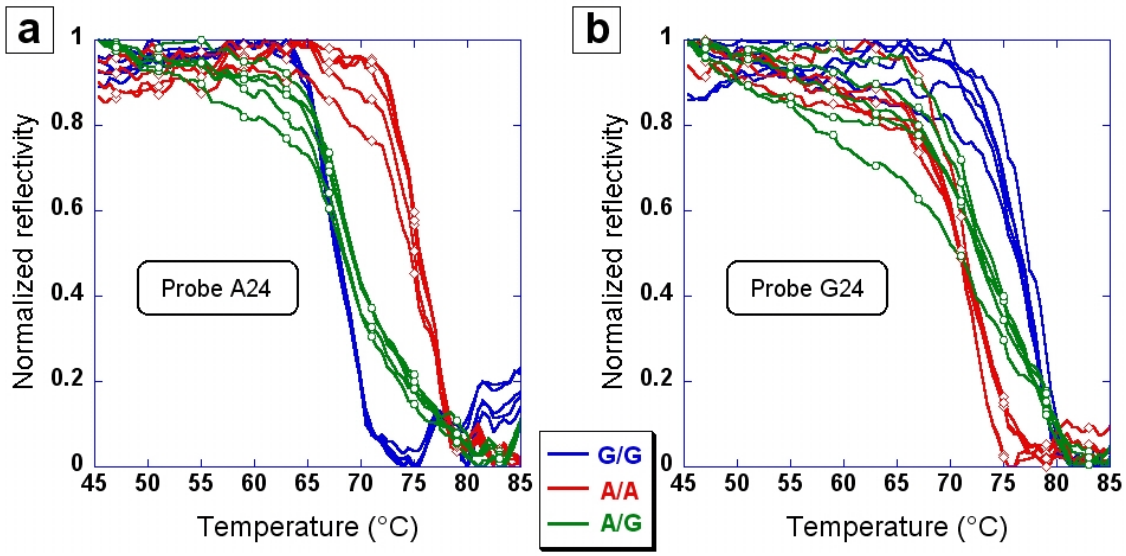

Figure 5.10: PCR detection using unpurified single stranded samples. a) Comparison of NTD curves obtained on spots A24 upon hybridization of genotype G/G, A/A and A/G. b) NTD curves for the same injections obtained on spot G24.

sociation curves for a target mixture of equal proportions of PCR G/G and PCR A/A (in absence of a 'real' PCR sample of type A/G at the end of the Ph.D.). Also in the cased of mixed targets, dissociation is cooperative. As in the case of the oligonucleotides, we observe the subsequent dissociation of, at low temperatures, the target with one mismatch with respect to the probe, then, at higher temperatures, the perfectly complementary target is denatured and washed away. We so find once more the characteristic plateau in the melting curve. Contrarily to observations on ODN curves, the plateau is here not found at exactly the same proportion for each probe type. A20, which forms the less stable duplexes, shows an increased proportion of matched targets when compared to, for example, probe A24. This indicates that dissociation at the hybridization temperature is not negligible on this spot and some reorganization takes place. Mismatched targets are replaced by matched targets to some extend. Although it might be difficult to clearly find a plateau in the dissociation curve of probe G24, the derivatives shown in figure 5.9 reveal its presence. As predicted from the Langmuir based model in section 4.2.1, we find two minima indicating the presence of targets of different stability on the spot. We are thus able to correctly identify the genotype of the injected target. For correct identification, only two spots, complementary to each allele would be necessary in this approach.

Up to here, all results reported are obtained on purified targets, in the absence of enzymes or proteins of any types and with well controlled buffer conditions. We will now try to suppress the DNA extraction step, while still performing the enzymatic purification and generation of the ssDNA. Although we would like to have as little manipulation steps as possible, it is necessary to make one change to the buffer. A sufficient concentration of EDTA should be added in order to prohibit any activity of Taq DNA polymerase on the chip. An accidental 'result' during this work is the elongation of surface grafted 16mer probes during heating of the chip in presence of Taq polymerase and PCR targets. The probes are extended by the remaining 13 bases towards the 5' end of the target as indicated in figure 5.3. This renders the chip unusable for further SNP detection studies and should thus be suppressed by capture of free Mg^{2+} ions by EDTA.

Before unpurified PCR solutions are passed over the SPRi chip, a second blocking step, additional to BSA injection is done. A mixture of 36 µl solution of PCR control (absence of template DNA) and 4 µl EDTA at 100 mM is passed at a flow rate of 0.2 ml/h over the chip to block any

non-specific sites to which enzymes might attach. 31 µl PCR solution is adapted to contain 1 mM EDTA and 1 µM helper ODN in 40 µl final volume. The solution is denatured at 95°C for 3 min before annealing to the helper at 60°C for 1 min. Hybridization on the chip is carried out for 1 h at 45°C and yields a maximum signal of 0.35% reflectivity. Figure 5.10 shows a superposition of denaturation curves obtained after 1 h hybridization of genotype G/G (blue), A/A (red) and A/G (green). On the left, results on spot A24 sensing the mutant target are shown. We find a dissociation temperature of 76.5°C for hybridization of A/A, and a T_d of 69°C for injection of G/G. The heterozygous sample shows dissociation between these two temperatures. Here, we can not detect a clear plateau in the signal since hybridization signals are small. The findings on spot G24 are equivalent, the heterozygous genotype being detectable by its mid-position between the two dissociation curves. Although curves for each genotype can be clearly distinguished, a criterion based on the curve's derivative would fail here to detect genotype A/G. Probes of 20 bases are not shown since they lead to even smaller hybridization signals and on spot A20 hybridization is quasi absent for injection of G/G. The curves are also subject to a lot more noise than curves obtained with purified targets.

Although we show here that genotyping is possible even on complex samples containing several enzymes and proteins (Taq Polymerase, Exonuclease I, λ-exonuclease, BSA) and with low hybridization signals, it is quite evident that further optimization will be needed to improve hybridization signals. Since the buffer here is not the same as in previous experiments on purified samples, the hybridization temperature of 45°C might not be optimal. Also, while for purified samples, the total of one PCR amplification of 50 µl is concentrated in 40 µl at ∼1 µM, here, only 31 µl of PCR sample is used in a final volume of 40 µl, leading to a more diluted concentration of ∼620 nM. Hybridization kinetics can therefore be slower.

The results with unpurified PCR targets are preliminary and represented here to show that our detection system can be applicable to more complex samples. It is clear that for an unambiguous and automated detection of PCR amplified detection a series of optimization and validation experiments will still be needed. Also, only few steps have been taken until today to validate the detection of mutated targets at low percentages in a large DNA background as previously introduced in section 4.6.2 for oligonucleotides. Preliminary experiments show that the main limitation is the slow hybridization, even when hybridization takes place during a steady cooling process at 1°C/min. Protocols that worked well for ODN targets can thus not be applied in a 1:1 fashion to PCR amplified targets. For complicated protocols with heating and cooling cycles over long durations, we expect problems due to signal drift in the SPRi, especially in the presence of proteins that may change properties during heating and lead to high background signal. For optimization of protocols searching for low proportions of mutated targets, purified DNA samples should thus be used. The oligonucleotide based detection limit of 5% that we found earlier is encouraging, since other PCR based methods report detection limits that are higher or equal to ∼5% minority allele in the sample [213, 285]. So, with the help of temperature assisted dynamic hybridization, we might be able to push these limits to lower percentages.

In the summary, we demonstrated here that point mutation detection using a temperature scan based SPRi detection method can be applied to biological samples of high complexity. Problems related to secondary structures, hybridization with surface proximal tails, low sample volumes and low sample availability have been overcome. This work reveals, however, that even our temperature scan based method needs optimization of the hybridization protocol. SPRi has a low sensitivity, compared to fluorescence detection where PCR targets could be detected even with not optimized, standard hybridization protocols. Once hybridization exceeds a signal-to-noise ratio of 10, genotyping of the targets is possible. Our NTD curves obtained on long targets show a sharp, reproducible dissociation profile as opposed to ODN samples with a large transition. This renders the discrimination between different curves easier and thus favors point mutation detection. The reason for this cooperative behavior is not completely clear, but might be attributed to interactions of dangling ends with their environment or dangling ends of proximal targets.

5.3 Detection of samples from Nucleic Acid Sequence-Based Amplification (NASBA)

In this section, we will learn about a second DNA amplification strategy as an alternative to PCR. The project on Nucleic Acid Sequence-Based Amplification (NASBA) is led in collaboration wit K. Brengel-Pesce and N. Beaufet from bioMérieux. The NASBA amplification strategy is patented and commercialized by bioMérieux. Due to the industrial background of this study, some experimental information, such as DNA probe and target sequences or exact buffer components have not been known during the work and are thus not stated here.

This project has been started during the Master 2 project of Carole Lecossois. The motivation of this project is to study a second biological target type with our temperature scan based detection method, which is this time RNA from NASBA amplification. The RNA targets are between 100 and 200 bases long and considerations as previously made for PCR samples do also apply here. We have to take into account that our samples have dangling ends, may form secondary structures and, especially, that they are provided in complex sample solutions that need careful preparation and blocking of the biochip to reduce non-specific interactions. Since NASBA is an isothermal method, it is seductive to use NASBA directly 'in situ' in our SPRi heated cell, so that we would obtain a real-time amplification and detection method. The results presented here will only reach the 'proof-of-concept' state since our laboratory is not equipped to work in contamination free environments which would be necessary to optimize and validate the detection method for screening applications.

5.3.1 NASBA detection and applications

Like PCR and other DNA amplification methods, NASBA is a *in vitro* amplification system suitable for nucleic acid detection. The NASBA reaction as developed by Compton in 1991 produces antisense RNA from RNA templates [286]. In some cases also DNA templates can be used, eventually with a slightly altered experimental protocol [287]. One advantage of NASBA is the RNA amplification in a huge DNA background making it suitable for mRNA detection. Moreover, NASBA is an attractive amplification method in the field of microbial detection since no intermediate cDNA is needed. A huge variety of viruses, bacteria and fungi have been detected using NASBA for applications in disease detection [288, 289, 290, 291, 292, 293, 294, 295, 296, 297, 298], food screening [299, 300, 301] and water control [302]. NASBA recently finds an increasing interest and several studies undertake comparisons to classical detection methods like (real-time) RT-PCR or ELISA [293, 294, 295, 296]. Results however diverge and although NASBA is reported as a very simple and sensitive method, it is not always the method of choice. Especially, primer design is a critical factor, as in all primer based methods, since here the process is isothermal and no specific annealing at the primer's temperature takes place. So, it can happen that multiplex NASBA sometimes fails to yield positive results where other methods do [290]. The addition of internal controls may here be favorable in order to increase the assay precision and detect amplification failure [291, 303]. Also secondary structures in RNA templates may lead to failure of amplification due to suppressed primer annealing when only few templates are available [300]. Nakahara et al. reported an increased efficiency of NASBA amplification upon addition of inosine 5'-triphosphate to the reaction medium for targets with strong secondary structures [304]. A detailed review on NASBA amplification and detection has been published by Deiman et al. which delivers general rules for probe and primer design [287]. A more specific review for food and environmental screening is published by Cook et al. [301]. Classical NASBA amplification is detected by electro-chemiluminescence, but methods based on enzyme-linked gel assay, NASBA-linked oligonucleotide capture or a RNA biosensor in a membrane base format with liposome reporter probes have be reported, too [301, 302, 298]. However, since this time, a real-time NASBA assay based on fluorescence detection using specific molecular beacons has been developed and is now widely applied because of its availability in the NucliSens technology developed by bioMérieux [305, 297, 291, 290]. Further, a quantitative mathematical model for molecular

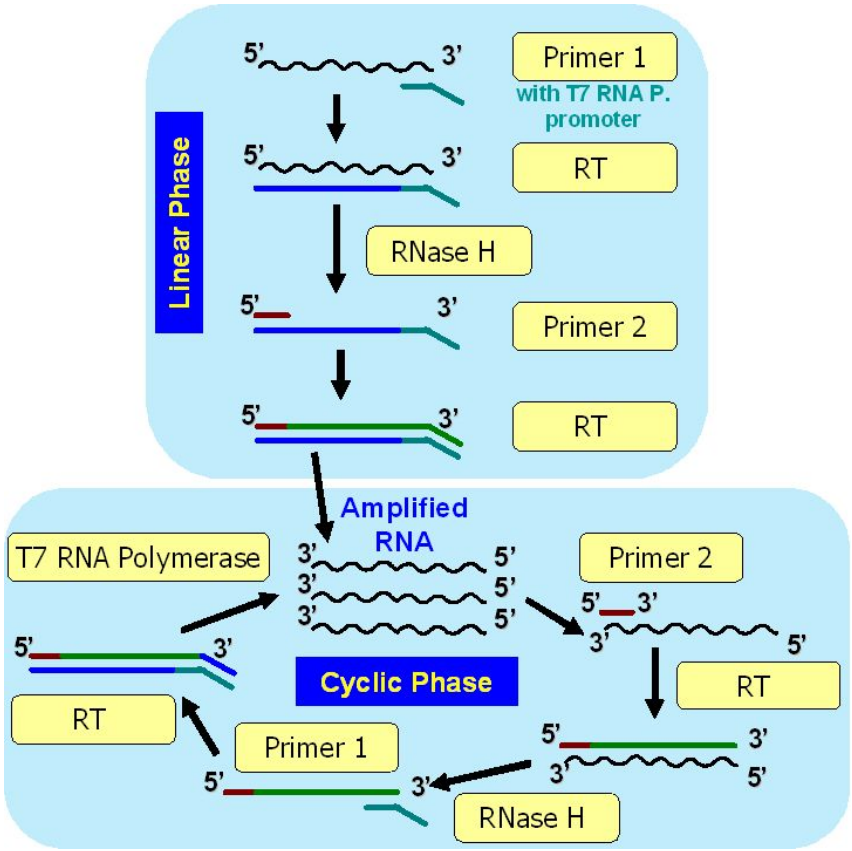

Figure 5.11: Reaction scheme of isothermal RNA amplification using Nucleic Acid Sequence-Based Amplification (NASBA).

beacon based NASBA detection has been presented by Weusten et al., making real-time NASBA a fast and attractive detection system [306]. The real-time NASBA system has also been proved to be compatible with point mutation detection due to the good specificity of molecular beacons [307, 205].

5.3.2 Amplification of RNA by NASBA

Nucleic Acid Sequence-Based Amplification is an isothermal, enzymatic reaction that produces single stranded RNA targets of determined sequence and length. As PCR, the method makes use of primers to select the correct region in the template that can either be DNA or RNA. The amplification works at 41°C and needs three different enzymes. Contrarily to exponential PCR target amplification, NASBA gives rise to linear amplification with 10^{12}-10^{14} copies at the end of amplification.

The amplification strategy is depicted in figure 5.11. In the scheme, RNA is distinguished by wave lines from DNA represented by solid lines. Sense RNA is here chosen as template. We distinguish a linear and a cyclic phase of the amplification but both take place simultaneously. Before the amplification can start, the template is denatured for 3 min at 65°C. Only when the reaction mix is cooled down to 41°C, the enzymes are added and the amplification begins. First, primer 1 needs to anneal to its position on the template. The primer has a 5' dangling end composed of the T7 RNA polymerase promoter sequence (5'-TAA-TAC-GAC-TCA-CTA-TAG-GG-3'). The primer is then extended in the 5'→3' direction by reverse transcriptase (RT), using AMV-RT, an enzyme from avian myeloblastosis virus. In this way a DNA strand complementary to the template is produced. This DNA/RNA duplex can now be recognized by *RNase H*, an

enzyme that specifically hydrolyzes RNA that is bound to DNA. Now, the new DNA strand is accessible for annealing of primer 2 at its 3' end and can be once again extended by RT. Note that during this extension, also the T7 promoter sequence is copied that is not part of the original sequences of the template. This linear phase generates thus continuously double stranded DNA that corresponds to the template sequence in between the primers plus a functional T7 promoter site. The T7 promoter is important for the cyclic phase, since it is recognized by the T7 RNA polymerase which produces hundreds of antisense RNA copies. The reaction product will thus be complementary to the original template strand. Although this RNA is the final target, it also contributes to the amplification by production of more dsDNA strands with T7 promoter. Therefore, primer 2 anneals to the RNA target and is extended by RT as before. After RNA digestion by *RNase H*, primer 1 can hybridize to the remaining DNA strand and once again be extended by RT. Actually, both 3' ends of the double stranded portion are extended since also the T7 promoter is copied. In this way, a new dsDNA strand is produced for RNA transcription by T7 RNA polymerase. The reaction is allowed to proceed for 1-2 h.

It is clear that the reaction scheme involving three different enzymes needs careful buffer optimization to ensure a good activity of each individual enzyme. Also triphosphates (dNTP and NTP) for DNA and RNA strand production must be available in sufficient quantity. The NASBA amplification is commonly used with real-time detection based on molecular beacons that bind to a specific target site on the ssRNA product. By fluorescence measurements, the apparition of fluorescence is detected once sufficient amounts of targets are produced. The amplification protocol can be multiplexed in order to amplify several targets at one time. Of course, as any multiplexing approach, this needs a lot of optimization to allow specific and efficient amplification of several targets. Also the detection system must then be chosen to present different fluorophores that can be distinguished during detection by their emission wave length.

In this study, we use the NucliSens basic kit® by bioMérieux for NASBA reactions. Enzymes, reagents and buffers are provided with a detailed experimental protocol. The reaction takes place in a volume of 20 µl. As only parameter, the amount of template DNA can be chosen and is here 500-10^4 copies. Amplification is carried out in absence of any molecular beacon probe so that amplified targets are free for surface hybridization. The reaction needs a precisely controlled temperature of 41.0±0.5°C, so we used a thermocycler platform (DNA thermal Cycler 480, Perkin Elmer/Cetus, Waltham, MA, USA) and DNAse-RNAse free Eppendorfs of 500 µl for amplification at 41°C for 90 min.

A control of our NASBA reaction is done by electrophoresis on a 2% agarose gel stained by ethidium bromide (EtBr) (figure 5.12). We find amplified products in lane 1 to 7. The first three lanes correspond to samples after RNA purification using phenol/chloroform extraction followed by ethanol precipitation. Lane 4 is a sample that was amplified at bioMérieux and stocked frozen until use. Lanes 5-7 represent amplifications from 10^4 copies of template carried out at our laboratory. In amplification No. 6, no template was added, but due to contamination, we find also here the same amount of target RNA. The NASBA reaction is very sensitive and works with solutions containing only very few templates. Only sample 8 does not show amplification, since no enzymes were added to the solution. This proves that the detected lines are produced by amplification and that the lines do not represent our templates. From the size markers and the DNA band, we can conclude that the detected RNA product is about 200 nt long.

5.3.3 Detection of DNA/RNA on-chip hybridization

To study surface hybridization of NASBA products by Surface Plasmon Resonance imaging, we need to prepare a chip with the corresponding probes. bioMérieux provided probe sequences of 20-22 nt length with 28-33% G·C content that correspond to specific detection regions in targets A, B and IC that are about 100-200 nt long. A and B represent sequences corresponding to two types of influenza viruses and IC is the internal control used for molecular beacon based NASBA quantification. In the molecular beacon based assay, the probe sequence would correspond to the loop of the beacon. All probes have here a 10-thymine spacer on the 5' end. Probes are modified by

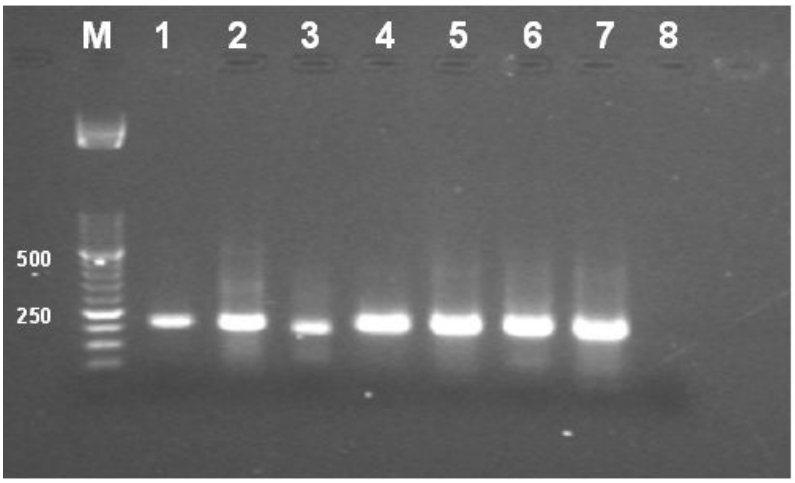

Figure 5.12: Fluorescence image of NASBA product A migrated on 2% agarose gel stained with ethidium bromide. The smear shows ssRNA products, while the band is the dsDNA with T7 promoter sequence: M=size marker, ladder of 50 bp. 1-3) Purified samples, 4) Sample amplified at bioMérieux, 5-7) Amplification at SPrAM. In No. 6, no transcripts had been deposited, but unsterile working conditions led to contamination and amplification. 8) NASBA control without enzymes.

an amine function (NH_2) on the 5' end and by a DABSYL molecule (4-dimethylaminoazobenzene-4"- sulfonyl chloride) on the 3' end, that serves here to prevent probe extension in the presence of a reverse transcriptase enzyme in the sample. C. Lecossois coupled the probes to N-hydroxy-succinimide ester modified pyrrole (Py-C_{11}-NHS) monomers using sodium bicarbonate ($NaHCO_3$) as coupling agent with a equivalent of 80 pyrrole monmers per ODN. Probes are then purified on C-18 columns by H.P.L.C. to purify the proportion of probes coupled to a pyrrole moiety as described earlier for probes synthesized at our laboratory (section 3.4). Complementary ODN targets obtained from bioMérieux served to control the spotting by SPRi. Probe A and IC show good, specific hybridization signals as response to ODN injection at 250 nM in PBS 450 mM NaCl. Coupling of probe B to pyrrole had a low efficiency and probe B signals will therefore not be analyzed in this work. As positive control, M5 is spotted on each chip and ppy spots are used as negative control.

For hybridization of the targets, we first analyzed purified NASBA products. The extracted RNA is concentrated in water and approximately quantified using the NanoDrop UV Spectrometer using an estimated absorption coefficient. Targets are stocked frozen and only diluted to working concentrations in our standard hybridization buffer PBS at 450 mM NaCl and pH 7.4 before injection in the SPRi. Typically, sample volumes are 20-100 µl and we thus use the Hamilton syringe and 3-way valve injection system for target injection. Initially, we did heat denaturation and quenching on ice before injection of the targets at 25°C at ∼250 nM-1 µM. However, this precaution turned out to be unnecessary since these RNA targets hybridize rather well even without this treatment. Figure 5.13 shows a typical prism prepared for detection of RNA targets. The kinetic curves show a hybridization event of RNA target A on its complementary spot. Due to a slight buffer change, a global base line shift occurs during hybridization, but the obtained signal can be found during rinsing. Each curve represents the average of 5 spots bearing the same probe. We can see on the kinetic curves as well as on the differential image that the hybridization signal is specific. The 100 µl sample is here passed at a continuous flow rate of 0.5 ml/min, allowing for ∼13 min hybridization. In this short hybridization time, we obtain a detectable hybridization signal.

The ease of signal detection with RNA targets is in the beginning surprising, after having worked on our difficult PCR targets. Two explanations can however be brought forward. On one

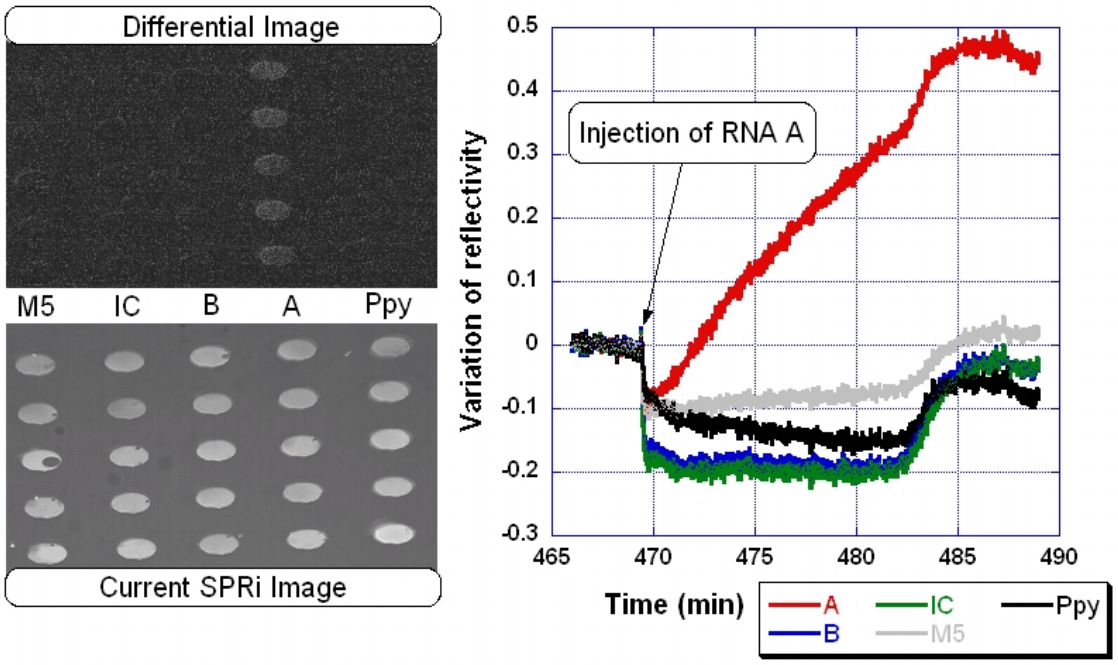

Figure 5.13: *On the left:* Current SPRi image and differential image of the ppy functionalized prism after hybridization. Hybridization of RNA target A is specific. *On the right:* Corresponding kinetic curves of hybridization demonstrating the fast association. A slight buffer change occurs during injection and signal readout is done at t> 485 min in rinsing buffer.

hand, the system from bioMérieux is already used with a molecular beacon detection system and must thus be optimized with regards to secondary structure formation in the amplicon at least at 41°C. Here, the hybridizing part of our target seems not implicated in strong secondary structures since it is readily available to surface hybridization at low temperatures. This is especially true since RNA is commonly known to form stable secondary structures more easily than DNA. On the other hand, RNA is also known to form a more stable duplex with DNA than a corresponding DNA sequence on the same DNA probes. This may also contribute to the good affinity we find here for our immobilized probe.

5.3.4 In situ amplification and detection of RNA targets

Since RNA detection is possible on our DNA chip, we would like to go towards an integrated system that combines in-situ amplification using NASBA with our temperature scans for sequences identification. If we successfully amplify and hybridize RNA targets in the SPRi, we can then detect point mutations in the target during a subsequence non-equilibrium thermal dissociation experiment. Although the probe/target system provided by bioMérieux does not contain any point mutations, it can still be used as a proof of concept for an integrated amplification and detection system.

As hybridization of purified RNA could be readily performed, the next logical step is to work with solutions from the NASBA amplification without further treatment. Therefore, we use again the BSA based blocking strategy reported on page 89 to avoid non-specific adsorption of enzymes to the sensor surface. Moreover, we have to take into account eventual activity of enzymes on our sensor. To avoid any activity of reverse transcriptase on our probes, all probes furnished by bioMérieux are blocked on the 3' end by a DABSYL molecule. This is not the case on our positive control M5. Further, we must consider eventual target digestion by *RNase H*. When targets are hybridized to our DNA probes, they provide a substrate for *RNase H* hydrolysis and we might

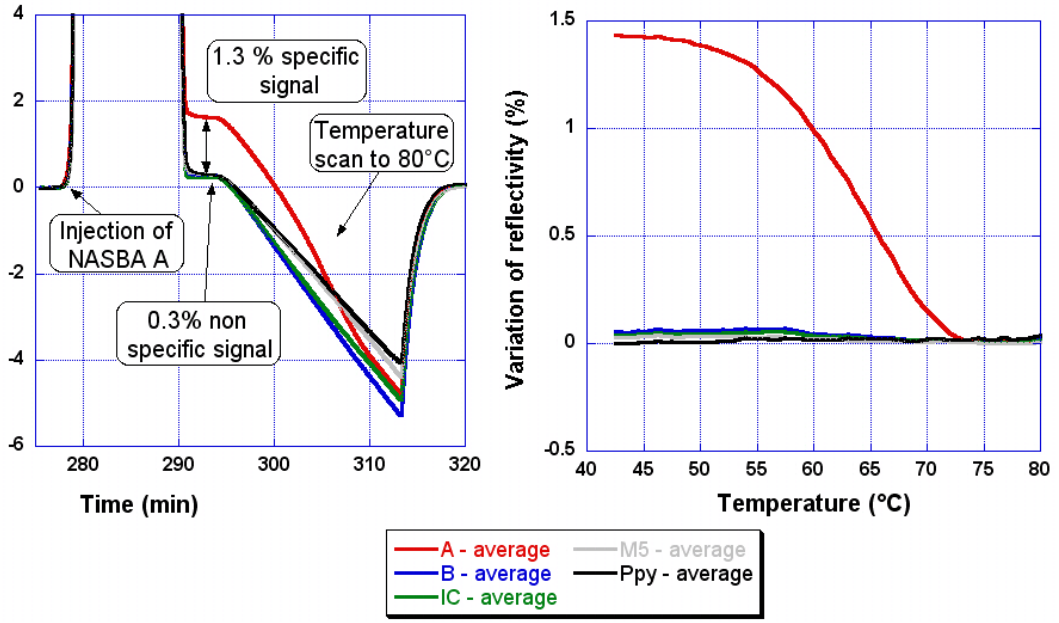

Figure 5.14: *On the left:* SPRi signal for NASBA RNA A injection and temperature scan detection. Signals are baseline subtracted and averaged over different spot families on the chip for better visibility. *On the right:* Corresponding dissociation curves as obtained after subtraction of a reference temperature scan. Only RNA A has been hybridized and can be detected with an average T_d of 63°C in PBS 450 mM NaCl.

loose hybridized targets in this way. Two facts are however encouraging. First, molecular beacon based detection also uses DNA probes and only slight signal decrease may be found at the end of the amplification. Thus, although some targets might be hydrolyzed, the overall amount is sufficient to provide good signals. Second, work in the group of R. M. Corn uses *RNase H* in SPRi experiments and shows that *RNase H* has a about 10-fold decreased activity on surface hybridization as opposed to solution experiment [265, 308, 123]. We can thus hope that digestion of targets plays a minor role and will not prohibit successful integration of NASBA in our SPRi heating cell. Finally, before trying to do in-situ NASBA reactions, we calibrated the heating cell with respect to the PCR thermo-cycler in which NASBA reaction is successfully performed.

For hybridization of non-purified NASBA products, targets from one amplification are diluted in a total volume of 100 µl PBS 450 mM NaCl, 1 mM EDTA and 0.05% Tween20 buffer. The sample is injected at 25°C at a flow rate of 0.5 ml/h resulting in 13 min hybridization. During the injection a very high buffer change of 6.5-8% reflectivity occurs so that association can not be followed in real-time and we only find the hybridization signal during rinsing. Although non-specific signal in the order of 0.4% of reflectivity is detected, we find a hybridization signal of 1.5% above this background noise with very good specificity for probe A. Similar hybridization signals are obtained for injections of 20 µl undiluted NASBA product with hybridization for 10 min at 41°C in absence of any net flow and with comparably low background signal. In figure 5.14a, one injection of 20 µl sample of amplified target A is shown. Due to the high refractive index change, hybridization is detected only after rinsing. At the end of the 5 min rinsing period at 5 ml/h a temperature scan to 80°C is applied. We distinguish already from the untreated signal where the DNA is dissociating. In figure 5.14b, the respective NTD curves are shown. We see that the background signal of ∼0.3% reflectivity does not affect the NTD curves that show a smooth dissociation. The target can be easily detected.

So, the next step is to perform NASBA reaction in-situ by maintaining the heated cell at 41°C.

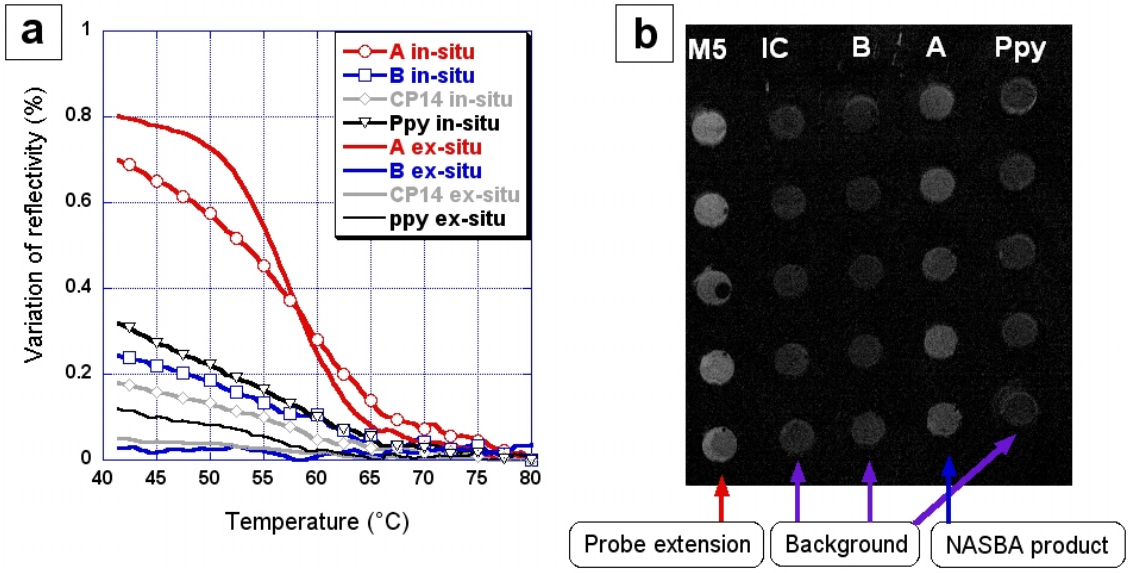

Figure 5.15: a) Comparison of dissociation curves of NASBA target A for in-situ amplified targets (markers) and ex-situ amplified RNA targets. For in-situ NASBA, we observe a smaller signal and higher background, as can be seen also in the differential image b). The image shows specific hybridization on A, but also strong signal on control M5 due to probe extension by reverse transcriptase. Probe A, B and IC are blocked by a DABSYL moiety at the 3' end.

First experiments did not succeed, due to inappropriate running buffer conditions. For small injection volumes (40 µl) of NASBA reaction mix in running PBS buffer, we detect a seriously changing reflectivity over the 90 min reaction time, indicating buffer exchange. Concentration gradients will appear that will induce net species flow. Especially salt ions are fast diffusing molecules with diffusion coefficients in the order of 1-2 $\times 10^5$ cm^2/s [309]. In the strong gradient applied, they will be drifting inside the reaction cell where they inhibit enzyme activity. At the same time, the reaction medium will be diluted and since NASBA reaction buffer is optimized for three enzymes simultaneously, surely at least one enzyme might fail in diluted buffer conditions with changing pH and salt concentration. So, we adapted a NASBA buffer from data from the literature to ensure that at all times the basic buffer components are maintained the closest possible to their original concentration [300, 289]. The NASBA buffer is based on 40 mM Tris-HCl at pH 8.5, 15% DMSO, 80 mM KCl, 12 mM $MgCl_2$, 5 mM freshly added Dithiotreitol (DTT) and 0.375 M sorbitol. As DMSO is denaturizing for DNA it adapts the melting temperature of each duplex formed in solution. KCl provides the necessary salt, while $MgCl_2$ is necessary for enzyme activity. Sorbitol is present since it is used for lyophilization of enzymes and is thus part of the buffer after enzyme dilution. The DTT is necessary for good functionality of T7 RNA Polymerase as indicated on the enzyme's data sheet by New Englands Biolabs, but is not always reported as ingredient in NASBA reaction buffers. In this reaction buffer, we succeeded to obtain a low hybridization signal after performing the NASBA reaction for 90 min at 41°C for 100 µl volume with 10^4 copies of template RNA. However, the SPRi base line change during injection is still huge so that real-time observation is suppressed. We adjust the sorbitol content to 0.5 M, but it is not possible to perfectly match the original reaction mix. However, this final buffer gave reproducible results that clearly showed the possibility to do NASBA in-situ amplification combined to NTD scans for detection.

Figure 5.15 shows a comparison of NTD curves from the same NASBA amplification preparation, one obtained in-situ with 100 µl injected (symbols), and the other for the injection of 20 µl sample amplified in the classical Eppendorf format (plain lines). First, we see that noise is more

elevated for in-situ amplification and at the same time, we obtain a lower hybridization signal. So, for in-situ experiments we find here a signal-to-noise ratio of 2.3 while ex-situ amplification gives 6.7. The signal-to-noise ratio during T-scans could be raised to 10 by injections of 1.5 M NaCl during the rinsing period and before the T-scan. Thereby, proteins that adhere electrostatically with low affinity are detached, as observed for PCR solutions, too. There clearly is a need for better blocking strategies to lower the background. Various signals found after in-situ NASBA reaction can be distinguished in figure 5.15b, where a differential image is shown. We see the elevated background signal, hybridization signal on probes A and an even higher signal specific to M5. Since M5 is the only unblocked probe with a free 3' end, it has been subject to elongation which is revealed by the impossibility to regenerate the signal during the T-scan. This phenomenon is not systematically observed on all prepared prisms and occurred only during the second in-situ NASBA preparation on the same chip. Indeed, the extension should not take place at all since M5 shows no particular hybridization with target A. It has also been found that prisms undergo degradation when reused with in-situ amplification and signal loss is more elevated than for simple target hybridization and detection. About one third of the original hybridization signal is lost during each in-situ amplification process. Four independent in-situ amplifications and detections are carried out successfully at our laboratory with 500-10 000 templates for target A in the reaction mix.

In summary, this study shows the feasibility of a NASBA based integrated system combining in-situ amplification and detection. There are still some points to be addressed to optimize the system. First, a better background suppression would be needed. Second, the degradation of biochips during amplification is strong and prevents reusability. Then, the injected samples of 100 µl should be reduced to save enzyme and reactant cost. Also, the issue of contamination in the heating cell has not yet been addressed. To avoid false positive results, the SPRi system must be sterilized before the next amplification, which could, for example be done by injection of strong alkali solutions that upon heating degrade any RNA remaining in the system. Multiplex NASBA with A and IC was tried, too, but resulted in no detectable amplification for IC neither from in-situ nor ex-situ samples. Possibly, degradation of templates or competition between primers which are identical for target A and IC may be the cause. But also surface hybridization may be much slower so that we are just incapable of detecting IC with the same conditions as A. All these issues could not be addressed in this work and may be part of future validation studies in case of further application of the SPRi system for NASBA based point mutation detection.

5.4 Conclusions on detection of long targets on DNA chips

This chapter demonstrated the detection of two specific detection systems that use long DNA or RNA as target. While confronted to a very complicated system with strongly limited surface hybridization characteristics for the PCR target, we get easy and fast hybridization detection with the NASBA amplified target that is optimized for availability of the hybridization site. The importance of well chosen hybridization sites for on-chip experiments is evident and must be considered during probe and target design. Still, hybridization parameters like buffer, temperature and concentration are important for our SPRi setup to succeed in target detection. Main issues for detection of unpurified samples are also blocking strategies for background suppression and a running buffer that limits diffusion phenomena and permits at least partial control of the hybridization signal. Finally, any activity of enzymes on the immobilized probes needs to be prohibited. The last points are especially difficult to control and will need optimization for each new sample containing different enzymes and buffer. One point that has not been confronted experimentally is also target mixing to optimize mass transport towards the surface. Mixing systems or closed-loop circulation systems for small sample volumes below 100 µl will be useful. For in situ amplification, the injection system should optimally be separated from the running buffer to avoid dilution of carefully optimized reaction solutions.

Besides these 'optimization' issues, we also found a surprising cooperativity when studying

DNA non-equilibrium thermal denaturation with PCR targets. By comparison with the NASBA NTD curves, it gets clear that this is not a characteristic of all systems hybridizing long targets to a surface. It might instead be related to the possibility of interactions with neighboring DNA strands, which is surely favored in the case of our G·C rich PCR amplicon. Since we have no knowledge of the exact sequences of the NASBA amplicon, no direct comparison is possible. The favorable surface hybridization might however indicate the absence of strong secondary structure and indicate a sequence with rather low G·C content. The cooperative dissociation is welcome since it enhances point mutation discrimination. We successfully detect homozygous and heterozygous cases with wild type and mutant in PCR amplicons.

Chapter 6

DNA repair: enzyme interaction with damaged DNA

Ce chapitre présente du travail réalisé en étroite collaboration avec le 'Laboratoire des Lésions des Acides Nucléiques' (LAN) du CEA Grenoble et représente une partie du projet de thèse de Christelle Corne sous la direction de D. Gasparutto et A. Favier. Les expériences SPRi réalisées ont débutées avec J.-B. Fiche et ont été continuées tout le long de ma thèse.

Dans cette dernière partie présentant des résultats expérimentaux, nous allons étudier différentes enzymes impliquées dans la réparation des lésions de l'ADN. L'étude est focalisée sur le mécanisme de réparation appelé 'réparation par excision de base' (BER). Ce mécanisme intervient notamment dans la réparation des lésions d'ADN suite à une désamination spontané, des dommages oxydatives ou par méthylation de l'ADN. Ce mécanisme de réparation par excision de base fait intervenir des enzymes qui ont une reconnaissance spécifique pour une certaine lésion, leur 'substrat'. Cette spécificité rend une analyse par SPRi de l'interaction enzymatique avec l'ADN endommagé attractive. Ici, nous allons observer notamment des enzymes impliquées dans la réparation de la lésion 7,8-dihydro-8-oxoguanine, une lésion oxydative de la guanine. La formamidopyrimide-DNA-glycosylase (FPG) d'*E. coli* et son équivalent humain la 8-oxoguanine DNA glycosylase (hOGG1) seront étudiées. Nous analyseront l'interaction de ces enzymes avec différentes lésions d'ADN naturelles ou synthétiques ainsi que leur activité d'excision de base. Pour cela, nous profiterons à nouveau de la possibilité de réguler la température. En un deuxième temps, nous étudierons également des endonucléase, Endo IV de *E. coli* et APE 1, son équivalent humain. Tandis que les glycosylases FPG et hOGG1 sont bivalentes, c'est-à-dire, elles excisent la base et coupent ensuite le squelette de l'ADN, les endonucléases n'interviennent qu'une fois la base endommagée est excisée. On étudiera ainsi leur activité sur des sites abasiques pour obtenir des informations fondamentales sur les processus de reconnaissance de la lésion et l'activité enzymatique liée. Une étude d'intérêt biologique est menée pour déterminer l'activité enzymatique sur des lésions multiples qui peuvent apparaître lors d'une irradiation par UV, par exemple.

Cette étude sur la réparation d'ADN montre l'utilité d'une approche 'biopuce à ADN' pour l'étude des enzymes. Bien qu'il soit difficile de quantifier l'activité enzymatique, les cinétiques offrent de nombreuses informations sur l'interaction de l'enzyme avec son substrat. Grace à une construction de puce dite 'universelle', nous pouvons comparer différentes lésions en parallèle et ainsi conclure sur leurs effets inhibitoires ou bénéfiques à la réparation enzymatique. Une telle étude servira notamment à développer de nouvelles stratégies pour la lutte contre le cancer. L'identification des inhibiteurs de la réparation d'ADN permettra d'améliorer des traitements de cancer par irradiation ou médicaments anticancéreuses, qui visent à endommager l'ADN de la tumeur pour tuer la cellule. Egalement, la possibilité de détecter rapidement l'activité de réparation cellulaire d'un patient pourrait être la base d'un traitement de cancer personnalisé.

6.1 Introduction

While in previous chapters, our main interest lay in the detection of point mutations in DNA, we will now take one step back and study the origin of variation in the genetic information. Contrarily to what we might guess, DNA is intrinsically instable and may be degenerated spontaneously in the cell [310]. In our natural environment, the DNA of each cell is constantly exposed to damaging effects. Those can have their origin in normal metabolic processes or be of external nature like, for example, the sun's UV light. Each of our cell suffers about 10 000 DNA lesions per day [311]. Hence, it is not astonishing that evolution early developed specific procedures to recognize and repair damage in the genetic information. DNA repair is crucial for gene expression since transcription of a gene is often interrupted at a damaged site. Thus, no messenger RNA (mRNA) is produced nor is the corresponding protein which is necessary in cell functioning. So, the DNA has to be constantly repaired to ensure a correct metabolism of the cell. But even more important is the 'sanity' of the genetic material for DNA replication, just before the cell divides. Any damage that has not been repaired or occurs at this state may lead to permanent change of the genetic information. Unprocessed or badly processed DNA damage is the origin of base substitutions, deletions or insertions, that may lead to defects, disease or cancer formation. By the way, also the aging process has been linked to alteration of the genetic information. It must however be said, that the cell has an intrinsic control mechanism that can give rise to programmed cell death, i.e. apoptosis, if the genes encounter too much damage. One cell is sacrificed for the good of the whole organism.

6.1.1 DNA repair pathways and their importance in cell survival

Cells are in systematic surveillance of eventual DNA damage. DNA repair can use one of the four main DNA repair pathways that are known today. The nucleotide excision repair (NER) pathway applies for a large number of lesions. NER is based on the recognition of the lesion followed by local unwinding of the DNA in order to excise a region of about 30 nt in the damaged strand. Then, the gap is filled by copying from the remaining strand and ligation of the DNA backbone. Another DNA repair mechanism is the base excision repair pathway (BER). It usually applies for lesions generated by spontaneous deamination of a base, oxidative damage due to irradiation or free radicals and DNA methylation. Here, only the damaged base is recognized and excised so that a DNA polymerase can then fill in the gap. Repair is completed by ligation of the remaining ends. A third repair pathway is specialized in DNA mismatch repair (MMR). MMR intervenes after replication and corrects mismatches or insertion/deletion loops that may occur when polymerases 'slip' on the strand to be copied. As already mentioned in section 2.3, DNA polymerases have a high, but limited fidelity and errors occur every 10 000-1 000 000 bases [43]. Last, the recombinational repair pathway exists for the serious damage of double strand breaks. In the case of double strand breaks, two ends of the helix have to be correctly combined to restore the original information. Non-homologous repair joins the two strands and repairs by ligation while homologous repair makes use of the fact that each chromosome exists twice so that the duplicate can provide the necessary information for repair. In some cases, also single strand annealing may serve for alignment before homologous repair. All these pathways are detailed in [311] and references therein.

In this work, we will focus on enzymes that are part of the BER pathway. Enzymes involved in this repair process are often very specific for one type of DNA lesion, i.e. their substrate, which makes them an attractive target for SPRi studies. Here, we will only study the two first states in the BER pathway which are the base excision by the activity of a glycosylase and the incision of the DNA backbone as preparation for subsequent gap filling. We will not study the DNA synthesis and ligation process where two submechanisms are available, which are either short or long-patch BER with replacement of one or several nucleotides, respectively. Instead, we will study the activity of bifunctional glycosylase-lyase enzymes that excise the damaged base to create an abasic (apurinic, apyrimidic: AP) site. Then, in a second step, a single strand break (SSB) in the DNA backbone is created. This step is either carried out by bifunctional repair

enzymes or specific endonucleases that recognize the abasic site. In human beings, for each case the backbone will we cut at different places; the bifunctional glycosylases creating a 5' phosphate and a 3' blocking group containing the sugar that will recruit an endonuclease for further treatment, while an endonuclease directly cleaves at the 3' end of the AP site creating a 3' OH function and a 5'-deoxyribose-5-phosphate that needs no further treatment before polymerization [312, 313].

Here, we will present principally results for DNA repair enzymes from *Escherichia coli*. In particular, we will study formamidopyrimidine DNA N-glycosylase (FPG) specific for 7,8-dihydro-8-oxoguanine (8-oxoG), a current oxidative DNA damage [314]. As corresponding *E. coli* AP endonuclease, we will also study Endo IV. For comparison, some preliminary results obtained with the equivalent human enzyme hOGG1, a DNA glycosylase/β-lyase, and Ape1, the most current human AP endonuclease will be presented. For the study of these enzymes we dispose of several natural or artificial DNA lesions inserted in oligonucleotides at well defined positions. The combination of a system of lesions and repair enzymes with an on-chip approach provides interesting features. If we are able to detect specific enzyme activity on a whole set of DNA damages, we would be able to screen the repair capacities of an individual organism. This may find applications in the personalized therapy of patients that show pharmacoresistance for certain types of DNA damage inducing cancer treatments. Further, the identification of possible cytotoxic lesions that hamper a cell's repair machinery will be helpful in the development of agents that reduce resistance to cancer treatment and render medical interventions by photo-sensibilization, irradiation or chemotherapy more successful. A very recent publication explains, for example, that the resistance to platinum based anti-cancer drugs may be related to efficient repair of oxidative lesions such as 8-oxoG [315]. To develop better cancer treatments and avoid pharmacoresistance, a thorough understanding of the repair mechanisms and its reaction to different types of DNA damage must be gained.

In the following section, we will first summarize data from the literature that characterizes the enzymes we are going to study in our on-chip approach. Then, the experimental concepts for enzyme interaction studies will be introduced. The different DNA sequences as well as the DNA lesions to be studied will be shown. In particular, the virtues of a universally addressable DNA chip are presented and the temperature depending strategy for enzyme activity detection will be explained. Our experimental results will be reported in sections 6.3, where we will first discuss interaction between various enzymes and damaged DNA on the chip, before analyzing enzymatic activity. We will then focus on results obtained on double stranded DNA that contains two lesions in one of the strands. Indeed, such tandem lesions that are strongly localized occur in nature, e.g. as a result of oxidative damage. Radioactivity, for example, can create several DNA damages in a small volume where the energy of the incoming particle is deposited. But also oxidizing agents can be responsible for multiple lesions [314]. Such neighboring lesions will however affect the repair mechanism since DNA is additionally bended or deformed. Finally, in section 6.4, we will discuss the results from our enzyme interaction study and see how this format offers a flexible layout that can be adapted to various kinds of DNA repair studies.

6.1.2 Enzymes involved in oxidative damage repair of 8-oxoG or AP sites

In this work, we mainly focus on enzyme activity to repair the ubiquitous *endogenous* oxidative damage 7,8-dihydro-8-oxoguanine. 8-oxoG is probably one of the most abundant lesions created in response to oxidative stress and is often used as a marker in cell studies. In fact, is has been reported that during DNA attack by oxidizing agents, charge transfer along the DNA helix occurs and damage may so be inflicted at some distance from the original event. Guanine seems to have the role of a sink, i.e. an acceptor, leading to preferred chemical modification of this DNA base [314]. Adenine is less often affected by this process, but 7,8-deoxy-8-oxoadenine (8-oxoA) also occurs in nature. Also, guanine is reported to be the only target for attack by singlet oxygen [314]. The great mutagenic potential of 8-oxoG is generally admitted. While 8-oxoG pairs with cytosine in Watson-Crick style, it can also form hydrogen bonds in the Hoogsteen mode with

adenine [316]. So, misincorporation of adenine opposite 8-oxoG during replication and successive reparation of the 8-oxoG lesion or a second replication will lead to G·C→T·A transversion. Cells dispose of another repair mechanism that cleaves adenine paired with 8-oxoG in order to allow DNA polymerases another attempt to insert cytosine opposite the lesion. Still, this type of somatic mutations is commonly found in human cancers.

8-oxoG is repaired by the BER pathway and *E. coli* disposes of the FPG enzyme that is specific for the 8-oxoG lesion. FPG is a well studied enzyme that exists in several types of bacteria. *E. coli* FPG has a molecular weight of 30.2 kDa with an isoelectric point at 8.5 and is stable up to 65°C [317, 318, 319]. Its crystallographic structure has been resolved in presence or absence of a DNA substrate or for FPG/DNA assemblies that are stabilized by reduction of a naturally occurring Schiff base during enzymatic activity [320, 321, 322, 323]. FPG makes contact with about 9-10 DNA base pairs. For base excision, the lesion is flipped out of the helix and inserted in the active site, while the enzyme also senses the opposite DNA base. So, 8-oxoG is cleaved preferably when opposite a cytosine with a fast catalytic process starting ∼50 ms after initial contact [324]. At the same time FPG is much less specific for 8-oxoG opposite A preventing mutagenesis and leaving time for excision of A to restore the natural G·C pair [325, 324]. FPG kinetic and thermodynamic studies have been carried out using stepwise increase in ligand complexity (method involving competitors), electrophoretic mobility shift assay or stopped-flow fluorescence analysis [326, 327, 328]. It has been reported, that FPG exhibits a greater affinity for abasic sites or equivalents than for its natural substrate 8-oxoG [319, 329]. This may be explained by a larger pocket for accommodation of AP lesions than 8-oxoG lesions. At the same time, the smaller size of the recognition pocket for 8-oxoG allows better substrate recognition and a more favorable positioning for base excision. FPG nicks DNA by a β/δ elimination process creating 3' and 5' phosphates [318]. FPG, like other repair enzymes of the BER pathway, recognizes the DNA helix initially via electrostatic interactions. This explains why FPG activity is generally higher in low salt containing buffer of ≤ 100 mM NaCl or KCl [330, 331]. Kinetic constants have been derived using the Michaelis-Menten reaction for excision of 8-oxoG and subsequent AP lyase activity of FPG yielding a k_{cat} of 1.65 min^{-1} [330] although other authors suggested that due to several intermediate configurations, a more complex kinetic model than the Michaelis-Menten reaction should be used [326, 324]. An increasing turnover with increasing temperature has been reported [330].

In general, the affinity of FPG for dsDNA is about two orders of magnitudes higher than for corresponding ssDNA strands. The same difference can be found in affinity between non-substrate and substrate dsDNA. But the specificity for substrate DNA is 10^4-10^7 fold higher than for non-substrate DNA. When FPG makes contact with the DNA helix and proceeds at low salt concentrations with processive search on the strand by one dimensional sliding [332]; the interaction forces with the DNA in its positively charged cleft are week. At high salt concentration, the enzyme switches to a distributive mechanism. FPG scans in the average 275 bp per binding event while processing several 8-oxoG·C lesions [332, 333]. Only when FPG recognizes its substrate, a certain number of hydrogen bonds are formed with the backbone of each strand and the base opposite the lesion in order to kink the DNA strand and flip out the damaged base for catalysis. For more detailed information on structural and conformational interaction of FPG with DNA, the interested reader may be referred to the review by Zharkov et al. [334]. Finally, it should be noted, that although we will focus here on the 8-oxoG lesion, other substrates of FPG are known, such as formamidopyrimidine derivatives of A and G and dihydrothymine, for example [335, 336]. FPG has also been studied in the presence of multiple DNA damage on opposite DNA strands [335]. Clustered DNA damage can lead to substantial reduction of the enzymatic activity or even render the lesion inaccessible and presents thus an increased *cytotoxicity*.

Although FPG has a very high affinity for AP sites and chemically stable mimics, such as tetrahydrofuran (THF), it is not always capable of performing its AP lyase activity [337]. So, here we studied also the bacterial AP endonuclease Endo IV. As AP sites come with different chemical structures [338], several AP endonucleases exist in *E. coli* with varying functionality [337]. Endo IV has been shown to be more efficient in case of C1' or 4' oxidation of the abasic site and is associated to a cleaving mechanism that differs from other known *E. coli* endonucleases or

glycosylase/lyases [337]. This makes it an interesting enzyme to study in combination with FPG. Endo IV is an enzyme of 31 kDa that is involved in reparation of free-radical induced AP sites, but may also act on various 3' terminals of a DNA duplex [339, 336]. The second activity is useful to render incised strands with 3' blocking groups available for subsequent strand reparation by leaving an 3'OH end [339]. Endo IV works preferably on dsDNA substrates. The crystallographic structure of Endo IV bound to DNA has been resolved by Hosfield et al. [340] and reveals a double nucleotide flipping process with intervention of three zinc ions for the catalysis of an abasic sites. Further insight gained by mutation studies revealed that during Endo IV processing, product release may be the rate-limiting step [341]. Like FPG, Endo IV preferentially works at low salinity of ≤ 100 mM salt [342]. No cofactors are needed for activity. Endo IV can be inactivated by EDTA with a half-life of 10 min in 1 mM EDTA at 37°C in the absence of DNA. *In vivo*, Endo IV may act as counterpart of endonuclease III, since both have similar substrates, but differ in their specific DNA interaction [343]. Some exonuclease activity has been reported for Endo IV, with various efficiency depending on buffer conditions and the presence of 3' ends that are substrate for the enzyme [344].

As a complement, we will present here a comparison of the procaryotic FPG/Endo IV ensemble to the human equivalents hOGG1 and APE1. The human 8-oxoguanine-DNA glycosylase hOGG1 is becoming a well studied enzyme of the BER pathway specific for 8-oxoG and the formamidopyrimidine derivatives of G [345]. The enzyme of 39 kDa and 345 amino acids has been cloned by Radicella et al. in 1997 [346]. The enzyme's structure has been resolved by Bruner et al. [316] and reveals a catalytic process in which 8-oxoG is flipped out of the helix while other residues of the enzyme make contact with the opposite base by plugging [345]. The functionality is thus very similar to what has been found for FPG, although the overall structure of the two enzymes is quite different. hOGG1 has been shown to find its substrate by slipping on the DNA helix with a very high diffusion constant of $4.8 \times 10^6\,\mathrm{bp}^2/\mathrm{s}$ [347]. This diffusion constant arises from very specific contact between the enzyme and the DNA strands. So, while the average contact time with DNA is decreased with increasing salinity up to 100 mM, the diffusion constant remains unchanged [347]. It remains unclear how exactly hOGG1 recognized 8-oxoG in the helix since this lesion does not lead to discernible structural change and also gives rise to only small destabilization. The fast screening process and redundant passes may be combined with kinetically favorable insertion of 8-oxoG into the active pocket. Several studies are also devoted to hOGG1 enzymatic activity. hOGG1 is a bifunctional enzyme with glycosylase activity to excise the damaged base and a 3' lyase activity that incises the DNA backbone for further repair. Conformational analysis and associated kinetic rate constants have been derived from stopped-flow experiments [345], explaining how hOGG1 can efficiently distinguish the opposite base pair and why it operates best for 8-oxoG·C pairs. Indeed, although hOGG1 shows glycosylase activity also when C, T or A are opposite the 8-oxoG lesion, the enzyme does not proceed with β-elimination after base excision [348]. Another kinetic study by Vidal and co-workers derives the time the enzymes typically needs for each catalytic step using an electrophoretic mobility shift assay (EMSA) [349]. Their work reveals that hOGG1 needs more than 20 min in average to perform the base excision. Once the AP site is formed, the enzyme dissociates readily, leaving time for an AP endonuclease to process the AP site. If hOGG1 binds again to the AP site, it needs on the average over two hours to cleave the backbone. So, AP sites act as intrinsic inhibitor for glycosylase activity. The authors showed that it is most likely that *in vivo*, APE1 takes over once hOGG1 has created an AP site. Evidence for team working of hOGG1 with other enzymes has been found by Vidal, but also by Hill et al. and Saitoh et al. [350, 351].

The human apurinic/apyrimidic endonuclease 1 (APE1) can be seen as a homologue of *E. coli* endonuclease III. APE1 hydrolyzes the DNA backbone 5' of the AP site, generating a 3' OH function. Structural data of the 35 kDa enzyme has been resolved by Mol et al [352]. A very good introduction to how precisely APE1 scans the DNA strand for AP sites is demonstrated by Mol et al. and compared to the mechanism resolved for Endo IV [353]. This review provides relevant insight for the two 5' AP endonucleases that we will study here. Besides repair of AP sites, APE1 seems to have multiple functions in recruiting or stimulating other DNA binding enzymes and has been recently reported to present endoribonuclease activity [354, 353].

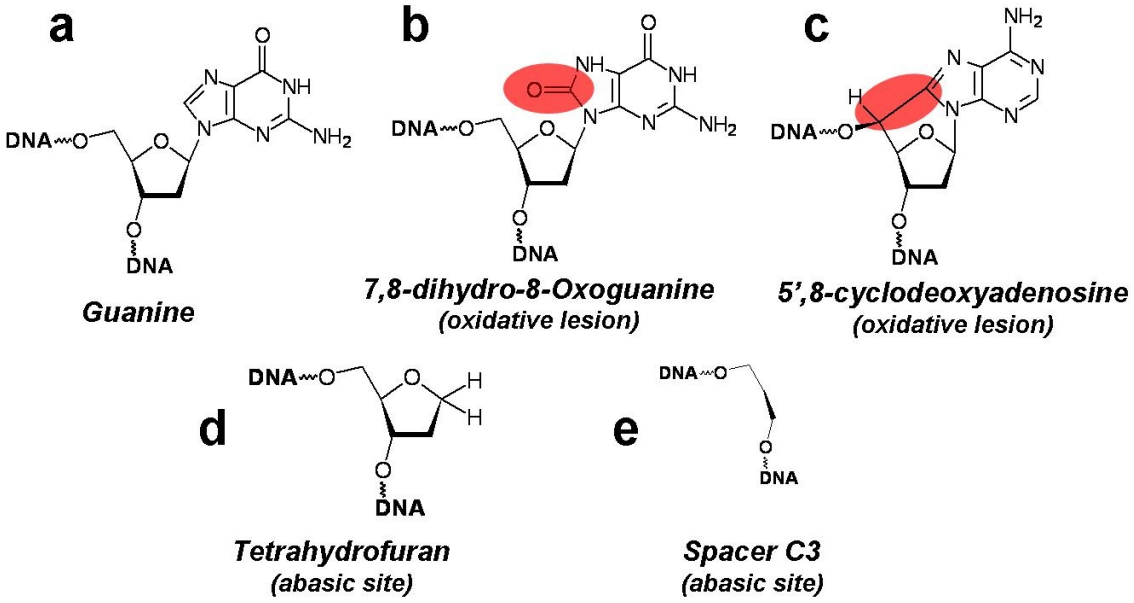

Figure 6.1: DNA lesions used in this study. a) Normal guanine base. b) 7,8-dihydro-8-oxoguanine, substrate for FPG and hOGG1 c) 5,8-cyclodeoxyadenosine, a rare oxidative lesion repaired by NER. d) Tetrahydrofuran (THF), a stable abasic site mimic and substrate of Endo IV. e) C3 spacer, a linker mimicking an abasic site, substrate of Endo IV.

For a detailed chemical understanding of BER enzyme repair mechanisms the reader may be referred to the review by P. J. Berti [355].

6.2 Experimental approach

To detect the previously introduced enzymes by SPRi, we use a universal, addressable DNA chip that provides a flexible, reusable support for DNA lesion attachment. The setup has been optimized in previous work by C. Corne and J.-B. Fiche [239]. This study will extend the format to new lesions that are studied primarily with FPG, but also with endonuclease IV (Endo IV), human 8-oxoguanine DNA glycosylase (hOGG1) and human apurinic/apyrimidic endonuclease 1 (APE1).

6.2.1 Universal addressable DNA chip

To obtain a flexible DNA biochip that is addressable by double stranded targets injected to the SPRi, we use the universal chip approach as reported by Gerry et al. [356]. The authors describe a construction mode that generates so-called Zip sequences, which have the useful feature to be a shuffle of building blocks used to construct sequences with similar stability, i. e. T_m. The sequences are constructed to have no cross-talk in spite of similar G·C contents. Several Zip sequences are available at our laboratory with the usual 10-thymine spacer and the 5' pyrrole moiety for poly-pyrrole electro-polymerization. Here, we use four Zip sequences: Zip2, Zip6, Zip7 and Zip9 as given in table 6.1. Since surface grafting has already been optimized in previous work [13], we use here the 1:2000 ratio between DNA-pyrrole and pyrrole monomers with 10 µM DNA and standard spotting conditions as introduced in section 3.5. Spots are grafted in quintuplets and CP14 is usually used as positive control for hybridization.

The four available Zip sequences constitute addressable sites to which we can hybridize DNA with well identified DNA sequences and damage. Therefore, a Zip-complementary sequence is

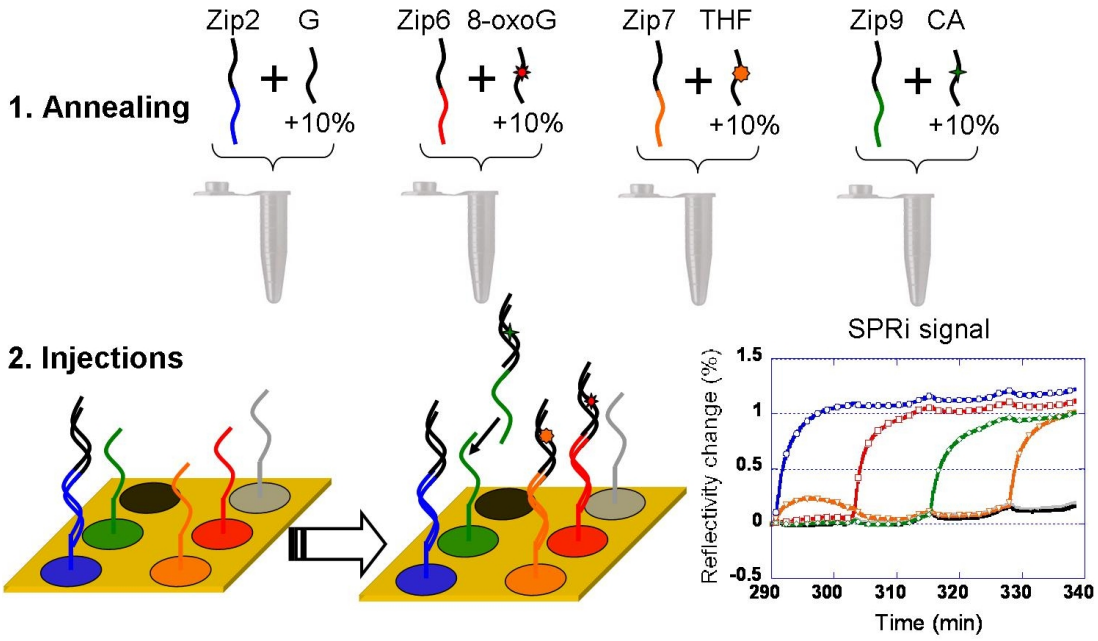

Figure 6.2: Principle of hybridization of the universal addressable chip. Each Zip complementary sequence is annealed ex situ to a 22mer with specific DNA damage (in 10% excess) by heat denaturation at 95°C for 3 min and slow cooling to room temperature. Each duplex is separately injected to control specificity by SPRi as shown.

available that has 24 bases corresponding to one of the Zips at its 3' end and additional 22 bases towards its 5' end with one certain sequence preserved for all Zips (see table 6.1). In this way, we can attach to each different Zip sequence an extremity pointing towards the solution with 22 identical bases. The exact hybridization strategy is depicted in figure 6.2. First, 250 nM Zip complementary sequences are mixed with one specific 22mer at 275 nM containing a DNA damage. The two strands are annealed by heating to 95°C for 3 min followed by slow cooling to room temperature. Each duplex is then injected separately to hybridize to its probe counterpart as shown in the figure. With the SPRi kinetics, we can control the specificity of the hybridization. In fact, while originally hybridization was carried out at 40°C, the addition of Zip7 to our ensemble of Zip sequences gave rise to cross-hybridization with Zip2. The hybridization temperature is consequently adapted to 45°C where Zip7c does no longer form a stable duplex with Zip2 probes. During Zip2c injection, we observe a small signal in Zip7 probes, as shown in figure 6.2 that disappears upon rinsing before Zip7c is hybridized.

The preserved region of 22 bases can be hybridized freely to any available Zip complementary sequence. The ODN-22mers are modified to bear one or several DNA damages. We use here the 8^{th} position from the 5' end of the 22mer as specific DNA damage site. In the natural DNA sequence, this base pair is a G·C pair, where the guanine will be substituted by the following DNA lesions:

- 7,8-dihydro-8-oxoguanine (8-oxoG), an oxidative lesion and FPG/hOGG1 substrate
- 5',8-cyclo-2-deoxyadenosine (CA), a naturally occurring oxidative lesion at low abundance
- Tetrahydrofuran (THF), a synthetic lesion mimicking an AP site with the advantage to be chemically stable
- C3 spacer, the probably simplest 'AP' site, where the deoxyribose is substituted by a three carbon linker

Name	Sequence 5'→3'
Poly-pyrrole probes	
Zip2	pyrrole-T_{10}-CAG CAC CTG ACC ATC GAT CGC AGC
Zip6	pyrrole-T_{10}-GAC CGG TAT GCG ACC TGG TAT GCG
Zip7	pyrrole-T_{10}-TGC GAT CGC AGC GGT AAC CTG ACC
Zip9	pyrrole-T_{10}-GAC CAT CGT GCG GGT AGG TAG ACC
CP14	pyrrole-T_{10}-GCC TTG ACG ATA CA
A24	pyrrole-T_{10}-CAA GTG TGA CCC AGT AAG TGA GGG
Zip complementary targets 3'→5' (part complementary to studied sequence in bold)	
Zip2c	GTC GTG GAC TGG TAG CTA GCG TCG **GTG AAG CCT AGC ACT GAC TAG A**
Zip6c	CTG GCC ATA CGC TGG ACC ATA CGC **GTG AAG CCT AGC ACT GAC TAG A**
Zip7c	ACG CTA GCG TCG CCA TTG GAC TGG **GTG AAG CCT AGC ACT GAC TAG A**
Zip9c	CTG GTA GCA CGC CCA TCC ATC TGG **GTG AAG CCT AGC ACT GAC TAG A**
CP14c	TCT CAC GGA ACT GCT ATG TCG ATT AAG TCT TAG TAA AAC A
Studied sequence with/without lesion 5'→3'	
ODN-G	CAC TTC G**G**A TCG TGA CTG ATC T
ODN-G-bio	CAC TTC G**G**A TCG TGA CTG ATC T -biotin
ODN-8oxoG	CAC TTC G**8-oxoG**A TCG TGA CTG ATC T
ODN-8oxoG-bio	CAC TTC G**8-oxoG**A TCG TGA CTG ATC T -biotin
ODN-Cyclo-A	CAC TTC G**CA**A TCG TGA CTG ATC T
ODN-THF	CAC TTC G**THF**A TCG TGA CTG ATC T
ODN-C3	CAC TTC G**C3**A TCG TGA CTG ATC T
Sequence with tandem lesions 5'→3'	
ODN-8G/8A-1st	CAC TTC G**8-oxoG 8-oxoA** TCG TGA CTG ATC T
ODN-8G/8A-7th	CAC TTC G**8-oxoG**A TCG TG **8-oxoA** CTG ATC T
ODN-THF/8A-1st	CAC TTC G**THF 8-oxoA** TCG TGA CTG ATC T
ODN-THF/8A-7th	CAC TTC G**THF**A TCG TG**8-oxoA** CTG ATC T

Table 6.1: Sequences of ZipX probes, ZipX complementary targets and studied sequence. The positive control is CP14 or A24.

The chemical structure of the lesions are shown in figure 6.1. The detailed sequences are available in table 6.1. In addition to this subset of single lesions, we will study four ODN-22mers in which we modify either the 1^{st} or 7^{th} position 3' of the principal damage site. These tandem lesions permit to analyze how enzymes react when encountering clustered DNA damage. Since DNA repair enzymes make contact with several base pairs during their enzymatic activity, any additional region that alters the DNA stability or conformation might be disturbing the repair process. However, in nature, such clustered damages are expected to arise frequently and are thus of relevance for biological studies.

6.2.2 Experimentation with enzymes on a solid support

We have already experienced in the previous chapters that each sample will need its specific experimental conditions to yield exploitable SPRi signals. Here, we will work with different enzymes on a DNA array environment which will impose certain constraints.

The first condition for successful experiments is the correct choice of the enzyme reaction buffer. The SPRi running buffer should be adapted to both, DNA hybridization and enzyme reaction conditions. Here, we use one standard buffer for all experiments that is composed of 30 mM Tris HCl at pH 8, 3 mM $MgCl_2$, 100 mM KCl, 1.3 mM EDTA Na_2 and 0.2 mM dithiotreitol (DTT) which is added at the beginning of the experiment. This buffer has been selected during previous studies [239]. It yields good activity with FPG and shows good DNA hybridization

signals for Zip sequences [13]. With Mg^{2+}, the necessary co-factor is provided. It should be noted, that within this study, no buffer optimization has been attempted for various enzymes and so it might not necessarily represent ideal conditions for all enzymes. Factors as salt content, pH, and presence of co-factors as well as absence of inhibitors may be individually adapted.

The next concern is the enzyme injection system. In fact, proteins in general are very sensitive to their environment and might readily undergo irreversible denaturation when coming into contact with solutions and surfaces that are not compatible. This is why for enzyme activity studies, we use a 500 µM injection loop made of PEEK, a biocompatible material [13]. Also, it might be useful to use Eppendorf tubes with low adsorption in order to reduce enzyme loss and denaturation during preparation.

Further, enzymes are normally stocked in a high percentage of glycerol (30-50%) in order to keep them at -20°C without freezing the buffer. All the same, repeated freeze-thaw cycles are usually unfavorable and enzymes are thus aliquoted into quantities suitable for one SPRi experiment. Enzyme concentrations are either available in mass/volume from which the concentration can be determined of in units/volume, where units (U) is a manufacturer defined activity of the enzyme. So, in our study, for each enzyme, the actual proportion of enzymes that show some catalytic activity is not known. Here, we use the obtained SPRi signal as indicator of enzyme activity, as in absence of non-specific adsorption; a certain concentration of active enzymes will give rise to a specific reflectivity change. So, the signal may serve for comparison between different enzyme solutions. When commercial enzymes are used, it should be made sure that their storage buffer does not contain any BSA which is sometimes used to stabilize the enzyme and avoid loss by adsorption. In SPRi, BSA provokes a high background signal and prevents observation of enzyme interactions.

Of course, the blocking strategy is of great concern. Here, we do not only want to suppress background signal that may arise from enzyme adsorption to the surface. Adsorption of the enzyme to the surface would deplete the solution and alter the injected concentration. Fewer enzymes will be available for DNA repair. Since the *isoelectric point* of FPG is ∼8.6 [317], BSA is not adapted as a blocking protein, since FPG and BSA would have opposite charges at buffer pH 8 and thus give rise to attractive interactions. It turns out that the 15 kDa protein Cytochrome C (Cyt C), extracted from horse hearts, is better adapted [13]. Each prism is blocked by at least three injections of Cyt C at 1 µM before enzymes are injected. As Cyt C is considerably smaller than BSA, it also has the advantage to only slightly increase SPRi reflectivity with signals around 1% reflectivity so that optimal SPRi regulations are easily maintained.

When finally all precautions are taken that the enzyme arrives functionally on the chip in presence of suitable buffer, we still have to ensure that the enzyme has access to the DNA damage. Therefore, grafting density will be important and will depend on the size of the enzyme that needs to penetrate the surface DNA layer. Since all enzymes used in this study are rather small, we can use standard grafting densities as in our DNA/DNA interaction studies. When larger entities like antibodies are to be detected, the surface grafting density should be reduced.

6.3 Enzyme interaction studies by SPRi

In this section, we will use different observation strategies to characterize and compare interactions of repair enzymes on surface grafted DNA with damages. Since SPRi is a real-time method, interaction kinetics can be studied. However, as we will see in the following, the time dependence we will measure will depend on various factors and several specific and non-specific interactions that all occur simultaneously. We can divide the influences in those that will depend on the experimental protocol and those that are linked to the observation of ligand binding to a biopolymer. Experimental factors that influence our experiments are for example:

- The flow rate, which will alter the probability that the enzyme encounters a surface grafted DNA. It will also determine the interaction frequency. At low flow rates, the enzyme has the possibility to make contact with several DNA strands on identical or different spots. At high flow rates, the frequency of reassociation will be lower, as the enzyme will be washed

away quickly. To access 'real' dissociation constants, the flow should be sufficiently high to suppress this kind of dissociation and reassociation phenomena where enzymes undergo down-stream 'hopping' from one spot to the next. A review of influences due to flow-cell design has been published by Ward et al. [357].

- Temporary or permanent interactions of the enzyme with the surface. Permanent interactions remain after enzyme elimination as base line increase and should possibly be suppressed. The Control spots, like CP14 in ssDNA form and ppy without any DNA, reveal temporary surface interactions but also global refractive index changes due to buffer changes during injection.

SPRi signals of interactions between enzymes or other ligands and surface grafted DNA will also depend on:

- Kinetics of FPG association on dsDNA and subsequent scanning for lesions [333]. This interaction type will have a lower affinity than enzyme/lesion recognition but provides multiple interaction sites per DNA strand [358]. Hence, at high concentration it is possible to have several enzyme interactions of this kind on one single DNA strand of total length of 46 bp. Here, we always have one control spot without DNA damage that serves to analyze dsDNA recognition.

- Kinetics of enzymatic activity. The affinity of interaction is high and very specific. Only one lesion per strand is available. However, the enzymatic activity is twofold, first presenting the glycosylase activity, then the lyase of the backbone. The enzyme might dissociate between these steps. AP sites also have a limited lifetime at pH 8.

Since global refractive index changes, temporary and permanent non-specific interactions all occur at the same time as dsDNA recognition and specific DNA damage catalysis, it is impossible to dissociate all these contributions to obtain intrinsic results. SPRi delivers only a signal average of everything near the surface and not microscopic details. So, we will analyze our results in the following in a qualitative or semi-quantitative way. The reader should however note, that in more simple cases, models can be developed that combine Langmuir adsorption kinetics with Michaelis-Menten enzymatic activity and so give access to reaction kinetics [359]. However, the model supposes that once the substrate is treated and the product is formed, no further recognition takes place, a prerequisite that is clearly not fulfilled in our case. A substantial review on the topic of protein/DNA interaction has been recently published by W. Bujalowski and provides also more complex models [360].

Still, we will see in the following that we can get quite interesting information on enzyme substrate specificity and also its activity by comparing one enzyme that interacts with multiple DNA lesions on our chip. Our experiments will be completed by more classical gel-based approaches where reactions are carried out in solution.

6.3.1 Former results from our laboratory

The foundations of this project are lain by J.-B. Fiche and C. Corne in from of a collaboration between the CREAB and the LAN, two laboratories located at the INAC at CEA Grenoble. Also E. Suraniti contributed to the initial work. The project is followed by D. Gasparutto and A. Favier from the LAN and T. Livache, R. Calemczuk and A. Buhot from the CREAB. The concept of the universal chip approach and the later on presented temperature related activity revelation have been published in 2008 [239]. We will shortly summarize the main results before explaining how this study has been extended here to new DNA lesions and repair enzymes.

The original work is carried out with the FPG enzyme, using three different Zip sequences (Zip2, Zip6, and Zip9) to study 8-oxoG, as a substrate for base excision repair, cycloadenine (CA) as a non-cleavable DNA lesions and the undamaged DNA strand with guanine. Interactions between FPG and these lesions have been studied and revealed that FPG recognizes all double stranded DNA on the chip with a preference for 8-oxoG and an even stronger affinity for CA.

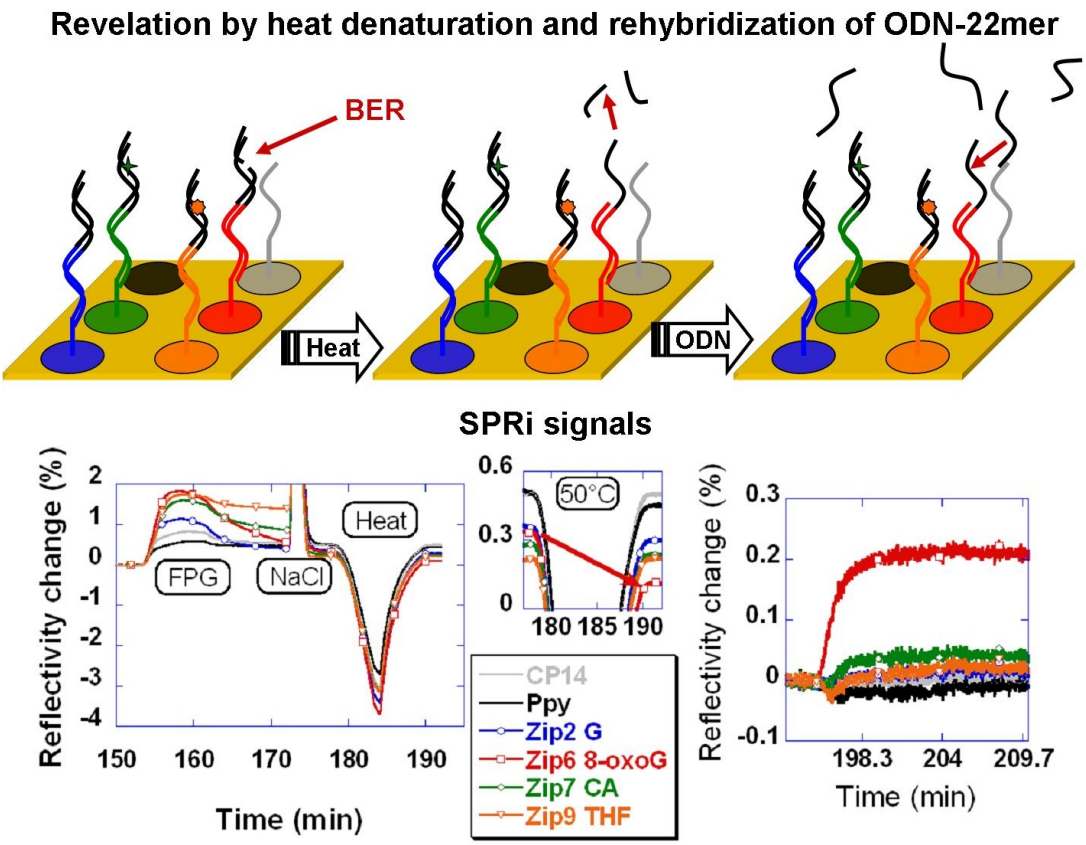

Figure 6.3: Enzymatic activity revelation using heating and rehybridization. *Top:* Schematic representation of experimental steps. *Bottom:* Corresponding SPRi signals for FPG activity on 8-oxoG. From left to right: FPG injection, regeneration and heating. Zoom on signal before and after heating. ODN-22mer injection and specific hybridization.

This is a surprising finding since CA is no substrate for FPG and so the detected slow dissociation reveals an inhibitory action of CA on FPG repair activity. Since FPG upon encounter with CA is bound with high affinity, it is not available for further repair processes, which would have bad consequences on DNA repair if similar binding affinities are found *in vivo*.

To characterize the activity of the FPG enzyme on our DNA chip, two approaches are presented. The first consists of a double injection of FPG protein on one DNA chip without any regeneration and reconstitution of the chip. As during the first injection 8-oxoG is processed by FPG and cut out of the double helix, a reduced interaction signal can be found on 8-oxoG sequences during the second injection. A repetition of this experiment is shown in figure 6.9a (see later on). While FPG has slow association kinetics on CA, fast dissociation is found on G and 8-oxoG. During the second injection of FPG, the signals reach the same amplitude on CA and G spots, while FPG interaction on 8-oxoG DNA is now decreased. This simple experiment demonstrates that most 8-oxoG lesions are excised in the time course of the first injection/rinsing step with a total duration of 20 min. The chip can be regenerated from enzymes by injection of NaCl at 1.5 M. The high salt concentration screens out any electrostatic interaction between DNA and enzymes. Since recognition is partly based on the positive charges in the enzyme's cleft for DNA, the salt provokes dissociation from the strands. In fact, on advantage of the NaCl regeneration is the increased stability of the DNA duplex at high salinity, as previously presented in section 4.5. In this way, the DNA chip may be reused for several interaction studies, provided that there is no enzymatic interaction that cleaves the studied damage.

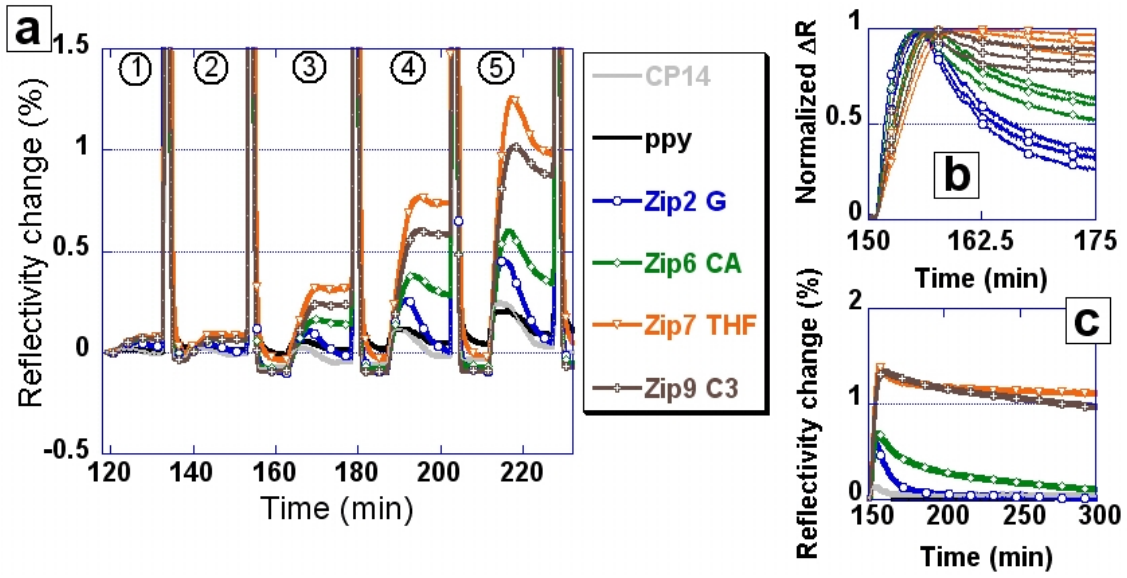

Figure 6.4: a) Consecutive FPG injections at various concentrations and 25°C. The prism is regenerated by 1.5 M NaCl between each FPG injection. 1) 6.25 nM. 2) 12.5 nM. 3) 25 nM. 4) 50 nM. 5) 100 nM. b) Normalized FPG injection on the same lesions. c) Long term dissociation observation for CA, THF and C3.

A second protocol for revelation of FPG activity on 8-oxoG has been developed by Fiche and Corne. The method makes use of the flexible temperature regulation. Briefly, after chip hybridization is completed, FPG is injected, followed by buffer rinsing and NaCl regeneration. To reveal the enzymatic activity, the chip is then heated moderately and cooled down again to 25°C. During the heating process, only those strands that have been subject to enzymatically catalyzed single strand breaks will dissociate. After base excision, two strands of 7 and 14 nt remain of the former ODN-22mer. These sequences are unstable at 45-50°C, while all other sequences with 22 (ODN) and 24 (Zip) bases remain hybridized. So, the heating process renders the Zip-complementary sequence accessible for a new ODN-22mer. An injection of single stranded ODN-22mer then leads to specific rehybridization on spots that formerly bore 8-oxoG lesions. This strategy is schematically depicted in figure 6.3.

6.3.2 FPG damage recognition and repair

In this work, a fourth Zip sequence is added to the ensemble of addressable positions to allow the comparison of three or four different DNA lesions simultaneously. As we will see, due to problems of cross-hybridization between Zip2 and Zip7 sequences, we will hybridize at 45°C to ensure specificity. Two new lesions, tetrahydrofuran (THF) and a C3 spacer are inserted into the ODN-22mer to mimic an abasic site at the position of 8-oxoG. Indeed, since FPG creates an abasic site as its intermediate, we expect these lesions to be a good substrate for FPG. Due to chemical modification, neither THF not C3 will be subject to lyase by FPG. Natural abasic sites with a hydroxyl function at the C1' positions of the deoxyribose are not sufficiently stable at the pH of our running buffer (pH 8) to serve as substrate in this study.

Characterization of the FPG enzyme on various lesions

In figure 6.4a, several injections of FPG enzyme at increasing concentrations are shown. The chip has been hybridized with Zip2-G, Zip6-CA, Zip7-THF and Zip9-C3. Each injection is carried out

for 10 min at 50 µl/min followed by 5 min buffer rinsing and 1 min NaCl. For FPG concentrations of 25 nM and higher, we obtain a discernible interaction signal. While at 25 nM and 50 nM the dissociation phase shows fast dissociation from Zip2-G, the signal on the DNA lesions is rather stable. So, all injected FPG enzymes on the surface interact with a DNA lesion. This is no longer the case for 100 nM, where FPG is found in excess on the DNA strands. Already before the start of the rinsing process, FPG shows strong dissociation from Zip6, 7 and 9. Only in a second time, dissociation slows down to lower dissociation rates as found at lower enzyme concentrations. The remaining signal can so be associated to the fraction of enzymes that recognized a DNA lesion. This supposition is strengthened by the observation that non-lesion specific DNA interaction on Zip2-G is almost completely washed off at the end of the rinsing period. This concentration range permits to fix optimal injection conditions which are found at 50 nM where only little excess FPG is bound. The determination of the optimal concentration must be repeated for each new batch of enzymes that may contain varying fractions of active versus inactive material. It has to be noted that unlike for DNA injections, enzyme injections show a surface position dependent signal. Spots downstream of the sample inlet will react later than spot in immediate vicinity to the inlet. Enzyme concentration is in the beginning depleted by capture on the first range of spots. This effect can be appreciated from the different on-rates for one spot type in the normalized signal plot in figure 6.4b.

Although not all lesions used in this interaction experiment are substrate for FPG repair, we find that they all have the ability to strongly bind the enzyme. The affinity of FPG is even higher for THF and C3 than previously found for CA as can be seen in the normalized signal plot in figure 6.4b. In another FPG experiment on the same lesions, the rinsing step is extended over one night. On a time scale of over 2 h as shown in figure 6.4c, it gets evident that FPG has the most stable interaction with THF, followed by the C3 spacer. During this period, FPG almost completely dissociates from CA, while C3 has about 30% signal loss and THF still shows 90% of initially bound FPG. After one night rinsing, there remains a notable signal of FPG on C3 and THF as revealed from the specific signal decrease obtained after NaCl injection. All other spots show no base line difference before and after salt injection.

These results emphasize the toxicity of such damages for FPG mediated base excision repair. Strong binding of the enzyme renders the site inaccessible to other repair agents and, at the same time, FPG is not available for 8-oxoG repair. Lesions of this type could be used in cancer treatment as inhibitors of the natural repair systems. As they strongly bind the repair enzymes, they hinder cancer cells to counteract DNA damaging treatments.

In the next step, we will show that dissociation rates represent only relative stabilities. When doing SPRi experiments, we must always keep in mind that the reflectivity change observed is an average over all mass changes that occur in the proximity of the surface. We are not able to distinguish, for example, the dissociation of an enzyme from one DNA duplex and its reassociation to another free site on the same spot. This reassociation hinders in fact the observation of real dissociation constants. To avoid multiple dissociation and reassociation effects, the flow rate can be increased. Similarly, we can alter the dissociation rate by the presence of competitors in solution. For FPG, competitors must be in form of double stranded DNA and the presence of a DNA lesion additionally increases the affinity. After FPG injection of 50 nM for 8 min, we inject during rinsing 100 nM of double stranded DNA with or without lesion to capture any FPG enzyme that dissociates from surface grafted DNA. Reassociation to the spot is so prevented.

Figure 6.5 shows five repeated injections of FPG 50 nM followed by 10 min rinsing in presence of different competitors. Between each injection the chip is regenerated from the enzyme by injection of NaCl 1.5 M. The chip presents the sequences G, CA, THF and C3, so that FPG has no specific activity and DNA strands remain intact after contact with the enzyme. In the first cycle, rinsing is carried out in buffer only, without any competitor. Dissociation is as before, slow on THF and C3, faster on CA and almost all signal disappears on G before the end of the rinsing period. The second injection is followed by rinsing with double stranded DNA without damage. We observe that dissociation is accelerated, showing that FPG is efficiently captured and carried away by free dsDNA in solution. From injection 3 and 4 with THF or CA rinsing, we observe that

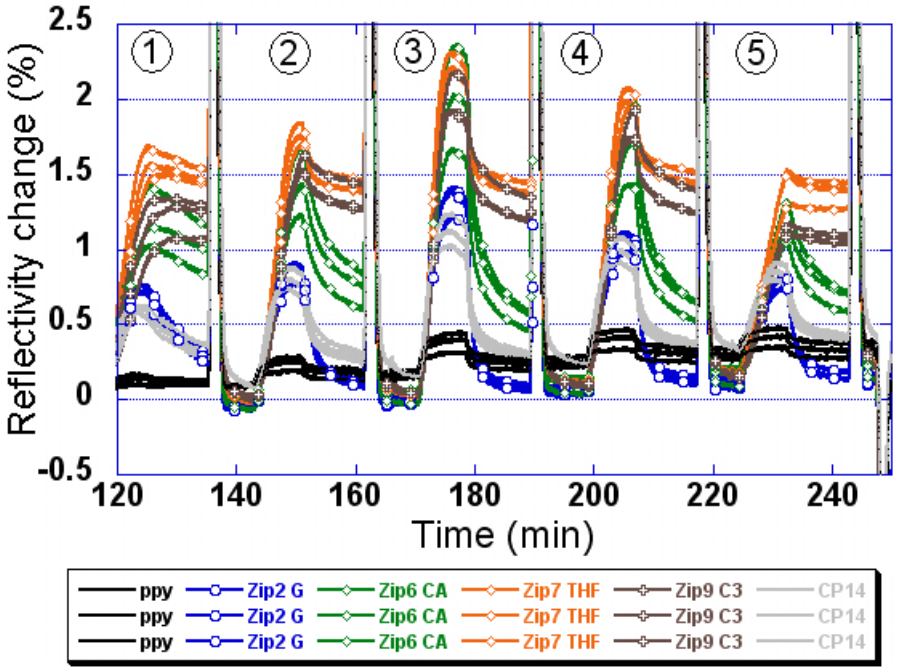

Figure 6.5: Consecutive FPG injections at 50 nM and 25°C followed by rinsing in presence of different dsDNA competitors at 100 nM. The prism is regenerated by NaCl 1.5 M NaCl between each FPG injection. 1) No competitor. 2) No lesion (G). 3) THF. 4) CA. 5) 8-oxoG.

not only fast capture of non-lesion specific bound FPG occurs, but also dissociation from surface bound DNA with lesions is slightly increased. FPG has a strong affinity for the competitors; hence they can accelerate dissociation of the enzyme from the surface. 8-oxoG seems to be slightly less efficient than CA and THF. This experiment can only show tendencies since exact comparison is hampered by a irreproducibility of the FPG concentration during injections. This variation is due to experimental errors in pipetting, since the concentrated stock of the enzyme required measurement of 0.6 µl volumes of enzyme for dilution in 1 ml to obtain 50 µl. However, the enzyme is stocked in 50% of glycerol. The viscosity of the solvent biases exact quantity measurements and leads to concentration variations as observed here on our signals. For example, the third injection of FPG show a lot higher percentage of non-lesion specific bound FPG on the spot which quickly dissociated upon rinsing with THF modified dsDNA. We can however show with this experiment that dissociation rates as observed during buffer rinsing do not represent necessarily only dissociation of FPG from DNA, but can be a mixture of dissociation and reassociation processes. The injection of competitors can serve to suppress secondary association of FPG on spots, especially when FPG has a high affinity for the injected competitor. In that way, unbiased dissociation rates can be observed.

Detection of base excision repair by FPG

This general interaction studies gave us a first insight of how FPG binds to our DNA and then dissociation from the spots. While single stranded DNA is only feebly recognized, FPG recognizes double stranded DNA and in particular certain DNA lesions. Its affinity is highest for THF, followed closely by C3, the two abasic sites. On CA, we observe a higher residence time of the enzymes, compared to DNA without lesion of 8-oxoG, too. In the next sections, we will concentrate on the revelation of enzymatic activity on different types of DNA damage. Therefore, we first present different strategies to detect enzymatic activity on our DNA chip by SPRi. Then, the simple case of one single lesion per DNA duplex is extended to the case, where a second lesion

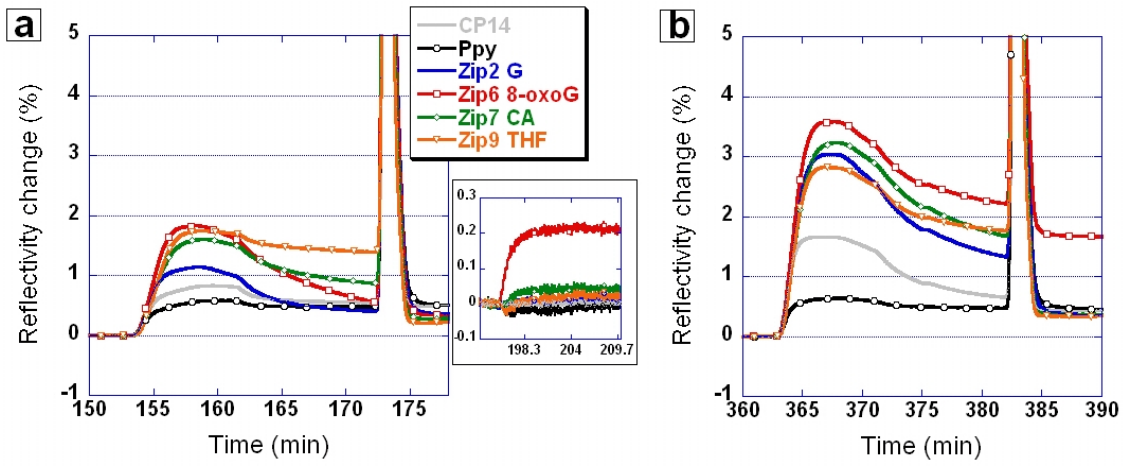

Figure 6.6: Comparison of interactions with normal FPG and mutated FPG that has lost any enzymatic activity. a) Injection of normal FPG at 50 nM. The inset shows the signal obtained for ODN-G revelation. The signal is specific to the 8-oxoG lesion. b) Injection of 500 nM mutant FPG. Interaction with 8-oxoG lesions is stable even after salt regeneration.

is present on the same strand in different distances to the initial damage site. Results are analyzed by comparison between different lesion types.

Temperature based revelation of enzyme activity: One first strategy to reveal enzymatic activity in base excision repair is based on thermal dissociation of cleaved DNA fragments that are then replaced by a new single stranded ODN that will hybridize specifically to sites rendered accessible during heating. Experiments of this type have the following experimental protocol:

- Hybridization of the DNA chip with dsDNA containing an identified damage as shown in figure 6.2.
- Injection of repair enzymes at a flow rate of 50 µl/min for 8 min.
- Chip rinsing (typically 10-20 min), determining the overall enzyme interaction time.
- Enzyme elimination by injection of 1.5 M NaCl for 1 min.
- Heating to 45-50°C at 2°C/min and 3 min at this temperature before cooling down to the initial temperature.
- Revelation of free hybridization sites by hybridization of ssODN-G (22mer), eventual biotinylated to use subsequent streptavidin amplification.
- Chip regeneration by 0.1 M NaOH.

For all experiments, the flow rate is set to 3 ml/h and hybridization temperature is 45°C. Enzymes are injected at 25°C (*E. coli*) or 37°C (human). The described strategy is depicted in figure 6.3 on page 124.

In figure 6.6a, an injection of 50 nM FPG on a 8-oxoG containing DNA chip is shown. We see that the most stable interaction is formed with THF and then CA while 8-oxoG shows a good association signal followed by fast dissociation. After 10 min rinsing, the enzyme is eliminated by NaCl and heating to 50°C follows. We find during the subsequent injection of ODN-G a specific signal on Zip6, the spots that carry 8-oxoG lesions. No significant signal is detected on other spots, showing that the heat denaturation is without effect for sequences of 22 bp hybridization length. FPG has no repair activity on CA or THF, nor on healthy DNA, so those spots will stay

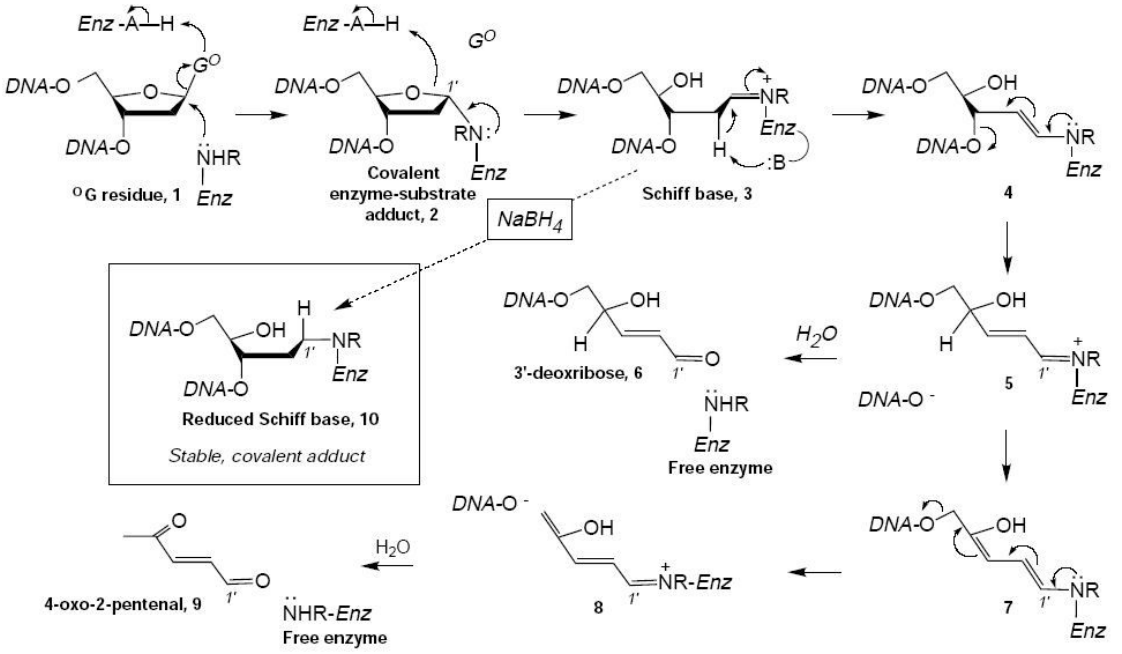

Figure 6.7: Reaction scheme of FPG on 8-oxoG in the presence of $NaBH_4$. The intermediate Schiff base is reduced by $NaBH_4$ and the enzyme gets covalently attached to the DNA.

intact. When observing closely the base line change before and after heating (figure 6.3), we can distinguish the signal loss on Zip6 8-oxoG spots that already indicated the dissociation that is later revealed by rehybridization. This shows that the heating is necessary to render the strands accessible for revelation.

This experiment with normal FPG can be compared to the interaction observed for FPG that has been mutated. The mutated FPG produced by B. Castaing conserves its specific recognition for 8-oxoG without any enzymatic activity on this lesion. Figure 6.6 shows that contrarily to normal FPG, all mutants that find a 8-oxoG lesion stay stably attached and do not even dissociate after salt injection. As the basic interaction mode is changed, also the contribution of electrostatic interactions between mutant FPG and DNA is influenced. The analysis of mutated enzymes can help to understand structural interplay, contact zones and mechanisms, but serves here only as control in our enzyme activity experiments.

Direct revelation of FPG activity by covalent capture: A direct revelation method of enzyme activity makes use of the chemical reduction of an intermediate Schiff base to covalently graft FPG or hOGG1 to its substrate. $NaBH_4$ reduction has been used in gel shift assays to reveal enzymatic activity. As the Schiff base between the enzyme and its substrate is only formed in the course of base excision as shown in the reaction scheme 6.7, the reduction mechanism and formation of a covalent adduct is a direct revelation of the activity. Although this method provides fast information on presence or absence of enzymatic activity, it does not give way to further information, since, once the covalent bond is formed, no further enzyme properties can be observed. So, this revelation protocol is only of minor biological relevance, but has been used here as a complementary proof of enzymatic activity on DNA chips.

This covalent grafting can be revealed by SPRi in the following way. The DNA chip is hybridized with Zip2-G, Zip6-8-oxoG, Zip7-THF and Zip9-CA in our usual FPG buffer. After hybridization, the buffer is changed: the usual amount of 100 mM KCl is replaced by the same concentration of $NaBH_4$. Since the addition of $NaBH_4$ to water provokes a reaction with release of hydrogen, the buffer must be prepared well in advance and is stirred for several hours under the

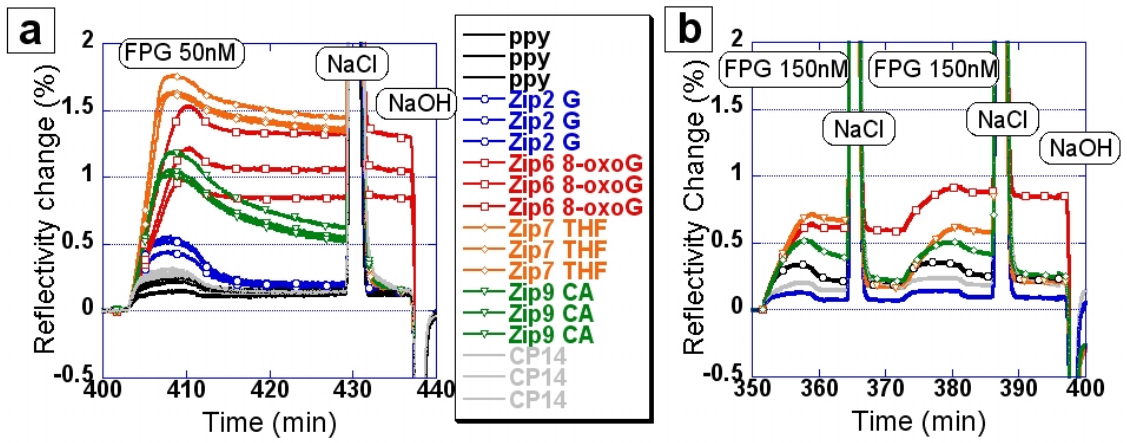

Figure 6.8: a) Covalent trapping of FPG at 50 nM on its substrate 8-oxoG in 100 mM $NaBH_4$ buffer. While FPG is regenerated by NaCl injection on all other DNA strands, it stays coupled to 8-oxoG. b) Same experiment with another FPG sample that shows much less activity. Two consecutive injections lead to accumulation of FPG on the 8-oxoG spots (signal averaged for 5 spots).

extraction hood and carefully degazed before use in SPRi. After buffer change to $NaBH_4$, FPG is injected in presence of this modified buffer on the chip. In figure 6.8, FPG covalent trapping in presence of $NaBH_4$ is presented. While FPG injection signals show the usual level of association on the spots, the rinsing period reveals that only a small part of FPG enzymes present on 8-oxoG spots are able to dissociate. The rest of the enzymes stay fixed, as revealed by the horizontal signal during rinsing and the identical reflectivity before and after enzyme elimination. The enzyme is covalently bound to its substrate. As a control, we can check that FPG has the usual affinity for THF, CA and G. Only regeneration of the DNA by 0.1 M NaOH regenerates the chip completely. In subfigure b, another experiment with two consecutive FPG injections in presence of $NaBH_4$ reveals that the signal is additive, and FPG can be added during the second step to available 8-oxoG lesions.

The same experiment has been carried out twice with hOGG1 and, astonishingly, we found no interaction at all between hOGG1 and the hybridized DNA on the spots. Either the presence of $NaBH_4$ in the buffer prohibits any interaction of the enzyme with DNA, or it denatures hOGG1 so that there is no recognition structure left. Other groups report trapping experiments with hOGG1 in $NaBH_4$, where the enzyme is allowed to interact with 8-oxoG for ~15 min before stopping the reaction [361]. The successful covalent trapping is then detected by gel shift assays. In two independent experiments with two different batches of hOGG1, no interaction of hOGG1 on immobilized DNA could be found in our SPRi setup. One alternative that has not been tested yet would be to proceed with hOGG1 injection in the normal buffer and flow only after some time $NaBH_4$ over the chip to trap any enzyme in the correct configuration.

Revelation of activity by two consecutive enzyme injections: Another approach to reveal enzymatic activity, as already mentioned (see 6.3.1), is by consecutive injections of enzymes. In figure 6.9, we compare this approach for the revelation of enzymatic activity of FPG and hOGG1 on the 8-oxoG lesion. In subfigure a we observe a smaller signal on 8-oxoG spots during the second injection of FPG, demonstrating that part of its substrate has been treated by enzymes during the first injection so that the 8-oxoG spots are now modified. This is underlined by the signal reproducibility for the two injections obtained on spots with other DNA lesions. However, as shown in subfigure b, we do not obtain the same properties with hOGG1. The same DNA chip has been hybridized as before. The first injection of hOGG1 reveals a 3.6-fold higher SPRi signal obtained with 50 nM hOGG1 on 8-oxoG than with 50 nM FPG. This mass increase can not

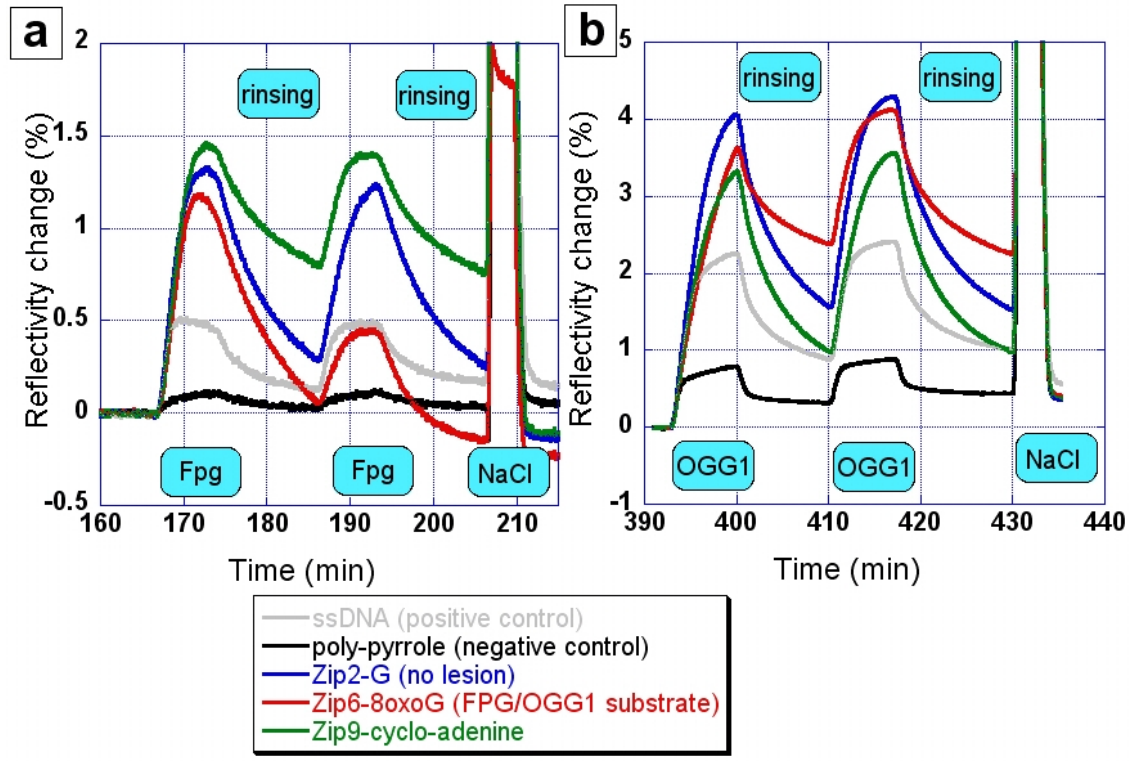

Figure 6.9: a) Two consecutive injections of FPG at 50 nM at 25°C. Signal loss on 8-oxoG indicates base excision. b) Identical experiment with hOGG1 at 50 nM and 25°C. No activity is detected at this temperature and time scale.

only be explained by the 30% increased mass of hOGG1 so that we conclude that also a much higher fraction of enzyme is bound to the dsDNA. The 12 min rinsing period, reveals further, that unlike FPG, no high affinity of hOGG1 for CA can be detected. The stability compares rather to dsDNA without lesion. However, hOGG1 shows a more stable interaction with 8-oxoG than FPG. The substrate recognition process of the two enzymes is hence based on different interactions and proceeds on different time scales. The second injection of hOGG1 does not present any basic difference compared to the first, so that here, we can not observe 8-oxoG repair by signal comparison. The slow dissociation process, however, indicates that the enzymatic repair process takes place on a longer time scale than our experiment. Vidal et al. report an average base excision time of 20 min for hOGG1. Then, the enzyme dissociates to leave space for AP endonucleases to finish the work or stays on to process also the β-elimination. As this second step takes in average more than two hours, it gets clear why our consecutive injections carried out in overally 40 min assay time do no reveal huge differences. The first injection and rinsing cycle left about enough time to create AP sites, that then, during the second injection are still recognized as substrate.

6.3.3 Base excision repair by human 8-oxoguanine DNA glycosylase OGG1

The previous section introduced already some differences between hOGG1 and FPG, notably for the recognition of CA and the necessary time for base excision repair. The main difference is probably its enzymatic activity. FPG proceeds much faster with 8-oxoG excision, while hOGG1 is very slow and often relies on partners like APE1 to proceed with the lyase activity to remove the AP site [353, 349]. In figure 6.10a, a 50 nM injection of hOGG1 is shown that is followed by heat revelation. The injection is represented for two distinguished lines of spots on the DNA chip

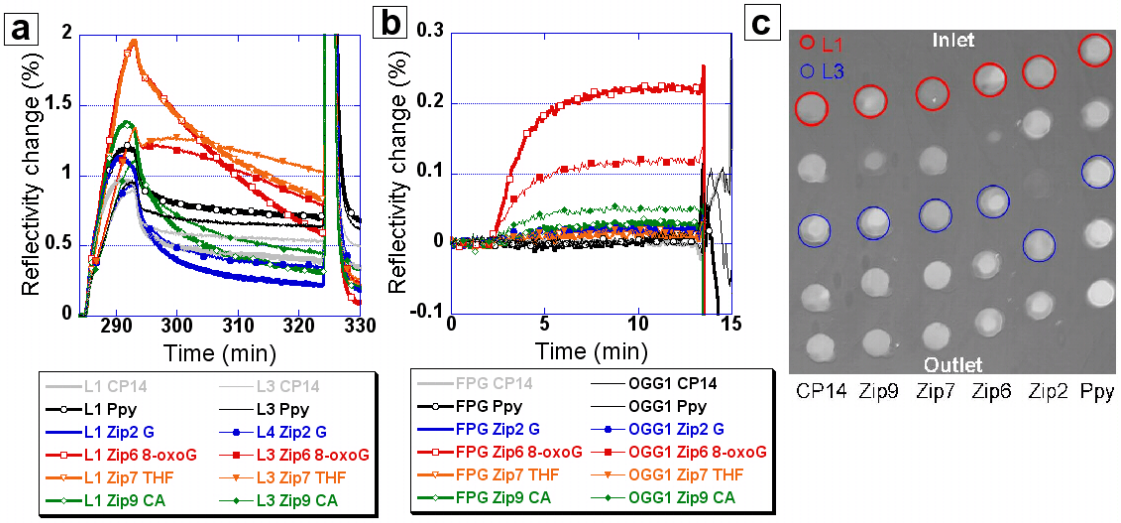

Figure 6.10: a) Injection of hOGG1 at 50 nM represented for 2 different lines as indicated in (c). b) Revelation by ODN-G injection after heating. The signal obtained after hOGG1 activity is compared to the signal obtained after an identical experiment with FPG on the same chip. c) SPRi image of DNA spots.

as indicated in subfigure c. While the first line is rapidly in contact with enzymes and shows fast association, we find for downstream spots, as for line 3 represented here, a clearly diffusion limited behavior. While the global refractive index change indicates that the injected solution arrives quasi simultaneously on all spots on the surface, the hOGG1/DNA recognition on line 3 shows signs of a slower, diffusion limited association. With proceeding injection, the association rate grows, due to increasing enzyme concentration near the surface. This initial depletion phenomenon is in contrast to signals found in line 1 where association is fastest in the beginning and then decreasing with increasing saturation of the spots with enzymes. Also the dissociation phase shows big differences depending on the spot's position on the chip. The highest affinity is found for THF, followed by 8-oxoG. The fraction of enzymes on lesions dissociates slowly from these spots. For equivalent spots in line 3 we even observe signal increase in the beginning of the rinsing step, which demonstrates the fact that hOGG1 can dissociate from one spot and bind further downstream to another one. This downstream hopping prevents the detection of the intrinsic dissociation rate for our enzyme. hOGG1, as shown, can be fully regenerated by NaCl injection. To reveal enzyme activity, the heat revelation protocol is used. Figure 6.10b compares ODN-22mer revelation signals observed after FPG interaction on the hybridized chip to signals obtained after incubation with hOGG1. We find that hOGG1 injection results in about 50% less excised bases than a FPG injection with identical experimental conditions. The enzyme is thus significantly less active or needs more time to complete the BER. For OGG1, we observe also a very small but specific signal on CA that is not observed with FPG. This result has been reproduced in an independent experiment on another prism. Although the signal is almost invisible, it might indicate a small activity of hOGG1 on cycloadenine lesions. However, as the signal is barely over noise and no such information is available in the literature, it rests to be confirmed by other methods if hOGG1 can excise also the CA lesion.

6.3.4 Repair of abasic sites by Endonuclease IV

As we have seen, THF and C3 are lesions that can be toxic to the BER pathway if they are not repaired. As well FPG as hOGG1 form a stable complex with THF; FPG with even higher affinity than hOGG1. When these artificial lesions are injected into a cell, crucial enzymes may

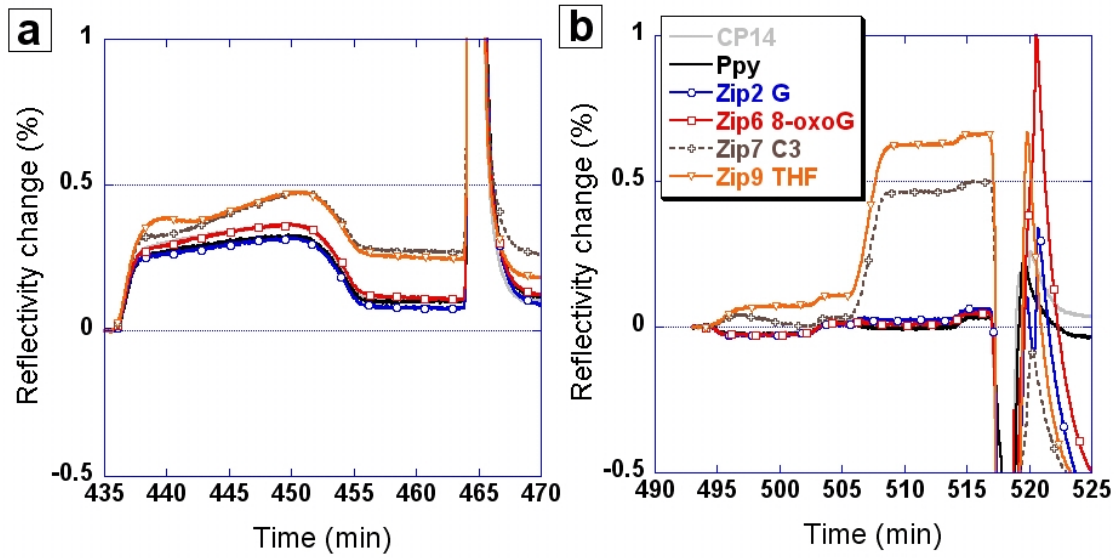

Figure 6.11: Revelation of Endo IV activity. a) Injection of Endo IV at 4 U/ml on a DNA chip with 8-oxoG, C3 and THF. b) Revelation of activity on THF and C3 by rehybridization of ODN-G-biotin and amplification by streptavidin.

be fixed and will no longer be available for repair of their natural substrate. So, the identification of enzymes that repair these toxic lesions will decide on eventual applications in cancer treatment. Consequently, it is interesting to characterize the activity and recognition potential of natural AP repair enzymes on these lesions. Endo IV, as introduced before, is a powerful 5' AP-endonuclease and 3' diesterase. Its activity is the excision of abasic sites in the helix by incision of the backbone and subsequent removal of the remaining 3' blocking groups. The resulting 3'OH groups are then compatible with ligation to complete DNA repair.

Here, we study two artificial mimics of abasic sites: THF and C3. Using the heat revelation protocol, we are able to determine enzyme activity. In figure 6.11a, the enzyme interaction with surface grafted DNA is represented. Although injections are carried out at 4 U/ml corresponding to a high concentration of ~130 nM, the SPRi interaction signal remains low. Endo IV has a molecular weight comparable to FPG. With this information we can conclude that interactions of FPG and Endo IV with dsDNA are not comparable. The average residence time of Endo IV on dsDNA without lesions has either a very low half-life or a very low interaction frequency. Only on DNA strands with THF and C3 lesions, a small signal due to enzyme binding can be found. Regeneration by NaCl does not show any effect on the enzyme's dissociation, revealing that the nature of interaction of Endo IV with abasic sites is not dominated by electrostatic interactions. Indeed, Endo IV is an enzyme that interacts mainly with the DNA's minor groove and it makes use of some residues inserted in the AP site to kink the DNA. Electrostatic interactions seem to have a contribution during scanning of DNA strands but are less important during enzyme activity. Although our injection signal stays very low, heating and injection of ODN-G reveal a specific hybridization signal on C3 and THF spots. Figure 6.11 shows the hybridization signal of ODN-G-biotin followed by revelation with streptavidin. The hybridization signal of ODN-G is interesting, as mass is first increased and then lost again as the signal regains almost its initial base line. As the streptavidin injection reveals the presence of the newly injected ODN, only one other explanation for this signal decrease can be found. The enzyme stays on the DNA during heating and is only displaced by rehybridization of ODN-G. We can, however, not determine where exactly the enzyme is fixed. Since the incised small DNA fragments seem released as the Zip-complementary strand is available for hybridization, it would be possible that Endo IV fixes the artificial strand break between the surface grafted probe and the small ODN containing the

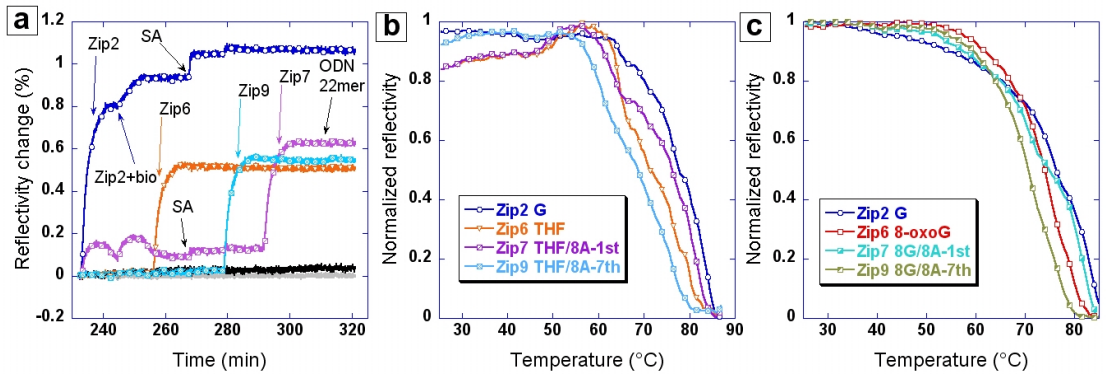

Figure 6.12: a) Hybridization of Zip complementary sequences with various lesions as indicated in legend at 400 nM. For optimization, a first Zip2 G injection is without the biotinylated ODN-22mer, the second is with biotin, so that the fraction on Zip2 and Zip7 of this second injection can be revealed by streptavidin (SA). b) Temperature scan at 2°C/min on the THF tandem lesion system after hybridization as in (a). c) Equivalent T-scan on the 8-oxoG tandem lesion system.

lesion. This typical increasing/decreasing signal during ODN-G injection is observed repeatedly for Endo IV, so we may exclude artifacts due to small signal variations. The revelation of enzyme activity shows a higher signal on THF spots compared to C3 spots, indicating a more efficient repair on the former lesion.

6.3.5 Enzyme activity on tandem lesion

After characterization of FPG, hOGG1 and Endo IV on simple DNA lesions, we will now work with a small system of clustered DNA damage. Clustered DNA damage describes the appearance of two or more DNA lesions in proximity either on the same or on the opposite strand. These lesions can be induced during local energy deposit by ionizing radiation as shown by Sutherland et al. [336], but may also originate from anti-cancer drugs. Clustered DNA lesions are supposed to be a challenge for DNA repair mechanisms and may have increased mutagenic or lethal potential [362]. It is thus of biological relevance to understand to which extend cells are able to repair neighboring DNA damage. As each damage changes the properties of the double helix by inducing bends or altering the chain's flexibility, DNA repair enzymes may have trouble to treat certain configurations. Several studies on this topic are available, but due to the large variety of DNA lesions that may occur during an oxidizing event, it is difficult to analyze all possibilities. David-Cordonnier et al., for example, studied 8-oxoG repair by yeast OGG1 (yOGG1) in the presence of various lesions at position 1, 3 and 5 on the opposite strand 3' and 5' of the 8-oxoG damage site [363]. They report a strong inhibitory effect for abasic sites or single strand breaks (SSB) that is not found when the second damage is a lesion like uracil or a second 8-oxoG damage. In the case of a second lesion, one can find inhibition or activation of the enzyme's catalytic activity. The strong inhibition by AP sites and SSB is attributed to the high risk of formation of double strand breaks during 8-oxoG repair, which would call for one of the most error prone repair mechanisms in the cell's DNA repair. Similar results have been found for FPG and hOGG1 [335, 364]. In the case of a second lesion, the highest inhibition is often detected when the lesion is next to the initial lesion, but on the complementary strand. When two lesions appear in the same strand, it may depend on the order of repair if the system hampers or not normal repair mechanisms. So, Budworth et al. studied 8-oxoG/8-oxoG or 8-oxoG/ U tandem lesions separated by two bases on the same strand that are repaired by hOGG1 and APE1 [365]. They find that 8-oxoG excision is mainly inhibited when located near the 3' terminus of an AP site formed during repair of the first lesion. Cunniffe et al. studied tandem lesions in the same strand for 8-oxoG/AP lesions and showed that the presence of 8-oxoG reduces efficient AP site incision by FPG and Endo III [366]. Lomax et al. also studied

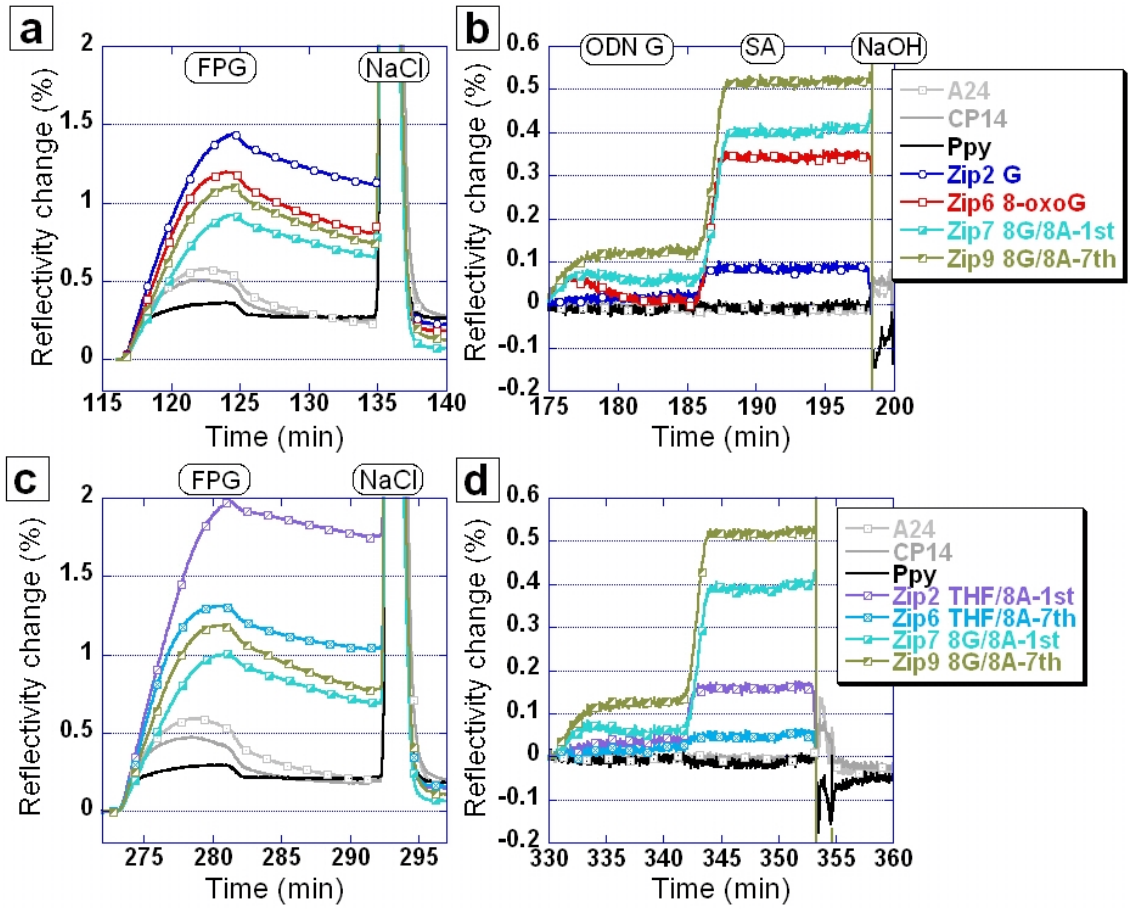

Figure 6.13: FPG base excision repair on tandem lesions a) Injection of FPG at 200 nM and 25°C on 8-oxoG tandem lesions. b) Revelation of FPG activity by ODN-G and SA after heating to 45°C for 3 min c) Injection of FPG 200 nM on THF and 8-oxoG tandem lesions at 25°C. d) Revelation of FPG activity by ODN-G and SA after heating to 45°C for 3 min. Both experiments are carried out on the same chip with similar hybridization signals for injections at 250 nM.

tandem lesions with AP sites located in vicinity of a 7,8-dihydro-8-oxoadenine (8-oxoA) lesion [367]. They determined that the presence of 8-oxoA next to an AP site strongly inhibits repair by FPG. 8-oxoA is not a substrate for FPG and hOGG1 provided that the opposite base is a thymine [361, 367]. According to the system of Lomax et al. we studied 8-oxoG BER in the presence of an 8-oxoA lesion on the same strand. Two positions are here compared: a neighboring position where 8-oxoA is the first base 3' of the 8-oxoG lesion and another position where 8-oxoA is in the 7th position 3' of 8-oxoG. The proximal tandem lesions is analog to the AP/8-oxoA position denoted +1 in the system of Lomax et al. [367]. From their study, we expect this position to have a 20-fold inhibition compared to enzymatic activity on a single lesion. The distal position at the 7th neighboring base should not show any particular influence on base excision repair. Analog to the 8-oxoG/8-oxoA tandems, we also dispose of THF/8-oxoA tandems for repair by endonuclease activity and trapping assays. The sequences are given in table 6.1.

To characterize the tandem lesions and the enzyme's repair activity, we will once again make use of the heat revelation using rehybridization. Our tandem lesion sequences are biotinylated, so that also an indirect detection is possible by the loss of biotin on the spot. A first experiment showed, that without heating, none of the cleaved 14mer strands part at 25°C, justifying the heating before ODN revelation. Further, the presence of biotin on the strands imposes the necessity

of a first SA injection before revelation with ODN-G. In this way, we obtain 'differential' information. First, we observe everything that has not been cleaved during the SA injection. Then, we reveal free hybridization sites with the ODN and then the ODN with a second SA injection. Of course, a simpler and also efficient way would be simple rehybridization with a biotinylated oligonucleotide on spots that do not present any biotin in the beginning, as for example in figure 6.11. As our sequences present now two lesions in one 22mer strand, we first control the validity of the temperature based revelation. Therefore, a classical temperature scan is applied to our DNA chip after hybridization with the tandem lesion system. In figure 6.12a, the injection signal is shown for an optimization experiment. As mentioned previously, there is a specificity problem between Zip2 and Zip7. In the plot, we see that Zip7 reacts to both injections of Zip2c, but as the stability is poor at 45°C, the signal decreases and when streptavidin is injected, almost no signal is found on Zip7. However, as shown by the subsequent injections of Zip2, at 250 nM the Zip2 spots are not saturated within one injection. This may leave space for Zip7 cross hybridization on this spots, which can create parasite signals. To avoid this problem, we increased the hybridization concentration to 500 nM Zip complementary sequence. As the ODN 22mer is hybridized in 10% excess, we only have one type of lesion per spot as all Zip complementary targets are saturated before injection of the duplex. This is controlled by the injection of a ODN-22mer at the end of the injection step, to demonstrate that no dissociation occurs at 45°C. The thermal stability is further controlled in a T-scan experiment for tandem lesions as shown in figure 6.12b+c. All hybridized DNA is found to be stable up to temperatures of >55°C. We choose here a revelation protocol with heating to 45°C maintained for 3 min to dissociate incised DNA strands. By the way, on some sequences, we observe the stability difference between the 22mer with lesions and the perfect match on Zip sequences of 24 bp, revealed by a plateau, analog to our mutation studies in the previous chapter for the case of spots with perfectly matched and mismatched targets (see for example the plateau in Zip7 8G/8A-1st).

First, we evaluate the tandem lesion system with our *E. coli* enzyme FPG. In the beginning, we worked with a commercial enzyme purchased from Sigma-Aldrich. However, it turned out that due to impurity of the solution (presence of other proteins), we were unable to follow FPG recognition on lesions and half of our signal stayed on as non-specific signal. From these experiments, we could only evaluate the enzyme activity by revelation during ODN-G hybridization. These experiments showed that FPG has better base excision efficiency on distal tandem lesions than on the proximal tandem lesions. For injections of 50 nM during 8 min followed by 10 min rinsing, we find only ∼40% ODN signal on 8G/8A-1st compared to the signal obtained on the distal tandem lesions.

We obtained the gracious gift of a purified batch of FPG from Bertrand Castaing that allowed us to have more detailed information on interactions of FPG with tandem lesions. In figure 6.13a, we show the FPG interaction on 8-oxoG tandem lesions. For this batch of enzymes, we used injections of 200 nM to obtain good interaction signals. We can see that FPG interacts well with all dsDNA strands on the chip. The high signal on duplex without lesions correlates to higher hybridization signals for Zip2 on this prism. Dissociation of FPG is slower on the proximal tandem lesion than on 8-oxoG alone and also the distal tandem. During revelation with the ODN-G (figure 6.13b), we find the highest signal on 8G/8A-7th and a similar efficiency on 8-oxoG and 8G/8A-1st neighbor that represents about 70-80% of the signal obtained on 8G/8A-7th neighbor. A parasite signal is observed on Zip2 due to cross hybridization with Zip7c for these hybridizations at 250 nM, as explained here above. A similar experiment is shown, where A24 is hybridized with Ac26 to provide a reference of healthy dsDNA, so that all Zip sequences are available to accommodate all tandem lesions. In figure 6.13c, we see that once again the highest signal is obtained on Zip2. We further observe that FPG does not show the exceptional stability on THF lesions found when THF is the only defect. Although THF tandem lesions lead once again to slower dissociation of FPG than 8A/8G-7th, for example, the differences are small. FPG injection signals on 8-oxoG tandem lesions are reproducible and so are the ODN revelation signals shown in 6.13d. Base excision repair is found to be less efficient when another lesion is next to the 8-oxoG damage. However, in contrast to results reported by Lomax et al. [367], we do not observe a 20-fold decreased efficiency for strand incision. However, relative values surely depend on enzyme concentration and

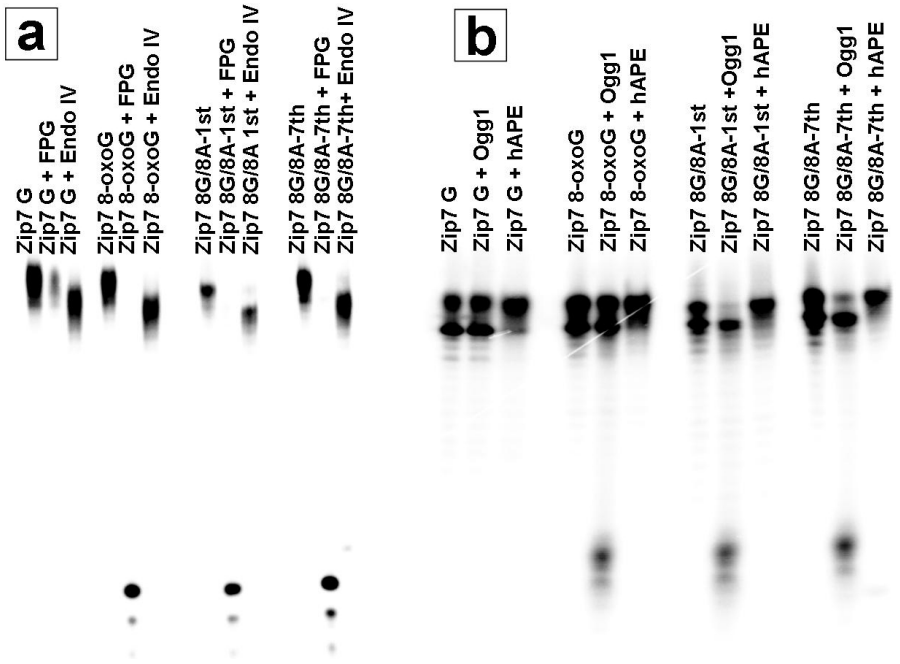

Figure 6.14: a) Electrophoresis DNA migration of 5'-P32 labeled 22mers. Each ODN 22mer is aligned with Zip7 in 10% excess before treatment with FPG of Endo IV. b) Same gel shift assay on tandem lesions with incubation with hOGG1 and hAPE1.

interaction time as well as accessibility of the lesion and so a direct comparison to results from solution is difficult. Still, FPG activity is reduced for the proximal lesion. An astonishing finding is that we systematically find a higher rehybridization signal on distal tandem lesions than on strands with only 8-oxoG. The reasons are not clear, but one may speculate that the presence of a second lesion near the 3' end close to the bulk can have the role of a recruiter and lead to more efficient damage recognition. The efficient cleaving of our tandem lesions by FPG has further been confirmed by electrophoresis in a denaturizing polyacrylamide gel for 5'P32 labeled ODN-22mer. The gel in figure 6.14a shows strand cleavage for 8-oxoG, 8G/8A-1st and 8G/8A-7th, confirming the capacity of FPG to excise the 8-oxoG lesion in presence of 8-oxoA. The presence of products of different length is due to different 3' end functions. Some enzymes may proceed with β but not δ-elimination and it is also possible that other molecules like DTT attach to the processed end. At the analyzed conditions with high FPG concentration, all initial substrate is processed, so that no difference due to the position of 8-oxoA can be found. Futur experiments will be done using a concentration range of FPG to access kinetic information.

We further analyzed the efficiency of Endo IV activity on THF tandem lesions. Figure 6.15 shows two enzyme activity revelation experiments for the excision of the artificial AP site. As already shown in figure 6.11, Endo IV has hardly any binding signal, so the enzyme injection is not represented here. In subfigure a, we observe ODN hybridization on all three spots containing THF lesions. The highest signal is obtained on the distal tandem lesions, analog to the observation with FPG. However, as before, we observe first association of ODN-G and, at the same time, dissociation so that Zip6-THF drops back to the initial base line. In subfigure b, an analog ODN-G-biotin injection is shown with a subsequent SA injection. It should be noted that tandem lesions already dispose of 3' biotin ends, like the ODN G on Zip2. Only the single THF lesion does not bear initially a biotin moiety. So, we expected to find approximately the same SA signal on Zip2, Zip7 and Zip9 since each duplex on these spots is biotinylated. Only THF represents the proportion of rehybridized 22mers with biotin. We find a similar SA signal on all spots with

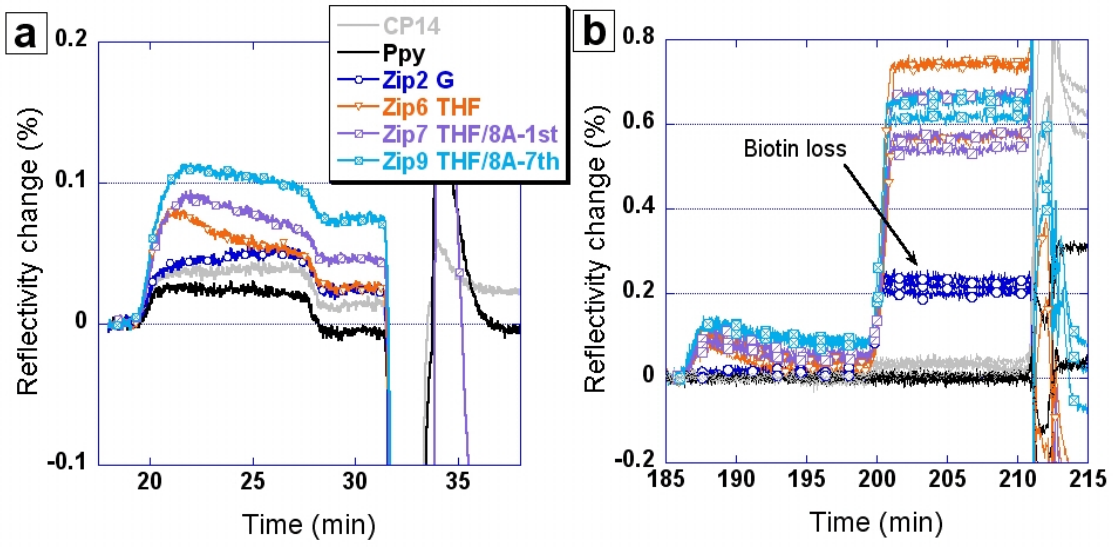

Figure 6.15: Revelation of Endo IV activity on tandem lesions with THF. a) Revelation of Endo IV activity for 4 U/ml and total interaction time of 30 min. b) Same experiment but revelation with ODN-G-biotin at 250 nM followed by streptavidin amplification.

lesions, indicating that also the Zip6-THF spots bears a similar amount of biotin moieties ODN-G-biotin hybridization. The big surprise is the small signal on Zip2. Since no repair takes place on these spots, as indicated by the absence of ODN-G hybridization, we would expect a SA response identical to the other spots. The only possible explanation for the small signal is a loss of biotin on these spots. This assumption is controlled in two different experiments. First, in figure 6.14, each tandem lesion with 3' biotin and ODN-G-biotin are labeled 5' by P32 and then hybridized to 10% excess of Zip7c. The duplex is then incubated with Endo IV in our reaction buffer. After migration on a denaturing polyacrylamide gel, we find that the Endo IV incubation leads to a slightly shorter product than the original 22mer. The size of this loss corresponds to the 570 Da of the biotin-TEG label. Attempts have been done to characterize this cleavage by mass spectrometry to identify the remaining 3' end function, but the high salinity of the reaction buffer prohibited resolution of our product. However, a SPRi experiment is carried out to access further information on Endo IV activity on biotin-TEG functions.

The experiment shown in figure 6.16 aimed to determine eventual Endo IV activity on various biotin labels under different conditions. The experiment is carried out at 37°C to maintain the conditions from our Endo IV activity revelation. First, Zip2 is hybridized with ODN-G-biotin. A short heating to 45°C is used to regenerate the cross-hybridized part on Zip7. We inject 10 nM streptavidin to protect the biotin labels on the Zip2 spots. We then hybridize subsequently Ac26-bio, which has two bases as dangling ends and 5' biotin-TEG, Zip6 G-biotin as equivalent to what is hybridized on Zip2 and Zip9c-biotin with 5' biotin-TEG. Then, Endo IV is injected for 8 min at 130 nM. At this stage, we observe no signal loss on Zip2 that would indicate streptavidin loss. Next, Zip7c-biotin is hybridized as a control and finally, streptavidin at 10 nM is injected to reveal biotin labels on the chip. The SA injection shows normal signals on all spots except Zip6, where the 3' biotin-TEG has been cleaved by Endo IV. This experiment shows that Endo IV only treats 3' biotin-TEG labels and has no function on 5' labels either directly at the end of the duplex or free on 5' dangling ends. Also, the first injection of SA on the Zip2 spot seems to protect the biotin label from enzymatic activity. This is important since this shows that functionalizations using streptavidin-biotin recognition *in vivo* would probably not be destroyed by endonuclease activity. On the other hand, the catalytic activity of Endo IV on 3' biotin-TEG labels as commercialized by Eurogentech needs to be taken into account in the experimental design. It also provides a

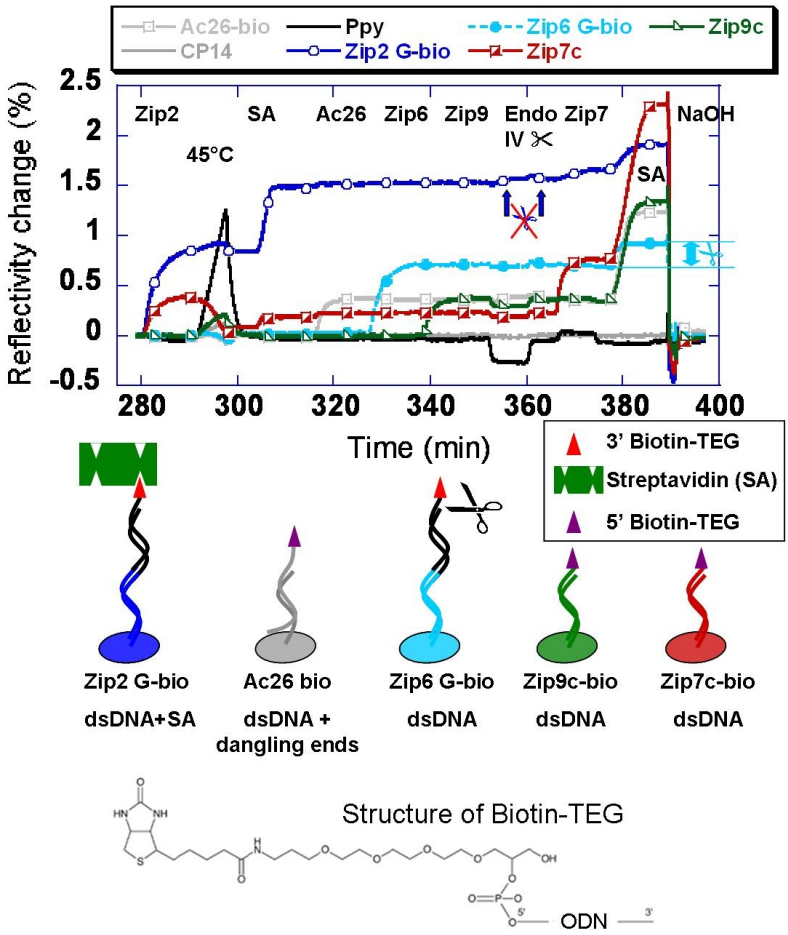

Figure 6.16: Experiment to control conditions under which Endo IV cleaves biotin. All oligonucleotides are injected at 500 nM and 37°C. Streptavidin injections use 10 nM and Endo IV corresponds to 4 U/ml. Only 3'biotin-TEG (from Eurogentech) is found to be cleaved by Endo IV when not blocked by streptavidin.

possibility to voluntarily cleave the label of oligonucleotides. In fact, the activity of Endo IV on DNA 3' ends is well known [339] and the structure of the biotin-TEG linker with its phosphate group is apparently compatible with the active site of the enzyme when used on the DNA 3' end. The structure as given by Eurogentech of 5' biotin-TEG is shown in figure 6.16. An experiment analog to the one described here has been carried out using APE1. While APE1 is able to incise THF just as Endo IV, no distinctive activity on the biotin label can be found. This is also the outcome of the gel electrophoresis after incubation of 8-oxoG tandem lesion with APE1. As shown in figure 6.14b, no modification of the 22mer is detected. From the APE1 experiment, we can estimate the efficiency of Endo IV biotin cleaving to be about 67% for the applied interaction time and concentration.

The results presented in the following are preliminary and have yet to be repeated. As clustered DNA repair is of biological relevance, we take also hOGG1 to study these lesions. One first experiment with hOGG1 at 12 U/ml and a total interaction time of about 50 min before NaCl regeneration indicated that hOGG1 preferably cleaves 8-oxoG when neighboring a 8-oxoA lesion. As the limiting step in BER by hOGG1 has been reported to be the β-elimination, a combined protocol with DNA glycosylase and endonuclease activity is tested. We first tried the model using

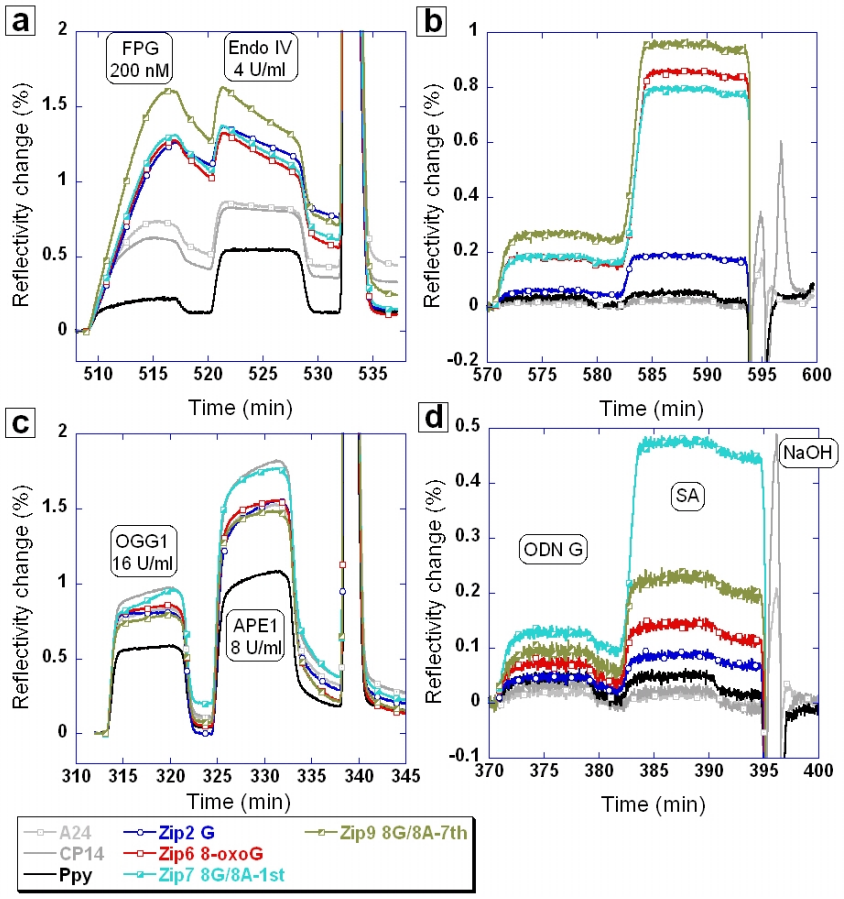

Figure 6.17: Enhanced 8-oxoG repair using first a DNA glycosylase (FPG, hOGG1) then an endonuclease (Endo IV, APE1). a) Injection of FPG followed by Endo IV at 37°C. b) Revelation of FPG activity by injection of ODN G followed by SA amplification. c) Injection of hOGG1 (Trevigen) followed by APE1 injection at 37°C. d) Revelation of hOGG1 activity by ODN-G and SA. Both experiments are carried out on the same chip with similar hybridization signals.

FPG and Endo IV, although no constructive interaction of these enzymes has yet been reported for *in vivo* studies, contrarily to hOGG1 and APE1. The double injection of the two enzymes is presented in figure 6.17. After FPG injection, Endo IV is injected, but as before no enzyme interaction is distinguishable and the signal basically represents a global refractive index change and FPG dissociation from the lesions. However, during revelation, we find that all tandem lesions are cleaved to about the same extend. From the exceptional high signal during the second SA injection as compared to the first that yields $\leq$0.15% reflectivity, we can conclude that SSB efficiency is 85% and higher. So, the injection of Endo IV assists FPG and the combination of FPG and Endo IV leads to fast and efficient base excision. The experiment is repeated for hOGG1 and APE1 as presented in figure 6.17c+d. Both enzyme injections are accompanied by a large global refractive index change the hides eventually interaction signals. During hOGG1 and APE1 injection, a specific signal is found on Zip7 carrying the proximal tandem lesions. Revelation by ODN-G-biotin confirms the higher activity of OGG1 on this type of tandem lesions. While activity is very small on 8-oxoG alone and also the distal lesions, the proximal tandem lesions shows a 3-fold increased for APE1 assisted repair than for hOGG1 alone. The cooperation between hOGG1 and APE1 in cells that undergo oxidative stress has been studied and an enhancement of hOGG1 activity by a factor 1.8 in the presence of APE1 has been observed by Sidorenko et al. [368, 369]. Other groups have also investigated the coordination between APE1 and hOGG1 and found a

2.5 and 5-fold increase of activity, respectively [351, 350]. The observation in the hOGG1/APE1 experiment confirms our first observation that hOGG1 has a preference for 8G/8A-1st. Compared to FPG, hOGG1 cleaves about 55% of the 8G/8A-1st lesions excised by FPG in the same time. On 8-oxoG alone, only 15% of FPG performance is recorded and 8G/8A-7th achieves about 25%. These reults may indicate more effective base excision for hOGG1 in the presence of multiple lesions in one strand. Denaturing gel migration as presented in figure 6.14b shows that hOGG1 is able to treat all tandem lesions. This gel migration experiment shows a double band that is absent for the FPG experiment in subfigure a, which probably indicates formation of secondary structures of some kind. The denaturing conditions provided by formamide and urea are not strong enough. Although this makes the experiment difficult to interpret, there might be a tendency of higher product formation on the proximal tandem lesion substrate. However, to truly confirm our SPRi results, the experiments will need to be repeated with a hOGG1 concentration range to obtain also kinetic information.

6.4 DNA repair studies: conclusions and perspectives

The results presented in this chapter are probably the closest to biological conditions amongst all studies within this work. So, it is not astonishing that a multitude of applications for the experimental design may be found. We provide here a universal chip design that can be upscaled to accommodate a large number of DNA lesions or clustered DNA damage, as started here with the tandem lesions. This provides a fast screening method that gives qualitative data on enzyme interaction and activity. In the first part, we show that interaction studies are an easy tool to compare the affinity of enzymes for specific kinds of DNA damage. We identified in this way THF and C3 as potential inhibitors for the base excision repair pathway. Both, hOGG1 and FPG show a longer half-life time on THF or C3 bearing DNA than on their natural substrates. As they further are not able to catalyze and repair this damage, the lesions may become a trap, fishing functional enzymes and keeping them away from their repair mission on the ubiquitous 8-oxoG lesion. 8-oxoG lesions are highly mutagenic when not repaired, as they induce a G·C to T·A transversion. Repair by FPG or OGG1 is highly specific for the opposite base of the lesion, ensuring that BER does not provoke or amplify wrong information. When these enzymes are no longer available, the cell is in danger of mutations that may even be lethal to its function. So, voluntary inhibition of hOGG1 may assist cancer treatment by reducing the efficiency of BER [315]. In cancer treatment, DNA damage is voluntarily increased in order to hinder a tumor to grow and, in the best case, the tumor will disappear. To achieve this, the cells must be forced in apoptosis by exogenous induction of DNA damage. This may be done in form of irradiation or chemotherapy, for example. Clustered DNA damage can be provoked by ionizing radiation already at low doses [336]. As we have seen here and elsewhere, clustered DNA damage may modulate the enzyme activity, by inhibition or activation [366]. So, a correct understanding of DNA repair can provide useful tools to find ways to destroy cancer cells. But our chip may also find applications in personalized treatment of patients insomuch as the repair mechanisms of each individual varies and screening of the repair activity on multiple lesions may allow for adapted cancer treatment.

While the clinical applications are still in the far future, a more immediate use for our design is found. During the last year of my Ph.D. two projects were started. The first collaboration with J. Breton and C. Bounaix du Puch from the 'Laboratoire des Lésions des Acides Nucléiques' (LAN) at the CEA Grenoble INAC/SCIB is aimed to study platinum induced DNA lesions as provoked by certain anti-cancer drugs. The lesions are studied in the same chip format as presented here with various enzymes that recognize the damage, but do not have any enzymatic activity. First results obtained on the SPRi system confirm affinities as obtained from other methods. The second project is led in collaboration with J.-F. Constant and M. Jourdan from the 'Département de Chimie Moleculaire' at the Université Joseph-Fourier Grenoble 1. This project is in close connection to our studies and extends the available lesions to a natural AP site produced during base excision of uracil in DNA strands by Uracil DNA glycosylase (UDG). Subsequent AP site

excision with FPG and our heating and hybridization revelation protocol showed that these AP sites are readily cleaved by FPG when inserted in a healthy DNA strand. However, this activity of FPG is strongly altered in clustered DNA damage, this time studied for AP sites on the opposite strand of 8-oxoG. First experiments using our SPRi concept permitted to follow real-time DNA strand breaks provoked during AP site repair and subsequent base excision and backbone incision on 8-oxoG by FPG. The SPRi experiments provide useful complementary kinetics information that can only indirectly be accessed in gel shift assays. Since our system is well adapted to any kind of specific DNA/ligand interaction, it could also be used for the systematic search for new DNA interacting proteins. When the surface is functionalized with one specific lesion, for example, and then exposed to nuclear extracts, the lesions can go 'fishing' for new proteins. SPRi preselected proteins may in a next step by analyzed by mass spectrometry. SPRi setups that are coupled to mass spectrometry are described in the literature and constitute a useful tool for such identification studies [370].

Chapter 7

Conclusions: DNA interaction studies with temperature regulation

With the work presented in this Ph.D. thesis we have demonstrated the manifoldness of our temperature regulated SPRi detection system. The aim of this project is to gain a fundamental understanding of DNA interactions on a solid support by the means of linear temperature scans that give rise to DNA denaturation curves. Our approach is as well theoretical with simulations within the framework of the Langmuir model as experimental using surface plasmon resonance imaging.

We have successfully conducted systematic studies to gain further insight in the surface hybridization process. Parameters like the buffer salinity and denaturing power are important for optimization of the assay specificity and we provide here the biochip dependency of non-equilibrium thermal denaturation of the denaturing agent formamide. Then, we successfully demonstrated the possibility of point mutation detection with our system with a very good sensitivity for target mixtures. The linear temperature scans are an important point in the detection process. As we can conclude on the genotype just from data obtained during the scan, we can use the most favorable conditions for surface hybridization. So, we chose to work in non-stringent salt concentrations of 350-450 mM NaCl and we use formamide to adapt the dissociation temperature to the accessible temperature range of the grafting method, i.e. thiols or ppy. Thanks to the temperature regulation, we can also increase or ramp the hybridization temperature to meet the requirements of the sample, as in the case of secondary structures in long targets. During heating, we can open up parts of the secondary structure in order to decrease competition between self-hybridization in solution and surface hybridization. Dynamic temperature regulated hybridization constitutes a flexible tool that allows to accumulate specifically the perfectly matched target to its corresponding probe.

All these fundamental studies allowed then the determination of hybridization parameters necessary to hybridize our PCR product that has an extremely unfavorable conformation for surface hybridization. We show here how the use of helper oligonucleotides can efficiently assist the accessibility of the hybridizing part of our target. After successful hybridization, we demonstrate that it is possible with our system to detect single nucleotide polymorphisms and to attribute the correct genotype also to heterozygous samples. For PCR denaturation curves, we find a very distinct curve shape with a sharp transition at the dissociation temperature. We attribute this phenomenon to interactions between targets on neighboring sites that lead to an interlaced network with cooperative features. However, this cooperativity seems to be related to the high G·C content of the target and possible cross-hybridization since we do not observe such an effect for the subsequent analysis of our RNA target from NASBA amplification. The NASBA system has been shown here to be a good approach to the development of integrated RNA or DNA detection systems that need low-cost screening, for example in food or environmental studies. As the SPRi approach does not need molecular beacons, we can profit here from the possibility to use our DNA

biochip for multiple experiments. The integrated system is also compatible with point mutation detection.

Finally, the study of enzymes from base excision repair (BER) provided a multivalent layout for a huge variety of applications in research of medical diagnosis. Here we analyze interactions between the bivalent glycosylases FPG and hOGG1 and their substrate 8-oxoG, but also other DNA damages of interest for the BER pathway. Our SPRi characterization can go beyond the simple characterization of recognition; indeed, we demonstrate a multi-step method that reveals the enzymatic activity of various enzymes that act by chemical generation of single strand breaks. To validate our strategy, we study a system of clustered DNA damages, as typically may arise from ionizing radiation. Our qualitative results are confirmed by other methods like polyacrylamide gel electrophoresis. Still, this project shows a lot of studies that might be interesting for future research and some new projects based on our universal addressable chip layout have already started during the last year.

Since the scope of this Ph.D. thesis is rather large, each individual project profits from the understanding gained in our earlier, more fundamental studies. The optimization using oligonucleotides allowed so the point mutation detection in long biological targets. Likewise, the knowledge of complex sample handling that involved blocking strategies and adapted regeneration methods is beneficial for optimization of our enzyme interaction studies. Maybe this wide range of research leads sometimes to a lack of time to develop further understanding of phenomena like the appearing plateau for targets with secondary structures, but in general the broad spectrum is favorable to develop rapidly conceptual approaches to new systems. So, in conclusion, the virtue of this work is the creative exploitation of a multivalent detection system.

Chapter 8

Perspectives

DNA chip technology is widely used in today's biomolecular research with many applications and much more that will arise. It is thus astonishing that DNA microarrays have not yet really found their way into clinical applications. The fact that DNA chip technology is rather costly, either the chip itself or the machinery needed for its production or read-out, plays certainly a role. Another reason is probably to be found in the technology itself and most of all in the reproducibility and reliability of results as discussed by Draghici et al. [371]. We have seen in this thesis that surface hybridization is far from being a simple and well understood concept. Although a lot of work has been devoted to the optimization of different parameters, the final performance is an interplay of a lot of connected interactions that are very specific for the detection method, but also for the sample to which it will be applied. The choice of the detection method should be guided by two main interests: the sensitivity must be sufficient for the sample in question and the signal that can be obtained should reflect all information that is needed for reliable data analysis. Real-time detection methods have surely the advantage to provide a multitude of data points and sample dependent information on the process of hybridization. With end point dependent detection methods, we obtain one data point, without any knowledge of the process. So, when hybridization times are long and rearrangements on the chip take place, the end point that will be measured may not reflect at all what we expect to be the sample's composition [55]. With this reflection, a real-time approach seems to be a good choice. The drawback is the huge amount of data that has to be treated which in fact limits the size of arrays to be analyzed. As optimization of DNA hybridization-based chip assays gets more and more complicated with the number of targets to be analyzed, it may make sense to limit the probes of analyzed sequences and rather apply the tool to screening of a large number of patients. Standard real-time detection methods like SPR and QCM are often used as biosensors without any possibility of parallelized measurements. For DNA, this is a rather impractical solution, since control surfaces would be needed separately and especially for SNP detection we have seen that it is useful to have at least both, the wild type complementary and the mutant complementary sequence to determine the correct genotype of the target. So, parallelized measurements are unavoidable and the choice of the method must take into account the capacity of sequences to be analyzed, in the right-sized 'package' to answer one or more specific questions.

This work shows that SPRi provides a tool that is easily adapted for up to 100 spots, which would already make a sufficient set for a sensor that would, for example, try to determine a patient's metabolism vis-à-vis a certain drug. We have shown here that SPRi can be used for DNA detection provided that the concentration is sufficiently high, more than 10 nM for oligonucleotides and 100-fold higher for longer targets with secondary structures. However, the SPRi technique is not sufficiently sensitive to screen for mRNA or even genetic material without amplification. Most of the more sensitive detection methods rely on labeling of the targets, like for example fluorescence. Indeed, fluorescence microscopy is today one of the most current techniques in DNA detection, which is facilitated by the ease of labeling of DNA. When PCR sample amplification is used, for example, the primers can already have the necessary label, like biotin, that can then be

used to attach the fluorophore. So, it may be a good choice to integrate fluorescence microscopy and real-time detection to obtain conclusive information on a very sensitive detection system. Another advantage of fluorescent labeling is also the insensitivity to buffer changes and buffer components that may interact with the surface. For optimal assay layout, the system should have an integrated temperature control which, as shown throughout this work gives way to elaborated detection protocols that help to adapt the method to complex samples and allows the detection of target mixtures even when one partner is present in low abundance. Some developments in this direction are proposed in form of integrated fluorescence-based and temperature regulated microarray readout systems equipped with a CCD camera. We can cite, for example, genewave, 4-MAT by innogenetics and nanogen as commercialized platforms for DNA detection [151, 153, 152].

For DNA experiments, due to the really well developed labeling methods and the good sensitivity provided, fluorescence analysis may be a good alternative to SPRi. However, when it comes to proteins or enzymes, it is much more difficult to use a labeling technique. Enzymes may loose their activity upon labeling, or alter their dynamics when, for example, labeled by the expression of the green fluorescent protein. When labeling is done by chemical linking after fabrication of the enzyme, it is often quite impossible to control and know the exact number of labels per protein. This may also bias the data analysis and complicates the signal interpretation. So, in this case, surface sensitive methods like SPRi are a very good opportunity. As these molecules are also of sufficient mass, they provide good SPRi signals. Also here, as we have seen, the temperature regulation presents an advantage: enzymes coming from different organisms have optimal working temperatures that can differ a lot. So, the activity will depend on the temperature of the system. This has been important here to make work the NASBA protocol in our SPRi setup. But also our heat revelation system constitutes a good example of such a temperature regulation application. In the near future, we can surely expect an increasing range of data obtained from temperature regulated, SPRi based protein or enzyme detection platforms.

Appendix A: Table of buffers

SPRi buffers		
Experiment	**Specification**	**Composition**
DNA running buffer	PBS 450 mM NaCl	Phosphate buffered saline: 0.01 M phosphate buffer, 0.0027 M potassium chloride, 0.137 M sodium chloride; pH 7.4 at 25°C. 3.66 g NaCl are added per 200 ml to adjust salinity to 450 mM NaCl
DNA regeneration buffer	NaOH	Sodium hydroxide at 0.1 M for ppy chips(0.2 g per 50 ml) or 0.01 M for thiol-DNA chips
DNA hybridization buffer	PBS 450 mM with DNA	DNA in water diluted in the running buffer. Since DNA stocks are available at 100 µM, the buffer is not significantly diluted. For hybridization of purified PCR products, EDTA is added at 1 mM
BSA blocking buffer	BSA	Solution of 1% bovine serum albumine in the running buffer
Protein/enzyme regeneration buffer	NaCl	NaCl dissolved at 1.5 M in water
NASBA running buffer	NASBA	40 mM Tris-HCl at pH 8.5, 15% DMSO, 80 mM KCl, 12 mM $MgCl_2$, 5 mM freshly added Dithiotreitol (DTT) and 0.5 M sorbitol
FPG running buffer	BER enzymes	30 mM Tris-HClpH 8, 3 mM $MgCl_2$, 100 mM KCl, 1.3 mM EDTA Na_2, 0.2 mM DTT (DTT added at the last moment)
Buffers for fluorescence essays		
Rinsing buffer	–	PBS 0.01 M, NaCl 0.537 M, KCl 2.7 mM, Tween20 0.05%
Hybridization buffer	2X	PBS 0.02 M, NaCl 1.047 M, KCl 5.4 mM, Tween20 0.1%, Salmon DNA, Denhardt's® solution
Spotting buffers		
Piranha solution	Piranha	70% sulfuric acid (H_2SO_4) and 30% hydrogen peroxide (H_2O_2). Wear protection gloves, mask and clothes. Be carefull, solution gets hot!
Ppy electrospotting	GDALi	In MilliQ water add 30% acetonitril, 20% DMSO, 0.5% glycerol and 0.1-0.15 M $LiClO_4$

Table 1: Recapitulation of the buffer solutions used in this work. All buffers are prepared with deionized water at a resistance of 18.2 MΩ and SPRi buffers are filtered successively by 0.8 µm and 0.2 µm filters.

Appendix B: Experimental protocol for fluorescence microscopy

This appendix gives the detailed experimental protocol that is used at our laboratory for fluorescence microscopy revelation of DNA hybridization. The experiments may use gold covered glass slides or gold covered prisms that are functionalized by probe DNA.

Use the rinsing buffer (tampon de rinçage) and the hybridization buffer (tampon d'hybridation 2X) at 2X concentration as given in the previous chapter on page 147.

- Cover the area of interest of the chip with deionized water for 5 min.
- Shake off the water and incubate with rinsing buffer for 5 min.
- Prepare 50-100 µl of hybridization solution with the appropriate DNA concentration in 1X final hybridization buffer. For oligonucleotides, 100 nM are sufficient. For PCR product, 250 nM or higher concentrations are advised.
- Remove rinsing buffer and incubate at the appropriate hybridization temperature for the appropriate hybridization time. For oligonucleotides of 20 bp or more, 15 min hybridization at 40-50°C is well adapted, the temperature will determine the specificity of hybridization for mutated targets. For PCR products, hybridization is here carried out at 42-45°C for 1 h-3 h.
- Rinse abundantly with 3-5 ml of rinsing buffer using the micro-pipette.
- Prepare 50-100 µl dilution of 5-10% SAPE in rinsing buffer
- Incubate for 5 min at room temperature with the SAPE solution in a dark environment (aluminum covered Petri dish, etc).
- Rinse with 1-2 ml rinsing buffer avoiding exposure to strong light sources
- Cover the wet chip with a cover slip avoiding air bubble formation and place the chip on a microscope slide.
- Proceed with microscopy fluorescence image acquisition using the adapted filter (WIG). Minimize exposure times by using the 'freeze image' option and closing the shutter before image acquisition. Adapt magnification (x1.25, x4, x10, x20), gain (=4) and exposure time to the fluorescence signal and the area of interest observed.
- After image acquisition, lift the cover slip off the chip carefully and regenerate by washing with 1-2 ml of NaOH at 0.1 M
- Rinse the chip abundantly with deionized water, dry and stock it at 4°C.

Appendix C: Details on SPRi data analysis

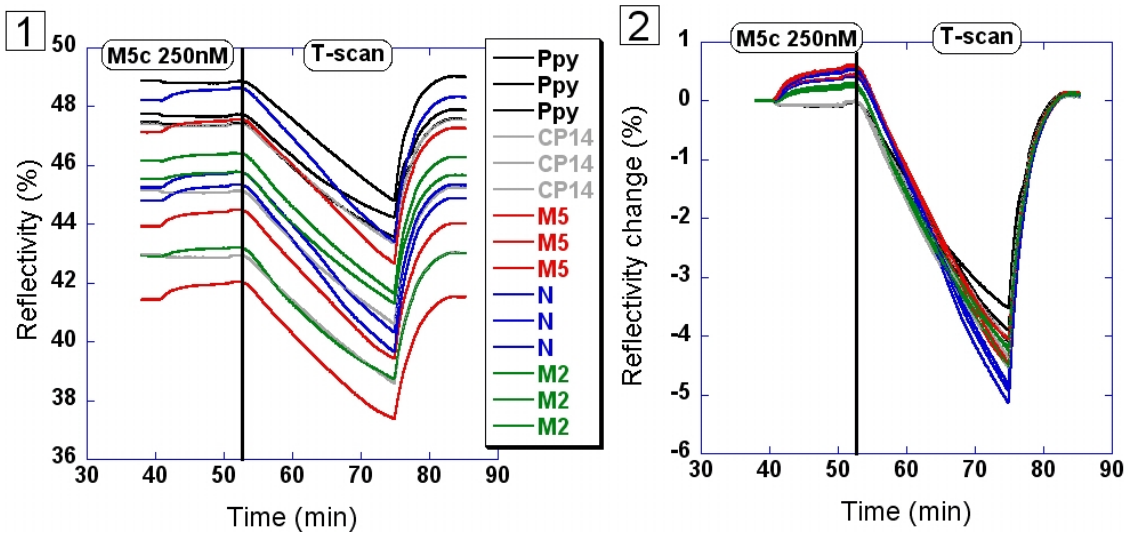

Figure 1: Data analysis - Base line subtraction: 1) Reflectivity as recorded by SPRi. 2) Base line subtraction before the start of the injection.

This appendix will present a step by step demonstration of how SPRi signals are analyzed in order to obtain the DNA denaturation or melting curves that are presented in this thesis. Here, an example of non-equilibrium thermal denaturation curves is taken corresponding to the 5% formamide experiment on a poly-pyrrole chip as presented in section 4.6.1. For better visibility, only 15 of the 42 spots on the chip are represented here. But of course, all spots undergo the same treatment, as the data analysis uses some Mathematica routines that automatically detect the number of spots and treat each spot in the same way.

Figure 1-1 shows the SPRi signal exactly the way it is acquired during the experiment. Each spot has its individual level of reflectivity as poly-pyrrole spots are not 100% reproducible. 'Good' prisms show a distribution over a 10% reflectivity range. Here, reflectivity differences of about 8% are found. The minimum of the plasmon curves of the gold layer on this prism is found at about 30.5% reflectivity, for poly-pyrrole spots this value lies around 33-35% reflectivity. TE saturation occurs at about 70% reflectivity in this experiment. Later, the new program by GenOptics shows TE saturation at ∼63% of reflectivity. As the curves are all between 40 and 50% reflectivity, they all lie inside the dynamic range and sufficiently high so that temperature scans stay in the linear range of the SPRi sensitivity. This can be seen from the signals as during the temperature scan, no spot approaches the minimum of the plasmon curve critically. The exact shape of the plasmon curve depends on the spot homogeneity. Ideally, for linear heating we should obtain linear reflectivity changes, but sometimes inhomogeneities in the spot may lead to slight curvatures, as found here on one poly-pyrrole control spot, for example.

The first step in data analysis is the subtraction of the base line. Therefore, a period of 1-2 min before an injection is chosen. In this period, the signal is averaged for each individual spot. Then, on each individual curve, this average value is subtracted from all data points. In this way, we set the base line before injection to zero as can be seen in figure 1-2. Although not shown here, the same step of baseline subtraction is also done for the reference temperature scan. We use the reference T-scan acquired in absence of DNA to extract the small signal due to DNA dissociation from the large signal due to global refractive index changes of the buffer during T-scans.

The second step of data analysis is the synchronization of reflectivity data and temperature

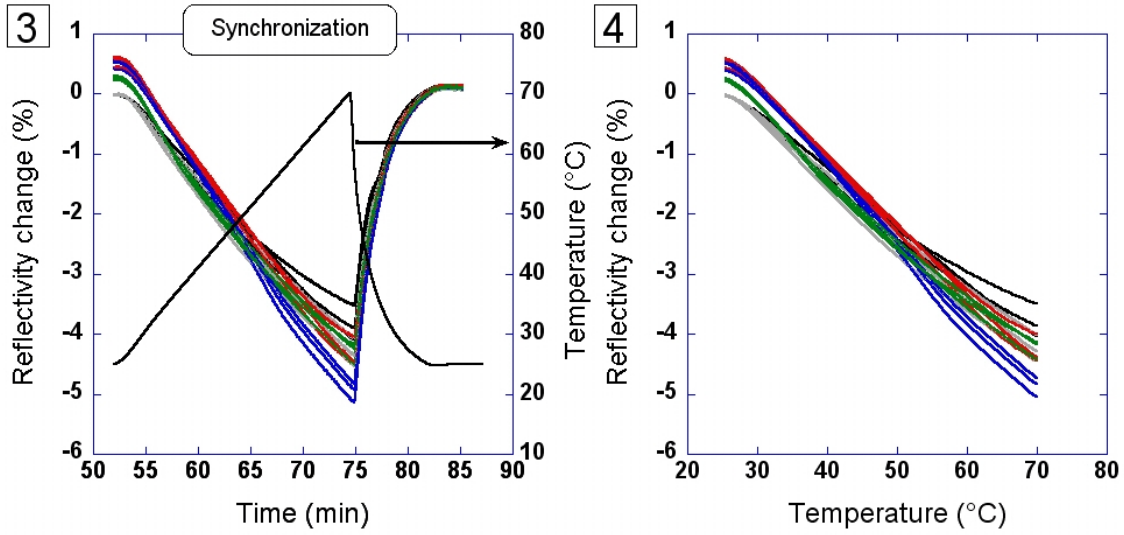

Figure 2: Data analysis- Synchronization with temperature: 3) Base line subtracted T-scan and simultaneously recorded temperature. 4) Synchronized T-scan.

data, as indicated in figure 2. During this synchronization, the number of data points are also reduced to one point ever 0.5°C. To do so, linear fits to the data are applied around the temperature to analyze and the reflectivity of this local data interpolation is taken for chosen temperatures. This local interpolation results also in soft data smoothing, thereby reducing noise on our data set. This reduced data set at discrete temperatures is also obtained for the reference T-scan. During the second year of my Ph.D. a new SPRi camera and program has been installed. As the new LabView program was available as open code, I could integrate the temperature data into the file saving the reflectivity, so that synchronization of temperature and SPRi data was no longer necessary.

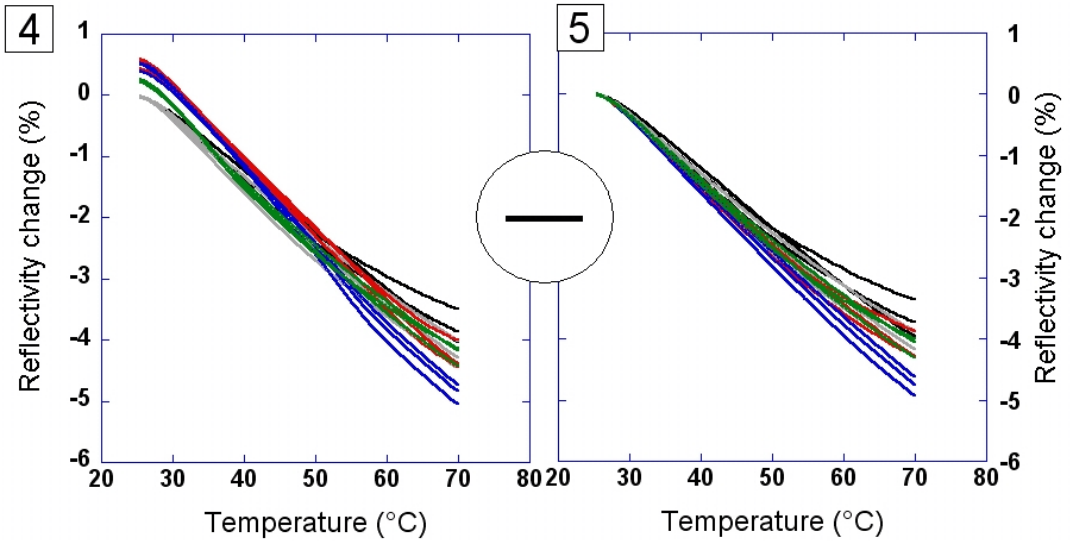

Figure 3: Data analysis - Subtraction of reference scan: 4) Synchronized T-scan with DNA. 5) Synchronized T-scan without DNA.

To obtain DNA denaturation curves, the reference scan has to be subtracted of data acquired

during DNA denaturation. In figure 3, the two sets of curves to be subtracted are represented. Close comparison reveals the subtle changes during the T-scan that are introduced by DNA dissociation. In figure 4, the result of the subtraction is given. We can now clearly see the DNA denaturation signal. However, small variations can occur that change the behavior of the spots in a global way. If this is the case, the global changes will be revealed on our control spots. It is always necessary to look if all controls represent the same tendency or if each spot has an individually shaped curve. When all spots show a common phenomenon, this may be attributed to a global event and base line correction can be done. Therefore, one control spot that represents the environment of surface grafted DNA without undergoing any DNA related event, i.e. a positive control spot like CP14, may be subtracted point by point from all other spots. However, it may happen that some spots show different signals, for example when an air bubble is formed and perturbs its neighboring spots, or when the prism has been exposed to proteins that may adhere in a non-uniform way on the surface. In these cases, it is delicate to do base line correction using the subtraction of a reference spot, signals should better be kept individual and the experiment must be repeated.

In our example, we can observe from figure 4-6 that all spots are subject to a small uniform base line drift. The exact 'size' of the perturbation is spot dependent, as each spot has a slightly differing SPRi sensitivity. In figure 4-7, the result of such a base line subtraction is shown. We see that curves are only slightly altered and that we obtain a more proper base line. It has to be noted that due to better reproducibility of thiol spots leading to more uniform sensitivity, the base line correction for thiol spots gives way to very homogeneous results.

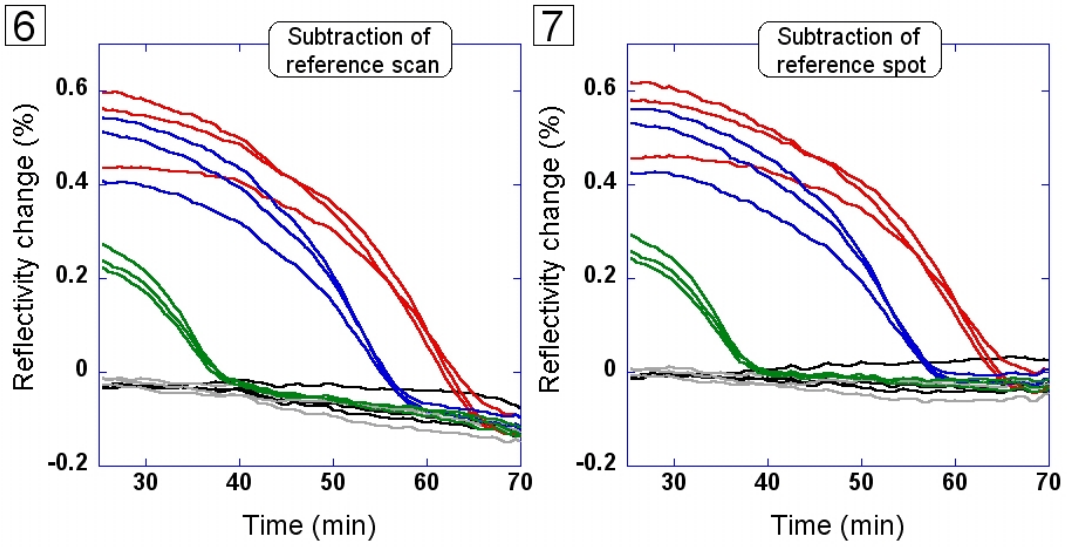

Figure 4: Data analysis - Subtraction of a reference spot: 6) DNA dissociation curves as obtained after subtraction of the reference temperature scan. 7) The same curves after subtraction of one positive control spot to correct the base line.

After base line correction, various spots have still different DNA hybridization signals due to varying grafting density and hybridization efficiency. However, for NTD-curves of individual DNA strands, these parameters should not influence our non-equilibrium analysis and each spot of one family is expected to show the same dissociation temperature. To better observe this, curves can be normalized. We therefore set the lowest signal x_{min} to zero and the highest signal x_{max} to 1 by the simple relation $y = (x - x_{min})/(x_{max} - x_{min})$. This normalization is shown in figure 5-8. Of course, normalization of control spots makes no sense, so they are no longer shown in this graph. These final DNA thermal denaturation curves can now be analyzed. For example, the derivative of the curves is calculated using a sliding local linear fit so that each data point has an attributed slope. The frame of data points used for the calculation of the linear fit will of course influence

the level of noise and the actual values. Typically, a frame of 3-8 point is used at each side of the data point. Smooth curves as shown in figure 5-9 are the result of larger frames.

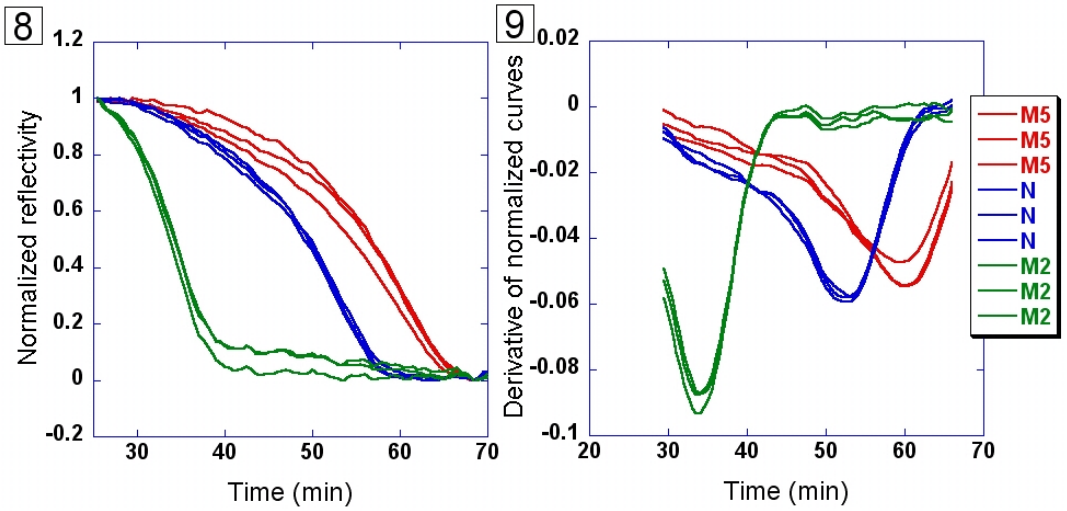

Figure 5: Data analysis - Normalization and derivatives: 7) DNA denaturation curves are normalized with the highest point at '1' and the lowest point at '0'. 8) Derivatives are calculated using a local linear fit, so that the slop can be attributed to each data point.

Finally, the normalized curves are used to extract the dissociation temperature at 50% of the initial signal. A Mathematica program therefore applies a soft smoothing using a moving average of size 3 which has been determined to be the smallest intervention as it does not provoke a shift of the curves towards lower temperatures. Then, the data is interpolated and the temperature corresponding to 0.5 is extracted for each DNA spot. Dissociation temperatures of spots from one family can be averaged and the standard deviation is calculated.

The data analysis for enzyme injections is less extensive as the extraction of DNA thermal denaturation information. Typically, for DNA injections or enzyme interactions the first step is the base line subtraction as in figure 1 to put all curves to 0. Then, a reference spot can be subtracted to take into account global refractive index changes. This can only be done in the limits of control spots that show no interaction with the injected species. Typically, for DNA, the positive control spot is used. As enzymes also interact with single stranded DNA and to some extend with poly-pyrrole spots, no reference spot has been subtracted for enzyme injections. Subtraction of reference spots works very well for thiol grafting as spots show homogeneous sensitivity. It is more delicate on poly-pyrrole spots where some remaining signal can be found on spots that have a significantly higher or lower sensitivity than the subtracted positive control. One example for this effect can be seen in figure 6.16 on page 139 for poly-pyrrole spots during the heating process to 45°C. In fact, as the first poly-pyrrole spot is spotted with longer pulse duration, it always has a reduced sensitivity, but due to its high SPRi signal serves to identify the spots matrix. So, it is not astonishing here that ppy differs from other spots.

Bibliography

[1] J. D. Watson and F. H. C. Crick. Molecular structure of nucleic acids: A structure for deoxyribose nucleic acid. *Nature*, 171(4356):737–738, 1953.

[2] J. C. Venter, M. D. Adams, E. W. Myers, and et al. The sequence of the human genome. *Science*, 291(5507):1304–1351, 2001.

[3] G. Ramsay. DNA chips: State-or-the-art. *Nature Biotechnology*, 16:40–44, 1998.

[4] J. D. Hoheisel. Microarray technology: beyond transcript profiling and genotype analysis. *Nature Reviews Genetics*, 7(3):200–210, 2006.

[5] M. Chee, R. Yang, E. Hubbell, A. Berno, X. C. Huang, D. Stern, J. Winkler, D. J. Lockhart, M. S. Morris, and S. P. A. Fodor. Accessing genetic information with high-density DNA arrays. *Science*, 274(5287):610–614, 1996.

[6] D. J. Lockhart, H. L. Dong, M. C. Byrne, M. T. Follettie, M. V. Gallo, M. S. Chee, M. Mittmann, C. W. Wang, M. Kobayashi, H. Horton, and E. L. Brown. Expression monitoring by hybridization to high-density oligonucleotide arrays. *Nature Biotechnology*, 14(13):1675–1680, 1996.

[7] D. G. Wang, J. B. Fan, C. J. Siao, A. Berno, P. Young, R. Sapolsky, G. Ghandour, N. Perkins, E. Winchester, J. Spencer, L. Kruglyak, L. Stein, L. Hsie, T. Topaloglou, E. Hubbell, E. Robinson, M. Mittmann, M. S. Morris, N. Shen, D. Kilburn, J. Rioux, C. Nusbaum, S. Rozen, T. J. Hudson, R. Lipshutz, M. Chee, and E. S. Lander. Large-scale identification, mapping, and genotyping of single-nucleotide polymorphisms in the human genome. *Science*, 280(5366):1077–1082, 1998.

[8] R. Levicky and A. Horgan. Physicochemical perspectives on DNA microarray and biosensor technologies. *Trends in Biotechnology*, 23(3):143–149, 2005.

[9] M. Campas and I. Katakis. DNA biochip arraying, detection and amplification strategies. *Trac-Trends in Analytical Chemistry*, 23(1):49–62, 2004.

[10] G. J. Vora, C. E. Meador, D. A. Stenger, and J. D. Andreadis. Nucleic acid amplification strategies for DNA microarray-based pathogen detection. *Applied and Environmental Microbiology*, 70(5):3047–3054, 2004.

[11] J. Wang. From DNA biosensors to gene chips. *Nucleic Acids Research*, 28(16):3011–3016, 2000.

[12] F. R. R. Teles and L. R. Fonseca. Trends in DNA biosensors. *Talanta*, 77(2):606–623, 2008.

[13] J. B. Fiche. *Etude thermique des puces à ADN par imagerie de résonance de plasmons de surface: vers la détection des mutations ponctuelles.* Ph.d. thesis, Université Joseph Fourier - Grenoble 1, 2006.

[14] UPPSALA UNIVERSITET. Figure adapted from `http://www.linnaeus.uu.se/online/phy/microcosmos/gifs/dna2.gif`, 2008.

[15] M. D. Frank-Kamenetskii. Biophysics of the DNA molecule. *Physics Reports-Review Section of Physics Letters*, 288(1-6):13–60, 1997.

[16] M. Ageno, E. Dore, and C. Frontali. Alkaline Denaturation of DNA. *Biophysical Journal*, 9(11):1281–1311, 1969.

[17] R. M. Wartell and A. S. Benight. Thermal-Denaturation of DNA-Molecules - a Comparison of Theory with Experiment. *Physics Reports-Review Section of Physics Letters*, 126(2):67–107, 1985.

[18] Wikipedia. Figures from `http://en.wikipedia.org/wiki/DNA`, 2007.

[19] R. M. Robertson, S. Laib, and D. E. Smith. Diffusion of isolated DNA molecules: Dependence on length and topology. *Proceedings of the National Academy of Sciences of the United States of America*, 103(19):7310–7314, 2006.

[20] D. M. Crothers and B. H. Zimm. Theory of Melting Transition of Synthetic Polynucleotides - Evaluation of Stacking Free Energy. *Journal of Molecular Biology*, 9(1):1–9, 1964.

[21] H. Devoe and I. Tinoco. Stability of Helical Polynucleotides - Base Contributions. *Journal of Molecular Biology*, 4(5):500–517, 1962.

[22] O. Gotoh and Y. Tagashira. Stabilities of Nearest-Neighbor Doublets in Double-Helical DNA Determined by Fitting Calculated Melting Profiles to Observed Profiles. *Biopolymers*, 20(5):1033–1042, 1981.

[23] N. Sugimoto, S. Nakano, M. Yoneyama, and K. Honda. Improved thermodynamic parameters and helix initiation factor to predict stability of DNA duplexes. *Nucleic Acids Research*, 24(22):4501–4505, 1996.

[24] J. SantaLucia, H. T. Allawi, and A. Seneviratne. Improved nearest-neighbor parameters for predicting DNA duplex stability. *Biochemistry*, 35(11):3555–3562, 1996.

[25] J. SantaLucia. A unified view of polymer, dumbbell, and oligonucleotide DNA nearest-neighbor thermodynamics. *Proceedings of the National Academy of Sciences of the United States of America*, 95(4):1460–1465, 1998.

[26] Y. Zeng, A. Montrichok, and G. Zocchi. Bubble nucleation and cooperativity in DNA melting. *Journal of Molecular Biology*, 339(1):67–75, 2004.

[27] D. M. Gray. Derivation of nearest-neighbor properties from data on nucleic acid oligomers .2. Thermodynamic parameters of DNA center dot RNA hybrids and DNA duplexes. *Biopolymers*, 42(7):795–810, 1997.

[28] S. Bommarito, N. Peyret, and J. SantaLucia. Thermodynamic parameters for DNA sequences with dangling ends. *Nucleic Acids Research*, 28(9):1929–1934, 2000.

[29] J. SantaLucia and D. Hicks. The thermodynamics of DNA structural motifs. *Annual Review of Biophysics and Biomolecular Structure*, 33:415–440, 2004.

[30] S. H. Ke and R. M. Wartell. The thermal stability of DNA fragments with tandem mismatches at a d(CXYG)·d(CY'X'G) site. *Nucleic Acids Research*, 24(4):707–712, 1996.

[31] B. N. Bourdélat-Parks and R. M. Wartell. Thermodynamic stability of DNA tandem mismatches. *Biochemistry*, 43(30):9918–9925, 2004.

[32] H. T. Allawi and J. SantaLucia. Thermodynamics and NMR of internal G·T mismatches in DNA. *Biochemistry*, 36(34):10581–10594, 1997.

[33] H. T. Allawi and J. Santalucia. Thermodynamics of internal C · T mismatches in DNA. *Nucleic Acids Research*, 26(11):2694–2701, 1998.

[34] H. T. Allawi and J. SantaLucia. NMR solution structure of a DNA dodecamer containing single G · T mismatches. *Nucleic Acids Research*, 26(21):4925–4934, 1998.

[35] H. T. Allawi and J. SantaLucia. Nearest neighbor thermodynamic parameters for internal G · A mismatches in DNA. *Biochemistry*, 37(8):2170–2179, 1998.

[36] H. T. Allawi and J. SantaLucia. Nearest-neighbor thermodynamics of internal A · C mismatches in DNA: Sequence dependence and pH effects. *Biochemistry*, 37(26):9435–9444, 1998.

[37] N. Peyret, P. A. Seneviratne, H. T. Allawi, and J. SantaLucia. Nearest-neighbor thermodynamics and NMR of DNA sequences with internal A · A, C · C, G · G, and T · T mismatches. *Biochemistry*, 38(12):3468–3477, 1999.

[38] Gerald S. Manning. On the application of polyelectrolyte 'limiting laws' to the helix-coil transition of DNA. I. Excess univalent cations. *Biopolymers*, 11(5):937–949, 1972.

[39] R. Owczarzy, Y. You, B. G. Moreira, J. A. Manthey, L. Y. Huang, M. A. Behlke, and J. A. Walder. Effects of sodium ions on DNA duplex oligomers: Improved predictions of melting temperatures. *Biochemistry*, 43(12):3537–3554, 2004.

[40] R. T. Koehler and N. Peyret. Effects of DNA secondary structure on oligonucleotide probe binding efficiency. *Computational Biology and Chemistry*, 29(6):393–397, 2005.

[41] N. Peyret and J. SantaLucia Jr. HYTHER TM, 1999.

[42] R. Owczarzy, A. V. Tataurov, Y. Wu, J. A. Manthey, K. A. McQuisten, H. G. Almabrazi, K. F. Pedersen, Y. Lin, J. Garretson, N. O. McEntaggart, C. A. Sailor, R. B. Dawson, and A. S. Peek. IDT SciTools: a suite for analysis and design of nucleic acid oligomers. *Nucleic Acids Research*, 36(suppl_ 2):W163–169, 2008.

[43] E. C. Friedberg and P. L. Fischhaber. DNA Replication Fidelity. In Ltd. John Wiley & Sons, editor, *Encyclopedia of life sciences*. Wiley Interscience, 2005.

[44] K. A. Eckert and T. A. Kunkel. DNA polymerase fidelity and the polymerase chain reaction. *PCR Methods and Applications*, 1(1):17–24, 1991.

[45] L. D. Stein. Human genome: end of the beginning. *Nature*, 431(7011):915–916, 2004.

[46] A. F. Wright. Genetic Variation: Polymorphisms and Mutations. In Ltd. John Wiley & Sons, editor, *Encyclopedia of life sciences*. Wiley Interscience, 2005.

[47] R. Devoret. Mutation. In Ltd. John Wiley & Sons, editor, *Encyclopedia of life sciences*. Wiley Interscience, 2005.

[48] S. B. Carroll. Genetics and the making of Homo sapiens. *Nature*, 422(6934):849–857, 2003.

[49] W. Vercoutere and M. Akeson. Biosensors for DNA sequence detection. *Current Opinion in Chemical Biology*, 6(6):816–822, 2002.

[50] T. F. Orntoft and M. Kruhoffer. DNA chips and microarrays. In Ltd. John Wiley & Sons, editor, *Encyclopedia of life sciences*. Wiley Interscience, 2005.

[51] P. A. E. Piunno and U. J. Krull. Trends in the development of nucleic acid biosensors for medical diagnostics. *Analytical and Bioanalytical Chemistry*, 381(5):1004–1011, 2005.

[52] A. Sassolas, B. D. Leca-Bouvier, and L. J. Blum. DNA biosensors and microarrays. *Chemical Reviews*, 108(1):109–139, 2008.

[53] Pui-Yan Kwok. Methods for Genotyping Single Nucleotide Polymorphisms. *Annual Review of Genomics and Human Genetics*, 2(1):235–258, 2001.

[54] A. Schulze and J. Downward. Navigating gene expression using microarrays - a technology review. *Nature Cell Biology*, 3(8):E190–E195, 2001.

[55] A. Chagovetz and S. Blair. Real-time DNA microarrays: reality check. *Biochemical Society Transactions*, 37:471–475, 2009.

[56] X. Y. Mao, B. D. Young, and Y. J. Lu. The application of single nucleotide polymorphism microarrays in cancer research. *Current Genomics*, 8(4):219–228, 2007.

[57] W. Knoll. Interfaces and thin films as seen by bound electromagnetic waves. *Annual Review of Physical Chemistry*, 49:569–638, 1998.

[58] J. M. Pitarke, V. M. Silkin, E. V. Chulkov, and P. M. Echenique. Theory of surface plasmons and surface-plasmon polaritons. *Reports on Progress in Physics*, 70(1):1–87, 2007.

[59] A. Otto. Excitation of Nonradiative Surface Plasma Waves in Silver by Method of Frustrated Total Reflection. *Zeitschrift Für Physik*, 216(4):398–410, 1968.

[60] E. Kretschmann. Determination of Optical Constants of Metals by Excitation of Surface Plasmons. *Zeitschrift Für Physik*, 241(4):313–324, 1971.

[61] E. Maillart. *Développement d'un système optique d'imagérie en résonance de plasmons de surface pour l'analyse simultanée de multiples interactions biomoléculaires en temps réel*. Ph.d. thesis, Université Paris XI Orsay, 2004.

[62] J. M. Brockman, B. P. Nelson, and R. M. Corn. Surface plasmon resonance imaging measurements of ultrathin organic films. *Annual Review of Physical Chemistry*, 51:41–63, 2000.

[63] G. Steiner. Surface plasmon resonance imaging. *Analytical and Bioanalytical Chemistry*, 379(3):328–331, 2004.

[64] N. Zhang, R. Schweiss, Y. Zong, and W. Knoll. Electrochemical surface plasmon spectroscopy - Recent developments and applications. *Electrochimica Acta*, 52(8):2869–2875, 2007.

[65] F. Yu, D. F. Yao, and W. Knoll. Oligonucleotide hybridization studied by a surface plasmon diffraction sensor (SPDS). *Nucleic Acids Research*, 32(9):e75, 2004.

[66] F. Yu, S. J. Tian, D. F. Yao, and W. Knoll. Surface plasmon enhanced diffraction for label-free biosensing. *Analytical Chemistry*, 76(13):3530–3535, 2004.

[67] K. Tawa and W. Knoll. Mismatching base-pair dependence of the kinetics of DNA-DNA hybridization studied by surface plasmon fluorescence spectroscopy. *Nucleic Acids Research*, 32(8):2372–2377, 2004.

[68] K. Tawa, D. F. Yao, and W. Knoll. Matching base-pair number dependence of the kinetics of DNA-DNA hybridization studied by surface plasmon fluorescence spectroscopy. *Biosensors & Bioelectronics*, 21(2):322–329, 2005.

[69] K. Tanaka, M. Tanaka, K. Katayama, and D. Miyahara. Propagation constants of guided waves in surface plasmon polariton gap waveguides excited through an I-shaped aperture. *Comptes Rendus Physique*, 9(1):16–23, 2008.

[70] K. A. Marx. Quartz crystal microbalance: A useful tool for studying thin polymer films and complex biomolecular systems at the solution-surface interface. *Biomacromolecules*, 4(5):1099–1120, 2003.

[71] A. Janshoff, H. J. Galla, and C. Steinem. Piezoelectric mass-sensing devices as biosensors - An alternative to optical biosensors? *Angewandte Chemie-International Edition*, 39(22):4004–4032, 2000.

[72] Günter Sauerbrey. Verwendung Von Schwingquarzen Zur Wägung Dünner Schichten Und Zur Mikrowägung. *Zeitschrift Für Physik*, 155(2):206–222, 1959.

[73] Q-Sense. http://www.q-sense.com, 2009.

[74] M. V. Voinova, M. Rodahl, M. Jonson, and B. Kasemo. Viscoelastic acoustic response of layered polymer films at fluid-solid interfaces: Continuum mechanics approach. *Physica Scripta*, 59(5):391–396, 1999.

[75] Q-sense. Study of viscoelastic films - a comparison between the Voigt model and the Sauerbrey relation. Technical report, Q-sense, 2009.

[76] Y. S. Li, X. Y. Zhou, and D. Y. Ye. Molecular beacons: An optimal multifunctional biological probe. *Biochemical and Biophysical Research Communications*, 373(4):457–461, 2008.

[77] W. T. Liu, J. H. Wu, E. S. Y. Li, and E. S. Selamat. Emission characteristics of fluorescent labels with respect to temperature changes and subsequent effects on DNA microchip studies. *Applied and Environmental Microbiology*, 71(10):6453–6457, 2005.

[78] S. A. E. Marras, F. R. Kramer, and S. Tyagi. Efficiencies of fluorescence resonance energy transfer and contact-mediated quenching in oligonucleotide probes. *Nucleic Acids Research*, 30(21):e122, 2002.

[79] A. V. Galland-Irmouli, L. Pons, M. Lucon, C. Villaume, N. T. Mrabet, J. L. Gueant, and J. Fleurence. One-step purification of R-phycoerythrin from the red macroalga Palmaria palmata using preparative polyacrylamide gel electrophoresis. *Journal of Chromatography B*, 739(1):117–123, 2000.

[80] T. Livache, E. Maillart, N. Lassalle, P. Mailley, B. Corso, P. Guedon, A. Roget, and Y. Levy. Polypyrrole based DNA hybridization assays: study of label free detection processes versus fluorescence on microchips. *Journal of Pharmaceutical and Biomedical Analysis*, 32(4-5):687–696, 2003.

[81] J. P. Alao, S. C. Gamble, A. V. Stavropoulou, K. M. Pomeranz, E. W. F. Lam, R. C. Coombes, and D. M. Vigushin. The cyclin D1 proto-oncogene is sequestered in the cytoplasm of mammalian cancer cell lines. *Molecular Cancer*, 5:7, 2006.

[82] M. E. Ewen and J. Lamb. The activities of cyclin D1 that drive tumorigenesis. *Trends in Molecular Medicine*, 10(4):158–162, 2004.

[83] E. S. Schernhammer, G. J. Tranah, E. Giovannucci, A. T. Chan, J. Ma, G. A. Colditz, D. J. Hunter, W. C. Willett, and C. S. Fuchs. Cyclin DI A870G polymorphism and the risk of colorectal cancer and adenoma. *British Journal of Cancer*, 94(6):928–934, 2006.

[84] B. Persson, K. Stenhag, P. Nilsson, A. Larsson, M. Uhlen, and P. A. Nygren. Analysis of oligonucleotide probe affinities using surface plasmon resonance: A means for mutational scanning. *Analytical Biochemistry*, 246(1):34–44, 1997.

[85] Z. Guo, Q. H. Liu, and L. M. Smith. Enhanced discrimination of single nucleotide polymorphisms by artificial mismatch hybridization. *Nature Biotechnology*, 15(4):331–335, 1997.

[86] T. Livache, A. Roget, E. Dejean, C. Barthet, G. Bidan, and R. Teoule. Preparation of a DNA Matrix Via an Electrochemically Directed Copolymerization of Pyrrole and Oligonucleotides Bearing a Pyrrole Group. *Nucleic Acids Research*, 22(15):2915–2921, 1994.

[87] Sigma-Aldrich. Sigma-Proligo: Oligo-Calculation `http://proligo2.proligo.com/Calculation/calculation.html`, 2009.

[88] P. Guedon, T. Livache, F. Martin, F. Lesbre, A. Roget, G. Bidan, and Y. Levy. Characterization and optimization of a real-time, parallel, label-free, polypyrrole-based DNA sensor by surface plasmon resonance imaging. *Analytical Chemistry*, 72(24):6003–6009, 2000.

[89] A. W. Peterson, L. K. Wolf, and R. M. Georgiadis. Hybridization of mismatched or partially matched DNA at surfaces. *Journal of the American Chemical Society*, 124(49):14601–14607, 2002.

[90] T. Weidlich, S. M. Lindsay, and A. Rupprecht. The optical properties of Li- and Na-DNA films. *Biopolymers*, 26(3):439–453, 1987.

[91] P. Mailley, A. Roget, and T. Livache. Conducting Polymers for DNA Sensors and DNA Chips: From Fabrication to Molecular Detection. In E. Palecek, F. Scheller, and J. Wang, editors, *Electrochemistry of Nucleic Acids and Proteins*, volume 1 of *Perspectives in Bioanalysis*, pages 297–330. Elsevier, 2005.

[92] J. C. Love, L. A. Estroff, J. K. Kriebel, R. G. Nuzzo, and G. M. Whitesides. Self-assembled monolayers of thiolates on metals as a form of nanotechnology. *Chemical Reviews*, 105(4):1103–1169, 2005.

[93] C. D. Bain, E. B. Troughton, Y. T. Tao, J. Evall, G. M. Whitesides, and R. G. Nuzzo. Formation of Monolayer Films by the Spontaneous Assembly of Organic Thiols from Solution onto Gold. *Journal of the American Chemical Society*, 111(1):321–335, 1989.

[94] C. D. Bain, J. Evall, and G. M. Whitesides. Formation of Monolayers by the Coadsorption of Thiols on Gold - Variation in the Head Group, Tail Group, and Solvent. *Journal of the American Chemical Society*, 111(18):7155–7164, 1989.

[95] C. D. Bain and G. M. Whitesides. Formation of Monolayers by the Coadsorption of Thiols on Gold - Variation in the Length of the Alkyl Chain. *Journal of the American Chemical Society*, 111(18):7164–7175, 1989.

[96] C. D. Bain, H. A. Biebuyck, and G. M. Whitesides. Comparison of Self-Assembled Monolayers on Gold - Coadsorption of Thiols and Disulfides. *Langmuir*, 5(3):723–727, 1989.

[97] T. Livache, P. Guedon, C. Brakha, A. Roget, Y. Levy, and G. Bidan. Polypyrrole electrospotting for the construction of oligonucleotide arrays compatible with a surface plasmon resonance hybridization detection. *Synthetic Metals*, 121(1-3):1443–1444, 2001.

[98] B. Kong, Y. Kim, and I. S. Choi. pH-dependent stability of self-assembled monolayers on gold. *Bulletin of the Korean Chemical Society*, 29(9):1843–1846, 2008.

[99] T. M. Herne and M. J. Tarlov. Characterization of DNA probes immobilized on gold surfaces. *Journal of the American Chemical Society*, 119(38):8916–8920, 1997.

[100] M. Büttner, T. Belser, and P. Oelhafen. Stability of thiol-passivated gold particles at elevated temperatures studied by X-ray photoelectron spectroscopy. *Journal of Physical Chemistry B*, 109(12):5464–5467, 2005.

[101] T. Kawaguchi, H. Yasuda, K. Shimazu, and M. D. Porter. Electrochemical quartz crystal microbalance investigation of the reductive desorption of self-assembled monolayers of alkanethiols and mercaptoalkanoic acids on Au. *Langmuir*, 16(25):9830–9840, 2000.

[102] L. Malic, T. Veres, and M. Tabrizian. Biochip functionalization using electrowetting-on-dielectric digital microfluidics for surface plasmon resonance imaging detection of DNA hybridization. *Biosensors & Bioelectronics*, 24(7):2218–2224, 2009.

[103] K. A. Peterlinz, R. M. Georgiadis, T. M. Herne, and M. J. Tarlov. Observation of hybridization and dehybridization of thiol-tethered DNA using two-color surface plasmon resonance spectroscopy. *Journal of the American Chemical Society*, 119(14):3401–3402, 1997.

[104] R. Levicky, T. M. Herne, M. J. Tarlov, and S. K. Satija. Using self-assembly to control the structure of DNA monolayers on gold: A neutron reflectivity study. *Journal of the American Chemical Society*, 120(38):9787–9792, 1998.

[105] A. B. Steel, R. L. Levicky, T. M. Herne, and M. J. Tarlov. Immobilization of nucleic acids at solid surfaces: Effect of oligonucleotide length on layer assembly. *Biophysical Journal*, 79(2):975–981, 2000.

[106] E. Southern, K. Mir, and M. Shchepinov. Molecular interactions on microarrays. *Nature Genetics*, 21:5–9, 1999.

[107] A. Halperin, A. Buhot, and E. B. Zhulina. Sensitivity, specificity, and the hybridization isotherms of DNA chips. *Biophysical Journal*, 86(2):718–730, 2004.

[108] S. Blair, M. C. Williams, J Bishop, and A. Chagovetz. Microarray temperature optimization using hybridization kinetics. In Martin Dufva, editor, *DNA microarrays for biomedical research: Methods and Protocols*, volume 529, pages 171–196. Humana Press, 2009.

[109] N. K. Chaki and K. Vijayamohanan. Self-assembled monolayers as a tunable platform for biosensor applications. *Biosensors & Bioelectronics*, 17(1-2):1–12, 2002.

[110] R. Wang, S. Tombelli, M. Minunni, M. M. Spiriti, and M. Mascini. Immobilisation of DNA probes for the development of SPR-based sensing. *Biosensors & bioelectronics*, 20(5):967–974, 2004.

[111] A. Halperin, A. Buhot, and E. B. Zhulina. On the hybridization isotherms of DNA microarrays: the Langmuir model and its extensions. *Journal of Physics-Condensed Matter*, 18(18):S463–S490, 2006.

[112] J. B. Fiche, A. Buhot, R. Calemczuk, and T. Livache. Temperature effects on DNA chip experiments from surface plasmon resonance imaging: Isotherms and melting curves. *Biophysical Journal*, 92(3):935–946, 2007.

[113] I. Rouzina and V. A. Bloomfield. Heat capacity effects on the melting of DNA. 1. General aspects. *Biophysical Journal*, 77:3242–3251, 1999.

[114] A. Halperin, A. Buhot, and E. B. Zhulina. Hybridization isotherms of DNA microarrays and the quantification of mutation studies. *Clinical Chemistry*, 50(12):2254–2262, 2004.

[115] J. G. Wetmur and N. Davidson. Kinetics of renaturation of DNA. *Journal of Molecular Biology*, 31(3):349–370, 1968.

[116] B. M. Pettitt, A. Vainrub, and K. Y. Wong. DNA Saline Solutions Near Surfaces. In D. Henderson, M. Holovko, and A. Trokhymchuk, editors, *Ionic Soft Matter: Modern Trends in Theory and Applications*, volume Volume 260, pages 381–393. Springer, 2005.

[117] X. Gao, E. Gulari, and X. Zhou. In situ synthesis of oligonucleotide microarrays. *Biopolymers*, 73(5):579–596, 2004.

[118] S. Taylor, S. Smith, B. Windle, and A. Guiseppi-Elie. Impact of surface chemistry and blocking strategies on DNA microarrays. *Nucleic Acids Research*, 31(16):e87, 2003.

[119] T. Okamoto, T. Suzuki, and N. Yamamoto. Microarray fabrication with covalent attachment of DNA using Bubble Jet technology. *Nature Biotechnology*, 18(4):438–441, 2000.

[120] S. Venkatasubbarao. Microarrays–status and prospects. *Trends in Biotechnology*, 22(12):630–637, 2004.

[121] Claire E. Jordan, Anthony G. Frutos, Andrew J. Thiel, and Robert M. Corn. Surface Plasmon Resonance Imaging Measurements of DNA Hybridization Adsorption and Streptavidin/DNA Multilayer Formation at Chemically Modified Gold Surfaces. *Analytical Chemistry*, 69(24):4939–4947, 1997.

[122] J. M. Brockman, A. G. Frutos, and R. M. Corn. A Multistep Chemical Modification Procedure To Create DNA Arrays on Gold Surfaces for the Study of Protein-DNA Interactions with Surface Plasmon Resonance Imaging. *Journal of the American Chemical Society*, 121(35):8044–8051, 1999.

[123] H. J. Lee, A. W. Wark, Y. Li, and R. M. Corn. Fabricating RNA microarrays with RNA-DNA surface ligation chemistry. *Analytical Chemistry*, 77(23):7832–7837, 2005.

[124] Y. Chen, A. Nguyen, L. Niu, and R. M. Corn. Fabrication of DNA microarrays with poly(L-glutamic acid) monolayers on gold substrates for SPR imaging measurements. *Langmuir*, 25(9):5054–5060, 2009.

[125] A. Bietsch, M. Hegner, H. P. Lang, and C. Gerber. Inkjet deposition of alkanethiolate monolayers and DNA oligonucleotides on gold: Evaluation of spot uniformity by wet etching. *Langmuir*, 20(12):5119–5122, 2004.

[126] A. P. Quist, E. Pavlovic, and S. Oscarsson. Recent advances in microcontact printing. *Analytical and Bioanalytical Chemistry*, 381(3):591–600, 2005.

[127] E. Descamps, T. Leïchlé, B. Corso, S. Laurent, P. Mailley, L. Nicu, T. Livache, and C. Bergaud. Fabrication of Oligonucleotide Chips by Using Parallel Cantilever-Based Electrochemical Deposition in Picoliter Volumes. *Advanced Materials*, 19(14):1816–1821, 2007.

[128] N. Yang, X. Su, V. Tjong, and W. Knoll. Evaluation of two- and three-dimensional streptavidin binding platforms for surface plasmon resonance spectroscopy studies of DNA hybridization and protein-DNA binding. *Biosensors & Bioelectronics*, 22(11):2700–2106, 2007.

[129] E. Mercey, R. Sadir, E. Maillart, A. Roget, F. Baleux, H. Lortat-Jacob, and T. Livache. Polypyrrole oligosaccharide array and surface plasmon resonance imaging for the measurement of glycosaminoglycan binding interactions. *Analytical Chemistry*, 80(9):3476–3482, 2008.

[130] S. Da Silva, L. Grosjean, N. Ternan, P. Mailley, T. Livache, and S. Cosnier. Biotinylated polypyrrole films: an easy electrochemical approach for the reagentless immobilization of bacteria on electrode surfaces. *Bioelectrochemistry*, 63(1-2):297–301, 2004.

[131] E. Suraniti, E. Sollier, R. Calemczuk, T. Livache, P. N. Marche, M. B. Villiers, and Y. Roupioz. Real-time detection of lymphocytes binding on an antibody chip using SPR imaging. *Lab on a chip*, 7(9):1206–1208, 2007.

[132] C. Boozer, S. Chen, and S. Jiang. Controlling DNA orientation on mixed ssDNA/OEG SAMs. *Langmuir*, 22(10):4694–8, 2006.

[133] F. Mannelli, A. Minunni, S. Tombelli, R. H. Wang, M. M. Spiriti, and M. Mascini. Direct immobilisation of DNA probes for the development of affinity biosensors. *Bioelectrochemistry*, 66(1-2):129–138, 2005.

[134] A. W. Peterson, R. J. Heaton, and R. M. Georgiadis. The effect of surface probe density on DNA hybridization. *Nucleic Acids Research*, 29(24):5163–5168, 2001.

[135] R. Meunier-Prest, S. Raveau, E. Finot, G. Legay, M. Cherkaoui-Malki, and N. Latruffe. Direct measurement of the melting temperature of supported DNA by electrochemical method. *Nucleic Acids Research*, 31(23):e150, 2003.

[136] J. H. Watterson, P. A. E. Piunno, C. C. Wust, and U. J. Krull. Effects of Oligonucleotide Immobilization Density on Selectivity of Quantitative Transduction of Hybridization of Immobilized DNA. *Langmuir*, 16(11):4984–4992, 2000.

[137] Wolfram Research. Mathematica 5, 2004.

[138] E. S. Y. Li, J. K. K. Ng, J. H. Wu, and W. T. Liu. Evaluating single-base-pair discriminating capability of planar oligonucleotide microchips using a non-equilibrium dissociation approach. *Environmental Microbiology*, 6(11):1197–1202, 2004.

[139] H. Urakawa, P. A. Noble, S. El Fantroussi, J. J. Kelly, and D. A. Stahl. Single-base-pair discrimination of terminal mismatches by using oligonucleotide microarrays and neural network analyses. *Applied and Environmental Microbiology*, 68(1):235–244, 2002.

[140] R. Owczarzy, P. M. Vallone, F. J. Gallo, T. M. Paner, M. J. Lane, and A. S. Benight. Predicting sequence-dependent melting stability of short duplex DNA oligomers. *Biopolymers*, 44(3):217–239, 1997.

[141] R. Owczarzy, I. Dunietz, M. A. Behlke, I. M. Klotz, and J. A. Walder. Thermodynamic treatment of oligonucleotide duplex-simplex equilibria. *Proceedings of the National Academy of Sciences of the United States of America*, 100(25):14840–14845, 2003.

[142] A. V. Tataurov, Y. You, and R. Owczarzy. Predicting ultraviolet spectrum of single stranded and double stranded deoxyribonucleic acids. *Biophysical chemistry*, 133(1-3):66–70, 2008.

[143] P. J. Mikulecky and A. L. Feig. Heat capacity changes associated with nucleic acid folding. *Biopolymers*, 82(1):38–58, 2006.

[144] C. Brandfass and P. Karlovsky. Simultaneous detection of Fusarium culmorum and F. graminearum in plant material by duplex PCR with melting curve analysis. *BMC Microbiology*, 6:4, 2006.

[145] B. Sacca, R. Meyer, and C. M. Niemeyer. Temperature-dependent FRET spectroscopy for the high-throughput analysis of self-assembled DNA nanostructures in real time. *Nature Protocols*, 4(3):271–285, 2009.

[146] L. Zhou, L. Wang, R. Palais, R. Pryor, and C. T. Wittwer. High-resolution DNA melting analysis for simultaneous mutation scanning and genotyping in solution. *Clinical Chemistry*, 51(10):1770–1777, 2005.

[147] W. L. Chiu, C. N. Sze, N. T. Ma, L. F. Chiu, C. W. Leung, and S. C. Au-Yeung. NTDB: Thermodynamic Database for Nucleic Acids, Version 2.0. *Nucleic Acids Research*, 31(1):483–485, 2003.

[148] T. Liedl and F. C. Simmel. Determination of DNA melting temperatures in diffusion-generated chemical gradients. *Analytical Chemistry*, 79(14):5212–5216, 2007.

[149] M. C. Williams, I. Rouzina, and V. A. Bloomfield. Thermodynamics of DNA Interactions from Single Molecule Stretching Experiments. *Accounts of Chemical Research*, 35(3):159–166, 2002.

[150] R. Owczarzy. Melting temperatures of nucleic acids: discrepancies in analysis. *Biophysical Chemistry*, 117(3):207–215, 2005.

[151] Y. Marcy, P.-Y. Cousin, M. Rattier, G. Cerovic, G. Escalier, G. Béna, M. GuÁ©ron, L. McDonagh, F. le Boulaire, H. Bénisty, C. Weisbuch, and J.-C. Avarre. Innovative integrated system for real-time measurement of hybridization and melting on standard format microarrays. *BioTechniques*, 44(7):913–920, 2008.

[152] SNP for ID consortium, M. K. Balogh, K. Bender, and P. M. Schneider. Application of Nanogen microarray technology for forensic SNP analysis. *International Congress Series*, 1288:43–45, 2006.

[153] Innogenetics Biotechnology for Healthcare. Innogenetics achieves CE marking of 4-MAT ™ HLA-A system, its first microarray test for clinical molecular diagnostics `http://www.innogenetics.com/pressreleases.html?prid=211`, 2009.

[154] Roche Diagnostics. LightCycler ® Systems for Real-Time PCR `https://www.roche-applied-science.com/lightcycler-online/`, 2009.

[155] A. V. Fotin, A. L. Drobyshev, D. Y. Proudnikov, A. N. Perov, and A. D. Mirzabekov. Parallel thermodynamic analysis of duplexes on oligodeoxyribonucleotide microchips. *Nucleic Acids Research*, 26(6):1515–1521, 1998.

[156] P. A. E. Piunno, J. Watterson, C. C. Wust, and U. J. Krull. Considerations for the quantitative transduction of hybridization of immobilized DNA. *Analytica Chimica Acta*, 400:73–89, 1999.

[157] B. G. Moreira, Y. You, M. A. Behlke, and R. Owczarzy. Effects of fluorescent dyes, quenchers, and dangling ends on DNA duplex stability. *Biochemical and Biophysical Research Communications*, 327(2):473–484, 2005.

[158] S. L. Biswal, D. Raorane, A. Chaiken, and A. Majumdar. Using a microcantilever array for detecting phase transitions and stability of DNA. *Clin Lab Med*, 27(1):163–71, 2007.

[159] Y. Sun and C.-H. Kiang N.C. Harris. Melting transition of directly linked gold nanoparticles DNA assembly. *Physica A*, 350:89–95, 2005.

[160] J. Zhu and R. M. Wartell. The relative stabilities of base pair stacking interactions and single mismatches in long RNA measured by temperature gradient gel electrophoresis. *Biochemistry*, 36(49):15326–15335, 1997.

[161] N. Crews, C. T. Wittwer, J. Montgomery, R. Pryor, and B. Gale. Spatial DNA melting analysis for genotyping and variant scanning. *Analytical Chemistry*, 81(6):2053–2058, 2009.

[162] J. Petersen, L. Poulsen, H. Birgens, and M. Dufva. Microfludic device for creating ionic strength gradients over DNA microarrays for efficient DNA melting studies and assay development. *PLoS One*, 4(3):e4808, 2009.

[163] A. Russom, D. Irimia, and M. Toner. Chemical gradient-mediated melting curve analysis for genotyping of SNPs. *Electrophoresis*, 30(14):2536–2543, 2009.

[164] D. Erickson, D. Li, and U. J. Krull. Modeling of DNA hybridization kinetics for spatially resolved biochips. *Analytical Biochemistry*, 317(2):186–200, 2003.

[165] M. P. Nagata, K. Yamashita, M. Miyazaki, H. Nakamura, and H. Maeda. Enhanced thermal stability and mismatch discrimination of mutation-carrying DNA duplexes and their kinetic and thermodynamic properties in microchannel laminar flow. *Analytical Biochemistry*, 390(1):38–45, 2009.

[166] G. Shen, N. Tercero, M. A. Gaspar, B. Varughese, K. Shepard, and R. Levicky. Charging behavior of single-stranded DNA polyelectrolyte brushes. *Journal of the American Chemical Society*, 128(26):8427–8433, 2006.

[167] P. Furrer, J. Bednar, A. Z. Stasiak, V. Katritch, D. Michoud, A. Stasiak, and J. Dubochet. Opposite effect of counterions on the persistence length of nicked and non-nicked DNA. *Journal of Molecular Biology*, 266(4):711–721, 1997.

[168] P. L. Hansen, R. Podgornik, and V. A. Parsegian. Osmotic properties of DNA: critical evaluation of counterion condensation theory. *Physical Review E*, 64:021907, 2001.

[169] U. Rant, K. Arinaga, T. Fujiwara, S. Fujita, M. Tornow, N. Yokoyama, and G. Abstreiter. Excessive counterion condensation on immobilized ssDNA in solutions of high ionic strength. *Biophysical Journal*, 85(6):3858–3864, 2003.

[170] N. B. Adey, M. Lei, M. T. Howard, J. D. Jensen, D. A. Mayo, D. L. Butel, S. C. Coffin, T. C. Moyer, D. E. Slade, M. K. Spute, A. M. Hancock, G. T. Eisenhoffer, B. K. Dalley, and M. R. McNeely. Gains in sensitivity with a device that mixes microarray hybridization solution in a 25 µm-thick chamber. *Analytical Chemistry*, 74(24):6413–6417, 2002.

[171] P. Tabeling. A brief introduction to slippage, droplets and mixing in microfluidic systems. *Lab on a chip*, 9(17):2428–2436, 2009.

[172] A. Vainrub and B. M. Pettitt. Coulomb blockage of hybridization in two-dimensional DNA arrays. *Physical Review E*, 66(4):041905, 2002.

[173] A. Vainrub and B. M. Pettitt. Surface electrostatic effects in oligonucleotide microarrays: Control and optimization of binding thermodynamics. *Biopolymers*, 68(2):265–270, 2003.

[174] P. Gong and R. Levicky. DNA surface hybridization regimes. *Proceedings of the National Academy of Sciences of the United States of America*, 105(14):5301–5306, 2008.

[175] S. Y. Shaw and J. C. Wang. Knotting of a DNA Chain during Ring-Closure. *Science*, 260(5107):533–536, 1993.

[176] R. Owczarzy, B. G. Moreira, Y. You, M. A. Behlke, and J. A. Walder. Predicting stability of DNA duplexes in solutions containing magnesium and monovalent cations. *Biochemistry*, 47(19):5336–5353, 2008.

[177] F. Sanger, S. Nicklen, and A. R. Coulson. DNA Sequencing with Chain-Terminating Inhibitors. *Proceedings of the National Academy of Sciences of the United States of America*, 74(12):5463–5467, 1977.

[178] G. Bonner and A. M. Klibanov. Structural stability of DNA in nonaqueous solvents. *Biotechnology and Bioengineering*, 68(3):339–344, 2000.

[179] L. Levine, J. A. Gordon, and W. P. Jencks. The Relationship of Structure to the Effectiveness of Denaturing Agents for Deoxyribonucleic Acid. *Biochemistry*, 2(1):168–175, 1963.

[180] B. Hammouda and D. Worcester. The Denaturation Transition of DNA in Mixed Solvents. *Biophysical Journal*, 91(6):2237–2242, 2006.

[181] E. P. Geiduschek and T. T. Herskovits. Nonaqueous Solutions of DNA - Reversible and Irreversible Denaturation in Methanol. *Archives of Biochemistry and Biophysics*, 95(1):114–129, 1961.

[182] T. T. Herskovits, S. J. Singer, and E. P. Geiduschek. Nonaqueous Solutions of DNA - Denaturation in Methanol and Ethanol. *Archives of Biochemistry and Biophysics*, 94(1):99–114, 1961.

[183] R. D. Blake and S. G. Delcourt. Thermodynamic effects of formamide on DNA stability. *Nucleic Acids Research*, 24(11):2095–2103, 1996.

[184] C. Sadhu, S. Dutta, and K. Gopinathan. Influence of formamide on the thermal stability of DNA. *Journal of Biosciences*, 6(6):817–821, 1984.

[185] B. L. McConaughy, C. D. Laird, and B. J. McCarthy. Nucleic acid reassociation in formamide. *Biochemistry*, 8(8):3289–3295, 1969.

[186] A. E. Pozhitkov, R. D. Stedtfeld, S. A. Hashsham, and P. A. Noble. Revision of the nonequilibrium thermal dissociation and stringent washing approaches for identification of mixed nucleic acid targets by microarrays. *Nucleic Acids Research*, 35(9):e70, 2007.

[187] J. Casey and N. Davidson. Rates of Formation and Thermal Stabilities of Rna-DNA and DNA-DNA Duplexes at High-Concentrations of Formamide. *Nucleic Acids Research*, 4(5):1539–1552, 1977.

[188] W. I. Wood, J. Gitschier, L. A. Lasky, and R. M. Lawn. Base Composition-Independent Hybridization in Tetramethylammonium Chloride - a Method for Oligonucleotide Screening of Highly Complex Gene Libraries. *Proceedings of the National Academy of Sciences of the United States of America*, 82(6):1585–1588, 1985.

[189] U. Maskos and E. M. Southern. Parallel analysis of oligodeoxyribonucleotide (oligonucleotide) interactions. I. Analysis of factors influencing oligonucleotide duplex formation. *Nucleic Acids Research*, 20(7):1675–1678, 1992.

[190] S. Fang, H. J. Lee, A. W. Wark, and R. M. Corn. Attomole microarray detection of microRNAs by nanoparticle-amplified SPR imaging measurements of surface polyadenylation reactions. *Journal of the American Chemical Society*, 128(43):14044–14046, 2006.

[191] E. Hutter and M. P. Pileni. Detection of DNA hybridization by gold nanoparticle enhanced transmission surface plasmon resonance spectroscopy. *Journal of Physical Chemistry B*, 107(27):6497–6499, 2003.

[192] Y. Li, A. W. Wark, H. J. Lee, and R. M. Corn. Single-nucleotide polymorphism genotyping by nanoparticle-enhanced surface plasmon resonance imaging measurements of surface ligation reactions. *Analytical Chemistry*, 78(9):3158–3164, 2006.

[193] X. Yao, X. Li, F. Toledo, C. Zurita-Lopez, M. Gutova, J. Momand, and F. M. Zhou. Sub-attomole oligonucleotide and p53 cDNA determinations via a high-resolution surface plasmon resonance combined with oligonucleotide-capped gold nanoparticle signal amplification. *Analytical Biochemistry*, 354(2):220–228, 2006.

[194] A. Holmberg, A. Blomstergren, O. Nord, M. Lukacs, J. Lundeberg, and M. Uhlen. The biotin-streptavidin interaction can be reversibly broken using water at elevated temperatures. *Electrophoresis*, 26(3):501–510, 2005.

[195] M. Gonzalez, L. A. Bagatolli, I. Echabe, J. L. Arrondo, C. E. Argarana, C. R. Cantor, and G. D. Fidelio. Interaction of biotin with streptavidin. Thermostability and conformational changes upon binding. *The Journal of Biological Chemistry*, 272(17):11288–11294, 1997.

[196] O. H. Laitinen, V. P. Hytonen, H. R. Nordlund, and M. S. Kulomaa. Genetically engineered avidins and streptavidins. *Cellular and Molecular Life Sciences*, 63(24):2992–3017, 2006.

[197] T. Sano, S. Vajda, C. L. Smith, and C. R. Cantor. Engineering subunit association of multisubunit proteins: a dimeric streptavidin. *Proceedings of the National Academy of Sciences of the United States of America*, 94(12):6153–6158, 1997.

[198] S. C. Wu and S. L. Wong. Engineering soluble monomeric streptavidin with reversible biotin binding capability. *The Journal of Biological Chemistry*, 280(24):23225–23231, 2005.

[199] R. D. Stedtfeld, L. M. Wick, S. W. Baushke, D. M. Tourlousse, A. B. Herzog, Y. Xia, J. M. Rouillard, J. A. Klappenbach, J. R. Cole, E. Gulari, J. M. Tiedje, and S. A. Hashsham. Influence of dangling ends and surface-proximal tails of targets on probe-target duplex formation in 16S rRNA gene-based diagnostic arrays. *Applied and environmental microbiology*, 73(2):380–389, 2007.

[200] R. Peytavi, T. Liu-Ying, F. R. Raymond, K. Boissinot, L. Bissonnette, M. Boissinot, F. J. Picard, A. Huletsky, M. Ouellette, and M. G. Bergeron. Correlation between microarray DNA hybridization efficiency and the position of short capture probe on the target nucleic acid. *Biotechniques*, 39(1):89–96, 2005.

[201] A. Halperin, A. Buhot, and E. B. Zhulina. Hybridization at a surface: the role of spacers in DNA microarrays. *Langmuir*, 22(26):11290–11304, 2006.

[202] L. Poulsen, M. J. Soe, D. Snakenborg, L. B. Moller, and M. Dufva. Multi-stringency wash of partially hybridized 60-mer probes reveals that the stringency along the probe decreases with distance from the microarray surface. *Nucleic Acids Research*, 36(20):e132, 2008.

[203] M. S. Shchepinov, S. C. Case-Green, and E. M. Southern. Steric factors influencing hybridisation of nucleic acids to oligonucleotide arrays. *Nucleic Acids Research*, 25(6):1155–1161, 1997.

[204] G. Bonnet, O. Krichevsky, and A. Libchaber. Kinetics of conformational fluctuations in DNA hairpin-loops. *Proceedings of the National Academy of Sciences of the United States of America*, 95(15):8602–8606, 1998.

[205] G. Bonnet, S. Tyagi, A. Libchaber, and F. R. Kramer. Thermodynamic basis of the enhanced specificity of structured DNA probes. *Proceedings of the National Academy of Sciences of the United States of America*, 96(11):6171–6176, 1999.

[206] Y. Gao, L. K. Wolf, and R. M. Georgiadis. Secondary structure effects on DNA hybridization kinetics: a solution versus surface comparison. *Nucleic Acids Research*, 34(11):3370–3377, 2006.

[207] K. Halder and S. Chowdhury. Kinetic resolution of bimolecular hybridization versus intramolecular folding in nucleic acids by surface plasmon resonance: application to G-quadruplex/duplex competition in human c-myc promoter. *Nucleic Acids Research*, 33(14):4466–4474, 2005.

[208] X. Liang, H. Kuhn, and M. D. Frank-Kamenetskii. Monitoring single-stranded DNA secondary structure formation by determining the topological state of DNA catenanes. *Biophysical Journal*, 90(8):2877–2889, 2006.

[209] M. Zuker. Mfold web server for nucleic acid folding and hybridization prediction. *Nucleic Acids Research*, 31(13):3406–3415, 2003.

[210] K. U. Mir and E. M. Southern. Determining the influence of structure on hybridization using oligonucleotide arrays. *Nature Biotechnology*, 17(8):788–792, 1999.

[211] P. Yakovchuk, E. Protozanova, and M. D. Frank-Kamenetskii. Base-stacking and base-pairing contributions into thermal stability of the DNA double helix. *Nucleic Acids Research*, 34(2):564–574, 2006.

[212] C. Briones, E. Mateo-Marti, C. Gomez-Navarro, V. Parro, E. Roman, and J. A. Martin-Gago. Structural and functional characterization of self-assembled monolayers of peptide nucleic acids and its interaction with complementary DNA. *Journal of Molecular Catalysis a-Chemical*, 228(1-2):131–136, 2005.

[213] G. Feriotto, R. Corradini, S. Sforza, N. Bianchi, C. Mischiati, R. Marchelli, and R. Gambari. Peptide nucleic acids and biosensor technology for real-time detection of the cystic fibrosis W1282X mutation by surface plasmon resonance. *Laboratory Investigation*, 81(10):1415–1427, 2001.

[214] A. I. Lao, X. Su, and K. M. Aung. SPR study of DNA hybridization with DNA and PNA probes under stringent conditions. *Biosensors & Bioelectronics*, 24(6):1717–1722, 2009.

[215] H. Y. Mun, A. Girigoswami, C. Jung, D. Y. Cho, and H. G. Park. SNPs detection by a single-strand specific nuclease on a PNA zip-code microarray. *Biosensors & Bioelectronics*, 24(6):1706–1711, 2009.

[216] M. Castoldi, S. Schmidt, V. Benes, M. Noerholm, A. E. Kulozik, M. W. Hentze, and M. U. Muckenthaler. A sensitive array for microRNA expression profiling (miChip) based on locked nucleic acids (LNA). *Rna*, 12(5):913–920, 2006.

[217] A. Valoczi, C. Hornyik, N. Varga, J. Burgyan, S. Kauppinen, and Z. Havelda. Sensitive and specific detection of microRNAs by northern blot analysis using LNA-modified oligonucleotide probes. *Nucleic Acids Research*, 32(22):e175, 2004.

[218] Y. You, B. G. Moreira, M. A. Behlke, and R. Owczarzy. Design of LNA probes that improve mismatch discrimination. *Nucleic Acids Research*, 34(8):e60, 2006.

[219] G. Lahoud, V. Timoshchuk, A. Lebedev, M. de Vega, M. Salas, K. Arar, Y. M. Hou, and H. Gamper. Enzymatic synthesis of structure-free DNA with pseudo-complementary properties. *Nucleic Acids Research*, 36(10):3409–3419, 2008.

[220] G. Lahoud, V. Timoshchuk, A. Lebedev, K. Arar, Y. M. Hou, and H. Gamper. Properties of pseudo-complementary DNA substituted with weakly pairing analogs of guanine or cytosine. *Nucleic Acids Research*, 36(22):6999–7008, 2008.

[221] H. Auer, D. L. Newsom, and K. Kornacker. Expression Profiling Using Affymetrix GeneChip Microarrays. *Methods in Molecular Biology*, 509:35–46, 2009.

[222] M. T. Barrett, A. Scheffer, A. Ben-Dor, N. Sampas, D. Lipson, R. Kincaid, P. Tsang, B. Curry, K. Baird, P. S. Meltzer, Z. Yakhini, L. Bruhn, and S. Laderman. Comparative genomic hybridization using oligonucleotide microarrays and total genomic DNA. *Proceedings of the National Academy of Sciences of the United States of America*, 101(51):17765–17770, 2004.

[223] T. R. Golub, D. K. Slonim, P. Tamayo, C. Huard, M. Gaasenbeek, J. P. Mesirov, H. Coller, M. L. Loh, J. R. Downing, M. A. Caligiuri, C. D. Bloomfield, and E. S. Lander. Molecular classification of cancer: class discovery and class prediction by gene expression monitoring. *Science*, 286(5439):531–537, 1999.

[224] S. V. Tillib and A. D. Mirzabekov. Advances in the analysis of DNA sequence variations using oligonucleotide microchip technology. *Current Opinion in Biotechnology*, 12(1):53–58, 2001.

[225] D. Gresham, D. M. Ruderfer, S. C. Pratt, J. Schacherer, M. J. Dunham, D. Botstein, and L. Kruglyak. Genome-wide detection of polymorphisms at nucleotide resolution with a single DNA microarray. *Science*, 311(5769):1932–1936, 2006.

[226] K. B. Mullis and F. A. Faloona. Specific synthesis of DNA in vitro via a polymerase-catalyzed chain reaction. *Methods in Enzymology*, 155:335–350, 1987.

[227] C. Tse and J. Capeau. Real time PCR methodology for quantification of nucleic acids. *Annales de biologie clinique (Paris)*, 61(3):279–293, 2003.

[228] B. Schweitzer and S. Kingsmore. Combining nucleic acid amplification and detection. *Current Opinion in Biotechnology*, 12(1):21–27, 2001.

[229] S. C. Andras, J. B. Power, E. C. Cocking, and M. R. Davey. Strategies for signal amplification in nucleic acid detection. *Molecular Biotechnology*, 19(1):29–44, 2001.

[230] E. Khomyakova, M. A. Livshits, M. C. Steinhauser, L. Dauphinot, S. Cohen-Kaminsky, J. Rossier, F. Soussaline, and M. C. Potier. On-chip hybridization kinetics for optimization of gene expression experiments. *Biotechniques*, 44(1):109–117, 2008.

[231] J. C. Bres, Y. Merieux, V. Dugas, J. Broutin, E. Vnuk, M. Jaber, D. Rigal, J. R. Martin, E. Souteyrand, M. Cabrera, and J. P. Cloarec. New method for DNA microarrays development: applied to human platelet antigens polymorphisms. *Biomedical Microdevices*, 7(2):137–141, 2005.

[232] Z. He, L. Wu, X. Li, M. W. Fields, and J. Zhou. Empirical establishment of oligonucleotide probe design criteria. *Applied and Environmental Microbiology*, 71(7):3753–3760, 2005.

[233] J. C. Tan, J. J. Patel, A. Tan, J. C. Blain, T. J. Albert, N. F. Lobo, and M. T. Ferdig. Optimizing comparative genomic hybridization probes for genotyping and SNP detection in Plasmodium falciparum. *Genomics*, 93(6):543–550, 2009.

[234] M. Cerruti, S. Fissolo, C. Carraro, C. Ricciardi, A. Majumdar, and R. Maboudian. Poly(ethylene glycol) monolayer formation and stability on gold and silicon nitride substrates. *Langmuir*, 24(19):10646–10653, 2008.

[235] H. Vaisocherova, W. Yang, Z. Zhang, Z. Q. Cao, G. Cheng, M. Piliarik, J. Homola, and S. Y. Jiang. Ultralow fouling and functionalizable surface chemistry based on a zwitterionic polymer enabling sensitive and specific protein detection in undiluted blood plasma. *Analytical Chemistry*, 80(20):7894–7901, 2008.

[236] H. Vaisocherova, Z. Zhang, W. Yang, Z. Q. Cao, G. Cheng, A. D. Taylor, M. Piliarik, J. Homola, and S. Y. Jiang. Functionalizable surface platform with reduced nonspecific protein adsorption from full blood plasma-Material selection and protein immobilization optimization. *Biosensors & Bioelectronics*, 24(7):1924–1930, 2009.

[237] P. Y. J. Yeh, R. K. Kainthan, Y. Q. Zou, M. Chiao, and J. N. Kizhakkedathu. Self-assembled monothiol-terminated hyperbranched polyglycerols on a gold surface: A comparative study on the structure, morphology, and protein adsorption characteristics with linear poly(ethylene glycol)s. *Langmuir*, 24(9):4907–4916, 2008.

[238] E. Mercey. *Mesures parallelisées d'interactions oligosaccharides/protéines au moyen de biopuces.* Ph.d. thesis, Université Joseph Fourier - Grenoble 1, 2005.

[239] C. Corne, J. B. Fiche, D. Gasparutto, V. Cunin, E. Suraniti, A. Buhot, J. Fuchs, R. Calemczuk, T. Livache, and A. Favier. SPR imaging for label-free multiplexed analyses of DNA N-glycosylase interactions with damaged DNA duplexes. *Analyst*, 133(8):1036–1045, 2008.

[240] Sequence Manipulation Suite (SMS). Isoelectric Point calculation `http://annotathon.univ-mrs.fr/sms2/protein-iep.html`, 2009.

[241] M. Abrantes, M. T. Magone, L. F. Boyd, and P. Schuck. Adaptation of a surface plasmon resonance biosensor with microfluidics for use with small sample volumes and long contact times. *Analytical Chemistry*, 73(13):2828–2835, 2001.

[242] F. Raynal, A. Beuf, F. Plaza, J. Scott, P. Carriere, M. Cabrera, J. P. Cloarec, and E. Souteyrand. Towards better DNA chip hybridization using chaotic advection. *Physics of Fluids*, 19(1):017112, 2007.

[243] T. M. Squires, R. J. Messinger, and S. R. Manalis. Making it stick: convection, reaction and diffusion in surface-based biosensors. *Nature biotechnology*, 26(4):417–426, 2008.

[244] M. Minunni, S. Tombelli, J. Fonti, M. M. Spiriti, M. Mascini, P. Bogani, and M. Buiatti. Detection of fragmented genomic DNA by PCR-free piezoelectric sensing using a denaturation approach. *Journal of the American Chemical Society*, 127(22):7966–7967, 2005.

[245] O. A. Sadik, A. O. Aluoch, and A. Zhou. Status of biomolecular recognition using electrochemical techniques. *Biosensors & Bioelectronics*, 24(9):2749–2765, 2009.

[246] C. B. Christensen. Arrays in biological and chemical analysis. *Talanta*, 56(2):289–299, 2002.

[247] I. G. Gut. Automation in genotyping of single nucleotide polymorphisms. *Human Mutation*, 17(6):475–492, 2001.

[248] A. C. Syvänen. Toward genome-wide SNP genotyping. *Nature Genetics*, 37 Suppl:S5–10, 2005.

[249] D. Dell'Atti, S. Tombelli, M. Minunni, and M. Mascini. Detection of clinically relevant point mutations by a novel piezoelectric biosensor. *Biosensors & Bioelectronics*, 21(10):1876–1879, 2006.

[250] T. Jiang, M. Minunni, P. Wilson, J. Zhang, A. P. Turner, and M. Mascini. Detection of TP53 mutation using a portable surface plasmon resonance DNA-based biosensor. *Biosensors & Bioelectronics*, 20(10):1939–1945, 2005.

[251] N. Bianchi, C. Rutigliano, M. Tomassetti, G. Feriotto, F. Zorzato, and R. Gambari. Biosensor technology and surface plasmon resonance for real-time detection of HIV-1 genomic sequences amplified by polymerase chain reaction. *Clinical and Diagnostic Virology*, 8(3):199–208, 1997.

[252] G. Feriotto, M. Lucci, N. Bianchi, C. Mischiati, and R. Gambari. Detection of the deltaF508 (F508del) mutation of the cystic fibrosis gene by surface plasmon resonance and biosensor technology. *Human Mutation*, 13(5):390–400, 1999.

[253] S. Schwonbeck, A. Krause-Griep, N. Gajovic-Eichelmann, E. Ehrentreich-Forster, W. Meinl, H. Glatt, and F. F. Bier. Cohort analysis of a single nucleotide polymorphism on DNA chips. *Biosensors & Bioelectronics*, 20(5):956–966, 2004.

[254] A. Ho-Pun-Cheung, S. Choblet, T. Colineau, H. Abaibou, D. Zsoldos, K. Brengel-Pesce, J. Grenier, P. Cleuziat, and E. Lopez-Crapez. Detection of single nucleotide polymorphisms by minisequencing on a polypyrrole DNA chip designed for medical diagnosis. *Laboratory Investigation*, 86(3):304–313, 2006.

[255] A. J. Thiel, A. G. Frutos, C. E. Jordan, R. M. Corn, and L. M. Smith. In Situ Surface Plasmon Resonance Imaging Detection of DNA Hybridization to Oligonucleotide Arrays on Gold Surfaces. *Analytical Chemistry*, 69(24):4948–4956, 1997.

[256] S. C. Yim, H. G. Park, H. N. Chang, and D. Y. Cho. Array-based mutation detection of BRCA1 using direct probe/target hybridization. *Analytical biochemistry*, 337(2):332–337, 2005.

[257] E. Giakoumaki, M. Minunni, S. Tombelli, I. E. Tothill, M. Mascini, P. Bogani, and M. Buiatti. Combination of amplification and post-amplification strategies to improve optical DNA sensing. *Biosensors & Bioelectronics*, 19(4):337–344, 2003.

[258] B. M. Fuchs, F. O. Glockner, J. Wulf, and R. Amann. Unlabeled helper oligonucleotides increase the in situ accessibility to 16S rRNA of fluorescently labeled oligonucleotide probes. *Applied and Environmental Microbiology*, 66(8):3603–3607, 2000.

[259] R. H. Wang, M. Minunni, S. Tombelli, and M. Mascini. A new approach for the detection of DNA sequences in amplified nucleic acids by a surface plasmon resonance biosensor. *Biosensors & Bioelectronics*, 20(3):598–605, 2004.

[260] D. Yao, F. Yu, J. Kim, J. Scholz, P. E. Nielsen, E. K. Sinner, and W. Knoll. Surface plasmon field-enhanced fluorescence spectroscopy in PCR product analysis by peptide nucleic acid probes. *Nucleic Acids Research*, 32(22):e177, 2004.

[261] P. Nilsson, B. Persson, A. Larsson, M. Uhlen, and P. A. Nygren. Detection of mutations in PCR products from clinical samples by surface plasmon resonance. *Journal of Molecular Recognition*, 10(1):7–17, 1997.

[262] D. F. Yao, J. Kim, F. Yu, P. E. Nielsen, E. K. Sinner, and W. Knoll. Surface density dependence of PCR amplicon hybridization on PNA/DNA probe layers. *Biophysical Journal*, 88(4):2745–2751, 2005.

[263] L. G. Carrascosa, A. Calle, and L. M. Lechuga. Label-free detection of DNA mutations by SPR: application to the early detection of inherited breast cancer. *Analytical and Bioanalytical Chemistry*, 393(4):1173–1182, 2009.

[264] B. P. Nelson, T. E. Grimsrud, M. R. Liles, R. M. Goodman, and R. M. Corn. Surface plasmon resonance imaging measurements of DNA and RNA hybridization adsorption onto DNA microarrays. *Analytical Chemistry*, 73(1):1–7, 2001.

[265] T. T. Goodrich, H. J. Lee, and R. M. Corn. Enzymatically amplified surface plasmon resonance imaging method using RNase H and RNA microarrays for the ultrasensitive detection of nucleic acids. *Analytical Chemistry*, 76(21):6173–6178, 2004.

[266] G. Hayashi, M. Hagihara, and K. Nakatani. Genotyping by allele-specific L-DNA-tagged PCR. *Journal of Biotechnology*, 135(2):157–160, 2008.

[267] E. Kai, S. Sawata, K. Ikebukuro, T. Iida, T. Honda, and I. Karube. Detection of PCR products in solution using surface plasmon resonance. *Analytical Chemistry*, 71(4):796–800, 1999.

[268] J. Petersen, L. Poulsen, S. Petronis, H. Birgens, and M. Dufva. Use of a multi-thermal washer for DNA microarrays simplifies probe design and gives robust genotyping assays. *Nucleic Acids Research*, 36(2):e10, 2007.

[269] T Kajiyama, Y. Miyahara, L. J. Kricka, P. Wilding, D. J. Graves, S. Surrey, and P. Fortina. Genotyping on a thermal gredient DNA chip. *Genome Research*, 13:467–475, 2003.

[270] A. Ho-Pun-Cheung, E. Assenat, S. Thezenas, F. Bibeau, P. Rouanet, D. Azria, D. Cellier, J. Grenier, M. Ychou, P. Senesse, and E. Lopez-Crapez. Cyclin D1 gene G870A polymorphism predicts response to neoadjuvant radiotherapy and prognosis in rectal cancer. *International Journal of Radiation Oncology, Biology, Physics*, 68(4):1094–1101, 2007.

[271] R. G. Higuchi and H. Ochman. Production of single-stranded DNA templates by exonuclease digestion following the polymerase chain reaction. *Nucleic Acids Research*, 17(14):5865, 1989.

[272] P. G. Mitsis and J. G. Kwagh. Characterization of the interaction of lambda exonuclease with the ends of DNA. *Nucleic Acids Research*, 27(15):3057–3063, 1999.

[273] T. Hultman, S. Stahl, E. Hornes, and M. Uhlen. Direct solid phase sequencing of genomic and plasmid DNA using magnetic beads as solid support. *Nucleic Acids Research*, 17(13):4937–4946, 1989.

[274] N. C. Pagratis. Rapid preparation of single stranded DNA from PCR products by streptavidin induced electrophoretic mobility shift. *Nucleic Acids Research*, 24(18):3645–3646, 1996.

[275] D. O'Meara, P. Nilsson, P. A. Nygren, M. Uhlen, and J. Lundeberg. Capture of single-stranded DNA assisted by oligonucleotide modules. *Analytical Biochemistry*, 255(2):195–203, 1998.

[276] C. M. Niemeyer, W. Burger, and J. Peplies. Covalent DNA - Streptavidin conjugates as building blocks for novel biometallic nanostructures. *Angewandte Chemie-International Edition*, 37(16):2265–2268, 1998.

[277] B. R. Amirikyan, A. V. Vologodskii, and L. Lyubchenko Yu. Determination of DNA cooperativity factor. *Nucleic Acids Research*, 9(20):5469–5482, 1981.

[278] S. Ares, N. K. Voulgarakis, K. O. Rasmussen, and A. R. Bishop. Bubble nucleation and cooperativity in DNA melting. *Physical Review Letters*, 94(3):035504, 2005.

[279] T. Dauxois, M. Peyrard, and A. R. Bishop. Dynamics and thermodynamics of a nonlinear model for DNA denaturation. *Physical Review E*, 47(1):684–695, 1993.

[280] T. Dauxois, M. Peyrard, and A. R. Bishop. Entropy-driven DNA denaturation. *Physical Review E*, 47(1):R44–R47, 1993.

[281] T. A. Taton, C. A. Mirkin, and R. L. Letsinger. Scanometric DNA array detection with nanoparticle probes. *Science*, 289(5485):1757–17560, 2000.

[282] S. J. Park, T. A. Taton, and C. A. Mirkin. Array-based electrical detection of DNA with nanoparticle probes. *Science*, 295(5559):1503–1506, 2002.

[283] J. M. Gibbs-Davis, G. C. Schatz, and S. T. Nguyen. Sharp melting transitions in DNA hybrids without aggregate dissolution: proof of neighboring-duplex cooperativity. *Journal of the American Chemical Society*, 129(50):15535–15540, 2007.

[284] S. Y. Park, J. M. Gibbs-Davis, S. T. Nguyen, and G. C. Schatz. Sharp melting in DNA-linked nanostructure systems: thermodynamic models of DNA-linked polymers. *The journal of Physical Chemistry B*, 111(30):8785–8791, 2007.

[285] T. Pastinen, M. Raitio, K. Lindroos, P. Tainola, L. Peltonen, and A. C. Syvanen. A system for specific, high-throughput genotyping by allele-specific primer extension on microarrays. *Genome Research*, 10(7):1031–1042, 2000.

[286] J. Compton. Nucleic acid sequence-based amplification. *Nature*, 350(6313):91–92, 1991.

[287] B. Deiman, P. van Aarle, and P. Sillekens. Characteristics and applications of nucleic acid sequence-based amplification (NASBA). *Molecular Biotechnology*, 20(2):163–179, 2002.

[288] P. F. Mens, G. J. Schoone, P. A. Kager, and H. D. Schallig. Detection and identification of human Plasmodium species with real-time quantitative nucleic acid sequence-based amplification. *Malaria Journal*, 5:80, 2006.

[289] M. N. Widjojoatmodjo, A. Borst, R. A. Schukkink, A. T. Box, N. M. Tacken, B. Van Gemen, J. Verhoef, B. Top, and A. C. Fluit. Nucleic acid sequence-based amplification (NASBA) detection of medically important Candida species. *Journal of Microbiological Methods*, 38(1-2):81–90, 1999.

[290] K. Loens, T. Beck, D. Ursi, M. Overdijk, P. Sillekens, H. Goossens, and M. Ieven. Development of real-time multiplex nucleic acid sequence-based amplification for detection of Mycoplasma pneumoniae, Chlamydophila pneumoniae, and Legionella spp. in respiratory specimens. *Journal of Clinical Microbiology*, 46(1):185–191, 2008.

[291] E. T. Casper, S. S. Patterson, M. C. Smith, and J. H. Paul. Development and evaluation of a method to detect and quantify enteroviruses using NASBA and internal control RNA (IC-NASBA). *Journal of Virological Methods*, 124(1-2):149–155, 2005.

[292] B. Deiman, C. Schrover, C. Moore, D. Westmoreland, and P. van de Wiel. Rapid and highly sensitive qualitative real-time assay for detection of respiratory syncytial virus A and B using NASBA and molecular beacon technology. *Journal of Virological Methods*, 146(1-2):29–35, 2007.

[293] A. J. Lambert, R. S. Nasci, B. C. Cropp, D. A. Martin, B. C. Rose, B. J. Russell, and R. S. Lanciotti. Nucleic acid amplification assays for detection of La Crosse virus RNA. *Journal of Clinical Microbiology*, 43(4):1885–1889, 2005.

[294] M. C. Keightley, P. Sillekens, W. Schippers, C. Rinaldo, and K. St George. Real-time NASBA detection of SARS-associated coronavirus and comparison with real-time reverse transcription-PCR. *Journal of Medical Virology*, 77(4):602–608, 2005.

[295] A. Houde, D. Leblanc, E. Poitras, P. Ward, J. Brassard, C. Simard, and Y. L. Trottier. Comparative evaluation of RT-PCR, nucleic acid sequence-based amplification (NASBA) and real-time RT-PCR for detection of noroviruses in faecal material. *Journal of Virological Methods*, 135(2):163–172, 2006.

[296] W. van der Meide, J. Guerra, G. Schoone, M. Farenhorst, L. Coelho, W. Faber, I. Peekel, and H. Schallig. Comparison between quantitative nucleic acid sequence-based amplification, real-time reverse transcriptase PCR, and real-time PCR for quantification of Leishmania parasites. *Journal of clinical microbiology*, 46(1):73–78, 2008.

[297] J. H. Yoo, S. M. Choi, D. G. Lee, S. H. Park, J. H. Choi, E. Y. Kwon, and W. S. Shin. Comparison of the real-time nucleic acid sequence-based amplification (RTi-NASBA) with conventional NASBA, and galactomannan assay for the diagnosis of invasive aspergillosis. *Journal of Korean Medical Science*, 22(4):672–676, 2007.

[298] L. T. Lau, S. M. Reid, D. P. King, A. M. F. Lau, A. E. Shaw, N. P. Ferris, and A. C. H. Yu. Detection of foot-and-mouth disease virus by nucleic acid sequence-based amplification (NASBA). *Veterinary Microbiology*, 126(1-3):101–110, 2008.

[299] E. Churruca, C. Girbau, I. Martinez, E. Mateo, R. Alonso, and A. Fernandez-Astorga. Detection of Campylobacter jejuni and Campylobacter coli in chicken meat samples by real-time nucleic acid sequence-based amplification with molecular beacons. *International Journal of Food Microbiology*, 117(1):85–90, 2007.

[300] A. Nadal, A. Coll, N. Cook, and M. Pla. A molecular beacon-based real time NASBA assay for detection of Listeria monocytogenes in food products: role of target mRNA secondary structure on NASBA design. *Journal of Microbiological Methods*, 68(3):623–632, 2007.

[301] N. Cook. The use of NASBA for the detection of microbial pathogens in food and environmental samples. *Journal of Microbiological Methods*, 53(2):165–174, 2003.

[302] A. J. Baeumner, R. N. Cohen, V. Miksic, and J. Min. RNA biosensor for the rapid detection of viable Escherichia coli in drinking water. *Biosensors & Bioelectronics*, 18(4):405–13, 2003.

[303] S. S. Patterson, E. T. Casper, L. Garcia-Rubio, M. C. Smith, and 3rd Paul, J. H. Increased precision of microbial RNA quantification using NASBA with an internal control. *Journal of Microbiological Methods*, 60(3):343–352, 2005.

[304] K. Nakahara, T. Hataya, and I. Uyeda. Inosine 5'-triphosphate can dramatically increase the yield of NASBA products targeting GC-rich and intramolecular base-paired viroid RNA. *Nucleic Acids Research*, 26(7):1854–1856, 1998.

[305] G. Leone, H. van Schijndel, B. van Gemen, F. R. Kramer, and C. D. Schoen. Molecular beacon probes combined with amplification by NASBA enable homogeneous, real-time detection of RNA. *Nucleic Acids Research*, 26(9):2150–2155, 1998.

[306] J. J. Weusten, W. M. Carpay, T. A. Oosterlaken, M. C. van Zuijlen, and P. A. van de Wiel. Principles of quantitation of viral loads using nucleic acid sequence-based amplification in combination with homogeneous detection using molecular beacons. *Nucleic Acids Research*, 30(6):e26, 2002.

[307] C. Berard, M. A. Cazalis, P. Leissner, and B. Mougin. DNA nucleic acid sequence-based amplification-based genotyping for polymorphism analysis. *Biotechniques*, 37(4):680–686, 2004.

[308] S. Fang, H. J. Lee, A. W. Wark, H. M. Kim, and R. M. Corn. Determination of ribonuclease H surface enzyme kinetics by surface plasmon resonance imaging and surface plasmon fluorescence spectroscopy. *Analytical Chemistry*, 77(20):6528–6534, 2005.

[309] E. L. Cussler. *Diffusion-Mass Transfer in Fluid Systems.* Cambridge University Press, Cambridge, 2nd edition edition, 1997.

[310] T. Lindahl. Instability and decay of the primary structure of DNA. *Nature*, 362(6422):709–715, 1993.

[311] S. H. Reed and R. Waters. DNA repair. In Ltd. John Wiley & Sons, editor, *Encyclopedia of life sciences.* Wiley Interscience, 2005.

[312] T. Lindahl, P. Karran, and R. D. Wood. DNA excision repair pathways. *Current Opinion in Genetics & Development*, 7(2):158–169, 1997.

[313] J. S. Sung and B. Demple. Roles of base excision repair subpathways in correcting oxidized abasic sites in DNA. *The FEBS journal*, 273(8):1620–1629, 2006.

[314] J. Cadet, T. Douki, D. Gasparutto, and J. L. Ravanat. Oxidative damage to DNA: formation, measurement and biochemical features. *Mutation Research*, 531(1-2):5–23, 2003.

[315] T. J. Preston, J. T. Henderson, G. P. McCallum, and P. G. Wells. Base excision repair of reactive oxygen species-initiated 7,8-dihydro-8-oxo-2'-deoxyguanosine inhibits the cytotoxicity of platinum anticancer drugs. *Molecular Cancer Therapeutics*, 8(7):2015–2026, 2009.

[316] S. D. Bruner, D. P. Norman, and G. L. Verdine. Structural basis for recognition and repair of the endogenous mutagen 8-oxoguanine in DNA. *Nature*, 403(6772):859–866, 2000.

[317] S. Boiteux, T. R. O'Connor, F. Lederer, A. Gouyette, and J. Laval. Homogeneous Escherichia coli FPG protein. A DNA glycosylase which excises imidazole ring-opened purines and nicks DNA at apurinic/apyrimidinic sites. *The Journal of Biological Chemistry*, 265(7):3916–3922, 1990.

[318] B. Castaing, S. Boiteux, and C. Zelwer. DNA containing a chemically reduced apurinic site is a high affinity ligand for the E. coli formamidopyrimidine-DNA glycosylase. *Nucleic Acids Research*, 20(3):389–394, 1992.

[319] C. A. Minetti, D. P. Remeta, D. O. Zharkov, G. E. Plum, F. Johnson, A. P. Grollman, and K. J. Breslauer. Energetics of lesion recognition by a DNA repair protein: thermodynamic characterization of formamidopyrimidine-glycosylase (Fpg) interactions with damaged DNA duplexes. *Journal of Molecular Biology*, 328(5):1047–1060, 2003.

[320] M. Sugahara, T. Mikawa, T. Kumasaka, M. Yamamoto, R. Kato, K. Fukuyama, Y. Inoue, and S. Kuramitsu. Crystal structure of a repair enzyme of oxidatively damaged DNA, MutM (Fpg), from an extreme thermophile, Thermus thermophilus HB8. *The EMBO journal*, 19(15):3857–3869, 2000.

[321] L. Serre, K. Pereira de Jesus, S. Boiteux, C. Zelwer, and B. Castaing. Crystal structure of the Lactococcus lactis formamidopyrimidine-DNA glycosylase bound to an abasic site analogue-containing DNA. *The EMBO Journal*, 21(12):2854–2865, 2002.

[322] J. C. Fromme and G. L. Verdine. Structural insights into lesion recognition and repair by the bacterial 8-oxoguanine DNA glycosylase MutM. *Nature Structural Biology*, 9(7):544–552, 2002.

[323] R. Gilboa, D. O. Zharkov, G. Golan, A. S. Fernandes, S. E. Gerchman, E. Matz, J. H. Kycia, A. P. Grollman, and G. Shoham. Structure of formamidopyrimidine-DNA glycosylase covalently complexed to DNA. *The Journal of Biological Chemistry*, 277(22):19811–19816, 2002.

[324] N. A. Kuznetsov, V. V. Koval, D. O. Zharkov, Y. N. Vorobjev, G. A. Nevinsky, K. T. Douglas, and O. S. Fedorova. Pre-steady-state kinetic study of substrate specificity of Escherichia coli formamidopyrimidine–DNA glycosylase. *Biochemistry*, 46(2):424–435, 2007.

[325] J. Tchou, V. Bodepudi, S. Shibutani, I. Antoshechkin, J. Miller, A. P. Grollman, and F. Johnson. Substrate specificity of Fpg protein. Recognition and cleavage of oxidatively damaged DNA. *The Journal of Biological Chemistry*, 269(21):15318–15324, 1994.

[326] O. S. Fedorova, G. A. Nevinsky, V. V. Koval, A. A. Ishchenko, N. L. Vasilenko, and K. T. Douglas. Stopped-flow kinetic studies of the interaction between Escherichia coli Fpg protein and DNA substrates. *Biochemistry*, 41(5):1520–1528, 2002.

[327] A. A. Ishchenko, N. L. Vasilenko, O. I. Sinitsina, V. I. Yamkovoy, O. S. Fedorova, K. T. Douglas, and G. A. Nevinsky. Thermodynamic, kinetic, and structural basis for recognition and repair of 8-oxoguanine in DNA by Fpg protein from Escherichia coli. *Biochemistry*, 41(24):7540–7548, 2002.

[328] O. D. Schärer, H. M. Nash, J. Jiricny, J. Laval, and G. L. Verdine. Specific binding of a designed pyrrolidine abasic site analog to multiple DNA glycosylases. *The Journal of Biological Chemistry*, 273(15):8592–8597, 1998.

[329] V. Faure, M. Saparbaev, P. Dumy, and J. F. Constant. Action of multiple base excision repair enzymes on the 2'-deoxyribonolactone. *Biochemical and Biophysical Research Communications*, 328(4):1188–1195, 2005.

[330] C. A. Minetti, D. P. Remeta, and K. J. Breslauer. A continuous hyperchromicity assay to characterize the kinetics and thermodynamics of DNA lesion recognition and base excision. *Proceedings of the National Academy of Sciences of the United States of America*, 105(1):70–75, 2008.

[331] V. S. Sidorenko, G. V. Mechetin, G. A. Nevinsky, and D. O. Zharkov. Ionic strength and magnesium affect the specificity of Escherichia coli and human 8-oxoguanine-DNA glycosylases. *The FEBS Journal*, 275(15):3747–3760, 2008.

[332] A. W. Francis and S. S. David. Escherichia coli MutY and Fpg utilize a processive mechanism for target location. *Biochemistry*, 42(3):801–810, 2003.

[333] V. S. Sidorenko and D. O. Zharkov. Correlated cleavage of damaged DNA by bacterial and human 8-oxoguanine-DNA glycosylases. *Biochemistry*, 47(34):8970–8976, 2008.

[334] D. O. Zharkov, A. A. Ishchenko, K. T. Douglas, and G. A. Nevinsky. Recognition of damaged DNA by Escherichia coli Fpg protein: insights from structural and kinetic data. *Mutation research*, 531(1-2):141–156, 2003.

[335] M. H. David-Cordonnier, J. Laval, and P. O'Neill. Recognition and kinetics for excision of a base lesion within clustered DNA damage by the Escherichia coli proteins Fpg and Nth. *Biochemistry*, 40(19):5738–5746, 2001.

[336] B. M. Sutherland, P. V. Bennett, O. Sidorkina, and J. Laval. Clustered DNA damages induced in isolated DNA and in human cells by low doses of ionizing radiation. *Proceedings of the National Academy of Sciences of the United States of America*, 97(1):103–108, 2000.

[337] M. Häring, H. Rüdiger, B. Demple, S. Boiteux, and B. Epe. Recognition of oxidized abasic sites by repair endonucleases. *Nucleic Acids Research*, 22(11):2010–2015, 1994.

[338] J. Lhomme, J. F. Constant, and M. Demeunynck. Abasic DNA structure, reactivity, and recognition. *Biopolymers*, 52(2):65–83, 1999.

[339] J. D. Levin, A. W. Johnson, and B. Demple. Homogeneous Escherichia coli endonuclease IV. Characterization of an enzyme that recognizes oxidative damage in DNA. *The Journal of Biological Chemistry*, 263(17):8066–8071, 1988.

[340] D. J. Hosfield, Y. Guan, B. J. Haas, R. P. Cunningham, and J. A. Tainer. Structure of the DNA repair enzyme endonuclease IV and its DNA complex: double-nucleotide flipping at abasic sites and three-metal-ion catalysis. *Cell*, 98(3):397–408, 1999.

[341] E. D. Garcin, D. J. Hosfield, S. A. Desai, B. J. Haas, M. Bjoras, R. P. Cunningham, and J. A. Tainer. DNA apurinic-apyrimidinic site binding and excision by endonuclease IV. *Nature Structural & Molecular Biology*, 15(5):515–522, 2008.

[342] B. Demple and S. Linn. DNA N-glycosylases and UV repair. *Nature*, 287(5779):203–208, 1980.

[343] M. Takeuchi, R. Lillis, B. Demple, and M. Takeshita. Interactions of Escherichia coli endonuclease IV and exonuclease III with abasic sites in DNA. *The Journal of Biological Chemistry*, 269(34):21907–21914, 1994.

[344] S. M. Kerins, R. Collins, and T. V. McCarthy. Characterization of an endonuclease IV 3'-5' exonuclease activity. *The Journal of Biological Chemistry*, 278(5):3048–3054, 2003.

[345] N. A. Kuznetsov, V. V. Koval, G. A. Nevinsky, K. T. Douglas, D. O. Zharkov, and O. S. Fedorova. Kinetic conformational analysis of human 8-oxoguanine-DNA glycosylase. *The Journal of Biological Chemistry*, 282(2):1029–1038, 2007.

[346] J. P. Radicella, C. Dherin, C. Desmaze, M. S. Fox, and S. Boiteux. Cloning and characterization of hOGG1, a human homolog of the OGG1 gene of Saccharomyces cerevisiae. *Proceedings of the National Academy of Sciences of the United States of America*, 94(15):8010–8015, 1997.

[347] P. C. Blainey, A. M. van Oijen, A. Banerjee, G. L. Verdine, and X. S. Xie. A base-excision DNA-repair protein finds intrahelical lesion bases by fast sliding in contact with DNA. *Proceedings of the National Academy of Sciences of the United States of America*, 103(15):5752–5757, 2006.

[348] M. Bjorå s, L. Luna, B. Johnsen, E. Hoff, T. Haug, T. Rognes, and E. Seeberg. Opposite base-dependent reactions of a human base excision repair enzyme on DNA containing 7,8-dihydro-8-oxoguanine and abasic sites. *The EMBO Journal*, 16(20):6314–6322, 1997.

[349] A. E. Vidal, I. D. Hickson, S. Boiteux, and J. P. Radicella. Mechanism of stimulation of the DNA glycosylase activity of hOGG1 by the major human AP endonuclease: bypass of the AP lyase activity step. *Nucleic Acids Research*, 29(6):1285–1292, 2001.

[350] J. W. Hill, T. K. Hazra, T. Izumi, and S. Mitra. Stimulation of human 8-oxoguanine-DNA glycosylase by AP-endonuclease: potential coordination of the initial steps in base excision repair. *Nucleic Acids Research*, 29(2):430–438, 2001.

[351] T. Saitoh, K. Shinmura, S. Yamaguchi, M. Tani, S. Seki, H. Murakami, Y. Nojima, and J. Yokota. Enhancement of OGG1 protein AP lyase activity by increase of APEX protein. *Mutation Research*, 486(1):31–40, 2001.

[352] C. D. Mol, T. Izumi, S. Mitra, and J. A. Tainer. DNA-bound structures and mutants reveal abasic DNA binding by APE1 and DNA repair coordination. *Nature*, 403(6768):451–456, 2000.

[353] C. D. Mol, D. J. Hosfield, and J. A. Tainer. Abasic site recognition by two apurinic/apyrimidinic endonuclease families in DNA base excision repair: the 3' ends justify the means. *Mutation Research*, 460(3-4):211–229, 2000.

[354] T. Barnes, W. C. Kim, A. K. Mantha, S. E. Kim, T. Izumi, S. Mitra, and C. H. Lee. Identification of Apurinic/apyrimidinic endonuclease 1 (APE1) as the endoribonuclease that cleaves c-myc mRNA. *Nucleic Acids Research*, 37(12):3946–3958, 2009.

[355] P. J. Berti and J. A. McCann. Toward a detailed understanding of base excision repair enzymes: transition state and mechanistic analyses of N-glycoside hydrolysis and N-glycoside transfer. *Chemical Reviews*, 106(2):506–555, 2006.

[356] N. P. Gerry, N. E. Witowski, J. Day, R. P. Hammer, G. Barany, and F. Barany. Universal DNA microarray method for multiplex detection of low abundance point mutations. *Journal of Molecular Biology*, 292(2):251–262, 1999.

[357] L. D. Ward and D. J. Winzor. Relative merits of optical biosensors based on flow-cell and cuvette designs. *Analytical biochemistry*, 285(2):179–193, 2000.

[358] P. D. Munro, C. M. Jackson, and D. J. Winzor. On the need to consider kinetic as well as thermodynamic consequences of the parking problem in quantitative studies of nonspecific binding between proteins and linear polymer chains. *Biophysical Chemistry*, 71(2-3):185–198, 1998.

[359] C. H. Lee, A. W. Wark, T. T. Goodrich, S. Fang, and R. M. Corn. Surface Enzyme Kinetics for Biopolymer Microarrays: a Combination of Langmuir and Michaelis-Menten Concepts. *Langmuir*, 21:4050–4057, 2005.

[360] W. Bujalowski. Thermodynamic and Kinetic Methods of Analyses of Protein - Nucleic Acid Interactions. From Simpler to More Complex Systems. *Chemical Reviews*, 106(2):556–606, 2006.

[361] P. M. Girard, C. D'Ham, J. Cadet, and S. Boiteux. Opposite base-dependent excision of 7,8-dihydro-8-oxoadenine by the Ogg1 protein of Saccharomyces cerevisiae. *Carcinogenesis*, 19(7):1299–1305, 1998.

[362] B. M. Sutherland, P. V. Bennett, O. Sidorkina, and J. Laval. Clustered damages and total lesions induced in DNA by ionizing radiation: oxidized bases and strand breaks. *Biochemistry*, 39(27):8026–8031, 2000.

[363] M. H. David-Cordonnier, S. Boiteux, and P. O'Neill. Excision of 8-oxoguanine within clustered damage by the yeast OGG1 protein. *Nucleic Acids Research*, 29(5):1107–1113, 2001.

[364] M. H. David-Cordonnier, S. Boiteux, and P. O'Neill. Efficiency of excision of 8-oxo-guanine within DNA clustered damage by XRS5 nuclear extracts and purified human OGG1 protein. *Biochemistry*, 40(39):11811–11818, 2001.

[365] H. Budworth, G. Matthewman, P. O'Neill, and G. L. Dianov. Repair of tandem base lesions in DNA by human cell extracts generates persisting single-strand breaks. *Journal of Molecular Biology*, 351(5):1020–1029, 2005.

[366] S. M. Cunniffe, M. E. Lomax, and P. O'Neill. An AP site can protect against the mutagenic potential of 8-oxoG when present within a tandem clustered site in E. coli. *DNA Repair (Amst)*, 6(12):1839–1849, 2007.

[367] M. E. Lomax, H. Salje, S. Cunniffe, and P. O'Neill. 8-OxoA inhibits the incision of an AP site by the DNA glycosylases Fpg, Nth and the AP endonuclease HAP1. *Radiation Research*, 163(1):79–84, 2005.

[368] V. S. Sidorenko, G. A. Nevinsky, and D. O. Zharkov. Mechanism of interaction between human 8-oxoguanine-DNA glycosylase and AP endonuclease. *DNA Repair (Amst)*, 6:317–328, 2007.

[369] V. S. Sidorenko, G. A. Nevinsky, and D. O. Zharkov. Specificity of stimulation of human 8-oxoguanine-DNA glycosylase by AP endonuclease. *Biochemical and Biophysical Research Communications*, 368:175–179, 2008.

[370] E. Bouffartigues, H. Leh, M. Anger-Leroy, S. Rimsky, and M. Buckle. Rapid coupling of Surface Plasmon Resonance (SPR and SPRi) and ProteinChip based mass spectrometry for the identification of proteins in nucleoprotein interactions. *Nucleic Acids Research*, 35(6):e39, 2007.

[371] S. Draghici, P. Khatri, A.C. Eklund, and Z. Szallasi. Reliability and reproducibility issues in DNA microarray measurements. *Trends in Genetics*, 22(2):101–109, 2006.

[372] Heiner Grimm. Wasser - Eigenschaften, Daten und Phänomene `http://www.wissenschaft-technik-ethik.de/#wass`, 28.06.2009 2009.

[373] K. M. Hansen, H. F. Ji, G. Wu, R. Datar, R. Cote, A. Majumdar, and T. Thundat. Cantilever-based optical deflection assay for discrimination of DNA single-nucleotide mismatches. *Analytical Chemistry*, 73(7):1567–1571, 2001.

[374] R. J. Lipshutz, D. Morris, M. Chee, E. Hubbell, M. J. Kozal, N. Shah, N. Shen, R. Yang, and S. P. Fodor. Using oligonucleotide probe arrays to access genetic diversity. *Biotechniques*, 19(3):442–447, 1995.

[375] U. Maskos and E. M. Southern. A novel method for the parallel analysis of multiple mutations in multiple samples. *Nucleic Acids Research*, 21(9):2269–2270, 1993.

[376] S. V. Tillib, B. N. Strizhkov, and A. D. Mirzabekov. Integration of multiple PCR amplifications and DNA mutation analyses by using oligonucleotide microchip. *Analytical Biochemistry*, 292(1):155–160, 2001.

List of Figures

List of Tables

Glossary

Addressing	Bringing a molecule to a specific localization
Allele specific oligonucleotide	ODN sequence that is complementary to part of a specific allele of a gene containing the mutation site
Anion	Negatively charged ion
Apoptosis	Programmed cell death
Bimodal Distribution	Distribution with two distinct maxima
Biopsy	Extraction of cell samples from cancer tissue for analysis purposes
Cation	Positively charged ion
Chemisorption	Chemical specific adsorption involving forces comparable to interactions of chemical compounds. Activation energies are higher than in the physisorbed state and lower than covalent binding
Cytotoxicity	Substance or condition that is toxic for living cells and may lead to cell death
DNA sequence	Order of nucleotides in a DNA chain. The length of a DNA molecule is typically given in base pairs (bp)
Debye length	Characteristic length scale for charge screening in salty solutions
Detection limit	Lowest target concentration leading to signal that lies significantly over the background noise. Signal-to-noise ratios of 3-10 are often defined as lower limit of detection
Endogenous	Caused by factors within the body, as opposed to exogenous
Equilibrium melting	Used here as a synonym for thermal denaturation in the presence of a constant concentration of target DNA. This does not automatically imply that melting takes place reversibly in thermodynamic equilibrium, i.e. without a hysteresis effect
FISH	Fluorescence in situ hybridization, a method that studies intracellular binding of fluorescently labeled oligonucleotides to target RNA
Helix-coil transition	Passage of DNA from the double stranded helical form into a state of two separate DNA strands
Heterozygous case	Contrary of homozygous case: the genes on the chromosomes (alleles) differ so that the gene has not exactly the same DNA sequence
Homozygous case	When a cell is diploid, meaning that it has two times the same chromosomes, genes are called homozygous, when the DNA sequence on both chromosomes is identical
In vitro	Preparation of samples outside their natural environment, as opposed to *in vivo*, in laboratory assays
Isoelectric Point	Refers to the pH at which certain molecules do not present any net charges. It is important for proteins and enzymes to know their net charges in the experimental buffer
L-DNA	Left-handed mirror DNA that only hybridizes to PNA or other L-DNA targets
Melting temperature	Temperature at which statistically 50% of DNA is in the double helical state
Molecular beacon	Hairpin shaped ODN with specific recognition sequence in the loop. When the stem is closed, a fluorescent label at one end is quenched by a quencher on the other. Upon hybridization to a target, the stem opens up and fluorescence can be detected.
Mutagenesis	Process or condition that leads to mutations in the genetic information
Negative control	A surface area of the biosensor that should not lead to a detectable signal when exposed to relevant biological samples
Non-equilibrium thermal denaturation	DNA dissociation upon heating in absence of target DNA ($c = 0$). Normally, a constant buffer flow is applied. The dissociation temperature, corresponding to the temperature at which half of the initially hybridized strands are dissociated, depends on the heating rate (see section 4.4)

Oligonucleotide (ODN)	Synthetic DNA with a sequence length of ~ 10 to ~ 80 bases. Longer DNA is normally produced by polymerase chain reaction
Oncogene	Gene that contributes to formation of cancerous cells when mutated or over-expressed.
Physisorption	Adsorption promoted by intermolecular forces like Van-der-Waals forces, which do not significantly change the electronic orbitals of the interacting partners.
Positive control	Region of biosensor surface that is functionalized with a biological probe analog to the analyzed probe but without affinity for the target in question. When the sample contains, however, the corresponding specific target, the positive control gives a detectable signal
Point mutation	Exchange, addition or deletion of one single base at a given point in a DNA strand. Leads to mismatches in the double helix
Probe	DNA strand immobilized on a surface to explore the surrounding medium for targets
Proto-oncogene	A normal gene that becomes an oncogene in the presence of mutations
RNase H	Ribonuclease H is an endoribonulcease that hydrolyzes RNA hybridized to DNA starting from the 3' end. This process generates ssDNA from the RNA/DNA duplex. Single and double stranded DNA is not digested by the enzyme
Sample	Biological mixture, often extracted from cells or product of a molecular biology amplification protocol, which is to be tested for the presence or absence of the biological target
Sensitivity	Sensitivity refers to the slope of a detector at the onset of detection and is given as signal per target concentration. The higher the sensitivity of the system, the better the signal transduction
Specificity	The specificity of a biosensor refers to its capacity to produce a relevant signal only in the presence of its biological target. Specificity generally has to be controlled using the background signal produced on reference surfaces, like positive and negative controls
Static conditions	The flow rate replacing the liquid in the cuvette is stopped so that no exchange can take place
Target	Here: DNA in solution that has the complementary sequence to probes enabling specific recognition between the probe-target pair. More general, target refers to the molecule in solution to be recognized by the sensor leading to a detection signal
Template DNA	DNA sequence to be copied into complementary DNA during polymerase activity. The template defines the sequence of the newly synthesized DNA strand
Thiolate	R-S^-: Deprotonated form of a thiol group (R-SH), reactive form interacting for example with metal surfaces via valence bonds

Index

Physicochemical study of DNA biochips: DNA duplex stability, point mutation detection and beyond

This Ph.D. thesis studies phenomena concerning DNA duplex stability. Exploiting a real-time detection system based on Surface Plasmon Resonance imaging (SPRi), we use a temperature scan method to analyze DNA interactions on functionalized biochips. First, a detailed study about a comparison of two DNA immobilization methods and the influence of different buffer components on surface hybridized DNA duplexes is presented. Especially the influence of salt and denaturing agents in the buffer are discussed. Second, we apply the temperature scan methods to point mutation detection, as well for oligonucleotides as for longer DNA or RNA targets produced by Polymerase Chain Reaction (PCR) or Nucleic Acid Sequence Based Amplification (NASBA) amplification protocols, respectively. Competition between targets containing point mutations and surface hybridization is addressed. Also secondary structures in solution may alter target capture on probes. For the isothermal NASBA amplification, we show that it is possible to make an integrated system with amplification and detection on the SPRi chip. Finally, a study of DNA lesions and repair enzymes is presented in collaboration with the 'Laboratory of Nucleic Acids Lesions' (LAN) at the CEA Grenoble profiting once again from the flexible temperature regulation to characterize enzyme activity on surface grafted DNA.

Keywords: *Surface Plasmon Resonance imaging (SPRi), temperature scans, point mutation, poly-pyrrole, thiol self-assembling, PCR, NASBA, DNA lesions, Base Excision Repair (BER).*

Etude physico-chimique des puces à ADN : Stabilité du duplex d'ADN, détection des mutations ponctuelles et au-delà.

Le travail de cette thèse est axé autour de l'observation de la stabilité du duplexe de l'ADN. Exploitant un système de détection en temps réel basé sur le principe de l'imagerie par la résonance des plasmons de surface, nous utilisons des rampes de température pour mettre en évidence les interactions d'ADN sur une biopuce fonctionnalisée. Un premier travail porte ainsi sur une comparaison de chimies de greffages et l'influence du tampon sur la stabilité du duplexe d'ADN. Notamment, la salinité du milieu et l'influence d'un dénaturant de l'ADN sont étudiés. Dans un deuxième temps, la méthode des rampes de température est appliquée à la détection des mutations ponctuelles sur des cibles d'ADN et ARN longues, issus de la polymerase chain reaction (PCR) ou la nucleic acid sequence based amplification (NASBA), respectivement. L'effet de compétition entre cibles mutées et l'hybridation à la surface est abordé. De plus, les structures secondaires en solutions peuvent changer la capture des cibles sur les sondes. La possibilité d'intégrer l'amplification dans un système de détection sur puce est démontrée pour la NASBA. Enfin, en collaboration avec le laboratoire des lésions d'acides nucléiques (LAN) au CEA Grenoble, une étude des interactions et de l'activité de protéines réparatrices sur l'ADN endommagé est présentée, profitant, de nouveau du choix flexible de la température.

Mots clés : *Imagerie par résonance de plasmons de surface (SPRi), rampes de températures, mutation ponctuelle, poly-pyrrole, auto-assemblage de thiol, PCR, NASBA, lésions d'ADN, réparation par excision de base.*